

Washington University in St. Louis

## Washington University Open Scholarship

---

Arts & Sciences Electronic Theses and  
Dissertations

Arts & Sciences

---

Spring 5-15-2019

### The Role of IFRD1 in the Recruitment and Function of Reserve Stem Cells in Regeneration and Cancer

Mark Anthony Lewis

*Washington University in St. Louis*

Follow this and additional works at: [https://openscholarship.wustl.edu/art\\_sci\\_etds](https://openscholarship.wustl.edu/art_sci_etds)



Part of the [Cell Biology Commons](#), and the [Molecular Biology Commons](#)

---

#### Recommended Citation

Lewis, Mark Anthony, "The Role of IFRD1 in the Recruitment and Function of Reserve Stem Cells in Regeneration and Cancer" (2019). *Arts & Sciences Electronic Theses and Dissertations*. 1861.  
[https://openscholarship.wustl.edu/art\\_sci\\_etds/1861](https://openscholarship.wustl.edu/art_sci_etds/1861)

This Dissertation is brought to you for free and open access by the Arts & Sciences at Washington University Open Scholarship. It has been accepted for inclusion in Arts & Sciences Electronic Theses and Dissertations by an authorized administrator of Washington University Open Scholarship. For more information, please contact [digital@wumail.wustl.edu](mailto:digital@wumail.wustl.edu).

WASHINGTON UNIVERSITY IN ST. LOUIS

Division of Biology and Biomedical Sciences  
Molecular and Cellular Biology

Dissertation Examination Committee:

Jason C. Mills, Chair

David DeNardo

Blair Madison

Deborah Rubin

Ting Wang

The Role of IFRD1 in the Recruitment and Function of Reserve Stem Cells in Regeneration and  
Cancer

by

Mark Lewis

A dissertation presented to  
The Graduate School  
of Washington University in  
partial fulfillment of the  
requirements for the degree  
of Doctor of Philosophy

May 2019  
St. Louis, Missouri

© 2019, Mark Lewis

# Table of Contents

List of Figures .....	iv
List of Tables .....	vi
Acknowledgments.....	vii
Abstract.....	viii
Chapter 1: Introduction.....	1
1.1 Emergence of Paligenosis .....	1
1.2 Parallels between Apoptosis and Paligenosis .....	3
1.3 IFRD1 review.....	5
1.4 Paligenosis and GI Disease .....	13
1.5 IFRD1 review.....	20
1.6 Figures.....	21
1.7 References.....	27
Chapter 2: Regenerative proliferation of differentiated cells by mTORC1-dependent paligenosis (manuscript) .....	36
2.1 Introduction.....	36
2.2 Results.....	38
2.3 Discussion .....	49
2.4 Materials and Methods.....	55
2.5 Figures.....	61
2.6 References.....	93
Chapter 3: Increased IFRD1 Expression in Human Colon Cancers Predicts Reduced Patient Survival (manuscript).....	104
3.1 Introduction.....	104
3.2 Methods.....	106
3.3 Results.....	108
3.4 Discussion .....	110
3.5 Figures.....	113
3.6 References.....	122
Chapter 4: IFRD1 promotes survival and proliferation in the conserved cellular regeneration program (paligenosis) by suppressing p53 (manuscript in submission).....	125
4.1 Summary .....	125
4.2 Introduction.....	126
4.3 Results and Discussion .....	128
4.4 Conclusions.....	138
4.5 Figures.....	140

4.6	Methods.....	166
4.7	References.....	171
Chapter 5: Future Directions.....		175
5.1	Summary .....	175
5.2	Future Directions .....	176
5.3	Conclusions.....	184
5.4	Figures.....	185
5.5	References.....	189
Curriculum Vitae .....		192

# List of Figures

Figure 1.1: Metaplasias in Stomach and Pancreas .....	21
Figure 1.2: Schematic of Paligenosis.....	23
Figure 1.3: Identification of IFRD1 .....	24
Figure 1.4: <i>In silico</i> screen of paligenosis genes .....	25
Figure 1.5: Schematic of nucleolar stress .....	26
Figure 2.1: Changes in mTORC1 during paligenosis .....	61
Figure 2.2: Injury induced proliferation in the stomach and pancreas .....	62
Figure 2.3: mTORC1 in gastric tumorigenesis .....	63
Figure 2.4: GSEA and cell cycle gene analysis .....	64
Figure 2.5: Upregulation of lysosomal and autophagic machinery during paligenosis .....	65
Figure 2.6: Lysosomes are required for proliferation .....	66
Figure 2.7: Schematic of paligenosis .....	68
Figure S2.1: GSEA of SPEM, cell cycle and rapamycin sensitive genes .....	69
Figure S2.2: Time course of LAMP1 activity during paligenosis .....	71
Figure S2.3: Cerulein treated GNPTAB <sup>-/-</sup> mice demonstrate aberrant histology .....	72
Figure S2.4: Apoptosis during paligenosis in the stomach and pancreas .....	73
Figure EV2.1: pS6 as a marker for mTORC1 activity .....	78
Figure EV2.2: Paligenosis in liver and kidneys.....	80
Figure EV2.3: Pancreas and stomach histology with Rapamycin .....	82
Figure EV2.4: mTORC1 inhibition and metaplastic gene expression .....	84
Figure EV2.5: Representative IHC in human gastric cancer tissue microarray .....	86
Figure EV2.6: Histology of GNPTAB <sup>-/-</sup> mouse tissue .....	88
Figure EV2.7: GNPTAB <sup>-/-</sup> mice and mTORC1 activity .....	91
Figure 3.1: IFRD1 in human colon cancer .....	113
Figure 3.2: Survival analysis of colon cancer patients relative to IFRD1 expression .....	118
Figure 3.3: Survival analysis of colon cancer patients relative to country of origin .....	119
Figure 4.1: Characterization of IFRD1 in multiple tissues .....	140
Figure 4.2: IFRD1 is required for proliferation in pancreas and stomach .....	142
Figure 4.3: Loss of IFRD1 stabilizes p53 expression .....	145
Figure 4.4: IFRD1 is required for mTORC1 reactivation .....	147
Figure 4.5: <i>Ifrd1</i> <sup>-/-</sup> mice fail to proliferate due to p53 stabilization .....	149
Figure 4.6: mTORC1 suppresses p53 in the absence of IFRD1 .....	152
Figure 4.7: Schematic of IFRD1 in paligenosis .....	154
Figure S4.1: IFRD1 protein structure analysis .....	155
Figure S4.2: IFRD1 function is cell autonomous and required for proliferation .....	157

Figure S4.3: IFRD1 does not affect early stages of paligenosis .....	159
Figure S4.4: PS6 quantification using HALO software .....	161
Figure S4.5: Loss of p53 rescues mTORC1 phenotype .....	162
Figure S4.6: mTORC1 inhibition stabilized p53 .....	164
Figure 5.1: IFRD1 is required for gastric organoid formation .....	185
Figure 5.2: Yeast 2 hybrid assay results .....	186
Figure 5.3: Loss of IFRD1 affects DDX21 expression following cerulein .....	187
Figure 5.4: IFN Type 1 related gene expression in IFRD1 following cerulein .....	188

# **List of Tables**

Table S2.1: Gastric tumor microarray patient Demographics .....	75
Table S2.2: List of Antibodies .....	76
Table S2.3: List of qRT-PCR primers .....	77
Table 3.1: Colon cancer patient demographics.....	115
Table 3.2: Patient age and gender distribution.....	116
Table 3.3: Clinical characteristics of colon cancer patients.....	117

# Acknowledgments

I am grateful to have had the opportunity to attend Washington University School of Medicine. The rigorous scientific community and investment in training future scientists has prepared me for a bright future.

I am thankful to have had the opportunity to be mentored by Dr. Jason Mills. While I am certainly proud of the research project that we have created, my time in the Mills lab has meant more than that. Because of Dr. Mills, I now have the confidence to go forth, knowing that I am capable of more than I once believed.

I would like to thank my thesis chair, Dr. Deborah Rubin, whose previous work set the foundation for me to have a successful dissertation project. I would also like to thank each of the funding institutions and groups that have allowed me to achieve my dissertation research aims, including the National Institute of Diabetes and Digestive and Kidney Diseases, the Sally and Gerald DeNardo Family Grant, and the T32 training grant led by Dr. Phil Tarr. I would also like to thank Dr. David DeNardo, Dr. Blair Madison and Dr. Ting Wang for their support and advice as thesis committee members throughout my training.

Mark Lewis

*Washington University in St. Louis*

*May 2019*

This work is dedicated to my family, both near and far, for your unconditional love and support.

## ABSTRACT OF THE DISSERTATION

The Role of IFRD1 in the Recruitment and Function of Reserve Stem Cells in Regeneration and  
Cancer

by

Mark Lewis

Doctor of Philosophy in Biology and Biomedical Sciences

Molecular and Cellular Biology

Washington University in St. Louis, 2019

Professor Jason C. Mills, Chair

Mature cells can reprogram into a proliferative, progenitor-like state to repair tissue following injury and inflammation. Differentiated cells in diverse tissues can become proliferative via a dedicated, evolutionarily conserved program we termed *paligenosis*. We detailed how paligenosis occurs, in both gastric chief and pancreatic acinar cells, in a step-wise manner that involves: 1) autodegradation of mature cell components; 2) re-expression of progenitor genes; 3) re-entry into the cell cycle. This process is governed by mTORC1, a fundamental cellular energy sensor and regulator of protein translation. Blocking mTORC1 permitted autophagy and metaplastic gene induction but blocked cell cycle re-entry at S-phase. Because paligenosis is a shared, conserved process, we reasoned that genes likely evolved specifically to regulate it. We characterized IFRD1 as a gene that is conserved throughout eukaryotes, upregulated by paligenosis-inducing injury, and largely dispensable for homeostatic regulation of proliferation and differentiation. IFRD1 is critical for the injury-induced recruitment of cells into the cell cycle in *Drosophila* intestine and multiple mouse tissues. *Ifrd1*<sup>-/-</sup> mice showed decreased mTORC1-mediated proliferation and increased apoptosis in gastric and pancreatic paligenotic

cells. mTORC1 inhibition and *Ifrd1*<sup>-/-</sup>; *Trp53*<sup>-/-</sup> experiments revealed that IFRD1 works largely by preventing p53 from repressing the reactivation of mTORC1 during stage 3 of paligenosis. IFRD1 is the first gene shown to regulate the conserved cellular program that recruits mature cells for regeneration. Recruiting mature cells to proliferate following injury can reveal harbored mutations that increase the risk for preneoplastic lesions. Thus, we analyzed the expression of IFRD1 in colon cancer tumors and found it to be significantly associated with decreased 5-year patient survival. Pro-paligenotic genes like IFRD1 might be harnessed to increase cellular reprogramming to promote regeneration; alternatively, because recruiting old cells with potential stores of somatic mutations increases risk for cancer, blocking paligenosis might prevent or treat cancer.

# **Chapter 1: Introduction**

## **Chapter 1.1 The Emergence of Paligenosis**

Cellular plasticity in response to injury has become critical to understanding the role of mature, differentiated cells in human disease. Numerous species and nearly all tissues demonstrate instances of cellular plasticity. There have been relatively few investigations of the specific cellular and molecular mechanisms involved in this process. Limited research in this area is due to: 1) terminology, in that there has not been an accepted, singular term used to describe the process by which terminally differentiated cells revert their cellular state to repair injury; and 2) a general focus of investigators on the outcomes of dedifferentiation (vs. the process). This cellular “reprogramming” to a proliferative, regenerative state can occur in various contexts, such as when tissue undergoes metaplasia following injury. Metaplasia is described as a temporary change in differentiation state in a cell. Acutely, injury-induced metaplasia enables rapid tissue repair, with full restoration of normal tissue architecture. We primarily investigate the cellular processes involved in metaplasia in the stomach, where it is described as SPEM (Spasmolytic Peptide Expressing Metaplasia) (Figure 1A). High doses of tamoxifen causes SPEM and it is characterized by the loss of some differentiation markers and the emergence of cells that express both terminal differentiation markers such as Gastric Intrinsic Factor (GIF) or Pepsinogen-II (PGII) and a progenitor marker like Trefoil factor 2 (TFF2)<sup>1</sup>.

Building upon the work of former Mills lab members (Greg Sibbel, Ramon Jin, and Won Jae Huh), we understood that the first detectable morphological change in gastric chief cells is an induction of lysosomal and autophagic machinery. We proposed that pancreatic acinar cells, which share morphological and physiological function with gastric chief cells, would be an

important tissue to investigate and compare the acute injury response. Metaplasia in the pancreas is termed ADM (Acinar-to-Ductal Metaplasia) (Figure 1B). Repeated doses of cerulein causes ADM in pancreatic acinar cells, which is also characterized by the dedifferentiation of acinar cells to an embryonic progenitor phenotype that expresses ductal markers. Pancreatic acinar cells lose morphological features of a differentiated cell and express the combination of acinar-specific markers like Amylase or Carboxy-peptidase 1 (CPA1) and duct markers like cytokeratin 19 (CK19), Sry-related high-mobility group box 9 (SOX9) or mucin 1 (Muc1)<sup>2</sup>.

In addition to an upregulation of autophagic machinery, we observed that exocrine secretory cells in both the stomach and pancreas exhibited a specific and discrete set of events (Figure 2). The idea of a shared, conserved process of dedifferentiation was first proposed in the work of Dr. Jason Mills and Dr. Owen Sansom<sup>3</sup>. They described, based on preliminary observations in the lab and in the literature, that the stomach, pancreas and small intestine activate a similar program in response to injury and inflammation. They described how secretory cells in these tissues induced lysosomes to degrade mature cell components prior to the expression of progenitor markers (metaplastic gene expression). The last step is that these metaplastic cells will re-enter the cell cycle, in order to begin to repair and regenerate the damaged tissues. The sequential nature of this process was hypothesized to have specifically evolved to equip otherwise terminally differentiated cells with the capacity to revert to an embryonic state, and become mitotic again. Metaplasias in the stomach and pancreas are designed to be temporary cellular states that enable a cell to withstand certain injuries.

We proposed “paligenosis” as a dedicated term for this specific cellular process re-acquiring regenerative capacity. The term paligenosis encompasses the many terms that describe a “reprogramming” event in mature cells. Paligenosis represents a decision at the cellular level to

dedifferentiate and proliferate instead of being routed to programmed cell death. We predict that failure at any stage of paligenosis would result in cellular dysfunction or apoptosis. Here, we proposed paligenosis to define the process and demonstrate that it is a conserved program with shared molecular and cellular regulation similar to other basic cellular processes like mitosis or apoptosis.

## **Chapter 1.2 Parallels between paligenosis and apoptosis**

We proposed that paligenosis is a fundamental biological process, like mitosis or apoptosis. We believe that paligenosis is activated following injury and inflammation to enable a decision at the cellular level to either become proliferative or activate programmed cellular death. Apoptosis, like paligenosis, was named to describe a distinct program of cellular changes. The term apoptosis was first used in a hallmark paper by Kerr, Wyllie, and Currie in 1972 to describe a morphologically distinct form of cell death. While apoptosis as a term had only been described in 1972, components of the apoptosis concept had been explicitly described many years previously<sup>4-6</sup>. The cellular events involved in apoptosis include blebbing, cell shrinkage, nuclear fragmentation, chromatin condensation, chromosomal DNA fragmentation and global mRNA decay en route to death<sup>7</sup>. The understanding of the mechanisms involved in the process of apoptosis in mammalian cells emerged from the investigation of programmed cell death during the development of the nematode *Caenorhabditis elegans*<sup>8</sup>.

Kerr and colleagues described a mechanism by which the balance between cell division and cell loss can be managed in a newly named process termed apoptosis<sup>4</sup>. Like paligenosis, apoptosis was described to play a basic role in tissue homeostasis with wide-ranging biological implications<sup>4</sup>. After the initial characterization of apoptosis, little was known about the factors

that initiate apoptosis or of the nature of the proteins involved. At this time, apoptosis was described as a basic cellular process that was highly conserved and involved specific cellular mechanisms that were activated prior to the appearance of the characteristic morphological changes. The key events in the evolution of apoptosis, include: its naming, the identification of genes that are required for its execution and the description of subtypes that occur in a specialized manner. In the 1980's, the genetics of programmed cell death began to come into view. Initially, three genes- *ces-1*, *ces-2*, and *egl-1*- were identified in *C. elegans* that, when mutated reversed the life vs. death decision in a subset of cells<sup>9-11</sup>. Then, it was found that three different genes- *ced-3*, *ced-4* and *ced-9*- can mutate to cause the survival of all cells that otherwise would undergo apoptosis<sup>10,12</sup>. These three genes defined the killing or execution step of apoptosis. This time in apoptosis research represents the watershed moment when investigators began to elucidate not only the family of genes that are important for apoptosis (*ced* genes), but also the interplay between these genes and the genetics of apoptosis induction and function<sup>13-19</sup>. Another key moment was the cloning of the *ced-9* gene which revealed that the amino acid sequence of *ced-9* is similar to the protein product of the mammalian proto-oncogene *bcl-2*<sup>13</sup>. They found that, like *ced-9*, *Bcl-2* is sufficient to protect worm cells from apoptosis. This conservation of protein sequence and function was important in showing how basic cellular processes can be evolutionarily conserved and the ability to translate findings from simple to complex species.

Our hope is that paligenosis follows a similar trajectory. At this point, the set of cellular processes have been named. Like *ced* genes, we believe that there is a set of genes that have evolved specifically to regulate the paligenosis process. The most fundamental characteristic of a paligenosis gene would be for it to be highly conserved. We would also hypothesize that this

gene, whose primary role is to regulate reserve stem cell function, would be dispensable for normal cellular activity. We would also anticipate this gene to be called into action during the acute injury response in numerous tissues. Within this thesis, I will describe how we have identified the first gene specifically required for paligenosis.

### **Chapter 1.3 IFRD1 review**

We described paligenosis as a shared and conserved process activated in response to injury. Therefore, we initiated a bioinformatic screen to identify genes that are upregulated in the acute injury phase. Our initial criteria for a paligenosis gene was one that may be expressed at low or no levels normally, but then increase in response to stress. In addition, stresses that induce conserved mechanisms like fos/jun/AP1 would also likely signal through a protein that is important for a conserved process like paligenosis. We would, thus, expect this protein to only affect a certain kind of stress response, but not normal development or proliferation. Our initial screen included tissues that demonstrate metaplasia and dynamic mTORC1 activity following injury (Stomach, Pancreas, Kidney and Liver) (Figure 3). The screen led to the identification of 8 genes that we then analyzed further to include more diverse tissues that also demonstrate the ability to dedifferentiate in response to injury (lung and glia) (Figure 4). *Atf3* and *Ifrd1* were the only two genes to be significantly upregulated in diverse tissues during the acute injury response. My decision to pursue IFRD1 was influenced by the fact that our colleague, Dr. Deborah Rubin, is an expert on this protein and that would enable us to quickly leverage that expertise to investigate IFRD1 in paligenosis. ATF3 is also under active investigation in the lab.

IFRD1 (interferon related developmental regulator 1) was originally characterized as an immediate early gene that was found to respond to mitogens such as TPA, EGF, c-Jun and FGF.

IFRD1 associates with the Sin3 complex and was reported to play a role as a transcriptional co-regulator. Dr. Rubin described the role of IFRD1 in regulating intestinal lipid metabolism and epithelial cell proliferation<sup>20,21</sup>. To this point, there have no reports of homeostatic pathology in mice lacking IFRD1, other than a neurodegenerative disorder known as Spinocerebellar ataxia (SCA)<sup>22</sup>. Neurodegenerative disorders like SCA are generally progressive diseases associated with damage to neurons. Cells of the peripheral nervous system have an intrinsic ability to repair or regenerate<sup>22</sup>. For example, when an axon is damaged, the distal segment activates a repair process that begins with Wallerian degeneration. The proximal segment of the axon either undergoes apoptosis or chromatolysis in an attempt to repair the axon. Chromatolysis results in nuclear and nucleolar changes that enables a neuron to regenerate following injury<sup>22</sup>. This neuronal injury response mirrors the degradation, gene expression changes and regenerative capacity we describe in paligenosis. We hypothesize that the emergence of a defect related to IFRD1 in neuroregeneration would be due to the fact these long-lived cells may rely on a process like paligenosis to repair injury.

We began to generate specific criteria for a paligenosis gene and *Ifrd1* became a lead candidate for investigation. As a transcriptional co-regulator, IFRD1 could potentially regulate large sets of genes (like a specific genetic program) via chromatin modification, compared to a typical transcription factor which generally have more limited capacity to regulate genes. Preliminary experiments with GFP-tagged IFRD1 in Caco-2 cells revealed that this protein can be localized in various cell compartments (cytoplasm, nucleus and nucleolar). This suggested that IFRD1 may then function in different parts of the cell, potentially to interpret cellular stimuli in the cytoplasm or modify transcription in the nucleus or nucleolus. Since IFRD1 is activated rapidly in response to injury, it may function by associating with a complex that is already

present in all cells that rely on paligenosis to proliferate or regenerate. Alternatively, this protein may act as a scaffold, to bring together already present components needed for cell cycle re-entry after injury.

We would anticipate that IFRD1 function would impact human disease, as well. A recent paper has shown that mutations in IFRD1 are associated with gastric cancer<sup>23</sup>. Given the role of IFRD1 in driving the stress-induced proliferative response, we would also predict that IFRD1 expression in adult cancers could also be associated with increased tumorigenesis. Functionally, we might expect aberrant IFRD1 function to allow tumor cells to quickly switch from a quiescent to proliferative state. Further, IFRD1 has been shown to alter lipid metabolism in enterocytes and could, thus, regulate the metabolic status of cancer cells<sup>21,24</sup>. This metabolic flexibility could then influence the way that cancer cells adapt to the tumor microenvironment or it may modify sensitivity to adjuvant chemotherapy<sup>25</sup>.

Lastly, because paligenosis is shared and conserved process, we would also expect a protein evolved to regulate it to also be conserved. We found that the major domains of IFRD1 are conserved to *Schizosaccharomyces Pombe*. Publicly available datasets show that IFRD1 orthologs are upregulated in response to stress in both *S. pombe* and *D. melanogaster*. Thus, *Ifrd1* expression levels positively correlate with the processes of cell and tissue injury response and regeneration in humans, mice and in lower species. For these reasons, IFRD1 became a lead candidate as a critical regulator of paligenosis.

### **IFRD1 conservation and the Sin3A HDAC complex**

IFRD1 has been reported to interact with the SIN3 histone deacetylase (HDAC) complex<sup>26</sup>. SIN3 was initially identified via genetic screen by two groups in 1987-the MRC

Laboratory of Molecular Biology (Cambridge, England) and the University of California, San Francisco (San Francisco, CA)-that were independently investigating the phenomena of mating type switching in budding yeast<sup>27</sup>. SIN3 has not been shown to have intrinsic DNA-binding abilities, but instead is thought to act as a master scaffold, providing a platform for the assembly of numerous transcription factors and cofactors. More than two decades of research has implicated Sin3 in numerous biological functions including: scaffolding of core histone deacetylase (HDAC) complexes, regulation of DNA and histone methylation, nucleosome remodeling, and N-acetylglucosamine transferase activity. SIN3 has also been found to play a key role in the reprogramming of somatic cells by maintaining embryonic stem cell pluripotency and promotes the generation of induced pluripotent stem cells<sup>28</sup>. In *Drosophila*, Rpd3 is the ortholog for both HDAC1 and HDAC2. Inactivation of Rpd3 leads to apoptosis due to increased JNK activity and decreased Hippo signaling. Sin3A is a key component of the Rpd3-containing Sin3 complex and inhibition of either Rpd3 or Sin3a leads to apoptosis in *Drosophila* epithelial cells<sup>29</sup>. In mammals, the SIN3-HDAC complex represses CDKN1A which enables cell cycle progression. Loss of Sin3a in embryonic lung epithelial progenitor cells leads to upregulation of CDKN1A and permanent cell cycle arrest in G1<sup>30</sup>. In sum, loss of IFRD1 and SIN3A complex may lead to increased CDKN1A and cell cycle arrest.

Sin3 was originally isolated as a negative regulator of transcription in budding yeast (*Saccharomyces cerevisiae*). There is, however, no ortholog of IFRD1 in *S. cerevisiae*, but IFRD1 does emerge in *Saccharomyces pombe*. Both *S. pombe* and *S. cerevisiae* share genes with higher eukaryotes that they do not share with each other. For example, *S. pombe* has RNAi machinery genes like those in vertebrates, while this is missing from *S. cerevisiae*<sup>31</sup>. *S. cerevisiae* also has greatly simplified heterochromatin compared to *S. pombe*. Conversely, *S.*

*cerevisiae* has well-developed peroxisomes, while *S. pombe* does not. *S. cerevisiae* is in the G1 phase of the cell cycle for an extended period (as a consequence, G1-S transition is tightly controlled), while *S. pombe* remains in the G2 phase of the cell cycle for an extended period (as a consequence, G2-M transition is under tight control)<sup>32</sup>. Therefore, we would predict that IFRD1 has emerged as a chromatin modifier that interacts with SIN3 to regulate transcription programs required for G2-M transition higher eukaryotes.

### **IFRD1 is implicated in numerous cellular signaling pathways**

IFRD1 has been implicated in large number of cellular signaling pathways. The function of Sin3a in the cell cycle is a result of its regulation of its regulation STAT transcription activity<sup>33</sup>. IFRD1 has also been linked to fatty acid synthesis. Long chain acyl-CoA synthetases (ACSL) catalyze long-chain fatty acids (FA) conversion to acyl-CoAs<sup>34</sup>. Inactivation of ACSL1 in mouse hearts (*Acs11H*<sup>-/-</sup>) impaired FA oxidation and dramatically increased glucose uptake, glucose oxidation, and mTOR activation. The heightened cellular stress observed in *Acs11H*<sup>-/-</sup> mice resulted in increased *Atf3* and *Ifrd1* expression<sup>34</sup>. In keratinocytes treated with human papillomavirus, *Ifrd1* expression is significantly downregulated following inhibition of mTOR (rapamycin) or MAPK (MEK1- PD98059 and RAF- GW5074) pathways<sup>35</sup>. *Ifrd1* deficiency led to increased acetylation of p65 at residues K122 and K123, repressing NF-κB transcriptional activity<sup>36</sup>. PGC-1a which is an important cellular metabolic regulator is controlled by IFRD1 in adipocytes<sup>37</sup>. In osteoblasts, IFRD1 negatively regulates BMP-2, which is part of the TGF-β/SMAD and hedgehog pathways in development<sup>38</sup>. Lastly, IFRD1 has been predicted to downregulate B-catenin/Tcf4 transcriptional activity via its histone deacetylase activity<sup>39</sup>. All of these pathways play a role in injury response, progenitor activity or cell cycle re-entry following injury in our tissue models. The implication of IFRD1 in various cellular signaling pathways

increases its capacity to integrate the stress response in diverse cellular types and in different contexts.

### **IFRD1, ribosomes and nucleolar stress**

During the first stage of paligenosis, autodegradative machinery is upregulated in order to degrade mature zymogenic cell features such as secretory granules and rough ER. This degradation results in the release of free ribosomes. As the injury begins to resolve and metaplastic cells prepare to enter the cell cycle, ribosomal function needs to be restored and new ribosomes need to be generated. Ribosomes are composed of ribosomal proteins and ribosomal RNAs, which are synthesized in the nucleolus. Ribosomal RNA synthesis is regulated RAPTOR, an adaptor protein required for mTORC1 function<sup>40</sup>. The nucleolus is the largest structure within the nucleus and its primary function is to assemble ribosomes. CORD, a tool to identify coordinately expressed genes, reveals that *Ddx21* is one of the highest co-regulated genes that is co-regulated with *Ifrd1*. DDX21 is a key mediator of nucleolar ribosome biogenesis<sup>41</sup>. DDX21 associates with Pol I- and Pol II-transcribed genes and with diverse species of RNA. DDX21 occupies the transcribed rDNA locus, directly contacts both rRNA and snoRNAs, and promotes rRNA transcription, processing and modification<sup>41</sup>. In the nucleoplasm, DDX21 binds 7SK RNA and, as a component of the 7SK small nuclear ribonucleoprotein (snRNP) complex, is recruited to the promoters of Pol II-transcribed genes encoding ribosomal proteins and snoRNAs<sup>41</sup>.

Plasma cells are lymphocytes that secrete large amounts of Immunoglobulins. To achieve this, plasma cells expand their ER via continuous ER stress and activation of the Unfolded Protein Response (UPR). This ER stress must be delicately managed in order to not induce

apoptosis. Activating transcription factor 4 (ATF4), a predicted upstream regulator of IFRD1, is induced following LPS-induced ER stress in plasma cells. High levels of apoptosis was observed in cells that were engineered with overactive mTOR in the presence of ER stress<sup>42</sup>. This suggests, that protein synthesis in plasma cells is controlled by an ER stress-mediated mTOR regulation, which is needed for optimal cell viability<sup>42</sup>.

Tunicamycin is a drug used to experimentally induce the UPR, following treatment with Tunicamycin in erythroid progenitors, increased ribosome density is observed on *Ifrd1* transcripts<sup>43</sup>. Plasma cells are also the source of multiple myelomas and inactivation of histone methyltransferases in multiple myelomas increases *Ifrd1* (GEO dataset: GSE57863). During myogenesis, IFRD1 has been implicated in the induction histone-modifying enzymes<sup>44</sup>. Together, these data suggest that, in cells with high secretory activity (and ribosomes), like plasma cells, IFRD1 may help manage survival in stress conditions and function in global gene expression patterns via chromatin modification.

The regulation of translation factor eIF2 is also important in metaplasia-inducing stress. Phosphorylation of alpha unit of eIF2 results in the loss of its availability, but an increase in the translation of specific transcripts like *Atf3/4* and *Ifrd1*<sup>42</sup>. Several different serine kinases target eIF2- $\alpha$  in the presence of stresses like amino acid starvation (GCN2), the presence of dsRNA (PKR) or ER stress (PERK)<sup>45</sup>. The manner in which ribosomes, ER stress and the UPR influence human diseases hinges on TP53 (p53). The literature shows that ribosomes and nucleolar activity are key for the stabilization of p53<sup>46</sup>. There is also a close interconnection between ribosome biogenesis and cell proliferation. Further, we know that factors that stimulate cell proliferation also stimulate ribosome production while the ribosome biogenesis rate control cell cycle

progression<sup>46</sup>. p53 protein plays an important balancing role between ribosome biogenesis rate and progression through the cell cycle phases. The perturbation of ribosome biogenesis stabilizes and activates p53, resulting in cell cycle arrest and/or the transcription of pro-apoptotic genes<sup>46</sup>. The destabilization of ribosome biogenesis, or, potentially, through the mismatch of ribosomal proteins and ribosomal RNAs would result in the stabilization of p53 (Figure 5). As cells proceed through the paligenosis program, p53 could interfere, driving the cells toward quiescence or apoptosis.

### **IFRD1 and p53**

p53 is considered a master guardian of the genome and, like IFRD1, regulates diverse cellular pathways. The canonical function of p53 as a tumor suppressor is to mediate cell cycle arrest, apoptosis and the activation of DNA damage repair. p53 is known to repress target genes via multiple mechanisms, including by recruiting the Sin3/HDAC1/2 chromatin remodeling complex. SIN3 proteins (SIN3A and SIN3B) regulate gene expression at the chromatin level by serving as an anchor onto which the core Sin3/HDAC complex is assembled. There is a direct protein-protein interaction between the SIN3 complex and p53<sup>47</sup>. This suggests that IFRD1 and P53 may interact with each other and that IFRD1 may directly or indirectly regulate the cell cycle or apoptosis function of p53. Preliminary co-immunoprecipitation data from our lab also suggests that there is a physical interaction between IFRD1 and p53.

The role of p53, when activated upon DNA damage sensing is to prevent progress through cell cycle checkpoints and potentially activate apoptosis. We also know that p53 is mutated in countless adult tumors. Given the potential relationship between IFRD1 and p53, we would theorize that during paligenosis IFRD1 which would prevent p53 from acting prematurely (i.e. giving a cell the “all clear” signal to progress through the cell cycle following acute, but

manageable injury). However, a defect in IFRD1 function may instead result in reduced proliferation (and tumorigenesis in cancers) if associated with normal p53 or a much more devastating result in the presence of mutated P53.

## **Chapter 1.4 Paligenosis and GI Disease**

The process of undergoing paligenosis on its own could pose a pathological risk. The genetic changes that we observe during paligenosis (chromatin remodeling to re-express progenitor and proliferation associated genes) may expose differentiated cells to increased risk for mutation. A single mutation in a constitutively active stem cell is generally not thought to be harmful because that allele would be lost through differentiation to a daughter cell or through genetic drift. Long-lived differentiated cells, on the other hand, can harbor old mutations which can be revealed through activation of the paligenosis program in response to injury.

Differentiated cells can acquire mutations in tumor suppressors or activating mutations, like dominant-negative G12D KRAS, which are generally harmless, unless the cells undergo paligenosis. Thus, differentiated cells have become good candidates for cells of origin for cancers and, in particular, GI adenocarcinomas<sup>48</sup>. Pancreatic and gastric adenocarcinomas are often composed of cells which share morphology with differentiated, secretory cells of each organ. In the following sections, I will describe the potential impact of paligenosis on pancreatic and gastric cancer research.

### **Modeling Paligenosis in the pancreas**

Injury or inflammation can cause pancreatic acinar cells to reverse their post-mitotic, differentiated cell state. Acinar cells acquire morphological and molecular characteristics that are a hybrid between mature acinar cells and duct epithelial cells, which are the cells that link the

pancreatic ducts and facilitate the transport of secreted digestive enzymes to the duodenum. Historically, pathological analysis of ADM suggested that injury-induced duct complexes arose from the proliferation of ducts themselves, due to the organization of the ducts into tubules. Following the emergence of genetic lineage-tracing, it has become clear that proliferative, tubular, duct-like cells primarily arise from mature acinar cells, which account for more than 90% of the adult pancreas<sup>49-53</sup>. Thus, these lesions have been termed Acinar-to-Ductal Metaplasia (ADM). ADM is not the complete conversion of acinar cells to duct cells because these metaplastic cells maintain characteristics of mature acinar cells (digestive enzymes like amylase or carboxypeptidase 1) and those of mature duct cells (cytokeratin 19, Carbonic Anhydrase II, and Mucins 1 and 6)<sup>49</sup>. In mice, pancreatitis and ADM can be induced via drug administration or surgical resection<sup>54</sup>.

Prior to my joining the Mills lab, the primary focus was on the metaplastic changes in the gastric epithelium. However, as described above Mills and Samson 2015, there was a belief that pancreas and stomach may share a common program to dedifferentiate and repair injury. A review of the literature led to the utilization of cerulein which is the most commonly used method to induce ADM experimentally. Cerulein is a cholecystokinin (CCK) analog that induces hypersecretion of acinar secretory granules. High doses of intraperitoneally injected cerulein initially results in pancreatitis due to the damage associated with the inappropriate exocytosis of digestive enzymes and the direct induction of pro-inflammatory cytokines<sup>55</sup>. Another experimental model of ADM is through direct tissue injury by pancreatic duct ligation (PDL). This method involves the suturing of a pancreatic lobe, resulting in a blockade of digestive enzyme flow into the intestine and significant tissue injury and inflammation in the surgically affected lobe<sup>56</sup>. In each experimental model of ADM, it is known that inflammatory cells, are

critical for the progression to metaplasia<sup>56,57</sup>. However, the manner in which cells sense damage and which upstream signals induce acinar cells to dedifferentiate have not been elucidated.

Pathological studies of the pancreas show that ADM is a precursor to pre-cancerous lesions like pancreatic intraepithelial neoplasia (PanIN)<sup>58</sup>. Lineage tracing shows that mutations in key regulatory genes can result in PanIN lesions progressing to pancreatic ductal adenocarcinoma (PDAC)<sup>59,60</sup>. In contrast to gastric adenocarcinoma, models of pancreatic cancer in mice show that pancreatic acinar cells progress from pancreatitis to metastasis in a similar way to how it occurs in humans.

### **Paligenosis from ADM to Pancreatic Ductal Adenocarcinoma (PDAC)**

Pancreatic ductal adenocarcinoma is the fourth leading cause of cancer death in the United States and is projected to be the second by 2020<sup>61</sup>. The overall 5-year survival of PDAC is 7%<sup>61</sup>. The extremely poor prognosis of PDAC highlights the urgent need to understand and target the molecular aberrations that drive this disease. Pancreatic intraepithelial neoplasias (PanINs) are the most critical type of PDAC precursors. Tumorigenesis has been described as a stepwise progression from low-grade PanINs to high-grade PanINs and then to invasive adenocarcinoma<sup>62</sup>. Chronic pancreatitis is a significant risk factor for developing PDAC<sup>59,63,64</sup>.

The genetic events that drive pancreatic intraepithelial neoplasia (PanIN) formation and progression to PDAC are well known and have been validated in multiple mouse models. These involve mutations in tumor suppressor genes like *CDKN2A*, *TP53* and *SMAD4*, as well as activation of the *KRAS* oncogene<sup>65-67</sup>. To progress from ADM to PanIN and pancreatic cancer, the activities of endogenous and mutant alleles of *KRAS* are increased<sup>58,68</sup>. During the process of cancer initiation, crosstalk between acinar cells with *KRAS* mutations and inflammatory

macrophages contributes to ADM and formation of early lesions<sup>69</sup>. However, during progression to PDAC, the tumor microenvironment becomes immunosuppressive with a predominance of myeloid-derived suppressor cells and regulatory T cells<sup>70</sup>. Several studies have shown that inducing expression of constitutively active KRASG12D induces dedifferentiation and turning it off results in redifferentiation back the acinar state<sup>71</sup>. It should be noted that active KRAS is not sufficient to induce dedifferentiation, as injury or inflammation must also occur<sup>59,72</sup>. After dedifferentiation, KRAS, as well as multiple steps in the canonical Ras pathway, have been shown to be necessary and sufficient to promote and maintain the ADM state<sup>58,73,74</sup>. Upstream of KRAS, EGF or TGF $\alpha$  signaling and the key downstream mediator of the KRAS signal is Mitogen activated protein kinase 1 and 2 (MAPK1 and MAPK2; aka MEK1/2) upstream of extracellular signal-regulated kinase 1 and 2 (ERK1/1)<sup>53,58,75</sup>. Inhibitors at each stage can block or reverse ADM: Erlotinib and Cetuximab block EGFR interaction with its ligands, PD153035 blocks signaling from the EGFR, and the MEK inhibitors BAY 86–9766, PD325901, and U0126<sup>53,76-78</sup>.

Other important signaling pathways have been implicated in dedifferentiation and progression to PDAC including Hedgehog, Wnt, Akt-PTEM, Notch and TGF-B. A more recently described, non-KRAS pathway sufficient to induce ADM is the Hippo pathway. Induction of nuclear YAP1 activity (decreased signaling through the Hippo pathway) in adult mice is sufficient to cause ADM without affecting KRAS<sup>79</sup>. Together, these studies highlight the vast number signaling pathways involved in pancreatic cancer development and their impact on the initiation, maintenance and progression of oncogenic activity in pancreatic acinar cells.

## **Modeling Paligenosis in the Stomach**

An aspect of chief cell metaplasia that is arguably clearer than ADM is the cellular trigger that induces reprogramming. In the stomach, death of another key functional secretory cell, the acid-secreting parietal cell, causes loss of normal chief cell differentiation<sup>80-82</sup>. Loss or injury of parietal cells causes chief cells to downscale their large secretory granules containing digestive enzymes like Pepsinogen C and Carboxypeptidase B and re-express markers of mucous neck cells (which are the precursors of chief cells in adult stomachs), like TFF2 (Spasmolytic polypeptide), MUC6, the epitope for the lectin GS-II, and, in mice, Gastrokine 3<sup>80,82-88</sup>. The number of tools used to study the underlying mechanisms of SPEM in mice have increased over the last decade. The administration of chemicals like Tamoxifen or DMP-777 or treatment with the infectious bacterium *Helicobacter pylori* have recently been utilized to rapidly induce SPEM in animal models of gastric dysplasia<sup>89-91</sup>. The Mills lab originally contributed to this work by identifying that treatment with high doses of Tamoxifen can induce SPEM<sup>89</sup>. In humans, chief cells reprogram most frequently in the setting of infection by the bacterium *H. pylori*, especially in certain populations (e.g., in East Asians and in regions of Central and South Americans). In those populations, in particular, bacteria cause widespread parietal atrophy and chief cell metaplasia. More recently, the lab has generated a tool to directly target and kill Parietal Cells to test the sufficiency of parietal cell loss for SPEM initiation<sup>92</sup>. Work by our lab and others has clearly shown that chief cells reprogram to SPEM cells, however, there are no animal models of gastric cancer that resemble human adenocarcinoma in terms of morphology, invasion and metastasis.

## **Paligenosis from SPEM to Gastric Cancer**

The molecular mechanisms underlying how chief cells become metaplastic are just now starting to be elucidated<sup>1,80,83,93</sup>. The healthy stomach is subjected to daily chemical and microbial injuries, but manages to maintain epithelial integrity<sup>94</sup>. Studies have highlighted the epithelial plasticity of the gastric corpus, in particular, the ability of postmitotic zymogenic chief cells to re-enter the cell cycle and fuel the repair of injured epithelium. Plasticity of the gastric epithelium enables the stomach to withstand significant injury but could also increase the risk for developing gastric cancer. The glandular injury response is represented by the dedifferentiation of zymogenic cells when acid production is compromised or lost (oxyntic atrophy). This pattern of injury response has been termed SPEM and it is defined by the existence of cells deep in the gastric gland that co-express proteins such as chief cell progenitor marker TFF2 (spasmolytic peptide) and mature chief cell markers like pepsinogen (digestive enzyme). The lab of Dr. Jim Goldenring has identified many genes whose expression is increased specifically in SPEM: *Mal2*, *Wfdc2* (He4), *Tacc3*, *Mcm3*<sup>95,96</sup>. Most gastric cell and developmental biology research is done under the assumption that the loss of parietal cells and mature chief cells in the corpus is required for the development of gastric adenocarcinoma<sup>97</sup>.

Gastric Cancer, which consists predominantly of adenocarcinomas, is the fifth most common cancer globally, and third leading cause of cancer deaths in 2012<sup>98</sup>. As described earlier in section 1.4.1 studies in pancreatic models of tumorigenesis indicate that certain oncogenic mutations, such as constitutively active *KRAS*, do not have an effect in differentiated cells but can be unmasked when they are expressed in proliferating (metaplastic) cells. In the stomach, if mutations do not block re-differentiation as the gland recovers from injury, these mutations can be harbored in quiescent, seemingly normal differentiated chief cells. As in pancreatic ADM, the

initiation of SPEM (and/or parietal cell loss) is influenced by major signaling events including Notch, sonic hedgehog, gastrin, in the epithelium, as well as, immune factors like IFN $\gamma$ , IL-1B, and IL-33<sup>82,99-102</sup>. Global deletion of Amphiregulin, a gene encoding an EGFR ligand, causes spontaneous reprogramming and metaplasia of chief cells as they age<sup>103</sup>. A pERK $\rightarrow$ CD44 $\rightarrow$ pSTAT3 signaling pathway was identified as being key to parietal cell-damage-induced proliferation during metaplasia, suggesting pERK signaling in stomach may parallel the pancreas<sup>104</sup>.

There is a strong epidemiological link between chronic inflammation (pan-gastritis) and metaplasia in the gastric corpus, which has increased the clinical relevance of SPEM in relation to gastric cancer development<sup>105</sup>. There is, however, a disconnect between the location of glandular injury and the anatomical location of gastric tumors. The majority of human gastric adenocarcinomas seem to arise within the antrum or at the corpus–antrum transition, suggesting that parietal or chief cell loss and metaplasia are simply surrogate markers for the overall state of chronic inflammation in the stomach<sup>106-108</sup>. Inflammation is key to the reprogramming of gastric chief cells, but it is still unknown whether metaplastic cells are the origin of gastric cancer<sup>109</sup>. Most of the pathology literature related to gastric cancer focuses on gastric intestinal metaplasia (IM), a precursor lesion to gastric adenocarcinoma. Like SPEM, gastric IM emerges after the development of oxyntic atrophy<sup>97</sup>. Compared with SPEM, however, the cellular origin of intestinal metaplasia is less understood, largely due to a lack of adequate animal models. It remains to be seen whether SPEM gives rise to intestinal metaplasia or whether the two precursor lesions can independently give rise to gastric adenocarcinoma. It has, however, become more evident that the zymogenic chief cell plays a crucial role in the initiation of SPEM and in repairing glandular injury<sup>110</sup>.

In a clear parallel to ADM in the pancreas, MIST1 is also one of the first genes decreased during reprogramming of chief cells<sup>111,112</sup>. Mist1 (bhlha15) is a basic helix-loop-helix transcription factor that is required for the establishment and maintenance of mature secretory cells in the stomach and pancreas. Interestingly, the upregulation of *Ifrd1* that is observed following cerulein treatment in the pancreas is blocked in cells lacking MIST1 (GEO Dataset: GSE3644). This suggests that there may be a dependence of IFRD1 function on proper differentiation in the mature secretory cells that undergo paligenosis.

### **Chapter 1.5 Summary**

In summary, we describe a process by which terminally differentiated cells change their cellular state in order to repair injury. We generated the term paligenosis to describe this process as a shared and conserved basic cellular program and its role in the development of human diseases in the pancreas and stomach. Since paligenosis is a shared and conserved program, we hypothesized that there would be genes that specifically evolved to regulate this process. Through an *in silico* screen of genes that were upregulated during the acute injury phase in numerous diverse tissues, we identified *Ifrd1* as such a gene. IFRD1 is highly conserved, responsive to diverse cellular stimuli and has already been shown to be required for induced proliferation of intestinal cells after resection. We found IFRD1 to be associated with foundational cellular biology proteins like SIN3, p53 and mTOR and we also show that it is associated with cellular processes like ER stress and ribosome biogenesis. Together, our investigations show that IFRD1 may play an important role in differentiated cells that is required to evoke a change in cellular state to respond to injury.

Chapter 1.6 FIGURES

Figure 1.1

A

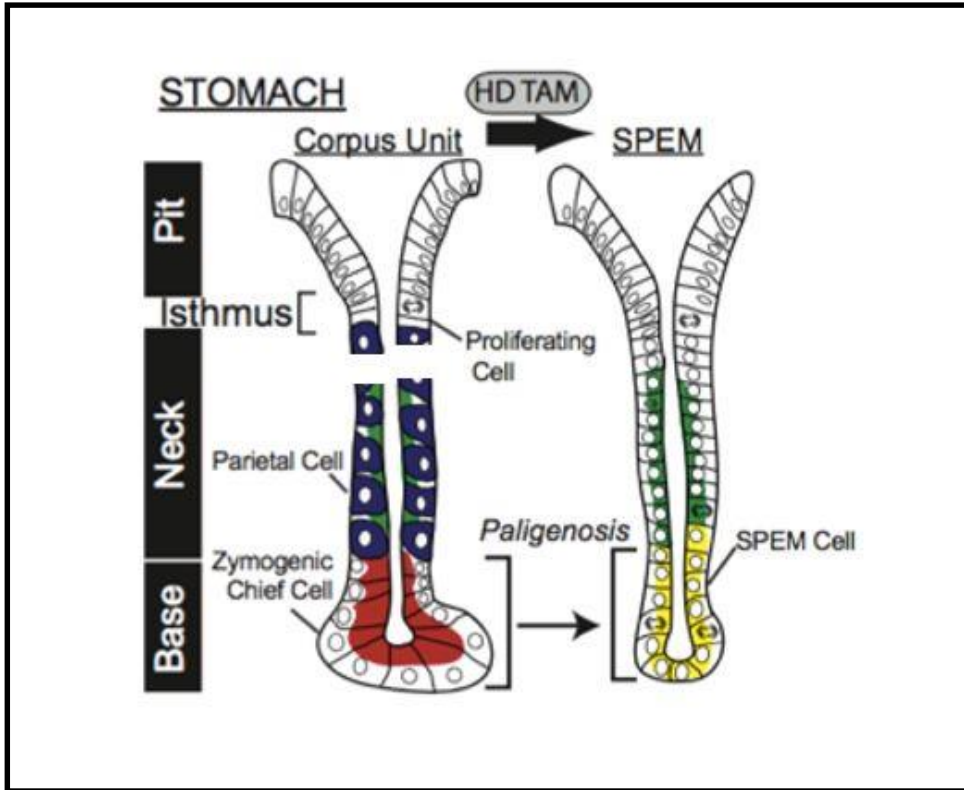


**Figure 1.1A.** Schematic representation of the cellular changes that occur during SPEM.

Zymogenic chief cells (RED) arise from mucous neck cells (GREEN). Following metaplasia inducing injuries like high doses of tamoxifen (HDTAM), DMP-777, or *Helicobacter pylori* infection leads to the cellular changes associated with SPEM. The SPEM cell (YELLOW) is a hybrid cellular state between the mucous neck cell and the terminally differentiated zymogenic chief cell.

**Figure 1.1**

**B**

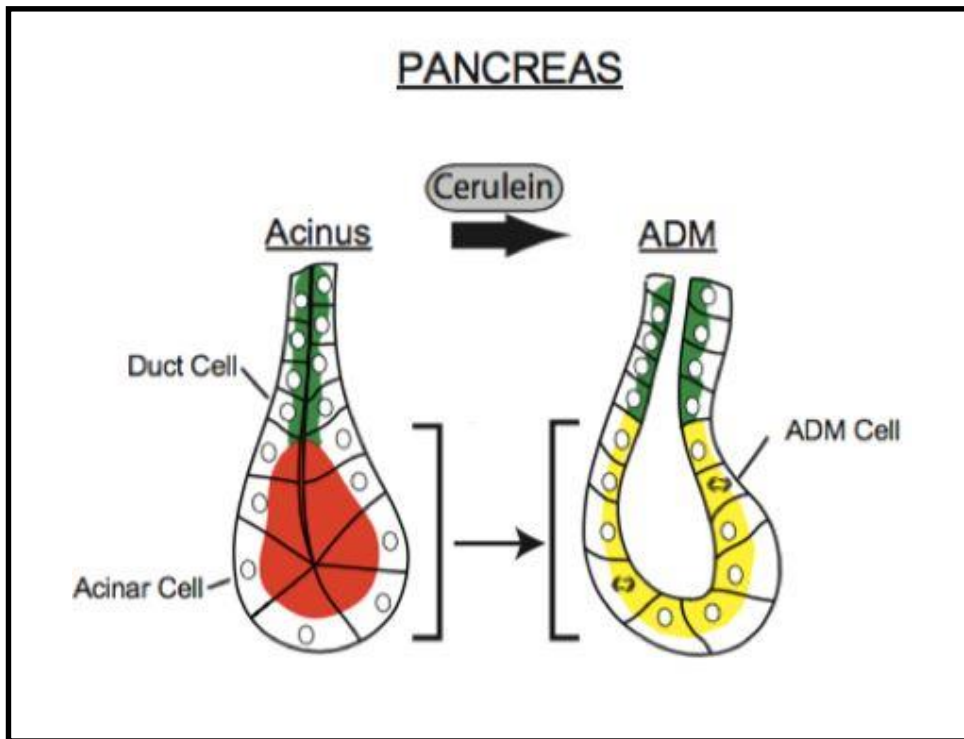


**Figure 1B.** Schematic representation of the cellular changes that occur during ADM. Pancreatic acinar cells (RED) arise from pancreatic duct cells (GREEN). Following metaplasia inducing injuries like pancreatic duct ligation or repeated doses of CCK-analog leads to the cellular changes associated with ADM. The ADM cell (YELLOW) is a hybrid cellular state between the pancreatic duct cell and the terminally differentiated pancreatic acinar cell.

**Figure 1.2**

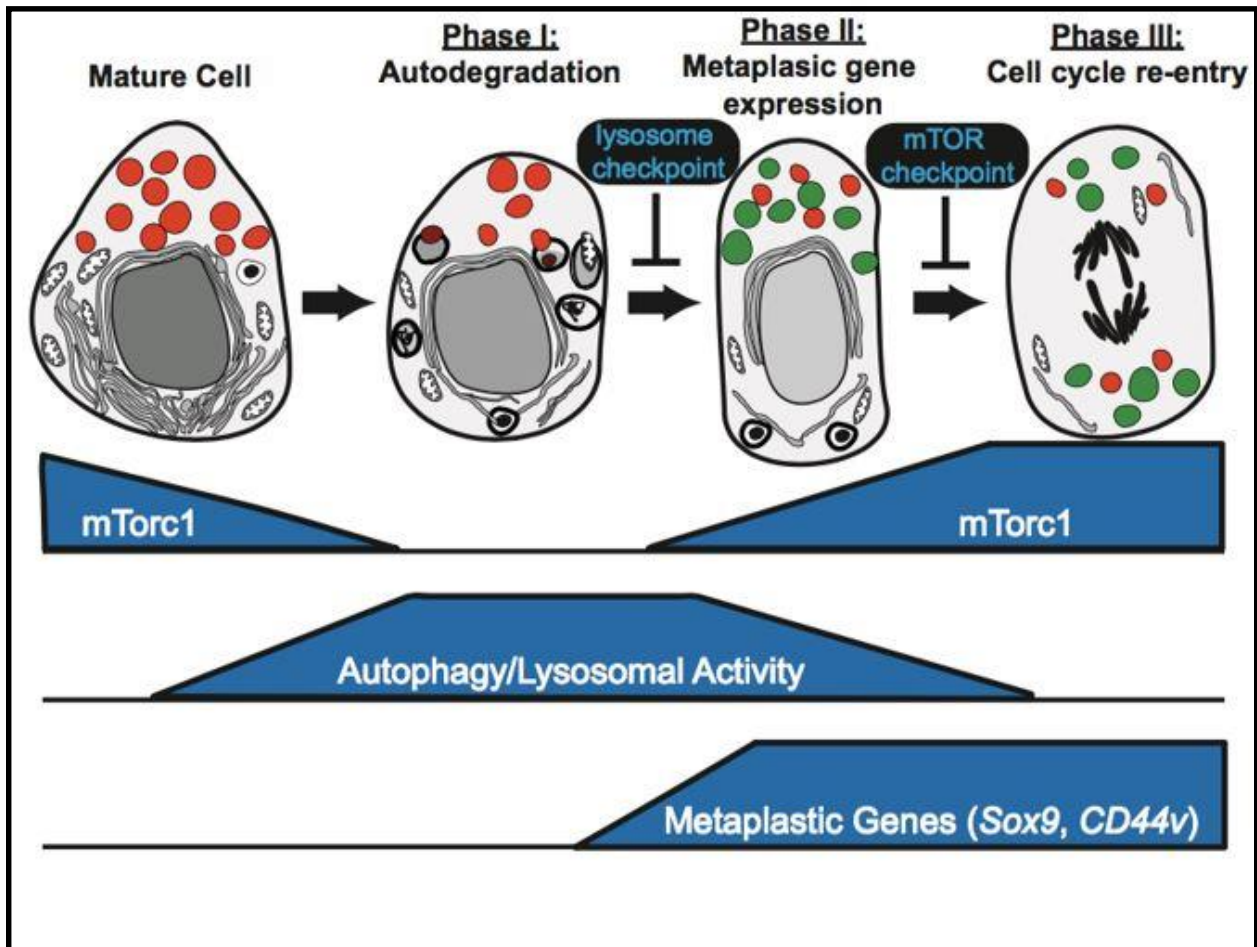


**Figure 1.2.** Schematic representation of the cellular and molecular changes that occur during Paligenesis. Paligenesis describes the process by which terminally differentiated cells can alter their cellular state to repair injury. We originally detail this process in the stomach in pancreas to include 3 steps: 1) upregulation of autophagic machinery, 2) expression of a metaplastic gene program and 3) re-entry into the cell cycle. This process is governed by mTORC1 which is a fundamental cellular energy sensor that controls translation.

**Figure 1.3**

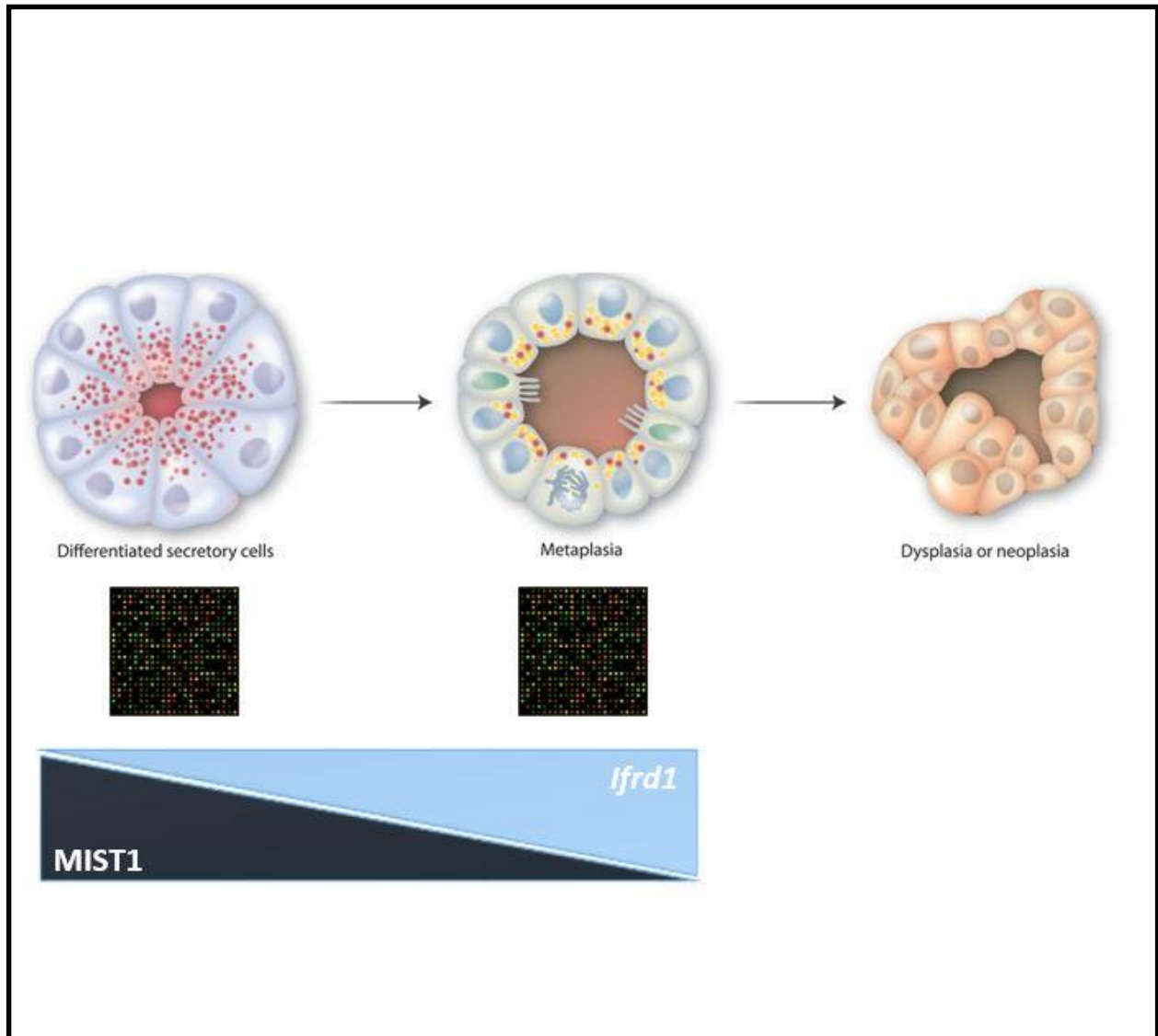


**Figure 1.3.** Schematic representation of the in silico screen used to identify IFRD1 as a gene that is important in the paligenosis process. I compared RNA expression in gene lists from gastric chief and pancreatic acinar cells at homeostasis to SPEM and ADM cells, respectively. *Ifrd1* was one of the few genes upregulated in both the pancreas and stomach during the acute injury response *en route* to metaplasia.

**Figure 1.4**

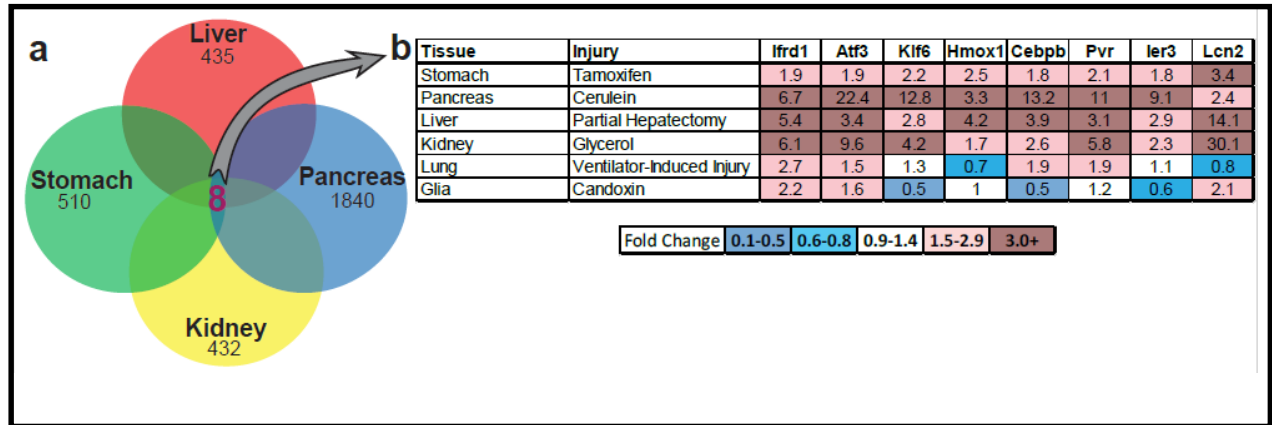


**Figure 4.** Representation of the in silico screen to identify genes that are important for paligenosis in multiple organs. a: Eight genes are upregulated in the pancreas, stomach, liver and kidney during the acute injury phase. These 4 tissues represent those that we have evidence for a paligenotic injury response. b: Expanded list of tissues that we hypothesize would also employ paligenosis to repair injury, due to the characteristics of dedifferentiation in both lung and glial cells. Atf3 and Ifrd1 are the only two genes to exhibit consistent upregulation during the acute injury phase in all 6 injury models.

**Figure 1.5**

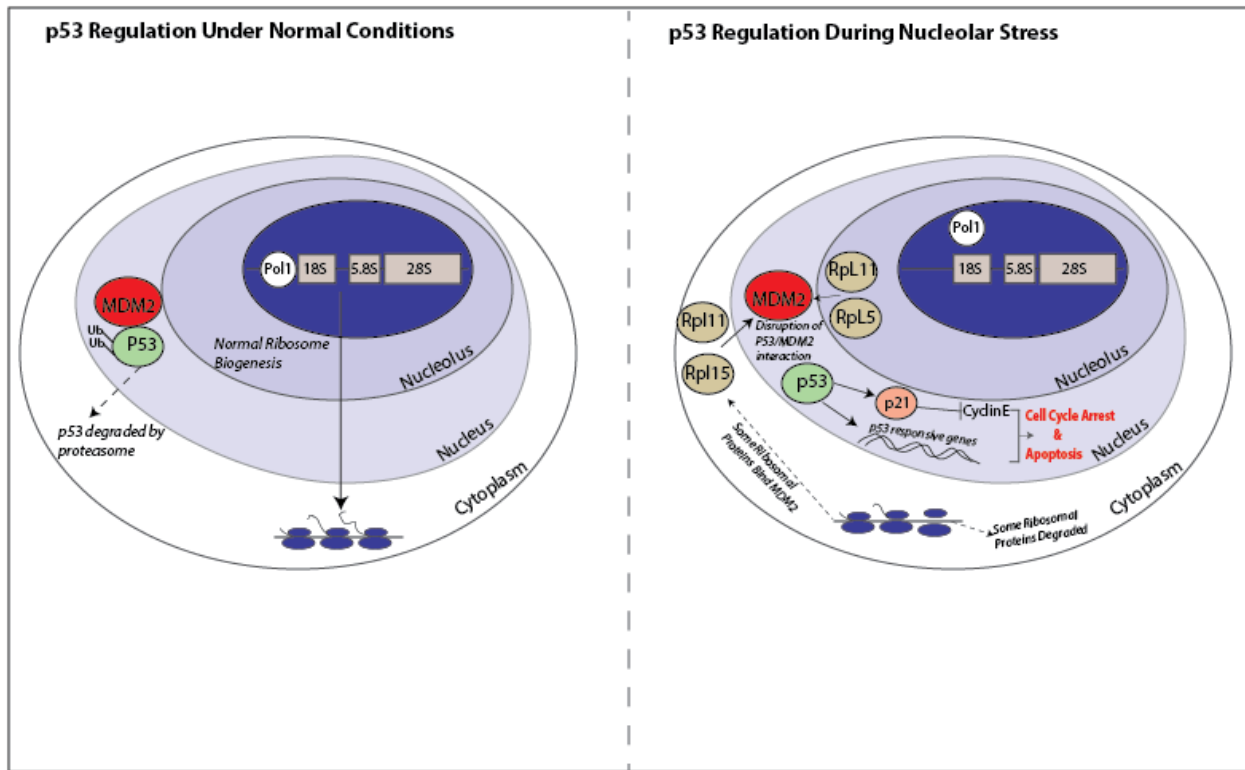


**Figure 5.** Schematic representation of the relationship between ribosomal/nucleolar stress and P53 expression and stabilization. Left: At homeostasis, p53 is bound by MDM2 and targeted for degradation through ubiquitination. Normal ribosomogenesis occurs. Right: During stress, there can be an imbalance between ribosomal RNAs and ribosomal proteins which can lead to an interaction between ribosomal proteins and MDM2. This results in the stabilization of p53 and transcription of p53 genes associated with cell cycle arrest and apoptosis.

## Chapter 1.7 REFERENCES

- 1 Nozaki, K. *et al.* A molecular signature of gastric metaplasia arising in response to acute parietal cell loss. *Gastroenterology* **134**, 511-522, doi:10.1053/j.gastro.2007.11.058 (2008).
- 2 Storz, P. Acinar cell plasticity and development of pancreatic ductal adenocarcinoma. *Nature reviews. Gastroenterology & hepatology* **14**, 296-304, doi:10.1038/nrgastro.2017.12 (2017).
- 3 Mills, J. C. & Sansom, O. J. Reserve stem cells: Differentiated cells reprogram to fuel repair, metaplasia, and neoplasia in the adult gastrointestinal tract. *Science signaling* **8**, re8-re8, doi:10.1126/scisignal.aaa7540 (2015).
- 4 Kerr, J. F., Wyllie, A. H. & Currie, A. R. Apoptosis: a basic biological phenomenon with wide-ranging implications in tissue kinetics. *British journal of cancer* **26**, 239-257 (1972).
- 5 Kerr, J. F. R. History of the events leading to the formulation of the apoptosis concept. *Toxicology* **181-182**, 471-474, doi:[https://doi.org/10.1016/S0300-483X\(02\)00457-2](https://doi.org/10.1016/S0300-483X(02)00457-2) (2002).
- 6 Paweletz, N. Walther Flemming: pioneer of mitosis research. *Nature Reviews Molecular Cell Biology* **2**, 72, doi:10.1038/35048077 (2001).
- 7 Elmore, S. Apoptosis: a review of programmed cell death. *Toxicologic pathology* **35**, 495-516, doi:10.1080/01926230701320337 (2007).
- 8 Shaham, S., Reddien, P. W., Davies, B. & Horvitz, H. R. Mutational analysis of the *Caenorhabditis elegans* cell-death gene *ced-3*. *Genetics* **153**, 1655-1671 (1999).
- 9 Trent, C., Tsuing, N. & Horvitz, H. R. Egg-laying defective mutants of the nematode *Caenorhabditis elegans*. *Genetics* **104**, 619-647 (1983).
- 10 Ellis, H. M. & Horvitz, H. R. Genetic control of programmed cell death in the nematode *C. elegans*. *Cell* **44**, 817-829, doi:[https://doi.org/10.1016/0092-8674\(86\)90004-8](https://doi.org/10.1016/0092-8674(86)90004-8) (1986).
- 11 Ellis, R. E., Jacobson, D. M. & Horvitz, H. R. Genes required for the engulfment of cell corpses during programmed cell death in *Caenorhabditis elegans*. *Genetics* **129**, 79-94 (1991).
- 12 Hengartner, M. O., Ellis, R. & Horvitz, R. *Caenorhabditis elegans* gene *ced-9* protects cells from programmed cell death. *Nature* **356**, 494, doi:10.1038/356494a0 (1992).
- 13 Hengartner, M. O. & Horvitz, H. R. Activation of *C. elegans* cell death protein CED-9 by an ammo-acid substitution in a domain conserved in Bcl-2. *Nature* **369**, 318, doi:10.1038/369318a0 (1994).

- 14 Xue, D., Shaham, S. & Horvitz, H. R. The *Caenorhabditis elegans* cell-death protein CED-3 is a cysteine protease with substrate specificities similar to those of the human CPP32 protease. *Genes & Development* **10**, 1073-1083 (1996).
- 15 Yuan, J., Shaham, S., Ledoux, S., Ellis, H. M. & Horvitz, H. R. The *C. elegans* cell death gene *ced-3* encodes a protein similar to mammalian interleukin-1 $\beta$ -converting enzyme. *Cell* **75**, 641-652, doi:[https://doi.org/10.1016/0092-8674\(93\)90485-9](https://doi.org/10.1016/0092-8674(93)90485-9) (1993).
- 16 Spector, M. S., Desnoyers, S., Hoepfner, D. J. & Hengartner, M. O. Interaction between the *C. elegans* cell-death regulators CED-9 and CED-4. *Nature* **385**, 653, doi:10.1038/385653a0 (1997).
- 17 Conradt, B. & Horvitz, H. R. The *C. elegans* Protein EGL-1 Is Required for Programmed Cell Death and Interacts with the Bcl-2-like Protein CED-9. *Cell* **93**, 519-529, doi:[https://doi.org/10.1016/S0092-8674\(00\)81182-4](https://doi.org/10.1016/S0092-8674(00)81182-4) (1998).
- 18 del Peso, L., González, V. c. M. & Núñez, G. *Caenorhabditis elegans* EGL-1 Disrupts the Interaction of CED-9 with CED-4 and Promotes CED-3 Activation. *Journal of Biological Chemistry* **273**, 33495-33500 (1998).
- 19 del Peso, L., Gonzalez, V. M., Inohara, N., Ellis, R. E. & Nunez, G. Disruption of the CED-9/CED-4 Complex by EGL-1 is a Critical Step for Programmed Cell Death in *C. elegans*. *Journal of Biological Chemistry* (2000).
- 20 Garcia, A. M. *et al.* *Tis7* deletion reduces survival and induces intestinal anastomotic inflammation and obstruction in high-fat diet-fed mice with short bowel syndrome. *American journal of physiology. Gastrointestinal and liver physiology* **307**, G642-G654, doi:10.1152/ajpgi.00374.2013 (2014).
- 21 Yu, C. *et al.* Deletion of *Tis7* protects mice from high-fat diet-induced weight gain and blunts the intestinal adaptive response postresection. *The Journal of nutrition* **140**, 1907-1914, doi:10.3945/jn.110.127084 (2010).
- 22 Lin, M. T. *et al.* Bidirectional Connections between Depression and Ataxia Severity in Spinocerebellar Ataxia Type 3 Patients. *European Neurology* **79**, 266-271, doi:10.1159/000489398 (2018).
- 23 Xu, R., Peng, C., Xiao, S. & Zhuang, W. IFRD1 polymorphisms and gastric cancer risk in a Chinese population. *Medical Oncology* **31**, 135, doi:10.1007/s12032-014-0135-0 (2014).
- 24 Wang, Y. *et al.* Targeted Intestinal Overexpression of the Immediate Early Gene *tis7* in Transgenic Mice Increases Triglyceride Absorption and Adiposity. *Journal of Biological Chemistry* **280**, 34764-34775 (2005).
- 25 Bhattacharya, B., Mohd Omar, M. F. & Soong, R. The Warburg effect and drug resistance. *British journal of pharmacology* **173**, 970-979, doi:10.1111/bph.13422 (2016).

- 26 Vietor, I. *et al.* TIS7 interacts with the mammalian SIN3 histone deacetylase complex in epithelial cells. *The EMBO Journal* **21**, 4621, doi:10.1093/emboj/cdf461 (2002).
- 27 Silverstein, R. A. & Ekwall, K. Sin3: a flexible regulator of global gene expression and genome stability. *Current Genetics* **47**, 1-17, doi:10.1007/s00294-004-0541-5 (2005).
- 28 Saunders, A. *et al.* The SIN3A/HDAC Corepressor Complex Functionally Cooperates with NANOG to Promote Pluripotency. *Cell reports* **18**, 1713-1726, doi:10.1016/j.celrep.2017.01.055 (2017).
- 29 Zhang, T., Sheng, Z. & Du, W. Loss of histone deacetylase HDAC1 induces cell death in Drosophila epithelial cells through JNK and Hippo signaling. *Mechanisms of development* **141**, 4-13, doi:10.1016/j.mod.2016.07.001 (2016).
- 30 Yao, C. *et al.* Sin3a regulates epithelial progenitor cell fate during lung development. *Development (Cambridge, England)* **144**, 2618-2628, doi:10.1242/dev.149708 (2017).
- 31 Kehayova, P. D. & Liu, D. R. In Vivo Evolution of an RNA-Based Transcriptional Silencing Domain in *S. cerevisiae*. *Chemistry & Biology* **14**, 65-74, doi:<https://doi.org/10.1016/j.chembiol.2006.11.008> (2007).
- 32 Price, C. M. *et al.* Evolution of CST function in telomere maintenance. *Cell cycle (Georgetown, Tex.)* **9**, 3157-3165, doi:10.4161/cc.9.16.12547 (2010).
- 33 Icardi, L. *et al.* The Sin3a repressor complex is a master regulator of STAT transcriptional activity. *Proceedings of the National Academy of Sciences of the United States of America* **109**, 12058-12063, doi:10.1073/pnas.1206458109 (2012).
- 34 Schisler, J. C. *et al.* Cardiac energy dependence on glucose increases metabolites related to glutathione and activates metabolic genes controlled by mechanistic target of rapamycin. *Journal of the American Heart Association* **4**, e001136, doi:10.1161/JAHA.114.001136 (2015).
- 35 Tummers, B. *et al.* The interferon-related developmental regulator 1 is used by human papillomavirus to suppress NFκB activation. *Nature communications* **6**, 6537-6537, doi:10.1038/ncomms7537 (2015).
- 36 Iezaki, T. *et al.* Transcriptional Modulator Ifrd1 Regulates Osteoclast Differentiation through Enhancing the NF-κB/NFATc1 Pathway. *Molecular and cellular biology* **36**, 2451-2463, doi:10.1128/MCB.01075-15 (2016).
- 37 Park, G. *et al.* The transcriptional modulator Ifrd1 controls PGC-1α expression under short-term adrenergic stimulation in brown adipocytes. *The FEBS Journal* **284**, 784-795, doi:10.1111/febs.14019 (2017).
- 38 Onishi, Y. *et al.* The transcriptional modulator Ifrd1 is a negative regulator of BMP-2-dependent osteoblastogenesis. *Biochemical and Biophysical Research Communications* **482**, 329-334, doi:<https://doi.org/10.1016/j.bbrc.2016.11.063> (2017).

- 39 Vietor, I., Kurzbauer, R., Brosch, G. & Huber, L. A. TIS7 regulation of the beta-catenin/Tcf-4 target gene osteopontin (OPN) is histone deacetylase-dependent. *J Biol Chem* **280**, 39795-39801, doi:10.1074/jbc.M509836200 (2005).
- 40 You, J.-S. *et al.* The role of raptor in the mechanical load-induced regulation of mTOR signaling, protein synthesis, and skeletal muscle hypertrophy. *The FASEB Journal*, fj.201801653RR, doi:10.1096/fj.201801653RR (2018).
- 41 Calo, E. *et al.* RNA helicase DDX21 coordinates transcription and ribosomal RNA processing. *Nature* **518**, 249-253, doi:10.1038/nature13923 (2015).
- 42 Goldfinger, M., Shmuel, M., Benhamron, S. & Tirosh, B. Protein synthesis in plasma cells is regulated by crosstalk between endoplasmic reticulum stress and mTOR signaling. *European Journal of Immunology* **41**, 491-502, doi:10.1002/eji.201040677 (2011).
- 43 Paolini, N. A. *et al.* Ribosome profiling uncovers selective mRNA translation associated with eIF2 phosphorylation in erythroid progenitors. *PloS one* **13**, e0193790-e0193790, doi:10.1371/journal.pone.0193790 (2018).
- 44 Lammirato, A. *et al.* TIS7 induces transcriptional cascade of methylosome components required for muscle differentiation. *BMC biology* **14**, 95-95, doi:10.1186/s12915-016-0318-6 (2016).
- 45 Kimball, S. R. Eukaryotic initiation factor eIF2. *The International Journal of Biochemistry & Cell Biology* **31**, 25-29, doi:[https://doi.org/10.1016/S1357-2725\(98\)00128-9](https://doi.org/10.1016/S1357-2725(98)00128-9) (1999).
- 46 Derenzini, M., Montanaro, L. & Trerè, D. Ribosome biogenesis and cancer. *Acta Histochemica* **119**, 190-197, doi:<https://doi.org/10.1016/j.acthis.2017.01.009> (2017).
- 47 Bansal, N. *et al.* Tumor suppressor protein p53 recruits human Sin3B/HDAC1 complex for down-regulation of its target promoters in response to genotoxic stress. *PloS one* **6**, e26156-e26156, doi:10.1371/journal.pone.0026156 (2011).
- 48 Chaffer, C. L. & Weinberg, R. A. How does multistep tumorigenesis really proceed? *Cancer discovery* **5**, 22-24, doi:10.1158/2159-8290.CD-14-0788 (2015).
- 49 Jensen, J. N. *et al.* Recapitulation of elements of embryonic development in adult mouse pancreatic regeneration. *Gastroenterology* **128**, 728-741, doi:<https://doi.org/10.1053/j.gastro.2004.12.008> (2005).
- 50 Zhu, L., Shi, G., Schmidt, C. M., Hruban, R. H. & Konieczny, S. F. Acinar cells contribute to the molecular heterogeneity of pancreatic intraepithelial neoplasia. *The American journal of pathology* **171**, 263-273, doi:10.2353/ajpath.2007.061176 (2007).
- 51 De La O, J.-P. *et al.* Notch and Kras reprogram pancreatic acinar cells to ductal intraepithelial neoplasia. *Proceedings of the National Academy of Sciences of the United States of America* **105**, 18907-18912, doi:10.1073/pnas.0810111105 (2008).

- 52 Habbe, N. *et al.* Spontaneous induction of murine pancreatic intraepithelial neoplasia (mPanIN) by acinar cell targeting of oncogenic Kras in adult mice. *Proceedings of the National Academy of Sciences of the United States of America* **105**, 18913-18918, doi:10.1073/pnas.0810097105 (2008).
- 53 Shi, G. *et al.* Maintenance of acinar cell organization is critical to preventing Kras-induced acinar-ductal metaplasia. *Oncogene* **32**, 1950-1958, doi:10.1038/onc.2012.210 (2013).
- 54 Hyun, J. J. & Lee, H. S. Experimental models of pancreatitis. *Clinical endoscopy* **47**, 212-216, doi:10.5946/ce.2014.47.3.212 (2014).
- 55 Zaninovic, V., Gukovskaya, A. S., Gukovsky, I., Mouria, M. & Pandol, S. J. Cerulein upregulates ICAM-1 in pancreatic acinar cells, which mediates neutrophil adhesion to these cells. *American Journal of Physiology-Gastrointestinal and Liver Physiology* **279**, G666-G676, doi:10.1152/ajpgi.2000.279.4.G666 (2000).
- 56 Watanabe, S., Abe, K., Anbo, Y. & Katoh, H. *Changes in the Mouse Exocrine Pancreas after Pancreatic Duct Ligation: A Qualitative and Quantitative Histological Study*. Vol. 58 (1995).
- 57 Liou, G.-Y. *et al.* Macrophage-secreted cytokines drive pancreatic acinar-to-ductal metaplasia through NF- $\kappa$ B and MMPs. *The Journal of cell biology* **202**, 563-577, doi:10.1083/jcb.201301001 (2013).
- 58 Shi, G. *et al.* Loss of the acinar-restricted transcription factor Mist1 accelerates Kras-induced pancreatic intraepithelial neoplasia. *Gastroenterology* **136**, 1368-1378, doi:10.1053/j.gastro.2008.12.066 (2009).
- 59 Guerra, C. *et al.* Chronic Pancreatitis Is Essential for Induction of Pancreatic Ductal Adenocarcinoma by K-Ras Oncogenes in Adult Mice. *Cancer Cell* **11**, 291-302, doi:<https://doi.org/10.1016/j.ccr.2007.01.012> (2007).
- 60 Hruban, R. H. *et al.* Pathology of Genetically Engineered Mouse Models of Pancreatic Exocrine Cancer: Consensus Report and Recommendations. *Cancer Research* **66**, 95, doi:10.1158/0008-5472.CAN-05-2168 (2006).
- 61 Rahib, L. *et al.* Projecting Cancer Incidence and Deaths to 2030: The Unexpected Burden of Thyroid, Liver, and Pancreas Cancers in the United States. *Cancer Research* **74**, 2913, doi:10.1158/0008-5472.CAN-14-0155 (2014).
- 62 Distler, M., Aust, D., Weitz, J., Pilarsky, C. & Grützmann, R. Precursor lesions for sporadic pancreatic cancer: PanIN, IPMN, and MCN. *BioMed research international* **2014**, 474905-474905, doi:10.1155/2014/474905 (2014).
- 63 Raimondi, S., Lowenfels, A. B., Morselli-Labate, A. M., Maisonneuve, P. & Pezzilli, R. Pancreatic cancer in chronic pancreatitis; aetiology, incidence, and early detection. *Best Practice & Research Clinical Gastroenterology* **24**, 349-358, doi:<https://doi.org/10.1016/j.bpg.2010.02.007> (2010).

- 64 Morris, J. P. I. V., Cano, D. A., Sekine, S., Wang, S. C. & Hebrok, M.  $\beta$ -catenin blocks Kras-dependent reprogramming of acini into pancreatic cancer precursor lesions in mice. *The Journal of Clinical Investigation* **120**, 508-520, doi:10.1172/JCI40045 (2010).
- 65 Hidalgo, M. Pancreatic Cancer. *New England Journal of Medicine* **362**, 1605-1617, doi:10.1056/NEJMra0901557 (2010).
- 66 Ying, H. *et al.* Genetics and biology of pancreatic ductal adenocarcinoma. *Genes & Development* **30**, 355-385 (2016).
- 67 Ryan, D. P., Hong, T. S. & Bardeesy, N. Pancreatic Adenocarcinoma. *New England Journal of Medicine* **371**, 1039-1049, doi:10.1056/NEJMra1404198 (2014).
- 68 Ji, B. *et al.* Ras Activity Levels Control the Development of Pancreatic Diseases. *Gastroenterology* **137**, 1072-1082.e1076, doi:<https://doi.org/10.1053/j.gastro.2009.05.052> (2009).
- 69 Liou, G.-Y. *et al.* Mutant KRAS–Induced Expression of ICAM-1 in Pancreatic Acinar Cells Causes Attraction of Macrophages to Expedite the Formation of Precancerous Lesions. *Cancer Discovery* **5**, 52, doi:10.1158/2159-8290.CD-14-0474 (2015).
- 70 Clark, C. E., Beatty, G. L. & Vonderheide, R. H. Immunosurveillance of pancreatic adenocarcinoma: Insights from genetically engineered mouse models of cancer. *Cancer Letters* **279**, 1-7, doi:<https://doi.org/10.1016/j.canlet.2008.09.037> (2009).
- 71 Collins, M. A. *et al.* Oncogenic Kras is required for both the initiation and maintenance of pancreatic cancer in mice. *The Journal of Clinical Investigation* **122**, 639-653, doi:10.1172/JCI59227 (2012).
- 72 Huang, H. *et al.* Oncogenic K-Ras requires activation for enhanced activity. *Oncogene* **33**, 532-535, doi:10.1038/onc.2012.619 (2014).
- 73 Jhappan, C. *et al.* TGF $\alpha$  overexpression in transgenic mice induces liver neoplasia and abnormal development of the mammary gland and pancreas. *Cell* **61**, 1137-1146, doi:[https://doi.org/10.1016/0092-8674\(90\)90076-Q](https://doi.org/10.1016/0092-8674(90)90076-Q) (1990).
- 74 Sandgren, E. P., Quaipe, C. J., Paulovich, A. G., Palmiter, R. D. & Brinster, R. L. Pancreatic tumor pathogenesis reflects the causative genetic lesion. *Proceedings of the National Academy of Sciences of the United States of America* **88**, 93-97 (1991).
- 75 Wu, C.-Y. C. *et al.* PI3K regulation of RAC1 is required for KRAS-induced pancreatic tumorigenesis in mice. *Gastroenterology* **147**, 1405-1416.e1407, doi:10.1053/j.gastro.2014.08.032 (2014).
- 76 Ardito, C. M. *et al.* EGF receptor is required for KRAS-induced pancreatic tumorigenesis. *Cancer cell* **22**, 304-317, doi:10.1016/j.ccr.2012.07.024 (2012).
- 77 Houbracken, I. *et al.* Lineage Tracing Evidence for Transdifferentiation of Acinar to Duct Cells and Plasticity of Human Pancreas. *Gastroenterology* **141**, 731-741.e734, doi:<https://doi.org/10.1053/j.gastro.2011.04.050> (2011).

- 78 Collins, M. A., Yan, W., Sebolt-Leopold, J. S. & Pasca di Magliano, M. MAPK signaling is required for dedifferentiation of acinar cells and development of pancreatic intraepithelial neoplasia in mice. *Gastroenterology* **146**, 822-834.e827, doi:10.1053/j.gastro.2013.11.052 (2014).
- 79 Gao, T. *et al.* Hippo Signaling Regulates Differentiation and Maintenance in the Exocrine Pancreas. *Gastroenterology* **144**, 1543-1553.e1541, doi:10.1053/j.gastro.2013.02.037 (2013).
- 80 Bredemeyer, A. J. *et al.* The gastric epithelial progenitor cell niche and differentiation of the zymogenic (chief) cell lineage. *Developmental biology* **325**, 211-224, doi:10.1016/j.ydbio.2008.10.025 (2009).
- 81 Li, Q., Karam, S. M. & Gordon, J. I. Diphtheria Toxin-mediated Ablation of Parietal Cells in the Stomach of Transgenic Mice. *Journal of Biological Chemistry* **271**, 3671-3676 (1996).
- 82 Nomura, S. *et al.* Alterations in gastric mucosal lineages induced by acute oxyntic atrophy in wild-type and gastrin-deficient mice. *American Journal of Physiology-Gastrointestinal and Liver Physiology* **288**, G362-G375, doi:10.1152/ajpgi.00160.2004 (2005).
- 83 Lennerz, J. K. M. *et al.* The transcription factor MIST1 is a novel human gastric chief cell marker whose expression is lost in metaplasia, dysplasia, and carcinoma. *The American journal of pathology* **177**, 1514-1533, doi:10.2353/ajpath.2010.100328 (2010).
- 84 Ramsey, V. G. *et al.* The maturation of mucus-secreting gastric epithelial progenitors into digestive-enzyme secreting zymogenic cells requires *Mist1*. *Development* **134**, 211, doi:10.1242/dev.02700 (2007).
- 85 Karam, S. M. & Leblond, C. P. Dynamics of epithelial cells in the corpus of the mouse stomach. I. Identification of proliferative cell types and pinpointing of the stem cell. *The Anatomical Record* **236**, 259-279, doi:10.1002/ar.1092360202 (1993).
- 86 Hanby, A. M., Poulsom, R., Playford, R. J. & Wright, N. A. The mucous neck cell in the human gastric corpus: a distinctive, functional cell lineage. *The Journal of Pathology* **187**, 331-337, doi:10.1002/(SICI)1096-9896(199902)187:3<331::AID-PATH241>3.0.CO;2-S (1999).
- 87 Menheniott, T. R. *et al.* A Novel Gastrokine, Gkn3, Marks Gastric Atrophy and Shows Evidence of Adaptive Gene Loss in Humans. *Gastroenterology* **138**, 1823-1835, doi:<https://doi.org/10.1053/j.gastro.2010.01.050> (2010).
- 88 Nomura, S. *et al.* Spasmolytic polypeptide expressing metaplasia to preneoplasia in H. felis-infected mice. *Gastroenterology* **127**, 582-594, doi:<https://doi.org/10.1053/j.gastro.2004.05.029> (2004).
- 89 Huh, W. J. *et al.* Tamoxifen induces rapid, reversible atrophy, and metaplasia in mouse stomach. *Gastroenterology* **142**, 21-24.e27, doi:10.1053/j.gastro.2011.09.050 (2012).

- 90 Goldenring, J. R. *et al.* Reversible drug-induced oxyntic atrophy in rats. *Gastroenterology* **118**, 1080-1093, doi:10.1016/S0016-5085(00)70361-1 (2000).
- 91 Yoshizawa, N. *et al.* Emergence of spasmolytic polypeptide-expressing metaplasia in Mongolian gerbils infected with *Helicobacter pylori*. *Laboratory Investigation* **87**, 1265, doi:10.1038/labinvest.3700682 (2007).
- 92 Burclaff, J., Osaki, L. H., Liu, D., Goldenring, J. R. & Mills, J. C. Targeted Apoptosis of Parietal Cells Is Insufficient to Induce Metaplasia in Stomach. *Gastroenterology* **152**, 762-766.e767, doi:10.1053/j.gastro.2016.12.001 (2017).
- 93 Goldenring, J. R., Nam, K. T. & Mills, J. C. The origin of pre-neoplastic metaplasia in the stomach: chief cells emerge from the Mist. *Experimental cell research* **317**, 2759-2764, doi:10.1016/j.yexcr.2011.08.017 (2011).
- 94 Giannella, R. A., Broitman, S. A. & Zamcheck, N. Gastric acid barrier to ingested microorganisms in man: studies in vivo and in vitro. *Gut* **13**, 251-256 (1972).
- 95 Nozaki, K., Weis, V., Wang, T. C., Falus, A. & Goldenring, J. R. Altered gastric chief cell lineage differentiation in histamine-deficient mice. *American journal of physiology. Gastrointestinal and liver physiology* **296**, G1211-G1220, doi:10.1152/ajpgi.90643.2008 (2009).
- 96 Weis, V. G. *et al.* Establishment of novel in vitro mouse chief cell and SPEM cultures identifies MAL2 as a marker of metaplasia in the stomach. *American journal of physiology. Gastrointestinal and liver physiology* **307**, G777-G792, doi:10.1152/ajpgi.00169.2014 (2014).
- 97 Correa, P. & Piazuelo, M. B. The gastric precancerous cascade. *Journal of digestive diseases* **13**, 2-9, doi:10.1111/j.1751-2980.2011.00550.x (2012).
- 98 Ferlay, J. *et al.* Cancer incidence and mortality worldwide: Sources, methods and major patterns in GLOBOCAN 2012. *International Journal of Cancer* **136**, E359-E386, doi:10.1002/ijc.29210 (2015).
- 99 Demitrack, E. S. *et al.* NOTCH1 and NOTCH2 regulate epithelial cell proliferation in mouse and human gastric corpus. *American journal of physiology. Gastrointestinal and liver physiology* **312**, G133-G144, doi:10.1152/ajpgi.00325.2016 (2017).
- 100 Syu, L.-J. *et al.* Transgenic expression of interferon- $\gamma$  in mouse stomach leads to inflammation, metaplasia, and dysplasia. *The American journal of pathology* **181**, 2114-2125, doi:10.1016/j.ajpath.2012.08.017 (2012).
- 101 Serizawa, T. *et al.* Gastric Metaplasia Induced by *Helicobacter pylori* Is Associated with Enhanced SOX9 Expression via Interleukin-1 Signaling. *Infection and Immunity* **84**, 562, doi:10.1128/IAI.01437-15 (2016).

- 102 Buzzelli, J. N. *et al.* IL33 Is a Stomach Alarmin That Initiates a Skewed Th2 Response to Injury and Infection. *Cellular and Molecular Gastroenterology and Hepatology* **1**, 203-221.e203, doi:<https://doi.org/10.1016/j.jcmgh.2014.12.003> (2015).
- 103 Nam, K. T. *et al.* Amphiregulin-deficient mice develop spasmodic polypeptide expressing metaplasia and intestinal metaplasia. *Gastroenterology* **136**, 1288-1296, doi:10.1053/j.gastro.2008.12.037 (2009).
- 104 Khurana, S. S. *et al.* The hyaluronic acid receptor CD44 coordinates normal and metaplastic gastric epithelial progenitor cell proliferation. *The Journal of biological chemistry* **288**, 16085-16097, doi:10.1074/jbc.M112.445551 (2013).
- 105 Sáenz, J. B. & Mills, J. C. Acid and the basis for cellular plasticity and reprogramming in gastric repair and cancer. *Nature Reviews Gastroenterology & Hepatology* **15**, 257, doi:10.1038/nrgastro.2018.5 (2018).
- 106 Camargo, M. C. *et al.* Divergent trends for gastric cancer incidence by anatomical subsite in US adults. *Gut* **60**, 1644-1649, doi:10.1136/gut.2010.236737 (2011).
- 107 You, W. C. *et al.* Comparison of the anatomic distribution of stomach cancer and precancerous gastric lesions. *Japanese journal of cancer research : Gann* **83**, 1150-1153, doi:10.1111/j.1349-7006.1992.tb02738.x (1992).
- 108 Wanebo, H. J. *et al.* Cancer of the stomach. A patient care study by the American College of Surgeons. *Annals of surgery* **218**, 583-592 (1993).
- 109 El-Zaatari, M. *et al.* Gli1 Deletion Prevents Helicobacter-Induced Gastric Metaplasia and Expansion of Myeloid Cell Subsets. *PLOS ONE* **8**, e58935, doi:10.1371/journal.pone.0058935 (2013).
- 110 Leushacke, M. *et al.* Lgr5-expressing chief cells drive epithelial regeneration and cancer in the oxyntic stomach. *Nature Cell Biology* **19**, 774, doi:10.1038/ncb3541  
<https://www.nature.com/articles/ncb3541#supplementary-information> (2017).
- 111 Nam, K. T. *et al.* Mature chief cells are cryptic progenitors for metaplasia in the stomach. *Gastroenterology* **139**, 2028-2037.e2029, doi:10.1053/j.gastro.2010.09.005 (2010).
- 112 Capoccia, B. J. *et al.* The ubiquitin ligase Mindbomb 1 coordinates gastrointestinal secretory cell maturation. *The Journal of clinical investigation* **123**, 1475-1491, doi:10.1172/JCI65703 (2013).

# **Chapter 2: Regenerative proliferation of differentiated cells by mTORC1-dependent paligenosis.**

Willet SG\*, Lewis MA\*, Miao ZF\*, Liu D, Radyk MD, Cunningham RL, Burclaff J, Sibbel G, Lo HG, Blanc V, Davidson NO, Wang ZN, Mills JC

\*Co-first author

## **Chapter 2.1 INTRODUCTION**

In 1900, George Adami wrote about the relationship between mitotic and differentiated cells, stating that he expected mitotic cells would generally devote energy toward replication and differentiated cells toward performing physiological functions (Adami, 1900). He also observed that upon injury, differentiated cells had the capacity to revert to a more primitive state, becoming mitotic again to promote tissue repair. Adami's observations on such cellular plasticity have largely been forgotten, as the focus in the 20th century was nearly exclusively on the unidirectional differentiation of stem cells into functional, "post-mitotic" cells.

However, over the past decade or two, numerous examples have emerged to support plasticity in differentiated cells. First, it became clear that normal, somatic cells could be reprogrammed to pluripotency (Takahashi & Yamanaka, 2006). Furthermore, in tissues, injury can induce a repair process that recruits largely post-mitotic, differentiated cells back into the cell cycle in most, if not all, organs and species, for example, glia (Boerboom et al, 2017; Mindos et al, 2017); lung (Logan & Desai, 2015); heart in mammals (Wang et al, 2017) and fish (Karra et al, 2015); in multiple gastrointestinal tract organs (Mills & Sansom, 2015). Each such

example to date has been studied essentially in isolation within the context of a particular type of injury and a single organ; however, because the process is so widespread, we have postulated that it may be governed by a shared, evolutionarily conserved molecular and cellular program that is independent of tissue and species (Mills & Sansom, 2015).

It has long been known that the response of both the corpus of the stomach and the digestive-enzyme-secreting (exocrine) pancreas to certain types of injury involves phenotypical changes in cell differentiation and tissue architecture, known as metaplasia. In the acute setting, the metaplastic response appears to be a tissue repair mechanism and can be temporary, with full restoration of normal tissue architecture (Nomura et al, 2005; Huh et al, 2012). Chronically, however, ongoing damage and long-term metaplasia are associated with and may fuel the majority of gastric and pancreatic adenocarcinomas (Mills & Sansom, 2015; Giroux & Rustgi, 2017; Storz, 2017). In both organs, the cells of origin for the metaplastic, proliferating epithelial cells are thought to be differentiated secretory cells (zymogenic chief cells in the stomach and acinar cells in the pancreas) that reprogram to re-enter the cell cycle (Mills & Sansom, 2015; Murtaugh & Keefe, 2015; Mills & Goldenring, 2017; Radyk & Mills, 2017).

Here, we report that differentiated cells in both pancreas and stomach exhibit high levels of mTORC1 activity during homeostasis. Proliferation-inducing injury caused rapid mTORC1 loss and a dramatic induction of autodegradative machinery (lysosomes and autophagy). As the functional and structural components were recycled, cells changed gene expression patterns (e.g., inducing the metaplastic marker Sox9); thereafter, they reactivated mTORC1 and re-entered the cell cycle. Such changes in mTORC1 activity were corroborated in tissues from human patients. Also, established models of injury to differentiated cells in mouse liver (Espeillac et al, 2011)

and kidney (Chang-Panesso & Humphreys, 2017) correlate mTORC1 activity with the recruited proliferating cells. Blocking mTORC1 with rapamycin in murine pancreas and stomach impaired only cell cycle re-entry but not earlier cellular changes. Differentiated cells in autophagy-defective *Gnptab*<sup>-/-</sup> mice were blocked from both SOX9 expression and cell cycle re-entry phases, consistent with the upstream autodegradative phase being necessary for downstream mTORC1-mediated S-phase entry.

Our results in the context of numerous previous reports on cellular reprogramming lead us now to propose that recruiting differentiated cells into a regenerative phenotype occurs via stepwise metabolic and molecular phases that constitute a conserved, fundamental, cellular program, akin to mitosis or apoptosis. This cellular program occurs during cell fate changes of various types (e.g., reversion, dedifferentiation, transdifferentiation, reprogramming). The lack of a standard term for the actual cellular process itself impedes finding shared features that transcend cell types, tissues, and model systems. We propose a new, unifying term: “paligenosis” from the Greek: *pali/n/m* (meaning backward or recurrence) + *genea* (born of, producing) + *osis* (an action or process).

## **Chapter 2.2 RESULTS**

### Diverse organs show similar changes in metabolic activity during acute injury

To induce injury in the stomach, we employed a high-dose tamoxifen (“HD-Tam”) injury model that has been used by us and others (Huh et al, 2012; Burkitt et al, 2017; Lee et al, 2017; Leushacke et al, 2017). HD-Tam causes loss of nearly all acid-secreting parietal cells in the body of the stomach (Figs EV1 and EV3) and induces mature, differentiated digestive-enzyme-

secreting chief cells at the base of the unit to give rise to a proliferating cell population (Radyk et al, 2018). These former chief cells maintain low-level expression of some mature chief cell markers and induce expression of wound repair-associated genes like mucins and TFF2 (aka spasmolytic polypeptide). The pattern of parietal cell loss and abundant, proliferative cells co-expressing TFF2 and chief cell markers has been called spasmolytic polypeptide-expressing metaplasia (SPEM) or pseudopyloric metaplasia (Schmidt et al, 1999). Maximal parietal cell loss and proliferation stemming from chief cells occurs at 3 days after the first dose of tamoxifen (Schematized in Fig 1A). By 7 days, parietal cells have returned, and the entire stomach regenerates to pre-treatment cell censuses within 14–21 days (Huh et al, 2012). HD-Tam is a rapid, synchronous method to model, in a manner that lends itself to molecular analyses, the mechanisms of stomach repair that also occurs in human stomachs infected with the bacterium *Helicobacter pylori*.

To induce injury in pancreas, we used a well-described rapid method involving daily injection of the secretagogue cerulein. Cerulein injections cause large-scale damage to the digestive-enzyme-secreting acinar cells of the exocrine pancreas (Adler et al, 1985; Niederau et al, 1985; Saluja et al, 1985). To repair the damage, acinar cells re-enter the cell cycle, forming duct-like structures called ADM (acinar-to-ductal metaplasia; schematic in Fig 1A). In our protocol, ADM peaks 5 days after commencement of cerulein. Thereafter, there is continued damage if cerulein administration is maintained, but the pancreas gradually adapts to the injury over 2 weeks. Similar to HD-Tam injury in the stomach, cerulein injury models a metaplastic process that can also be a precursor for pancreatic ductal adenocarcinoma.

To determine whether the reversion from the differentiated to the replicative state involves conserved shifts in cellular energy use, we examined metabolic activity in both tissues using phosphorylated ribosomal S6 protein (pS6). The principal mediator of S6 phosphorylation is the S6 kinase enzyme via the cellular metabolism hub mTOR complex 1 (mTORC1). To confirm that S6 phosphorylation depends on mTORC1 activity, we treated mice with rapamycin, a specific inhibitor of the mTORC1-mediated S6 kinase activity. We used an antibody against residues 240/244 of S6, because those sites are phosphorylated principally by pS6 kinase 1, whereas the 235/236 phosphorylation sites can have input from other signaling pathways. For example, 235/236 can be phosphorylated by p90 ribosomal S6 kinases that can be activated via ERK signaling (Roux et al, 2007). Figure EV1 shows that rapamycin, which is a specific inhibitor of mTORC1-mediated S6 Kinase activity, abolished pS6 240/44 staining, which was normally abundant in gastric pit cells nearer the stomach lumen and in gastric chief cells. Rapamycin also blocked S6 phosphorylation efficiently during the HD-Tam protocol (Fig EV1). Antibodies against 235/236 also showed strong phosphorylation at peak metaplasia as well as a similar abrogation of staining in the presence of rapamycin (Fig EV1). As anti-240/244 antibodies have stronger signal in our experiments and are more specific for mTORC1-mediated phosphorylation, we will use anti-240/244 pS6 as a surrogate for mTORC1 activity for the remainder of the manuscript unless otherwise mentioned.

HD-Tam or cerulein caused dramatic changes in pS6 expression. In stomach, pS6 was largely lost by 12 h. By 3 days, when SPEM is maximal in this system, the entire gastric unit expressed abundant pS6 (Fig 1B). Molecular and cellular changes in the stomach following HD-Tam are sufficiently synchronous across the whole stomach that quantitative, molecular approaches can be used (Huh et al, 2012). Quantitatively, phosphorylation status of both pS6

240/244 and 235/236 in the corpus of the stomach was decreased by nearly half within the first 4 h and returned to at or above baseline by 48 h (Fig 1C). In pancreas, despite a slower and less synchronous time course, the same pattern of mTORC1 activity could be observed by immunofluorescence. pS6 was abundant in acinar cells at baseline, was nearly undetectable by 24 h, and recovered in many cells by day 5, when ADM is maximal (Fig 1D).

Thus, both tissues, when recruiting proliferative cells for repair, undergo a well-defined pattern of changes in mTORC1 activity. During homeostasis, the organs are replete with differentiated secretory cells that are not dividing but are energetically active in synthesizing protein using their elaborate secretory apparatus (Mills & Taghert, 2012; Lo et al, 2017). When replicating cells must be recruited from those differentiated cells, the cells shut off mTORC1 temporarily, then re-induce it at the time of maximal regenerative proliferation.

To further assess whether the upregulation of pS6 is a common feature during the recruitment of differentiated cells to regenerate damaged tissue, we examined liver (two-thirds partial hepatectomy) and kidney (tunicamycin-induced acute injury) for changes in S6 phosphorylation. Both injury models have previously been shown to involve recruitment of differentiated cells back into the cell cycle (Newberry et al, 2008). In kidney, as expected, tubules in the cortex and outer medulla are damaged as evinced by vacuolation (Fig EV2). Non-damaged tubules show increased BrdU as cells re-enter the cell cycle (Fig EV2). The proliferative tubules show marked increase in pS6. Similarly, the well-known recruitment of hepatocytes into the cell cycle 48 h following partial hepatectomy is also accompanied by increased S6 phosphorylation (Fig EV2).

Rapamycin had equivalent effects on the pancreas. Metaplastic induction of SOX9 was not affected (Fig EV4); however, cell proliferation was even more substantially blocked than in the stomach (Fig 2D and E). This may be because the pancreas is entirely dependent on reprogramming acinar cells as a source for proliferation, whereas the stomach also has a constitutive stem cell that continues to proliferate even in the presence of rapamycin (Fig 1A). Continued HD-Tam injections kill mice, so we cannot study adaptation of stomachs; however, we have maintained cerulein injections for up to 2 weeks by which point wild-type pancreas usually adapts to the injury. Thus, we used the pancreas to determine whether mTORC1-dependent proliferation was required for pancreatic repair. Figure EV3 shows that 2-week cerulein with mTORC1 blocked led to tissue loss relative to cerulein treatment alone.

#### Changes in mTORC1 also characterize human metaplasia

To determine whether mTORC1 activity is modulated in human disease states, we first examined a database of stomach tissues from human patients exhibiting metaplastic response to *H. pylori* infection, previously compiled at Washington University (Lennerz et al, 2010; Radyk et al, 2018). A representative region from this dataset is shown in Fig 3A. As in mice, morphologically normal chief cells showed high pS6. In regions of SPEM, pS6 abundance varied. In lesions that had histological features of cells undergoing acute conversion to SPEM (what we have previously termed “hybrid SPEM” (Lennerz et al, 2010; Radyk et al, 2018) based on examination of a large dataset of SPEM lesions), pS6 levels were high (Fig 3A). In regions where basal cells showed more uniform metaplasia (“established SPEM”), pS6 levels were lower. In humans, SPEM is thought to be either transient and rapidly resolve (as in the mouse HD-Tam model) or chronic and persist for decades, involving large patches of the stomach

(Peterson, 2002). In the chronic case, SPEM is equivalent to the lesion pathologists call chronic atrophic gastritis (Rugge et al, 2008). In addition, SPEM is thought to progress to (or predate) another, proliferative, pre-cancerous lesion, intestinal metaplasia (Yoshizawa et al, 2007; Correa & Piazuelo, 2012; Spechler et al, 2017) and to increase risk for progression to a cytologically atypical lesion, dysplasia, as well as to cancer itself.

To further clarify the link between mTORC1 activity and metaplastic changes in humans, we analyzed pS6 levels in gastric tissue microarrays (Appendix Table S1) comprising tissue cores representing the following histological phenotypes: normal mucosa, SPEM, IM, dysplasia, and gastric adenocarcinoma. pS6 showed consistent, mid-level expression in nearly all normal mucosal samples, in agreement with our smaller sample showing expression of pS6 in normal chief cells and with our mouse data (Fig 3B). Both cancer and dysplastic lesions showed higher average pS6 expression, though there was also more variability in that over a third of such lesions showed much stronger expression than normal tissue, while about a third showed lower expression (Fig 3B). On average, intestinal metaplasia pS6 levels were close to those of normal mucosa (Figs 3B and EV5). SPEM lesions showed a clear biphasic pattern with the majority like the “established SPEM” with low-to-no detectable pS6 (cf. Figs 3A and EV5) but with some SPEM lesions having much stronger pS6 (Figs 3 and EV5).

SPEM lesions with lower pS6 activity tended to express abundant mucin as well as epitope for the SPEM-identifying lectin GSII (Fig 3A); nuclei tended to be flat and eccentric (Fig EV5). pS6-expressing SPEM cells were more cuboidal columnar, resembling the SPEM cells in the acute, proliferative mouse SPEM that resolves in a few days after HD-Tam. We hypothesized that SPEM with increased pS6 represented metaplastic cells that are actively proliferating (like

D3 HD-Tam in mice) to repair an injury, whereas the decreased pS6 lesions of established SPEM may be mitotically quiescent. Hence, we divided the SPEM lesions into mitotically active (“proliferative SPEM”) and inactive (“quiescent SPEM”) based on Ki-67 staining of the same tissue core on another microtome section (Fig EV5) and then correlated those phenotypes to the previously scored pS6 expression for that lesion. Proliferative SPEM was far more likely to be associated with pS6 expression, whereas quiescent SPEM was largely negative for pS6 (Fig 3C,  $P < 0.001$  by  $\chi^2$ ). Thus, pS6 is low-moderate in normal, physiologically active mucosa and high in most lesions that have increased proliferation (proliferative SPEM, IM, dysplasia, cancer). We conclude that metabolic activity correlates with differentiation state and recruitment into the cell cycle in humans as well as mice.

#### Loss of mTORC1 inhibits cell cycle progression at S-phase

Because gastric chief cells respond to injury more synchronously than pancreatic acinar cells, we are able to perform molecular analyses based on changes of gene expression. We used this approach to determine specifically where the block in cell cycle re-entry occurs when mTORC1 activity is inhibited. We analyzed Affymetrix GeneChips of whole gastric corpora  $\pm$ HD-Tam (3D)  $\pm$ rapamycin by Gene Set Enrichment Analysis (GSEA) with a combination of both a publicly available and custom gene sets. In a control experiment to validate our approach, we dissociated gastric epithelial cells from *Atp4b-Cre; ROSA26mTmG* mouse stomachs and used flow cytometry to isolate parietal cells (GFP+) from other epithelial cells (Tomato+). Expression of isolated, amplified RNA applied to GeneChips was analyzed by Partek Genomics Suite, and the 94 genes whose expression was enriched  $\geq$  eightfold in parietal cells vs. other epithelial cells was computed. As expected, GSEA showed that these PC-enriched genes were highly

preferentially expressed in control stomachs vs. HD-Tam stomachs; the addition of rapamycin did not affect this pattern (Appendix Fig S1). Thus, global gene expression profiling with GSEA can detect the loss of parietal cells that epitomizes HD-Tam-induced metaplasia and also shows that parietal cell loss is independent of mTORC1, consistent with the histological data. In another control experiment, we performed GSEA of a published gene set of mature chief cell enriched genes (Capoccia et al, 2013) and contrasted HD-Tam vs. HD-Tam + rapamycin. There was no substantial effect of rapamycin, suggesting that the change in chief cell gene expression induced by injury is also not substantially affected by loss of mTORC1 (Appendix Fig S1).

On the other hand, although many transcripts from a previously published gene set of SPEM-associated genes (Nozaki et al, 2008) did not show particular changes when rapamycin was administered in HD-Tam, there was a cluster of genes enriched only when mTORC1 levels were normal (Appendix Fig S1). Injury that causes metaplasia induces both wound-healing-associated genes (e.g., *Clu*, *Sox9*, *CD44v*) and proliferation-associated genes. Given that rapamycin blocks proliferation specifically in our histological analysis, we next examined the effects of rapamycin on the cell cycle using GSEA. Figure 4A shows that, indeed, rapamycin induces a marked de-enrichment of cell cycle gene expression in HD-Tam. The block appears specifically at the S-phase and beyond, as gene sets for G1-S, S, G2, and G2-M showed that G1-S genes were relatively similarly distributed regardless of mTORC1 activity, whereas genes expressed during the later stages in the cell cycle were skewed toward the HD-Tam alone condition (Fig 4B–E). We used a slightly different approach to further investigate the interaction of mTORC1 with cell cycle stage by first determining the top 20 genes skewed most toward the HD-Tam (vs. vehicle-treated controls) in each cell cycle stage gene set. We then determined the average increased expression of those genes in both HD-Tam and HD-Tam + rapamycin vs.

vehicle controls. Figure 4F shows that rapamycin decreased expression of the 20 top G1/S-phase HD-Tam-enriched genes by only  $16 \pm 3\%$ , whereas gene expression at other cell cycle stages was inhibited substantially more. Expression of G2/M-phase genes was decreased by  $49 \pm 3\%$  with rapamycin treatment ( $P < 0.001$ , HD-Tam vs. HD-Tam + rapamycin in G2-M genes;  $P < 0.05$  for G2-M vs. G1-S).

To independently validate the GeneChip findings, we performed qRT-PCR that showed that the expected decreases in a parietal cell (*Atp4b*) transcript and increase in a non-cell-cycle SPEM transcript (*Clu*) were not affected by rapamycin (Fig 4G). Also matching the GeneChip results, the G1 transcript, *Ccnd1*, was increased similarly regardless of mTORC1 status. As expected, a G2/M-phase transcript cohort was uniformly increased in HD-Tam but not in HD-Tam + rapamycin (Fig 4H). Thus, molecular analysis indicates that inhibition of mTORC1 activity does not substantially affect chief cell G1-phase entry from the quiescent, G0 state but slows S, G2, and M-phase progression. BrdU uptake and incorporation into DNA occurs during S-phase; thus, the block in BrdU seen histologically corroborates the molecular data suggesting that mTORC1 is required for G1 to S transition.

#### Autodegradative machinery is massively upregulated early following injury

We so far have observed that mTORC1 activity is rapidly extinguished within hours of inducing injury. Later, as cells re-enter the cell cycle, mTORC1 is rekindled. Blocking re-emergence of mTORC1 activity inhibits induced proliferation in both stomach and pancreas. In pancreas, where repair is entirely dependent on reprogramming, loss of mTORC1 activity blocks tissue regeneration. We hypothesized that the scaling down of mature cell architecture to “retool” a cell for more efficient proliferation would likely involve activation of lysosomes and

autophagic machinery. The autodegradation of cellular structure could then liberate key macromolecules (nucleotides, amino acids, lipids) that would both stimulate mTORC1 reactivation and provide building blocks for replication. Figure 5 shows that there is a massive increase of lysosomes (by luminal marker Cathepsin D, Fig 5A) and autophagosomal puncta (by LC3-GFP, Fig 5C) early following injury in gastric chief cells. Figure 5B quantifies a large spike in lysosomes, as a percentage of their PGC+ (pepsinogen C; chief cell marker) cell area, by 12–24 h of HD-Tam that begins to resolve by later stages, when many cells have re-entered the cell cycle. Increased lysosomes, autophagosomes, and autolysosomes can also be seen at the ultrastructure level (Fig 5D and E) on transmission electron microscopy (tEM). tEM analysis shows that rER, mitochondria, and secretory granules are all targeted for recycling during these early stages. The pancreas also shows an equivalent time course of changes in autodegradative machinery, with a spike in lysosome and autophagic puncta 8–24 h following cerulein, followed by decreasing, but still elevated levels, at D3 and near baseline levels at the time of maximal proliferation and pS6 activity (D5: Fig 5F, Appendix Fig S2).

#### Autodegradative machinery is required for normal progression to later stages

We next sought to address whether autodegradative machinery activation is both upstream of and required for metaplasia formation and proliferation. To do this, we used mice defective in lysosomal hydrolase trafficking that have been shown previously to have defects in autodegradative function specifically in exocrine secretory cells like chief and acinar cells (Boonen et al, 2011). *Gnptab*<sup>-/-</sup> mice are deficient in an enzyme required for the addition of mannose-6-phosphate to lysosomal enzymes to ensure their proper trafficking. We treated *Gnptab*<sup>-/-</sup> and littermate controls (*Gnptab*<sup>-/+</sup> and *Gnptab*<sup>+/+</sup>) with HD-Tam or cerulein. HD-Tam

treatment in *Gnptab*<sup>-/-</sup> mice caused the expected loss of parietal cells; however, chief cell reprogramming was dramatically compromised (Fig EV6). Most units did not show loss of large chief cells with eccentric nuclei at all (red arrowhead, Fig EV6), suggesting reprogramming did not occur, whereas some gastric units showed complete loss of the base zone where chief cells normally reside (green arrowhead, Fig EV6), indicating chief cells were aberrantly lost instead of reprogrammed. Rarer gastric units seemed to complete the reprogramming (yellow arrowhead, Fig EV6). In pancreas, we detected almost no ADM in *Gnptab*<sup>-/-</sup> mice (Fig EV6) by D5. Rather, cells remained in an aberrant acinar morphology with considerable loss of eosinophilic cytoplasm but no decrease in size. By 2 weeks, whereas wild-type controls had largely adapted to the cerulein injury, in *Gnptab*<sup>-/-</sup> mice, the exocrine pancreas comprised only scattered ducts and SOX9<sup>-</sup> acinar cells, still organized in typical lobules. Cytologically, these remnant cells were characterized by generous pale cytoplasm ranging from foamy to hyaline and lacking nearly all distinguishing features.

We next examined the molecular phenotype of the block in *Gnptab*<sup>-/-</sup> mice. In control stomachs in response to injury, reprogramming cells in the base showed the expected abundant increase in metaplastic genes like Sox9 (Fig 6A) and the epitope for GSII (Fig 6C). Proliferation in the base of the unit, where chief cells were reprogramming, was nearly equivalent to the rate of proliferation in the normal stem cell zone in the neck (Fig 6B and D). The bases of gastric units in *Gnptab*<sup>-/-</sup> mice were markedly compromised in both metaplastic changes and proliferation (Fig 6A–D). In *Gnptab*<sup>-/-</sup> mice, chief cells in the base remained both BrdU- and SOX9-negative (Fig 6E and F). They also failed to reactivate mTORC1, as pS6 in these mice was largely not detectable in the base (Fig EV7).

In the pancreas, there was a similar defect in both BrdU (Fig 6G and I) and Sox9 (Fig 6H). The remnant acinar cells that remained in *Gnptab*<sup>-/-</sup> mice following 2 weeks of cerulein treatment expressed E-cadherin and low levels of amylase but were not positive for other mature acinar nuclear markers like GATA4 or metaplasia markers like CK8/18 (Appendix Fig S3).

Finally, to determine whether the dropout of gastric bases was due to increased cell death in the absence of lysosomal hydrolase activity, we examined tissue for cleaved caspase 3. In wild-type mice (either with or without rapamycin), we did not detect substantial apoptotic death of the chief cells, consistent with our previous observations that death in HD-Tam is essentially confined to parietal cells (Huh et al, 2012; Radyk et al, 2018; Fig EV1). In *Gnptab*<sup>-/-</sup> mice, however, we frequently observed multiple cells in some bases of gastric units that were undergoing apoptosis (Appendix Fig S4). Thus, in stomach, aberrant autodegradative function leads either to stalling of the chief cell reprogramming process or cell death. In pancreas, we observed a pattern of scattered apoptosis of acinar cells in wild-type mice  $\pm$ rapamycin following cerulein treatment. Loss of GNPTAB did not seem to affect this basal rate of death, which is consistent with the survival of many acinar cell remnants out to 2 weeks, as discussed above.

## **Chapter 2.3 DISCUSSION**

There has been a recent burgeoning of examples of cellular plasticity in tissue in response to injury, not to mention a growing, already large literature on in vitro systems for reprogramming cells back to progenitors. The instances of such plasticity span numerous species and nearly all tissues. Despite the breadth of examples of cellular reprogramming, studies focusing on the specific molecular mechanisms responsible for the process are still relatively scant. This is particularly true in studies of cells in tissue, likely because investigators have

focused more on the outcome of cellular reprogramming—regeneration or tumorigenesis—than on the stepwise mechanisms differentiated cells use to contribute to those outcomes. Here, we have speculated that there could be a shared cellular program that governs the many diverse examples of differentiated cells changing their fate to facilitate repair. There have been many terms that either focus on the outcome of the program or are overly broad: “dedifferentiation”, “transdifferentiation”, “reversion”, “reprogramming”. We now propose “paligenosis” as a specific term describing the cellular process differentiated cells use to re-acquire regenerative capacity. We highlight that paligenosis may be a conserved cellular process with shared molecular and cellular regulation akin to other basic cellular processes like mitosis and apoptosis.

To support our assertion that there may be a shared program for recruiting differentiated cells, we have analyzed the cellular and molecular changes that occur during injury-induced reprogramming in two distinct organs. Upon injury, both the stomach and pancreas have the capacity to repair tissue damage through the recruitment of fully differentiated cells into a less differentiated, proliferative state to replenish cell numbers. This pattern of change in cell phenotype is known to pathologists as metaplasia. We find that the cellular and molecular changes that characterize cells undergoing such metaplastic injury response in either stomach or pancreas are remarkably similar. Specifically, we found that acutely following injury, autodegradative pathways increase alongside a decrease in mTORC1 activity (Fig 7). As the injury progresses, we observed the induction of genes that are known to occur during metaplasia followed by the rise of mTORC1 activity and increased proliferation (Fig 7). A similar pattern of changes in mTORC1 activity relative to metaplasia and the differentiated vs. proliferative phenotype was observed in human patients. We found that mTORC1 activity was specifically

required for progression through S-phase. Previous literature has also shown that mTORC1 activity is critical for S-phase progression of cancer cells following DNA damage, as mTORC1 is needed to generate pyrimidines in a nutrient-poor environment (Robitaille et al, 2013; Silvera et al, 2017; Zhou et al, 2017). mTORC1 activation is also needed for yeast to pass through G1 into S-phase as they emerge from quiescence (Dhawan & Laxman, 2015; Moreno-Torres et al, 2015). Using an animal model of lysosomal dysfunction, we uncovered that normal lysosomal function after injury is required for cell phenotype and gene expression changes associated with metaplasia. In pancreas, where constitutive stem cells are not available for regeneration, loss of either autodegradative function or mTORC1 activity compromised eventual organ repair.

Recent advances in the understanding of how mTORC1 is controlled have described a role for the lysosome as an activator of the pathway through the release of nutrients like key amino acids (Zoncu et al, 2011). Thus, our current working model is that due to injury-induced stress, autodegradative pathways are upregulated, and flux increases. The activation of autodegradative pathways appears to act in parallel with loss of the mature gene regulatory network, as forcing expression of key mature-cell-promoting transcription factors like MIST1 (BHLHA15) impairs the injury/repair process (Direnzo et al, 2012; Lo et al, 2017). MIST1 controls a cassette of genes that help direct a cell's energy toward secretion and away from lysosomal activation and autophagy (Mills & Taghert, 2012). We reason, as did Adami over a century ago, that to convert from the differentiated state (structurally complex, energetically active) to the replicative state (structurally simple, energetically active), cellular energy use must be repurposed as an autodegradative program is activated to convert differentiated cell structure into building blocks for replication. The release of nutrients through the lysosome is sensed in cells during the autodegradative phase, resulting in reactivation of mTORC1, which, once the

cell has reached sufficient energy levels, subsequently facilitates cell cycle progression and growth to replace cells lost during the injury.

Pancreatic adenocarcinoma and—to a lesser extent—gastric adenocarcinoma are commonly driven by oncogenic mutations in *Kras*. In mouse models in both the pancreas (Hingorani et al, 2005) and stomach (Choi et al, 2016), *Kras*G12D mutations, in concert with tissue inflammation, promote changes in gene expression and cell phenotypes resembling injury-induced metaplasia. In the pancreas, genetically disabling autophagy in the context of *K-Ras* mutations prevents *K-Ras* from driving high-grade lesions (Rosenfeldt et al, 2013). Furthermore, cells unable to phosphorylate S6 in the context of activating *K-Ras* mutations also exhibit less pancreatic cancer progression (Khalaileh et al, 2013). A similar critical role for mTORC1 downstream of another key driver oncogene pathway, Wnt activation mediated by APC mutation, has been described in intestinal carcinogenesis (Morran et al, 2014). Thus, tumorigenesis in diverse tissues may also involve modulating lysosomal activity and mTORC1, similar to what we observe in our injury models here. Other pathways downstream of *K-Ras*, such as PI3K/Rac1 signaling (Heid et al, 2011; Wu et al, 2014), also play similar roles in injury-induced metaplasia.

If there truly is a shared cellular program, paligenosis, underlying the process of recruiting mature cells to become regenerative cells, we would expect the general features we have described here in stomach and pancreas to be recapitulated in many other tissues and species. Obviously, it will be important to conduct new studies in other systems to begin to support that assertion; however, we can at this point re-examine the extant literature to determine whether roles for lysosomes/autophagy and/or mTORC1 in the process of cellular

reprogramming to a regenerative state have previously been described. One such previous study, using a different injury protocol, with the endpoint to determine the role of mTORC1 and autophagy in severity of pancreatitis, similarly showed a pattern of early autodegradation followed by mTORC1 activation (Hu et al, 2015). The authors also found that rapamycin worsened severity of pancreatitis. In liver, it has long been known that the earliest phase of hepatocyte response to partial hepatectomy is massive activation of autophagy/lysosomes (Becker & Lane, 1965). mTORC1 is required for the later stages of the process, when proliferation is maximal, consistent with observations we make in the current manuscript (Jiang et al, 2001; Nelsen et al, 2003; Buitrago-Molina et al, 2009; Espeillac et al, 2011). In kidney, the reprogramming process involves mTORC1 (Kato et al, 2012), and we show here that mTORC1 activity is increased specifically in the tubular cells, which are the cell population called back into the cell cycle to regenerate damaged tissue. To our knowledge, lysosomes/autophagy has not been examined in regenerating kidney. In mature glial cells that dedifferentiate following axonal injury, activation of autophagy/lysosomes is a well-established early event (Jessen & Mirsky, 2016). To our knowledge, mTORC1 activity has not been examined in the process. Furthermore, in tissue culture cellular reprogramming models to generate induced pluripotent stem cells, there is an emerging literature that an early autophagy phase is followed eventually by mTORC1 activation. Inhibition of either autophagy or prolonged inhibition of mTORC1 reduces reprogramming efficiency (He et al, 2012; Wang et al, 2013; Wu et al, 2015). Hence, the stages and checkpoints appear to be the same as the ones we examine in the current manuscript.

Thus, there are numerous reports indicating that the pattern we show here systematically of autodegradation first, then mTORC1 activation may be universal. Moreover, teleologically, it makes sense that a mature cell would first recycle cellular components required for physiological

function to use them as substrates for subsequent synthesis of components needed for proliferation. In organs like the vertebrate pancreas or liver, where there are no constitutively active stem cells, repair would likely depend in large part on paligenosis. In tissues with constitutive stem cells, like stomach and intestines, the tissues would have the choice of regenerating with either constitutive stem cells or paligenotic cells, depending potentially on type, extent, and location of injury.

Not all differentiated cells are likely to be able to undergo paligenosis. In the stomach, for example, we have never observed this phenomenon in mature parietal cells (Huh et al, 2012; Mills & Sansom, 2015). Cells that are constitutively undifferentiated and replicative like those of the isthmus of the stomach or LGR5+ crypt-base columnar cells should not need any stage of paligenosis (Fig 7). They may acquire the building block nucleotides and amino acids from the blood and/or extracellular environment, given that, by definition, their lack of differentiation means they contain limited non-nuclear components to recycle. Other cells, such as mucous neck cells in the stomach or +4 cells in the intestine (van Es et al, 2012; Roth et al, 2012; Buczacki et al, 2013), may be able to respond to injury but are less well differentiated and thus may be able to skip the autodegradative phase and go directly to the activating mTORC1 and cell division phase of paligenosis.

Paligenosis may be beneficial for its potential to provide lifelong tissue repair in adult organs, but this capacity also seems inherently tied to increased risk for tumorigenesis. Chronic injury of the type that repetitively induces paligenotic/metaplastic events has long been known to increase risk for acquisition of mutations and progression to neoplasm. We have proposed that the reason that risk increases with age is that cycles of paligenosis and subsequent

redifferentiation allow accumulation of mutations that may be stored in long-lived, differentiated cells. Eventually, a critical mutation may be unmasked during paligenosis, and a clone of cells that is unable to redifferentiate arises. We have termed this the “cyclical hit” model of tumorigenesis (Mills & Sansom, 2015; Saenz & Mills, 2018).

There are numerous questions that our current study prompts. What molecular events underlie the competence to pass through each stage of paligenosis? What is the relationship between paligenosis and chronic injury, and what causes the increased risk for cancer? Why are some cells able to undergo paligenosis, whereas others are not? We expect that the framework of sequential phases of paligenosis that we introduce here, along with the potential checkpoints that serve as molecular barriers between each stage of the process, can serve as a starting point for future questions.

## **Chapter 2.4 MATERIALS AND METHODS**

### Animal studies and reagents

All experiments using animals followed protocols were approved by the Washington University School of Medicine Animal Studies Committee. WT C57BL/6 mice were purchased from Jackson Laboratories (Bar Harbor, ME). Tg(Atp4b-cre)1Jig/JcmiJ (Atp4b-Cre) (Syder et al, 2004), Gt(ROSA)26Sortm4(ACTB-tdTomato,-EGFP)Luo/J (ROSA26mtmg) (Muzumdar et al, 2007), Gnptab (Gelfman et al, 2007), and LC3-GFP (Mizushima et al, 2004) mice were previously described. Gnptab mice were a kind gift from Dr. Stuart Kornfeld of Washington University. Tamoxifen (5 mg/20 g body weight; Toronto Research Chemicals) was injected intraperitoneally (IP) daily for 2–3 days to induce maximal gastric injury (Huh et al, 2012; Saenz

et al, 2016). Tamoxifen was prepared by first dispersing in 100% ethanol by sonication and then emulsifying in sunflower oil (Sigma-Aldrich) 9:1 (oil:ethanol). Pancreatitis was induced by 6 hourly IP injections of 50 µg/kg (in 0.9% saline) cerulein (Sigma-Aldrich) given every other day for up to 2 weeks. Mice were sacrificed 24 h after the final cerulein injection. Rapamycin (60 µg/20 g body weight; LC Laboratories) was injected IP in 0.25% Tween-20, 0.25% polyethylene glycol in PBS for 3–7 days prior to starting and throughout injury time course. Tunicamycin (Carlisle et al, 2014) and two-thirds partial hepatectomy (Blanc et al, 2010) injuries were performed as previously described. Mice were given an IP injection containing 5-bromo-2'-deoxyuridine (BrdU; 120 mg/kg) and 5-fluoro-2'-deoxyuridine (12 mg/kg) in sterile water 90 min before sacrifice for all BrdU labeling experiments.

For parietal cell isolation, stomachs were harvested and washed several times with PBS. The forestomach and antrum were carefully removed and the remaining corpus minced with a razor blade. The tissue was mechanically dissociated using a 50 µm Medicon (Beckman) for two 30-s pulses. Chunks of tissue were further dissociated by incubating in 10 ml HBSS with 5 mM EDTA and 1 mM DTT with vigorous shaking for 1 h at 37°C, and then, the solution was run through a 100-µm filter. Single cells were allowed to rest at 37°C, while filtered chunks were incubated in 10 ml RPMI 1640 with 5% BSA (Sigma) and 1.5 mg/ml Dispase II (Stem Cell Technologies) with vigorous shaking for 1.5 h at 37°C and then filtered again. Dissociated cells were pelleted and washed with cold HBSS three times and then resuspended in PBS with 1% BSA and 5 mM EDTA. Cells were sorted into a parietal cell population (GFP) and all remaining cells (tdTomato) using a MoFlo FACS machine (Dako/Cytomation).

## Imaging and tissue analysis

Mouse tissues were immediately excised and flushed with phosphate-buffered saline and fixed overnight in 4% paraformaldehyde in PBS. Tissues were washed, embedded in 3% agar, and then underwent routine paraffin processing. Sections prepared for immunofluorescence or immunohistochemistry underwent standard deparaffinization and rehydration protocols, were blocked in 5% normal serum, and left overnight with primary antibodies. Sections were washed in phosphate-buffered saline and incubated for 1 h with secondary antibodies and then washed prior to mounting. For antibodies used in this study, see Appendix Table S2.

Immunofluorescence images were taken on a Zeiss Apotome or LSM710 confocal (Zeiss). Bright field images were taken on a Nanozoomer (Hamamatsu) whole slide scanner or DP70 microscope (Olympus). Counting of stomach cell populations and proliferation was done as previously described (Burclaff et al, 2017), except for analysis of *Gnptab*<sup>-/-</sup> mice. To account for frequent gland loss in the base of these mice, a different approach was taken. For chief cell quantification (SOX9<sup>+</sup> and BrdU<sup>+</sup>), 10 random, 20× fields were chosen in three *Gnptab*<sup>-/-</sup> and three control animals, and chief cells scored in slides from SOX9 or BrdU immunostained sections. For BrdU, distribution, the 10 fields were further subdivided into two rectangular regions: a basal one 100 μm perpendicular and 450 μm parallel to the muscularis mucosa and a region of the same size immediately adjacent and encompassing the neck of the gastric unit. All BrdU<sup>+</sup> cells were scored and the proportion in each zone calculated. Quantification of proliferation in the pancreas was done by counting 10 randomly sampled whole 20× fields per condition. Cathepsin D<sup>+</sup> area was calculated by generating a region of interest around PGC<sup>+</sup> zymogenic cell cytoplasm and using particle counting analysis in ImageJ (NIH) to calculate

Cathepsin D+ area relative to total cytoplasmic area. Tissue preparation and imaging for electron microscopy was done as previously described (Ramsey et al, 2007).

### Human tissue studies

Human gastric pathological tissue specimens were obtained with approval by the Institutional Review Board of Washington University School of Medicine. Figure 3A is a representative image from a qualitative analysis of 44 separate curated gastric clinical samples that have been previously described (Lennerz et al, 2010; Radyk et al, 2018). The study of tissue microarray cases included in this paper was also approved by the China Medical University First Hospital Institutional Review Board and Ethics Committee. This patient cohort was initially treated at the China First Medical University, and routine standard of care specimens was obtained from patients treated between 2005 and 2009. Tumor, metaplastic, and uninvolved normal tissue from each patient was formalin-fixed and paraffin-embedded. Staining was scored on the following scale: 0, no staining; 1, minimal staining; 2, moderate to strong staining in at least 20% of cells; 3, strong staining in at least 50% of cells. The scoring system was designed, and independently verified, by a human pathologist.

### Bioinformatics, microarray, qRT-PCR, and statistical analyses

For qRT-PCR and microarray analyses of mouse stomach  $\pm$ rapamycin, two independent experiments were run and a total of two to three separate mice and corresponding microarrays were generated for each condition. All mice were harvested 3 days after first injection and treated as per protocol in (Fig EV1). Conditions were Veh-Veh (rapamycin vehicle regimen + 3 days of tamoxifen vehicle), Veh-Tam (3 days of rapamycin vehicle regimen + 3 days of HD-

Tam), Rap-Veh (rapamycin regimen, 3 days of tamoxifen vehicle); Rap-Tam (rapamycin regimen + 3 days of HD-Tam). RNA for microarray and qRT-PCR analysis was isolated as previously described (Lo et al, 2017). For microarray, samples were processed and hybridized to Affymetrix Mouse Gene 2.0 ST per the manufacturer's instructions by the Washington University Genome Technology Access Core (GTAC). GeneChips were analyzed with Partek Genomic Suite 6.6 (Partek, Inc.) analysis software using default settings (Lo et al, 2017). Mapping to Gene Symbols was done either via GSEA (Subramanian et al, 2005) or GenePattern software (Reich et al, 2006). GSEA was done using default 3.0 settings. GMX files were made using previously published microarray data in the case of laser-capture micro-dissected chief cells (Capoccia et al, 2013), generated de novo or acquired from GSEA molecular signatures database. For the list of parietal cell-specific genes generated de novo for the current manuscript, flow cytometry was used to sort parietal cells and control cells into 500  $\mu$ l RNA protect reagent (Qiagen). RNA was isolated using the RNeasy Micro Kit (Qiagen) following the manufacturer's instructions. Mouse Gene 2.0 ST Array (Affymetrix) was used to analyze gene expression, and the gene set whose expression was enhanced at least eightfold (96 separate genes) in parietal cells vs. control was determined by Partek. For primers used in qRT-PCR, see Appendix Table S3. Statistics for cell counts and qRT-PCR were done by Student's t-test (in the case of pair-wise analysis of significance) or ANOVA (if multiple conditions were compared). For determining statistically significant differences among various conditions in ANOVA, the post hoc tests were either Tukey's (for multiple crosswise comparisons of means) or Dunnett's (for comparisons of multiple experimental samples to a single control). For the tissue microarray, a  $\chi^2$  analysis was performed.

## Western blot

Approximately 100 mg mouse corpus stomach tissue was lysed in urea buffer (8 M urea, 1% SDS, 150 mM Tris-HCl, pH = 7.0) with 1× protease/phosphatase inhibitor cocktail (Thermo). Protein concentration was determined using the DC protein assay (Bio-Rad). Protein (30 µg) was separated using a 10% SDS-PAGE gel and transferred to PVDF membranes (Millipore). Membranes were incubated overnight at 4°C with Rabbit polyclonal pS6 240/244 or 235/236 (1:1,000 diluted, CST) and Rabbit polyclonal beta-tubulin antibody (1:1,000 diluted, CST) and then incubated with infrared fluorescent dye-conjugated secondary antibodies (LI-COR Biosciences). Protein signal intensities were normalized against a tubulin loading control for each sample. Fluorescent intensity values were determined and quantified on Western blots at non-saturating exposures using the ImageJ software. Statistical analysis with both antibodies was done using ANOVA with a post hoc Dunnett's test.

## Chapter 2.5 FIGURES

### Figure 2.1

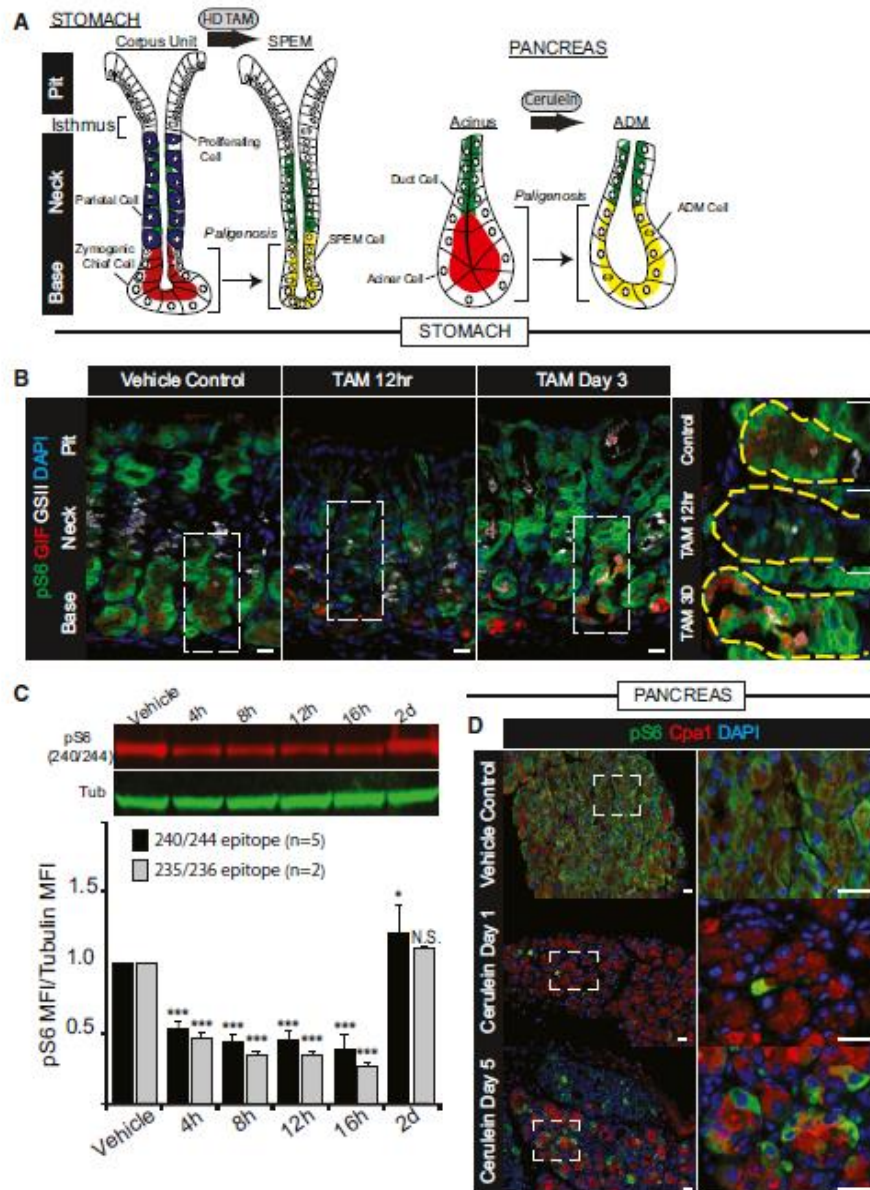


**Figure 1. mTORC1 activity undergoes dramatic changes during stomach and pancreas metaplastic injury response.**

A, B Digestive-enzyme-secreting (zymogenic) mature cell populations in the stomach (A) and pancreas (B) are recruited back into the cell cycle to fuel metaplasia in response to large-scale injury. Digestive enzyme expression (red) decreases, and markers of mucous neck cells (green, stomach) or duct cells (green, pancreas) increase in metaplastic, proliferating cells (red + green = yellow). Stomach is further characterized by loss of acid-secreting parietal cells (blue). (B) Representative epifluorescence images of mouse gastric corpus glands during homeostasis, early after injury (HD-Tam 12 h) and at maximal metaplastic response (HD-Tam Day 3), stained for mTORC1 activity using a downstream target, pS6 as a proxy. Green, pS6; red, GIF (gastric intrinsic factor, a chief cell marker); white, GSII (a mucous neck cell marker); blue, DAPI. Right—higher magnification images of boxed areas on left, focus exclusively on the base of the unit where the digestive-enzyme-secreting cells are reprogramming. Yellow dashed area outlines the base of a single gastric unit. Scale bar, 20  $\mu$ m; boxed area pull out, 10  $\mu$ m.

C Western blot of pS6 (red) and  $\beta$ -tubulin control (green) from whole corpus protein extracts at various injury time points; pS6 (240/244 or 235/6) vs. tubulin fluorescent intensity from replicate blots quantified below (error bars = standard deviation). \* $P < 0.05$ , \*\*\* $P < 0.001$ . Statistical analysis with both antibodies was done using ANOVA with a post hoc Dunnett's test.

D Representative epifluorescence images of pS6 staining of pancreas during homeostasis, acute injury (cerulein 12 h), and maximal injury (cerulein day 5). Green, pS6; red, amylase; blue, DAPI. Boxed areas on left depicted at higher magnification on right. Scale bar, 20  $\mu$ m; boxed area pull out, 10  $\mu$ m.

Figure 2.2

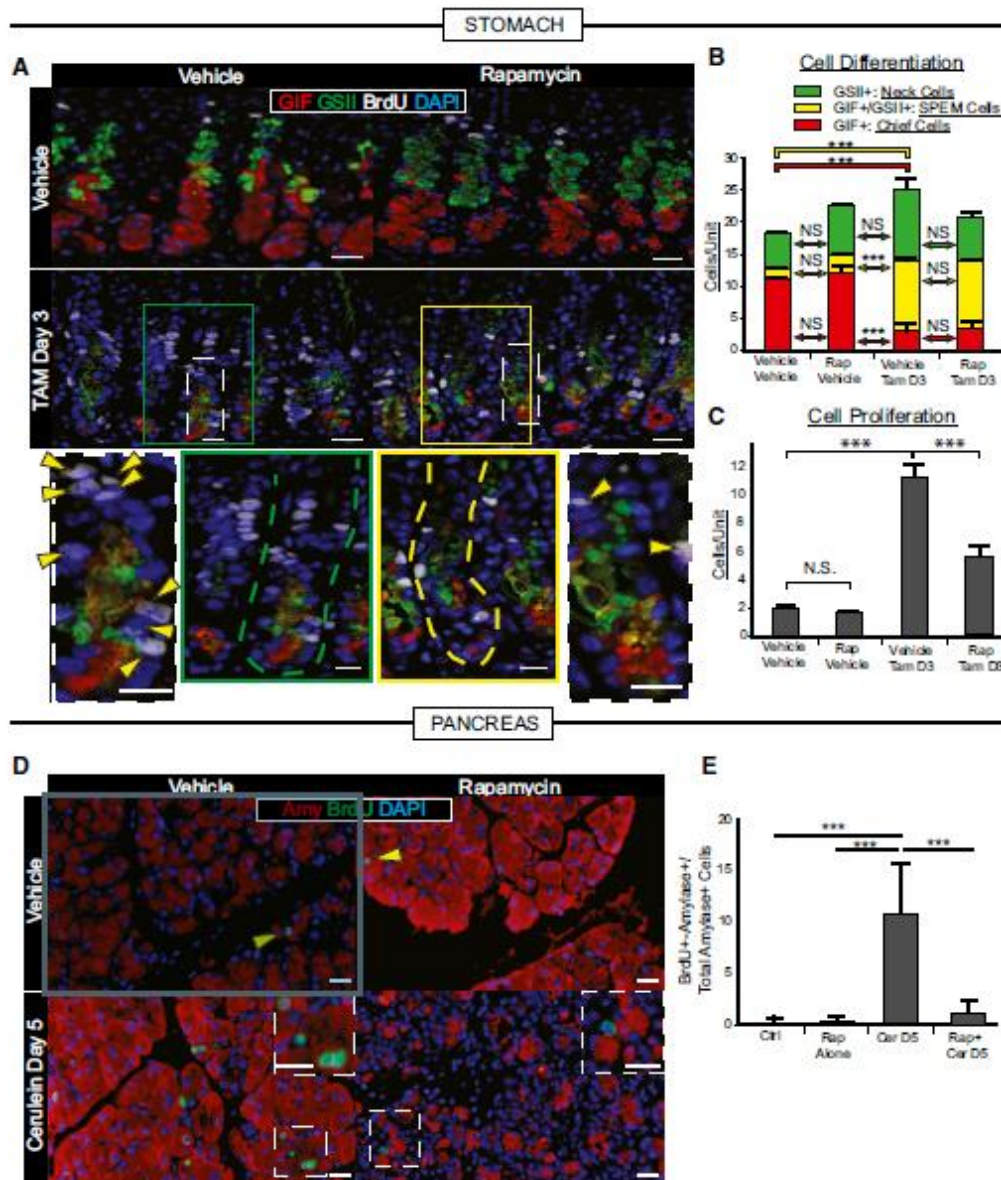
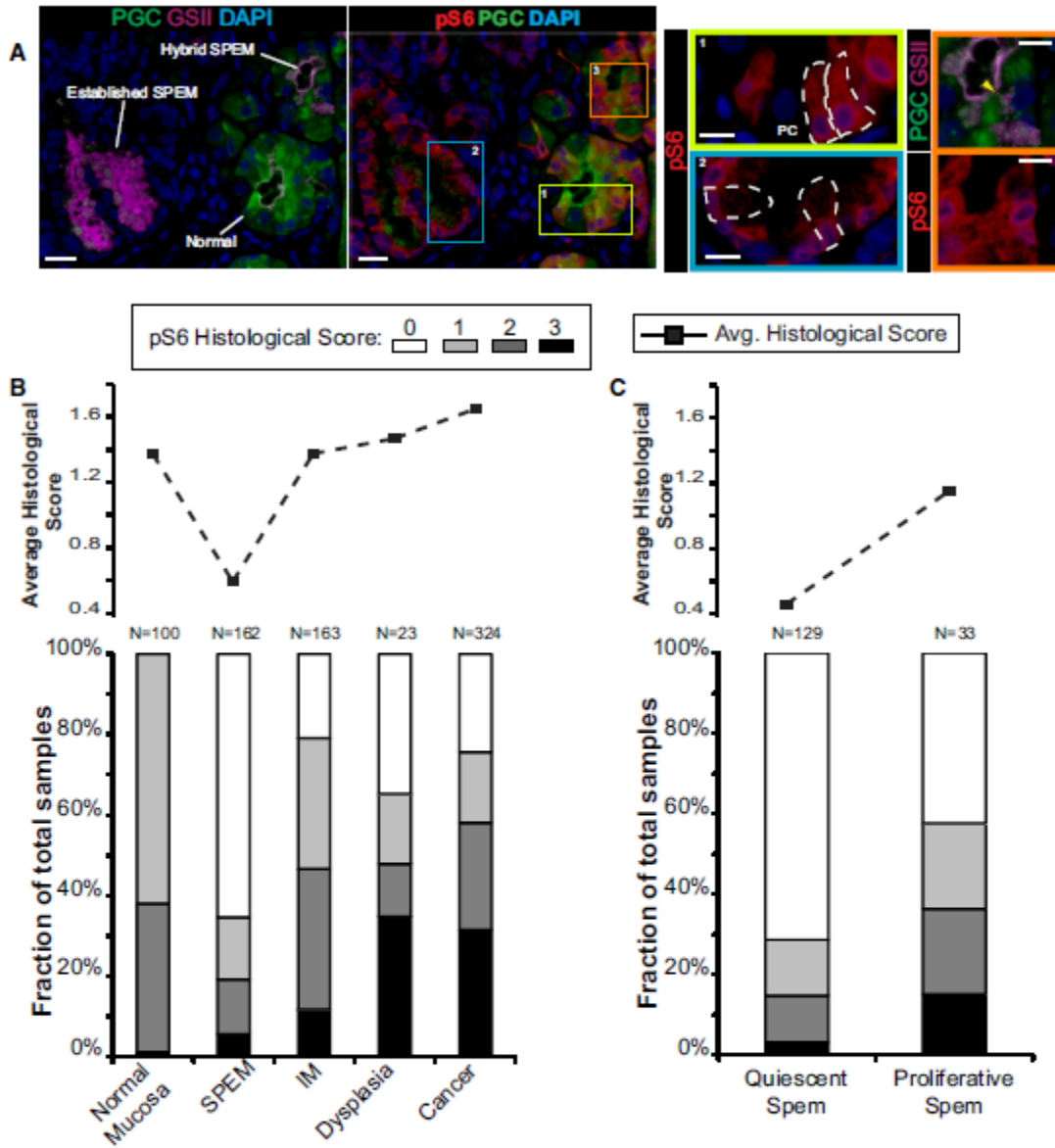


Figure 2. Recruitment of proliferating cells during stomach and pancreas metaplastic injury depends on mTORC1.

- A. Representative immunofluorescence images of stomach tissue  $\pm$  metaplastic injury  $\pm$  rapamycin treatment. Green, neck cells (GSII); red, chief cells (GIF); white, proliferating cells (BrdU); blue, nuclei (DAPI). Scale bars 20  $\mu$ m; 10  $\mu$ m for bottom images. Bottom—boxed areas from top pictures are shown at higher magnification with individual bases of gastric units (where reprogramming occurs) outlined by dashed lines and proliferating cells by arrowheads.
- B. Cells of each differentiation type, following scheme in Fig 1A, are quantified by scoring immunofluorescence images from multiple experiments. Metaplastic injury induces a massive accumulation of yellow (SPEM) cells and loss of red (Chief) cells (compare vehicle-vehicle with vehicle-Tam, D3) that is not significantly affected by rapamycin treatment (compare vehicle-Tam D3 with Rap-Tam D3).
- C. Proliferative cells are quantified as for panel (B). Injury induces massive proliferation (compare vehicle-vehicle with vehicle-Tam D3) significantly inhibited by rapamycin (compare vehicle-Tam D3 with Rap-Tam D3).
- D. Top panel arrowheads indicate rare proliferative acinar cells during homeostasis with or without rapamycin treatment. Cerulein induces proliferation of acinar cells recruited into the cell cycle that is inhibited by rapamycin. Boxed areas are magnified in insets. Note multiple BrdU<sup>+</sup> cells (green) staining with amylase (red) a digestive enzyme, indicating an acinar cell origin. BrdU<sup>+</sup> cells following rapamycin + cerulein treatment are often not co-stained with amylase. Blue, DAPI (nuclei). Scale bars 20  $\mu$ m; 10  $\mu$ m for insets.
- E. Quantification of multiple experiments with mice treated as in panel (D).

Data information: \*\*\*P < 0.001; N.S. = not statistically significant; data displayed as mean  $\pm$  SEM from 3 independent experiments with quantification from up to 13 low-power fields, from each of 4–5 total mice; significance determined by ANOVA with Tukey's post hoc test.

**Figure 2.3**



**Figure 3. mTORC1 activity correlates with stages of metaplasia during human gastric tumorigenesis.**

- A** Immunofluorescent images of human gastric tissue from a patient with intestinal-type gastric adenocarcinoma elsewhere. In this non-carcinoma containing region of the gastric corpus, various states of metaplasia can be observed that reflect mouse injury models. Extensive previous work (Lennerz *et al.*, 2010) of a dataset of such resection specimens and of biopsies showing SPEM in a non-cancer setting has indicated likely stages of progression of SPEM from essentially normal wherein large, pyramidal-columnar cells at the base express only chief cell markers like pepsinogen C (PGC, green) to "hybrid SPEM" (yellow arrowhead, inset) where smaller, cuboidal columnar cells label with varying degrees of PGC and the neck/SPEM cell marker GSII (purple) to "established SPEM" characterized by cells that label extensively with GSII and have scant PGC; established SPEM cells are mucus-stuffed, with peripheral, basal, flattened nuclei (blue, DAPI). Higher magnification of each cellular phenotype is shown by color-coded box on right. As parietal cells are lost in SPEM, the remnant one in the yellow boxed area (labeled "PC") is consistent with the normal chief cell phenotype (representative individual cells outlined by white dashed lines). Note that there is consistently high expression of pS6 (red) throughout the cytoplasm of such normal chief cells but that this pS6 varies in the hybrid SPEM lesion and is largely scaled down in the established SPEM region (note pS6 only around the nuclei of these cells). Scale bar; 20  $\mu$ m; pullouts 10  $\mu$ m.
- B** Analysis of a human gastric tissue microarray with normal, metaplastic, and cancer tissue all represented from patients with resections for gastric cancer. Serial tissues sections of the array were stained by immunohistochemistry with pS6 or Ki67, counterstained with hematoxylin, and visually graded by blinded observers, supervised by a human pathologist, for staining intensity (from score 0 meaning undetectable to 3 most intense). *Top*—average histological score is plotted for each phenotype. *Bottom*—the relative fraction of tissue cores with each score is plotted (total scores of each type provided at the top of each column).
- C** Given the biphasic nature of the SPEM histological score and given that established SPEM, as observed in panel (A), shows decreased pS6, we separated all the SPEM lesions into Ki-67<sup>+</sup> ("proliferative") and Ki-67<sup>-</sup> ("quiescent") and replotted as for panel (B).

**Figure 2.4**

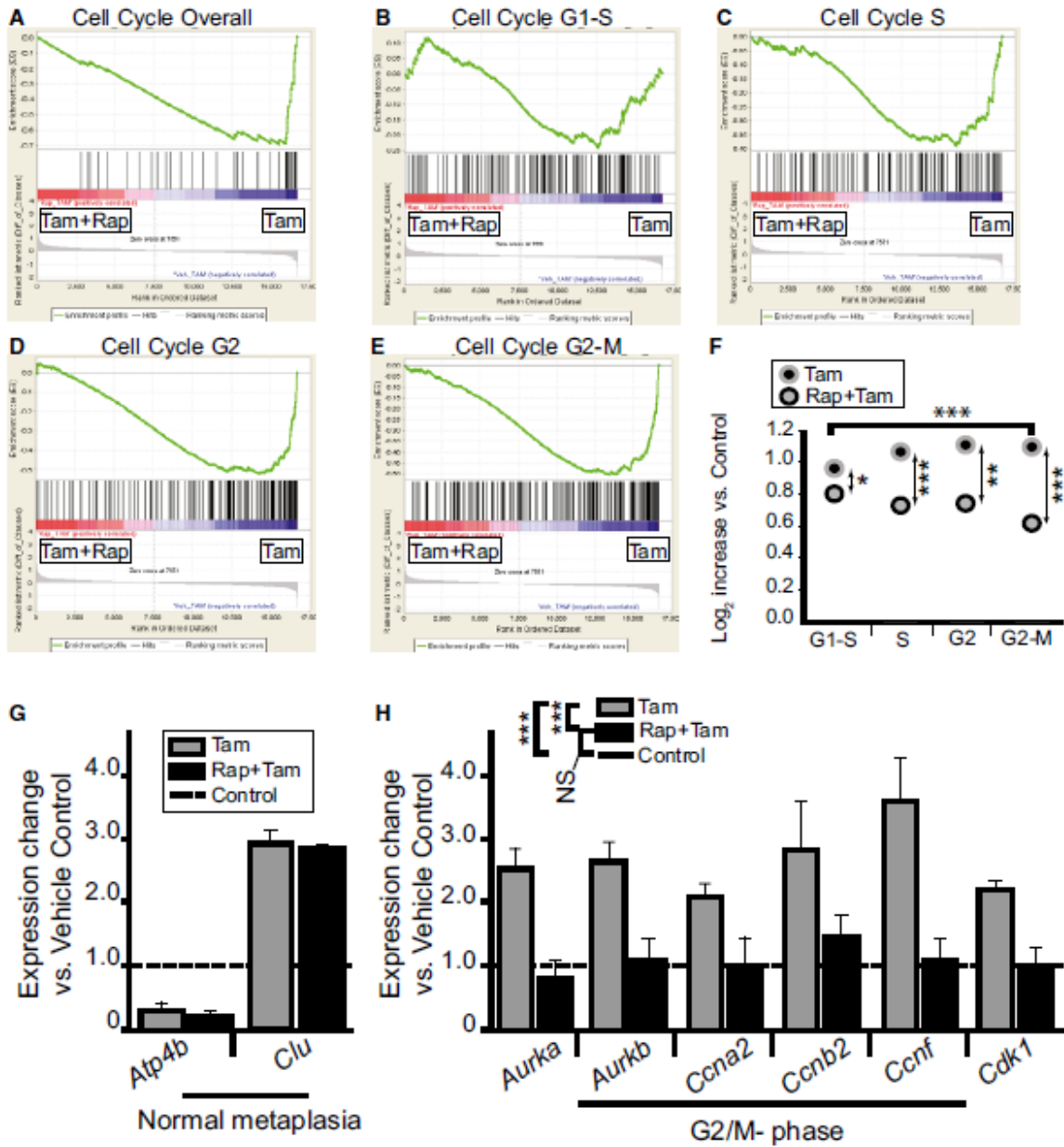


**Figure 4. mTORC1 activity is required predominately for progression through S-, G2-, and M-phases during metaplastic induction of proliferation.**

A-E Microarrays of stomach corpora at D3 ± HD-Tam ± rapamycin were analyzed using GSEA "Difference of Classes" function comparing rapamycin + HD-Tam ("Tam+Rap") vs. rapamycin vehicle + HD-Tam ("Tam"). Whitfield Gene Sets specific for either overall cell cycle genes or specific phases of cell cycle are depicted. Note that rapamycin correlates with decreased cell cycle gene expression that is largely due to decreased S-G2 phase gene expression.

F The dot plots are of the actual average expression levels (in rapamycin + HD-Tam and HD-Tam alone Genechips) of the top 20 genes enriched in various Whitfield Gene Sets GSEA comparisons of HD-Tam vs. vehicle controls (both without rapamycin). Expression levels of HD-Tam and HD-Tam + rapamycin for all genes were normalized to expression level in vehicle control Genechip to facilitate plotting and expressed as Log<sub>2</sub>, such that 1 = 2-fold enriched vs. control. Note that average expression of G1-phase genes is only somewhat reduced by rapamycin (by t-test of Tam vs. Rap-Tam, \**P* < 0.05, \*\*\**P* < 0.01; \*\*\*\**P* < 0.001), whereas later phases of the cell cycle are substantially reduced (decrease in G2/M-phase relative to G1-phase by ANOVA with Dunnett's *post hoc* test is \*\*\*\**P* < 0.001).

G, H qRT-PCR of select transcripts. Control genes known to be increased or decreased in SPEM (G) and genes associated with specifically with G2-M cell cycle phase (H). Expression was normalized to housekeeping gene *Tbp*, then vehicle control samples for each gene were set at 1, and HD-Tam and HD-Tam + rapamycin expression was normalized to the control sample (statistics for the entire set of cell cycle genes among the different treatments are shown in legend. \*\*\*\**P* < 0.001 by ANOVA with Tukey's *post hoc* test; data represented as mean ± SEM of the means from 3 replicates from a total of 3 independent experiments).

Figure 2.5

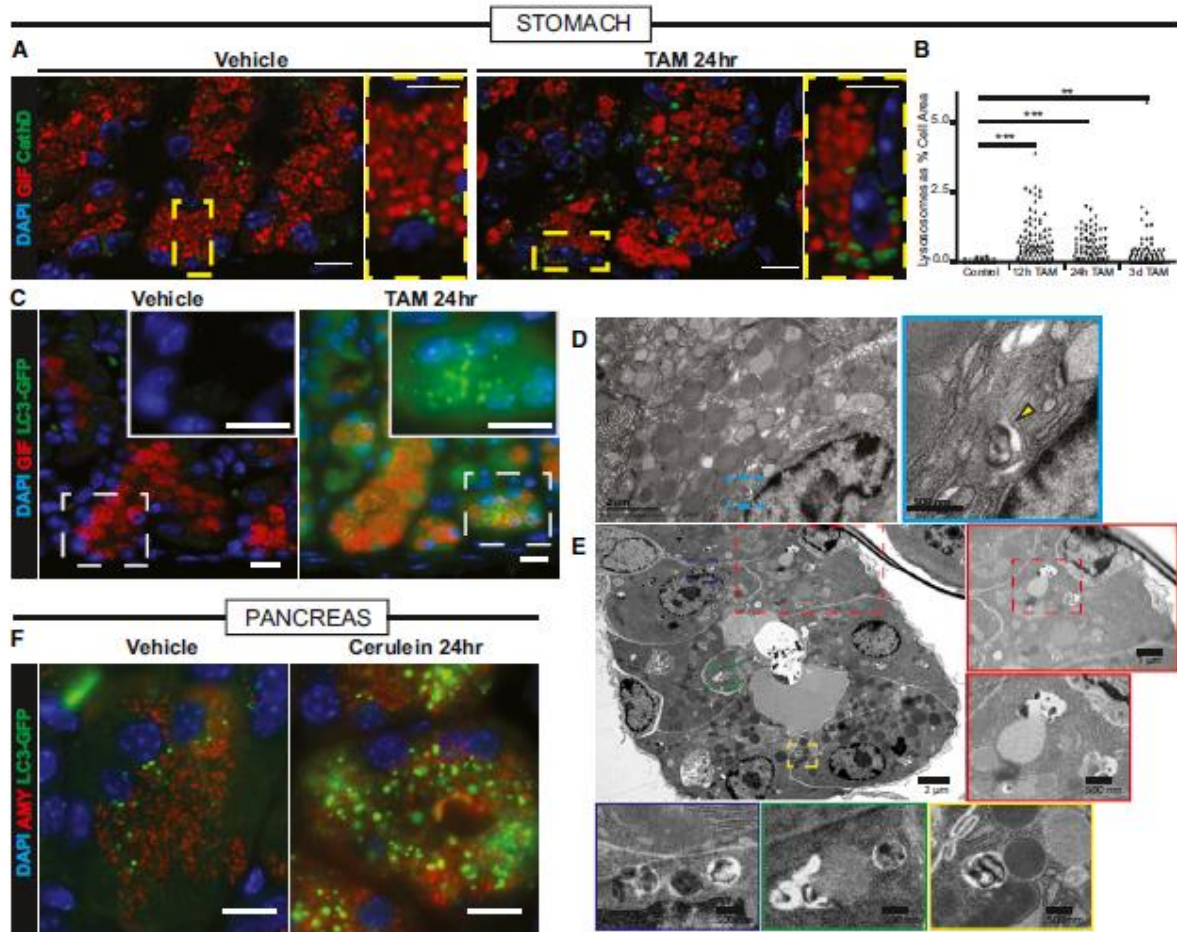


**Figure 5. Lysosomal and autophagic pathways are upregulated acutely following stomach and pancreas injury.**

**A** Injured zymogenic cells upregulate Cathepsin D<sup>+</sup> puncta (green) 24 h follow HD tamoxifen. Red, chief cells (GIF); blue, nuclei (DAPI). Boxed areas are shown at higher magnification at right of each panel. Scale bars 20  $\mu$ m; 10  $\mu$ m for pullouts.

**B** Quantification of Cathepsin D<sup>+</sup> area in chief cells at various stages following injury. \*\* $P < 0.01$ ; \*\*\* $P < 0.001$  by ANOVA with Dunnett's post hoc test. Each datapoint is an individual counted cell.

**C** LC3 puncta (detected by GFP fluorescence in *Lc3-gfp* mice) shows increased autophagosomal puncta paralleling Cathepsin D<sup>+</sup> results. Green, LC3-GFP; red, GIF; blue, DAPI. Boxed areas are shown at higher magnification and differing fluorescence channels in insets. Scale bars 20  $\mu$ m.

**D** Transmission electron micrographs of a normal zymogenic cell. Yellow arrowhead indicates a rare lysosome seen during homeostatic conditions.

**E** Transmission electron micrographs of corpus units 24 h follow tamoxifen injury. Various selected pullouts highlight double membrane-bound structures attacking cytosolic components in reprogramming chief cells.

**F** Acinar cells in pancreas have increased LC3-GFP<sup>+</sup> puncta following acute injury with cerulein. Green, LC3-GFP; red, GIF; blue, DAPI. Scale bar 20  $\mu$ m.

Figure 2.6

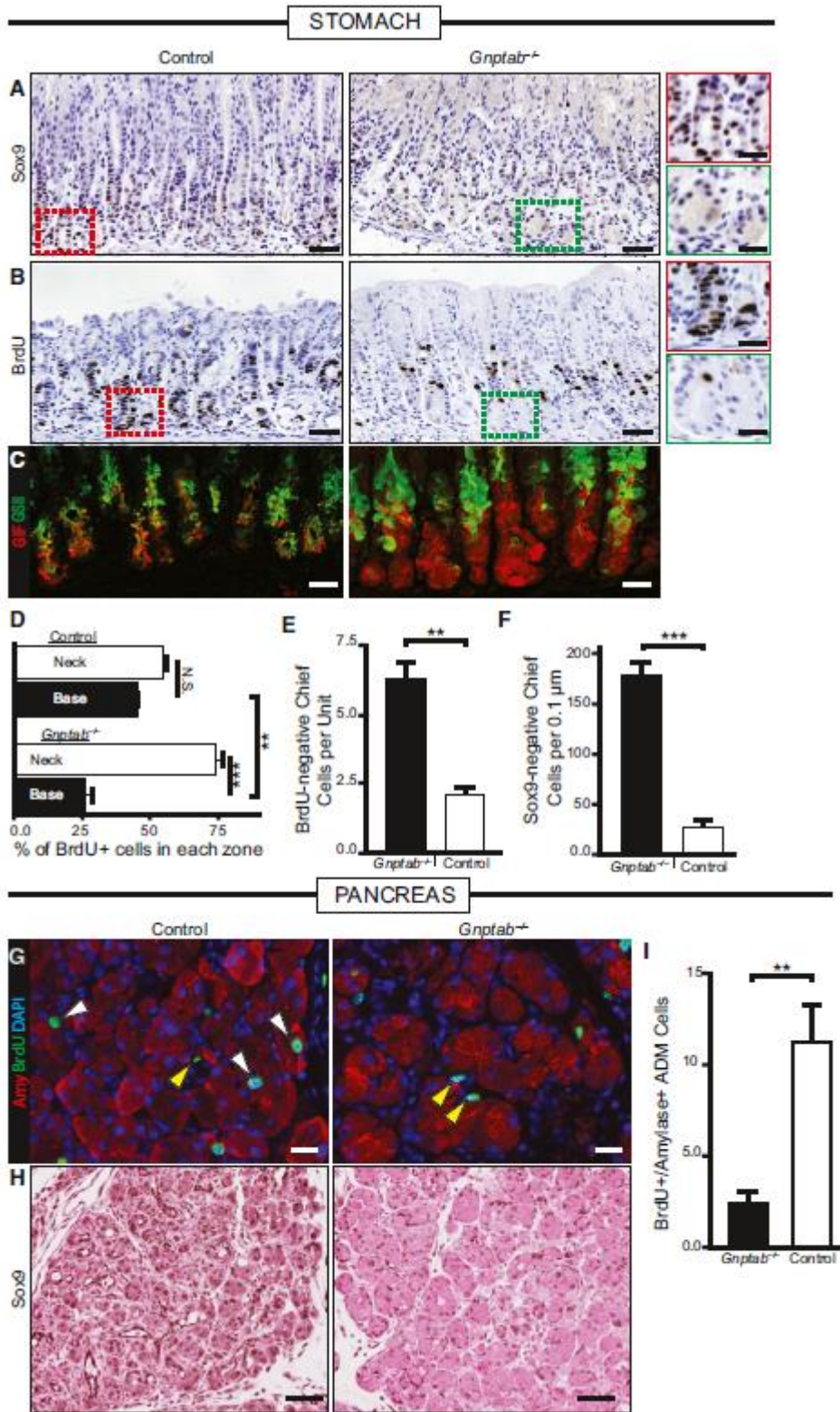


Figure 6.

◀ **Figure 6. Lysosomal function is required for metaplasia-associated gene expression and increased proliferation.**

- A Immunohistochemical analysis of SOX9 expression at peak SPEM stages following gastric injury. In control and *Gnptab*<sup>-/-</sup> mice, SOX9 becomes expressed in reprogramming chief cells in the bases of the corpus at SPEM stages, but not in *Gnptab*<sup>-/-</sup> mice. Color-coded boxes shown at higher magnification shown at right for panels (A and B). Scale bar, 50  $\mu$ m; 25  $\mu$ m pullout.
- B S-phase, cell cycle marker BrdU is incorporated throughout the gastric corpus unit at peak SPEM stages in control WT or *Gnptab*<sup>-/-</sup> mice. In *Gnptab*<sup>-/-</sup> mice, the gastric unit bases, where proliferation is recruited from chief cells, show a marked relative deficit in BrdU<sup>+</sup> cells. Scale bar, 50  $\mu$ m; 25  $\mu$ m pullout.
- C Immunofluorescence analysis of injured gastric tissue from *Gnptab*<sup>-/-</sup> and control mice. GIF/GSII co-expression is the hallmark of SPEM. In control mice, the vast majority of corpus unit bases are converted to GIF/GSII co-expression state. In *Gnptab*<sup>-/-</sup> mice, bases are resistant to conversion and remain as GIF single positive cells. Red, GIF; green, GSII. Scale bar, 20  $\mu$ m.
- D Quantification of randomly sampled 20 $\times$  fields stained with BrdU. Distribution of BrdU in neck region vs. base region (note total = 100%) is plotted. Note control mice have equivalent amounts of BrdU-labeled cells in the neck and base (~50% in each), whereas *Gnptab*<sup>-/-</sup> mice BrdU-labeled cells substantially shifted away from the paligenetic base of units and into the isthmal-neck region, where the constitutive stem cell is active.
- E Quantification of randomly sampled 20 $\times$  fields stained with BrdU in control and *Gnptab*<sup>-/-</sup> mice. *Gnptab*<sup>-/-</sup> mice have significantly more BrdU-negative base cells compared to control animals.
- F Quantification of control and *Gnptab*<sup>-/-</sup> corpus units stained for SOX9 scored for the amount of SOX9-negative chief cells per unit at peak SPEM stages. *Gnptab*<sup>-/-</sup> mice have significantly more SOX9-negative bases compared to control animals.
- G Representative immunofluorescence images of injured control and *Gnptab*<sup>-/-</sup> pancreatic tissue at cerulein 5 days. Red, amylase; green, BrdU; blue, DAPI. White arrows show proliferating, amylase<sup>+</sup> acinar-derived cells (note these are not seen in *Gnptab*<sup>-/-</sup> mice). Yellow arrowheads show proliferating stromal cells that are not affected by loss of GNPTAB. Scale bar, 20  $\mu$ m.
- H Representative immunohistochemistry of SOX9 stained control and *Gnptab*<sup>-/-</sup> pancreatic tissue at cerulein 5 days. *Gnptab*<sup>-/-</sup> tissue has reduced metaplastic phenotype and reduced expression of SOX9. Scale bar, 50  $\mu$ m.
- I Quantification of amylase<sup>+</sup>BrdU<sup>+</sup> cells of control and *Gnptab*<sup>-/-</sup> tissue in randomly sampled 20 $\times$  fields at 5 days of cerulein injury.

Data information: \*\*P < 0.01; \*\*\*P < 0.001 by t-test with unequal variance; data represented as mean  $\pm$  SEM of the means from 10 low-power fields each from 3 independent experiments.

Figure 2.7

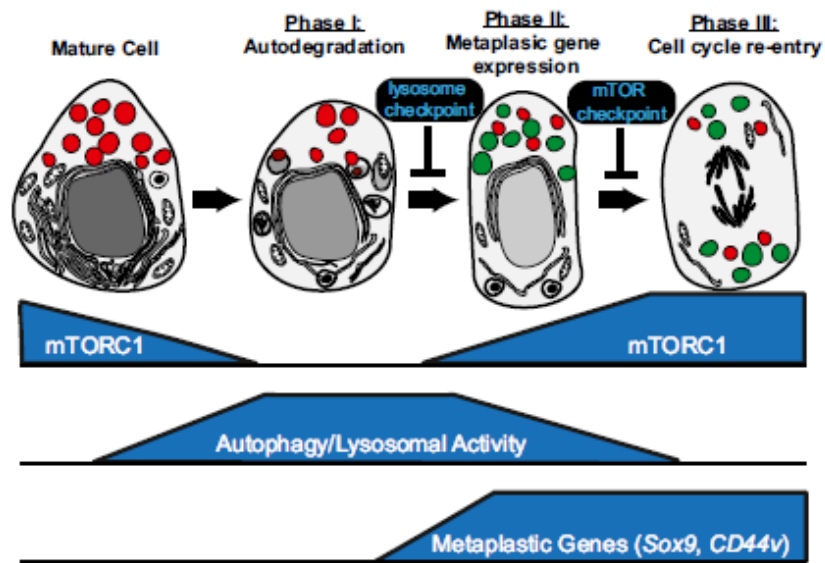
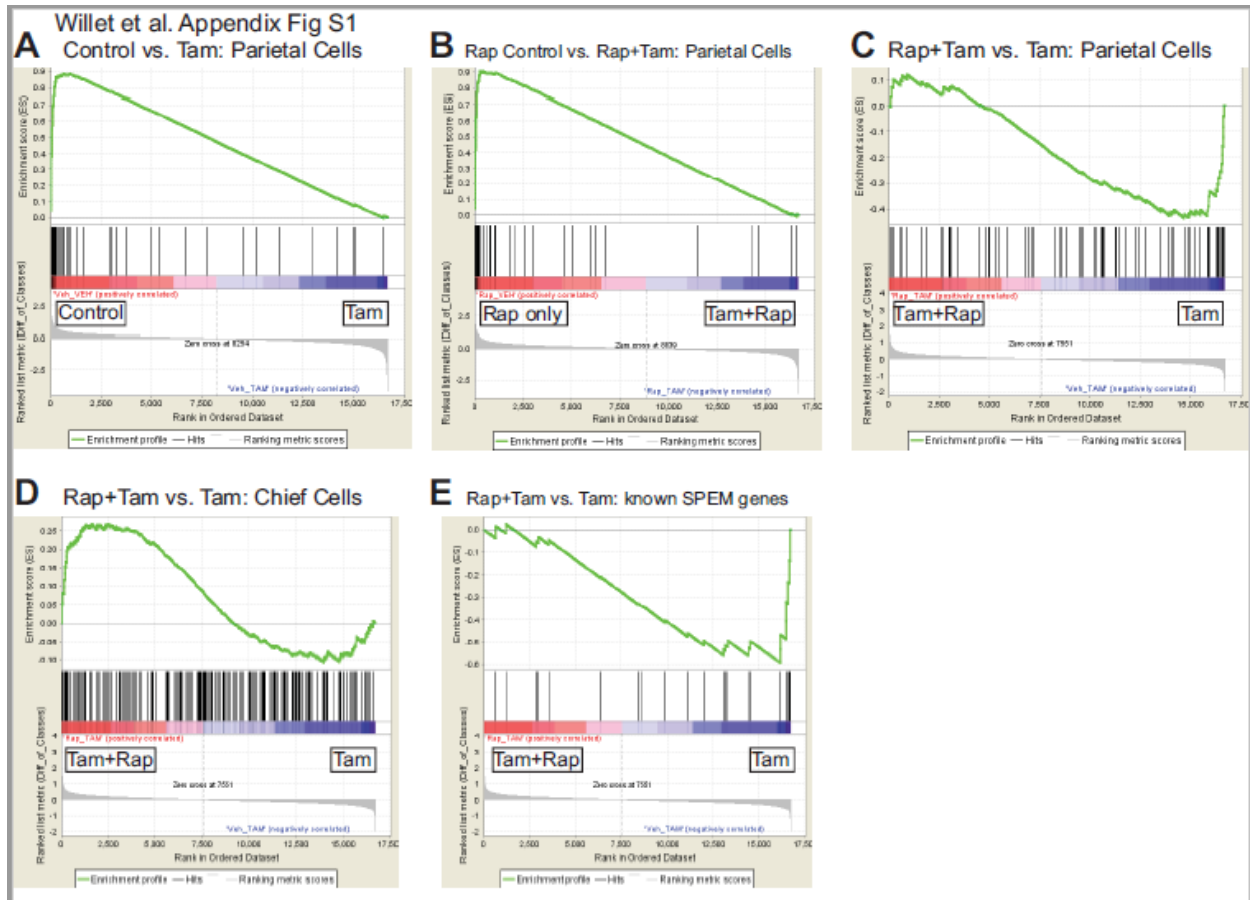


Figure 7. Schematic model of shared program: paligenosis.

Data presented in the paper suggest that differentiated cells revert to a regenerative/proliferative state via a program involving stepwise progression through three stages. Progression can be blocked at intervening checkpoints. The potential context-independent nature of this sequence of structural-energetic changes suggests that it is available to differentiated cells in multiple organs and species. We have termed this general program of differentiated cells acquiring regenerative potential "paligenosis".

## Appendix Figure S2.1



**Appendix Figure S1 - GSEA of microarray data shows that Rapamycin does not affect injury induced changes in parietal and chief cell gene expression but causes aberrant expression of a cohort of genes typically induced in SPEM.**

**A, B** GSEA and Genechip analyses were performed as for Fig.4, except panels **A** and **B** depict comparisons of a parietal cell specific gene set performed by flow cytometric purification of parietal cells (see Methods) with panel **A** showing how parietal cell gene expression is greatly enriched in vehicle control vs. HD-Tam and panel **B** showing that adding rapamycin with or without HD-Tam does not affect this pattern.

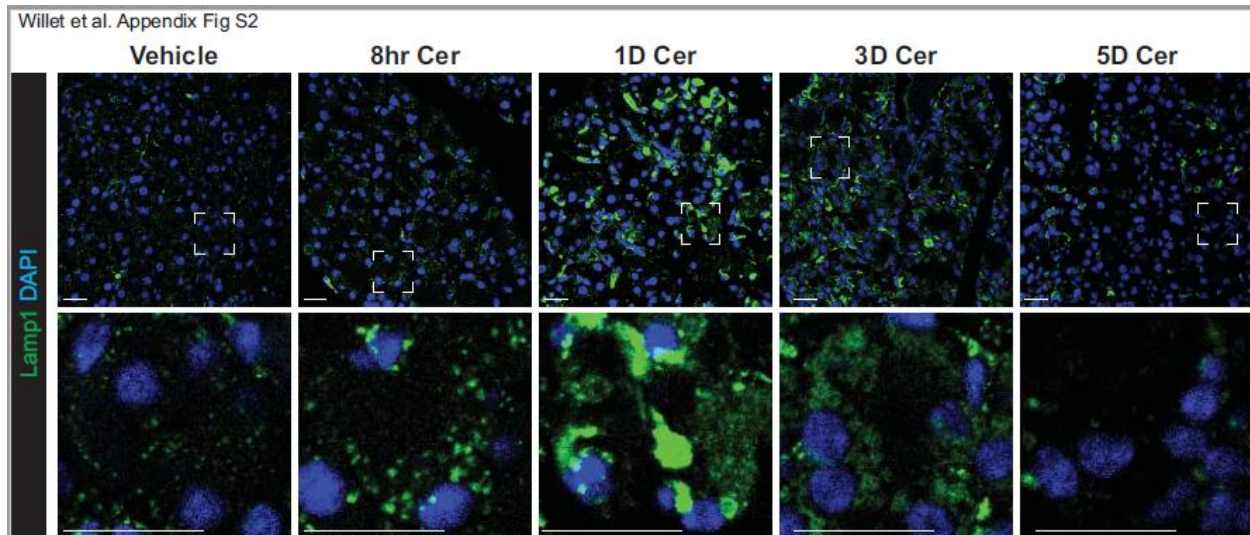
**C** Direct comparison of rapamycin+HD-Tam vs. HD-Tam shows that loss of parietal cell gene

expression after HD-Tam treatment is not affected by rapamycin; if anything, rapamycin causes even more parietal cell injury as there is some enrichment of parietal cell gene expression in HD-Tam alone.

**D** Previously published chief cell-specific gene set also shows no relative enrichment in HD-Tam vs. HD-Tam+rapamycin, indicating chief cell paligenosis is not affected by rapamycin.

**E** On the other hand, a previously published SPEM gene set shows enrichment in a specific subcluster of genes in HD-Tam vs. HD-Tam+rapamycin, indicating rapamycin blocks induction of a certain subset of SPEM genes. IM, intestinal metaplasia; pSPEM, proliferative SPEM; qSPEM, quiescent SPEM.

## Appendix Figure S2.2

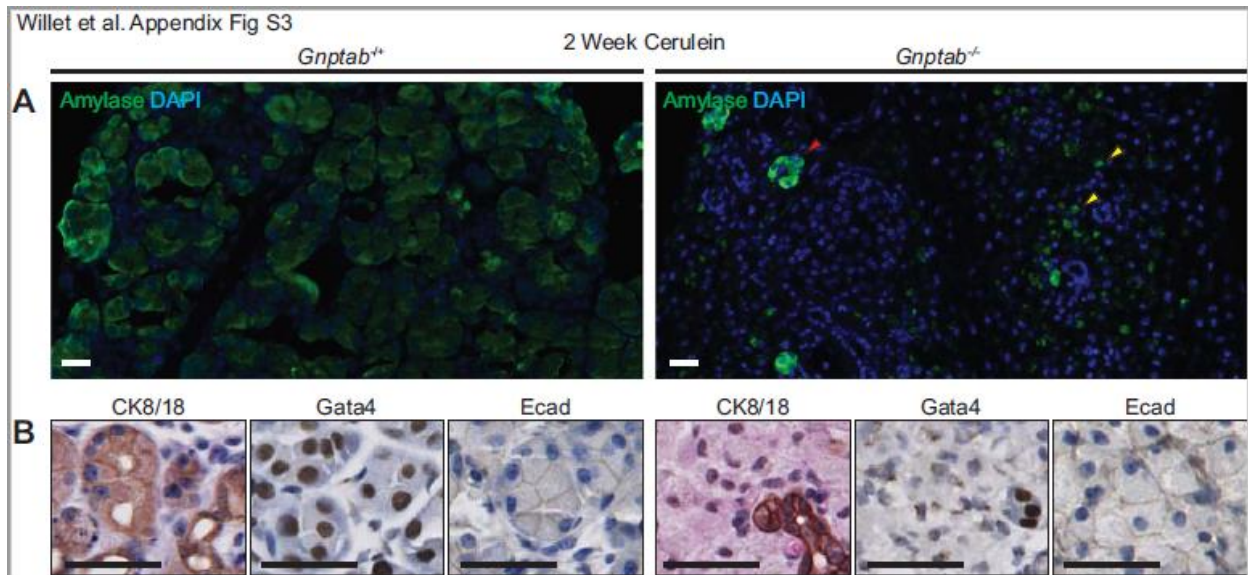


**Appendix Figure S2 - LAMP1 time course during cerulein injury shows a pattern of increased then decreased activation similar to that of stomach.**

Upon injury LAMP1 vesicles are induced in acinar cells starting around 8 hours and peak around 24 hours. By 3 to 5 days, the vesicles in exocrine cells begin to decrease back towards levels seen at homeostasis. Boxes in top panels are magnified to highlight acinar cells in bottom panels.

Scale bars:20  $\mu$ m

## Appendix Figure S2.3

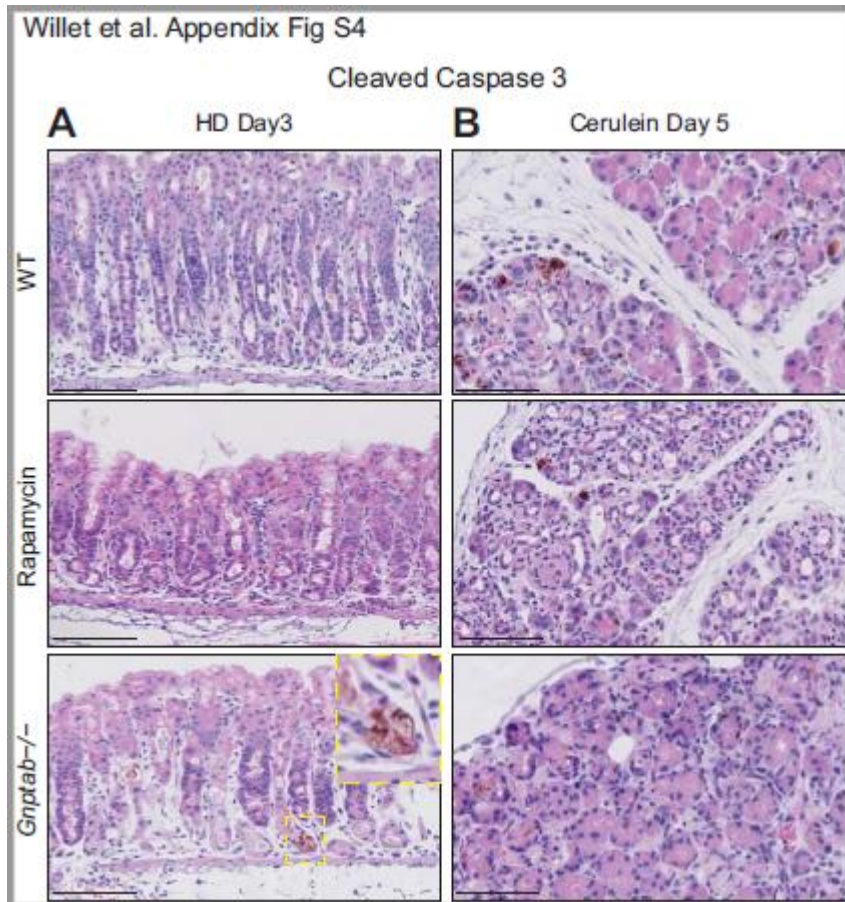


### Appendix Figure S3 - *Gnptab*<sup>-/-</sup> acinar cells after 2 week cerulein treatment remain cryptically acinar.

**A** Comparison of amylase staining between *Gnptab*<sup>-/-</sup> and *Gnptab*<sup>+/+</sup> following 2 weeks of cerulein treatment. In *Gnptab*<sup>-/-</sup> tissue, only scattered acinar cells remain highly positive for amylase (red arrowhead), with the vast majority only retaining weak positivity (yellow arrowheads). Scale bar: IF, 20  $\mu$ m; IHC, 50  $\mu$ m.

**B** Survey of metaplasia (CK8/18), mature acinar (GATA4), and epithelial markers (E-cadherin) on *Gnptab*<sup>-/-</sup> tissue. *Gnptab*<sup>-/-</sup> acinar tissue does not stain for the metaplasia marker CK8/18 or the mature acinar nuclear marker Gata4. The poorly differentiated acinar cells are positive for E-cadherin. Scale bar: IF, 20  $\mu$ m; IHC, 50  $\mu$ m.

## Appendix Figure S2.4



### Appendix Figure S4 - Apoptotic cells death during HD tamoxifen or cerulein-induced injury.

**A** At HD tamoxifen day 3 with or with rapamycin treatment, the stomach epithelium lacks apoptotic cells, indicating the main atrophy stage – in which parietal cells, but not chief cells, die by apoptosis – occurred earlier. In *Gnptab*<sup>-/-</sup> tissue, apoptotic cells can be found located at the base of some units consistent with the increased dropout of basal cells described in the results.

Scale bar, 100  $\mu$ m.

**B** During Cerulein at day 5, scattered apoptotic cells are seen in all experimental conditions, indicating the atrophy in this more asynchronous injury model is still occurring during this time window. No qualitative increase in cleave caspase positive cells were seen in rapamycin or *Gnptab*<sup>-/-</sup> tissue. Scale bar, 100 μm.

Appendix Table S2.1

**Appendix Table S1: Patient Demographics**

<b>Total Sample Number</b>	772
Normal Mucosa	100
SPEM	162
IM	163
Dysplasia	23
Cancer	324
Age Range	25-84
Average Age	64
<b>Gender</b>	
Male	448
Female	324

Appendix Table S2.2

<b>Appendix Table S2: Antibodies</b>			
<b>Antibody Table</b>			
<b>Antibodies</b>	<b>Company</b>	<b>Application</b>	<b>Dilution</b>
BrdU	DHSB (G3G4)	IF,IHC	1:500
GIF	Gift, David Alpers, WashU	IF	1:250
Ezrin	Santa Cruz (sc-58758)	IF	1:1000
pS6 240/244	Cell Signaling (D68F8)	IF,IHC,WB	1:500
pS6 235/236	Cell Signaling (57.2.2E)	IF,WB	1:100
Pgc	Abcam (ab 31464)	IF	1:500
Cpa1	R&D Systems (AF2765)	IF	1:250
Amylase	Sigma-Aldrich (A8273)	IF	1:250
Sox9	Millipore (ABE571)	IHC	1:1000
GSII	Molecular Probes (L32451)	IF	1:250
Lamp1	DHSB (1D4B)	IF	1:500
Cathepsin D	Santa Cruz (sc- 6486)	IF	1:1000
$\beta$ tubulin	Abcam (ab21057)	WB	1:1000
Ki67	Abcam (ab15580)	IHC	1:500
CK8/18	Abcam (ab194130)	IHC	1:1000
Gata4	Santa Cruz (sc-9053)	IHC	1:500
E-Cadherin	BD Biosciences (610182)	IHC	1:250

Appendix Table S2.3

**Appendix Table S3: qRT-PCR Primers**

Primers Name	Sequence 5' to 3'
Atp4b F	CAGGAGAAGAAGTCATGCAGC
Atp4b R	GAAACCTGCGTAGTACAGGCT
Clu F	CCAGCCTTTCTTTGAGATGA
Clu R	CTCCTGGCACTTTTCACACT
Aurka F	TCTAGAATATGCGCCCCTTG
Aurka R	CCGTTTGAGCCAAGCAGTA
Aurkb F	GAAGAAGAGCCGTTTCATCG
Aurkb R	TCCGACTCTTCTGCAGTTCC
Ccna2 F	CTTGTAGGCACGGCTGCTAT
Ccna2 R	AGCCAAGTCAAAGCAAGGA
Ccnb2 F	CCAAATCCGAGAAATGGAGA
Ccnb2 R	GCCACCTGAGAAGGATGGTA
Cdk1 F	CTGGGCAGTTCATGGATTCT
Cdk1 R	TCGGTATTCCAAACGCTCTG
Ccnd1 F	TTGACTGCCGAGAAGTTGTG
Ccnd1 R	CTGGCATTTTGGAGAGGAAG
TBP F	CAAACCCAGAATTGTTCTCCTT
TBP R	ATGTGGTCTTCCTGAATCCCT

EXPANDED VIEW FIGURE 2.1

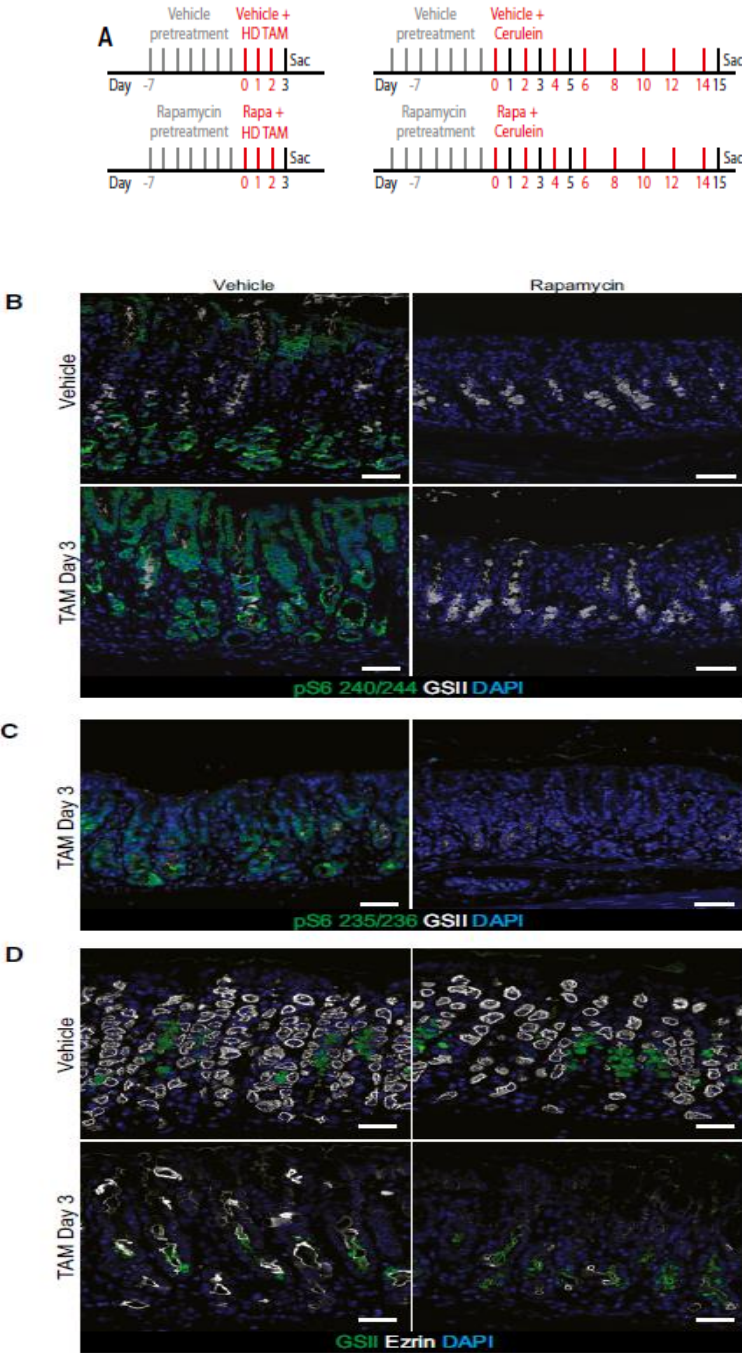


**Figure EV1.** pS6 is an accurate proxy for rapamycin-sensitive mTORC1 activity and shows that loss of mTORC1 does not affect parietal cell death or induction of metaplastic gene expression in reprogramming chief cells. A Injection schemes for injury experiments with rapamycin in stomach (left) and pancreas (right). B Representative epifluorescence images of the distribution of pS6 in the normal and injured stomach rapamycin treatment. pS6 is restricted to the chief cell zone (base) and pit zone of the normal corpus unit. At peak (HD-Tam day 3) SPEM stages, it is located at high level throughout the unit. Upon rapamycin treatment, all pS6 staining is lost throughout the normal and injured corpus unit. The characteristic induction of GSII staining in reprogramming chief cells at the base of gastric units (indicating SPEM) occurs at least as markedly in the presence of rapamycin, indicating mTORC1 is not required for metaplastic gene induction. Green, pS6; white, GSII; blue, DAPI. Scale bars: 50  $\mu$ m. C At peak metaplasia stages, pS6 235/6 is upregulated in the stomach epithelium and rapamycin treatment at this stage abolishes all staining. Scale bars: 50  $\mu$ m. D Representative epifluorescence images of the loss parietal cells (marked by ezrin) upon injury and rapamycin treatment. Treatment with HD-Tam caused the loss of the vast majority of parietal cells throughout the corpus. Rapamycin does not rescue that injury. Green, GSII; white, ezrin; blue, DAPI. Scale bars: 50  $\mu$ m.

EXPANDED VIEW FIGURE 2.2

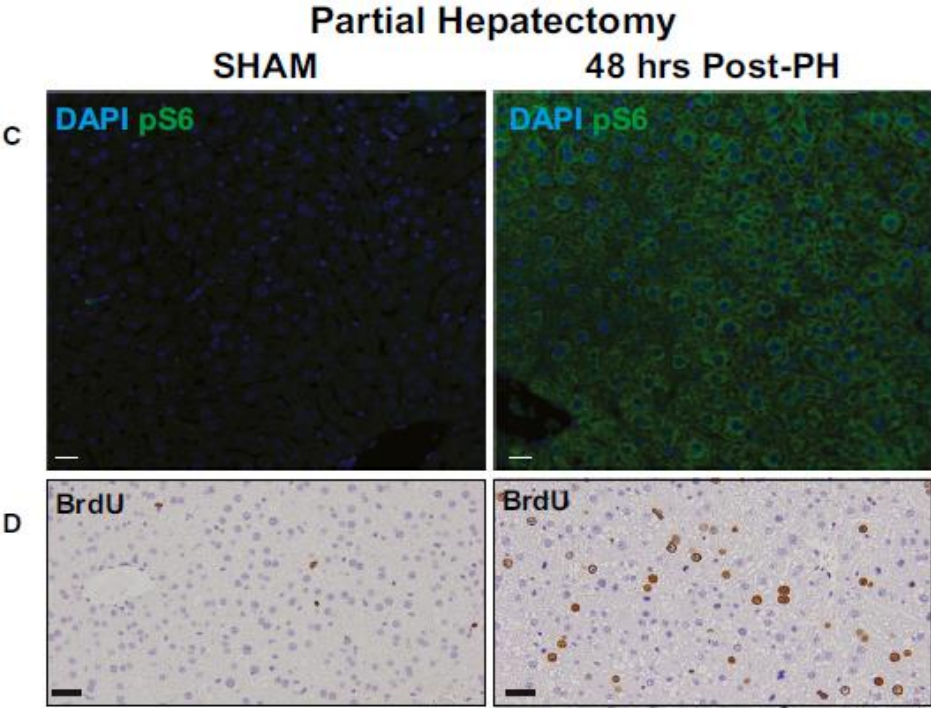
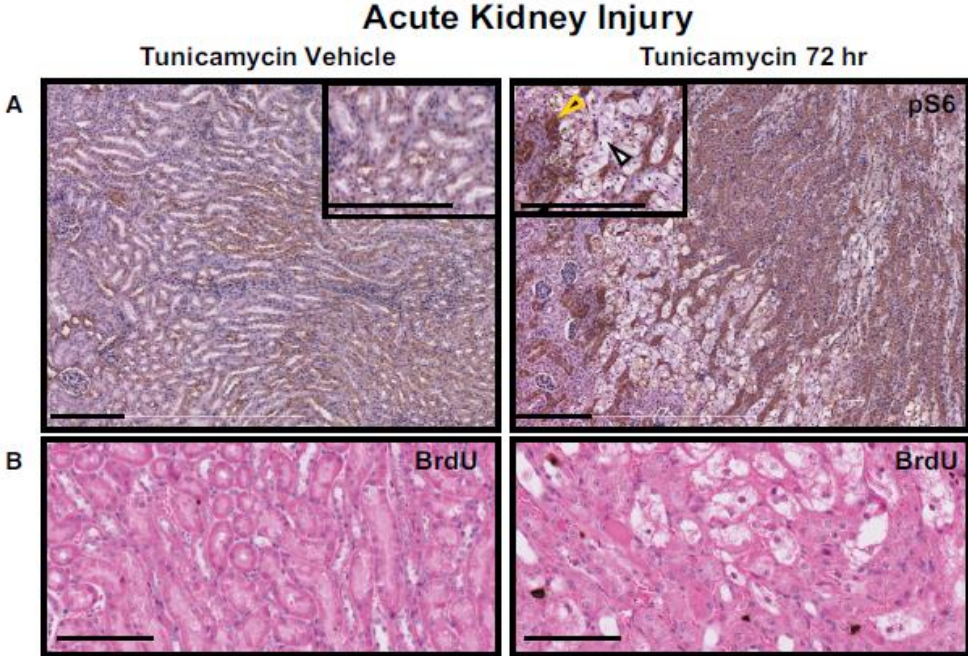


**Figure EV2.** Acute kidney injury and partial hepatectomy both cause upregulation of mTORC1 activity during proliferative phases.

A Upon injury with tunicamycin, tubule cells in the kidney are damaged (white arrowhead) and surviving tubule cells (yellow arrowhead) upregulate pS6. Scale bars: 100  $\mu\text{m}$ .

B Upregulation of the pS6 is associated with increased proliferation in this injury model as seen by BrdU+ nuclei. Scale bars: 100  $\mu\text{m}$ .

C Two-thirds partial hepatectomy causes a pronounced upregulation of pS6 in the remaining hepatocyte mass. Scale bars: 20  $\mu\text{m}$ .

D The pS6+ hepatocytes are highly proliferative at this stage. Scale bars: 20  $\mu\text{m}$ .

EXPANDED VIEW FIGURE 2.3

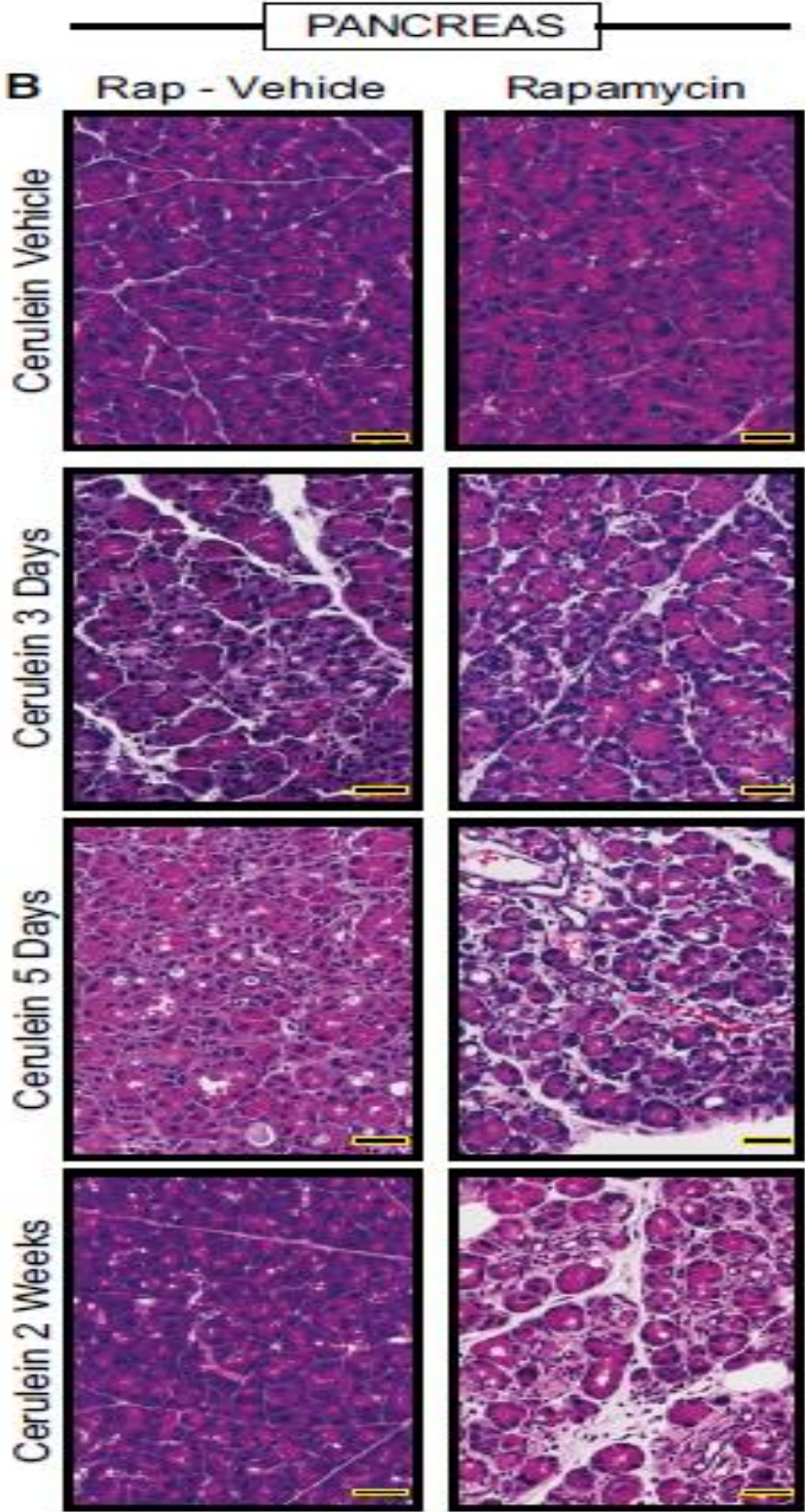


**Figure EV3.** Histological changes in the injured stomach and pancreas with and with rapamycin treatment.

A Representative hematoxylin and eosin counterstained images of HD-TAM stomach tissue rapamycin. Treatment with tamoxifen causes acute loss of parietal cells (large eosinophilic cells) by 12–24 h post-injury. By 3 days, chief cells have reprogrammed into SPEM cells. The general pattern of loss of parietal cells and conversion of chief cells to metaplastic cells is not affected by rapamycin (right panels). Scale bars, 50  $\mu\text{m}$ .

B Representative hematoxylin and eosin counterstained images of pancreas tissue injured with cerulein at various stages rapamycin. Cerulein injury causes mosaic, asynchronous conversion of acinar cells into proliferative, acinar-ductal metaplastic cells with maximal features of the process at day 5 in our protocol. By 2 weeks, the pancreas has compensated for the continuous injury and recovers a relatively normal morphology. Dual treatment with rapamycin and cerulein does not rescue the metaplastic response by day 5 and impedes normal tissue compensation by 2 weeks injury, with most of the tissue continuing to show abundant metaplastic forms. Scale bars, 50  $\mu\text{m}$ .

EXPANDED VIEW FIGURE 2.4

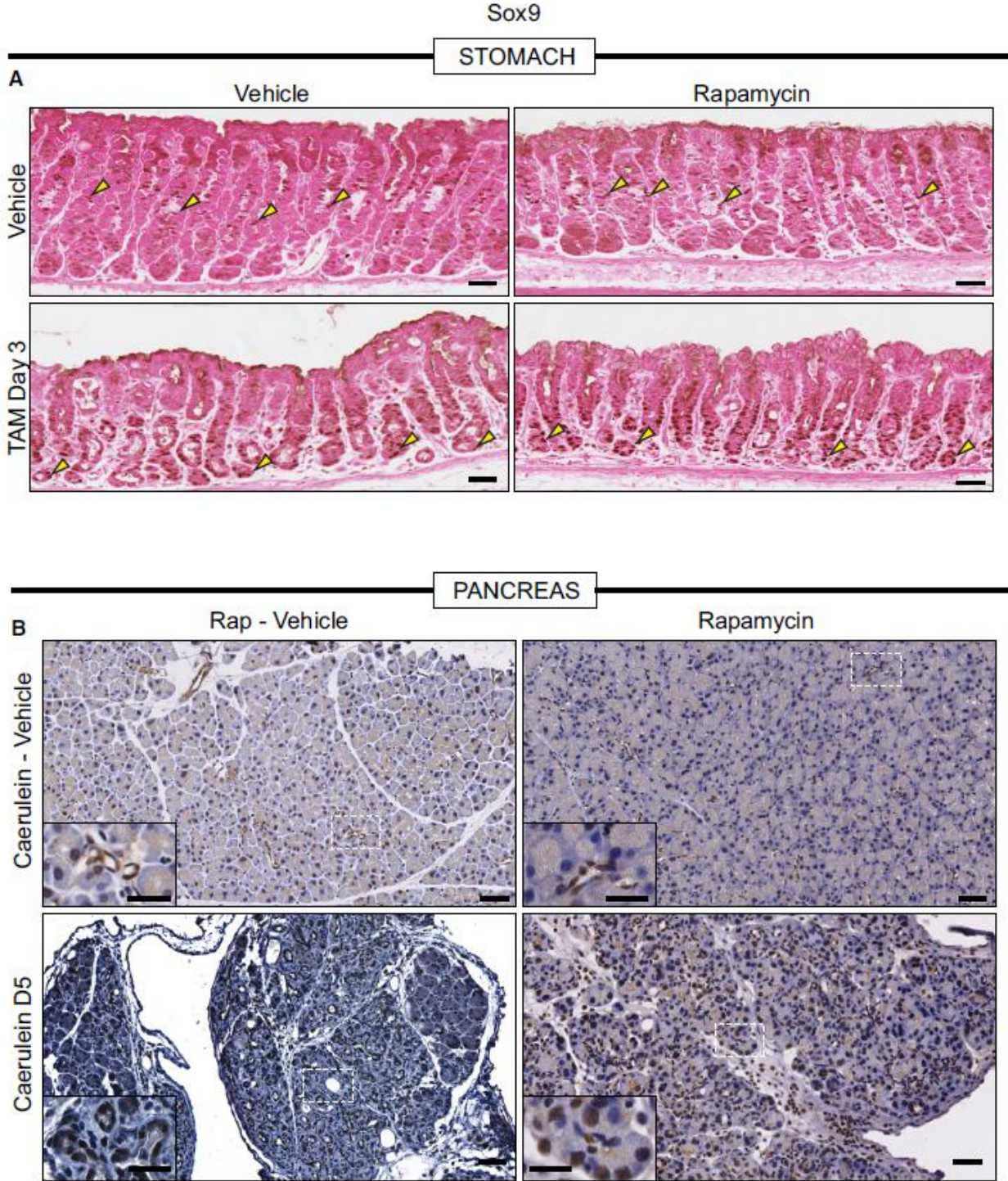


**Figure EV4.** mTORC1 is not required for increased SOX9 during metaplasia.

A Representative eosin counterstained IHC images of normal or metaplastic gastric tissue stained for SOX9. SOX9, in control tissue, stains the isthmal and mucous neck cells, which are proliferative progenitors (yellow arrowheads), of the corpus units and is generally excluded from the base of units. Upon injury with HD-TAM, SOX9 expression is induced in the base of units (yellow arrowheads). Treatment with rapamycin does not alter either the normal or metaplasia distribution of SOX9 (yellow arrowheads). Scale bars, 50  $\mu\text{m}$ .

B Representative hematoxylin counterstained IHC images of normal or metaplastic pancreatic tissue stained for SOX9. SOX9 expression in normal pancreatic tissue is restricted to the duct (see inset in top left panel which is a high magnification view of the boxed area). At peak metaplasia stages, SOX9 becomes expressed in dedifferentiating acinar cells (see bottom left inset). Treatment with rapamycin in normal (see top right inset) or injured (see bottom right inset) does not alter SOX9 expression. Scale bars 50  $\mu\text{m}$ ; inset 25  $\mu\text{m}$ .

EXPANDED VIEW FIGURE 2.5

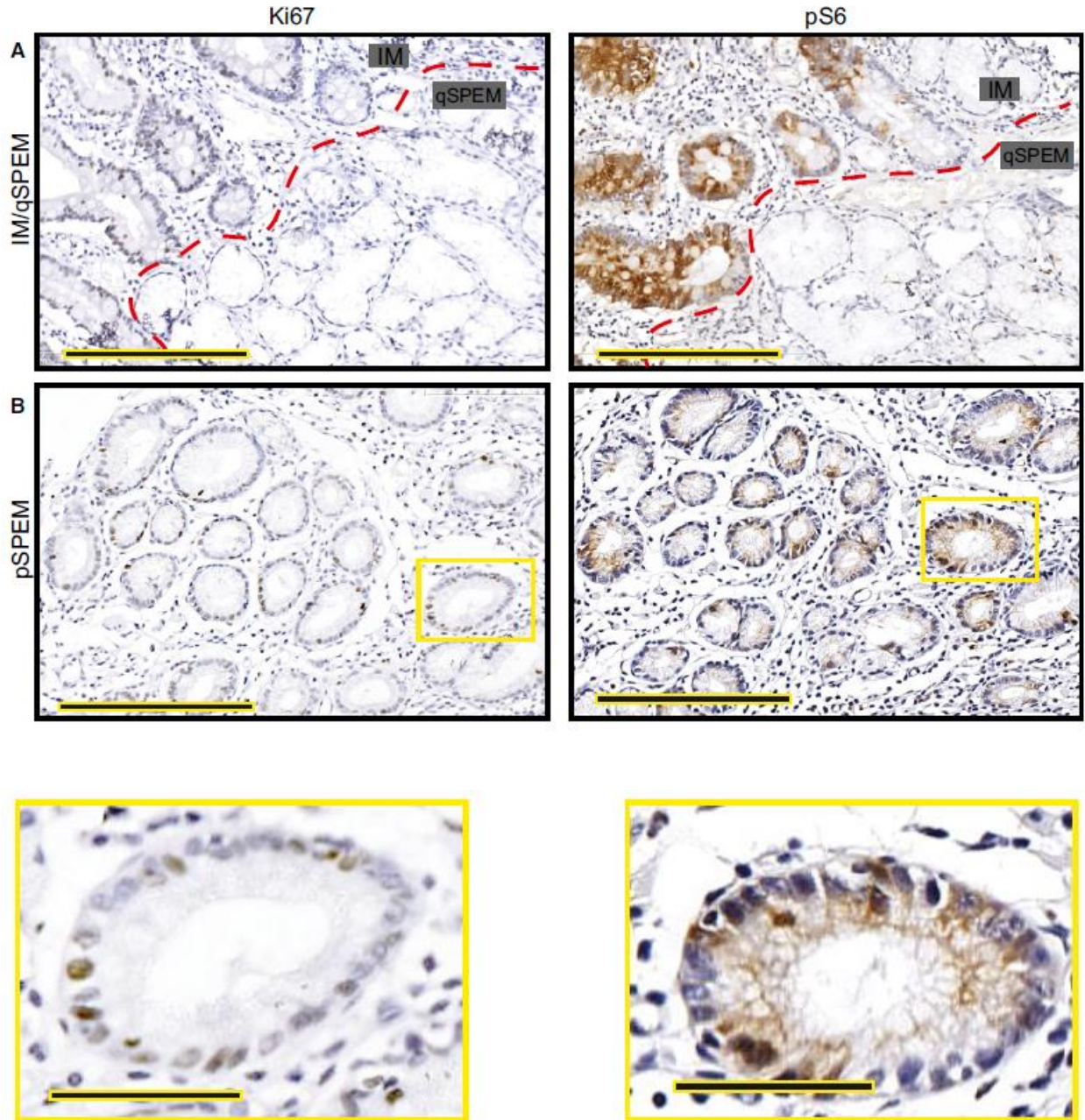


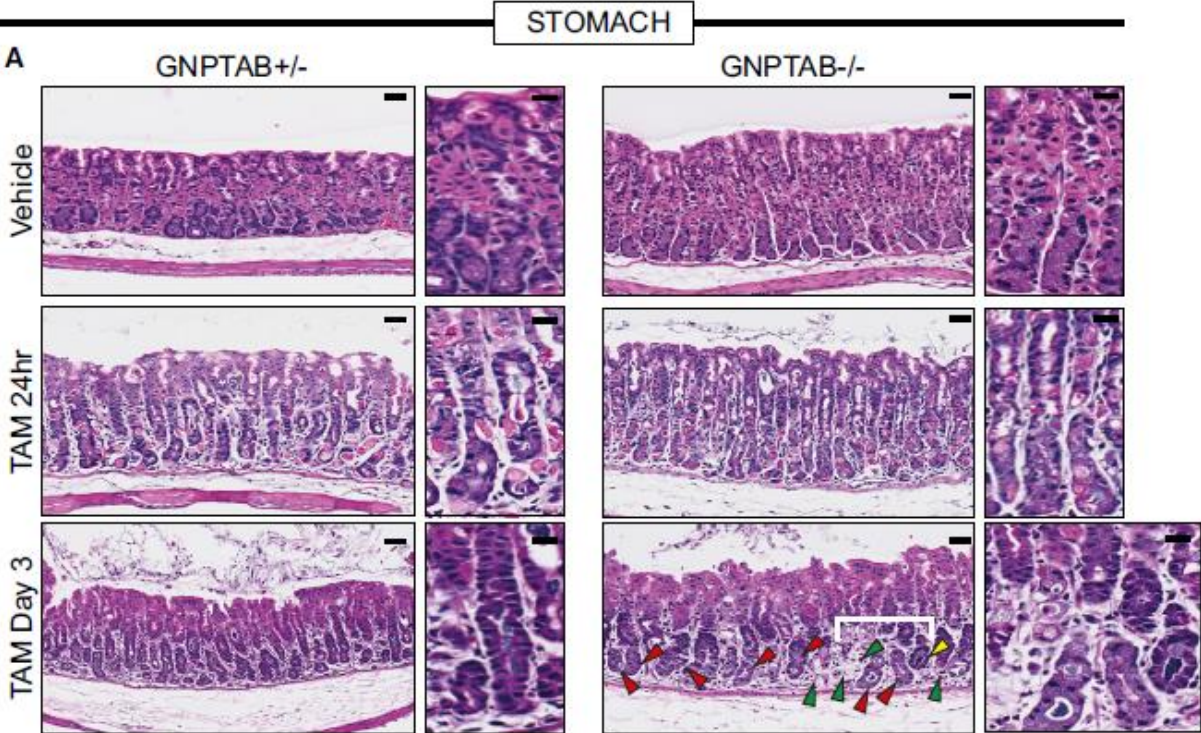
**Figure EV5.** Representative IHC images from human tissue microarray.

A Intestinal metaplasia (“IM” indicating the glands to upper left of red dashed line) is generally proliferative as evinced by frequent Ki-67+ cells (left) and is strongly pS6 positive. Most SPEM

has a quiescent phenotype (glands labeled on “qSPEM” side of panels) characterized by cells with abundant mucus, flattened basal nuclei, and a lack of both Ki-67 and pS6 staining Scale bar, 200  $\mu\text{m}$ .

B Rare SPEM lesions show cells with cuboidal columnar morphology. These lesions show Ki-67 positivity usually associated with pS6 positivity. Boxed regions are shown at higher magnification below. Scale bar, 200  $\mu\text{m}$ ; pullout, 50  $\mu\text{m}$ .

EXPANDED VIEW FIGURE 2.6



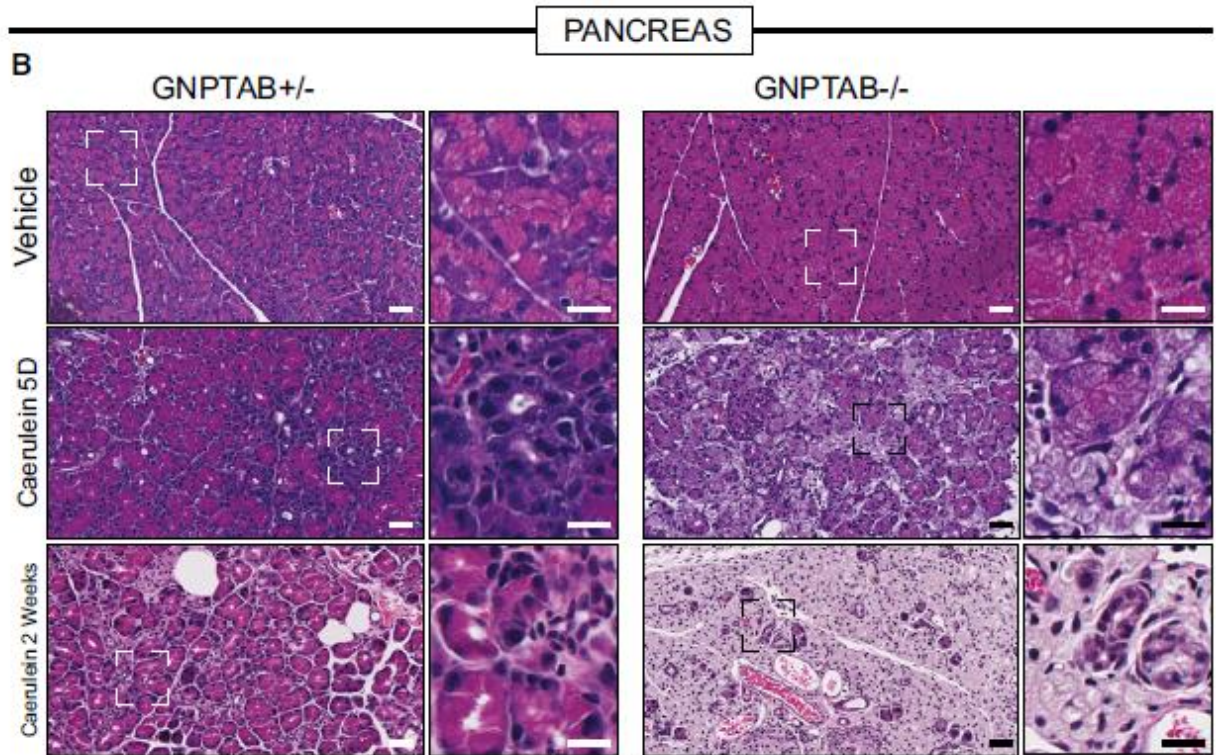


**Figure EV6.** Histological appearance of *Gnptab*<sup>-/-</sup> stomach and pancreas tissue at injury time points.

A Representative hematoxylin and eosin counterstained images of *Gnptab*<sup>+/-</sup> and *Gnptab*<sup>-/-</sup> stomach tissue. *Gnptab*<sup>-/-</sup> chief cell cytoplasm has a hypertrophic, frothy appearance compared to control zymogenic cells. Loss of parietal cells (fried-egg appearing eosinophilic cells) following HD-Tam is not affected by loss of GNPTAB; however, the base zones in *Gnptab*<sup>-/-</sup> mice at day 3 HD-Tam are usually resistant to dedifferentiation (red arrowheads) with large, frothy chief cells remaining largely non-reprogrammed. Another, less common phenotype is that all chief cells are lost such that most of the base of the unit disappears (green arrowheads). Rare units partially undergo morphological metaplastic changes, though usually those are also associated with loss of basal cells (yellow arrowheads). Higher magnification

views are to right of each panel, with white bracket delineating particular region of interest in  $Gnptab^{-/-}$  stomach Scale bar 50  $\mu\text{m}$ ; pullout, 25  $\mu\text{m}$ .

B Representative hematoxylin and eosin counterstained images of  $Gnptab^{-/+}$  and  $Gnptab^{-/-}$  pancreas. Similar to the stomach zymogenic cells, pancreatic acinar cells also have a hypertrophic, frothy appearance. Whereas control samples treated with cerulein show diffuse, asynchronous acinar-to-ductal metaplasia,  $Gnptab^{-/-}$  mice have acinar cells that simply become less eosinophilic and foamy over time without undergoing ADM. By 2 weeks, wild-type pancreas has largely adapted to cerulein, whereas  $Gnptab^{-/-}$  pancreas parenchyma comprises only lobules of excessively pale (hyaline), frothy acinar cells and scattered reactive ducts. Scale bar 50  $\mu\text{m}$ ; pullout, 25  $\mu\text{m}$ .

EXPANDED VIEW FIGURE 2.7

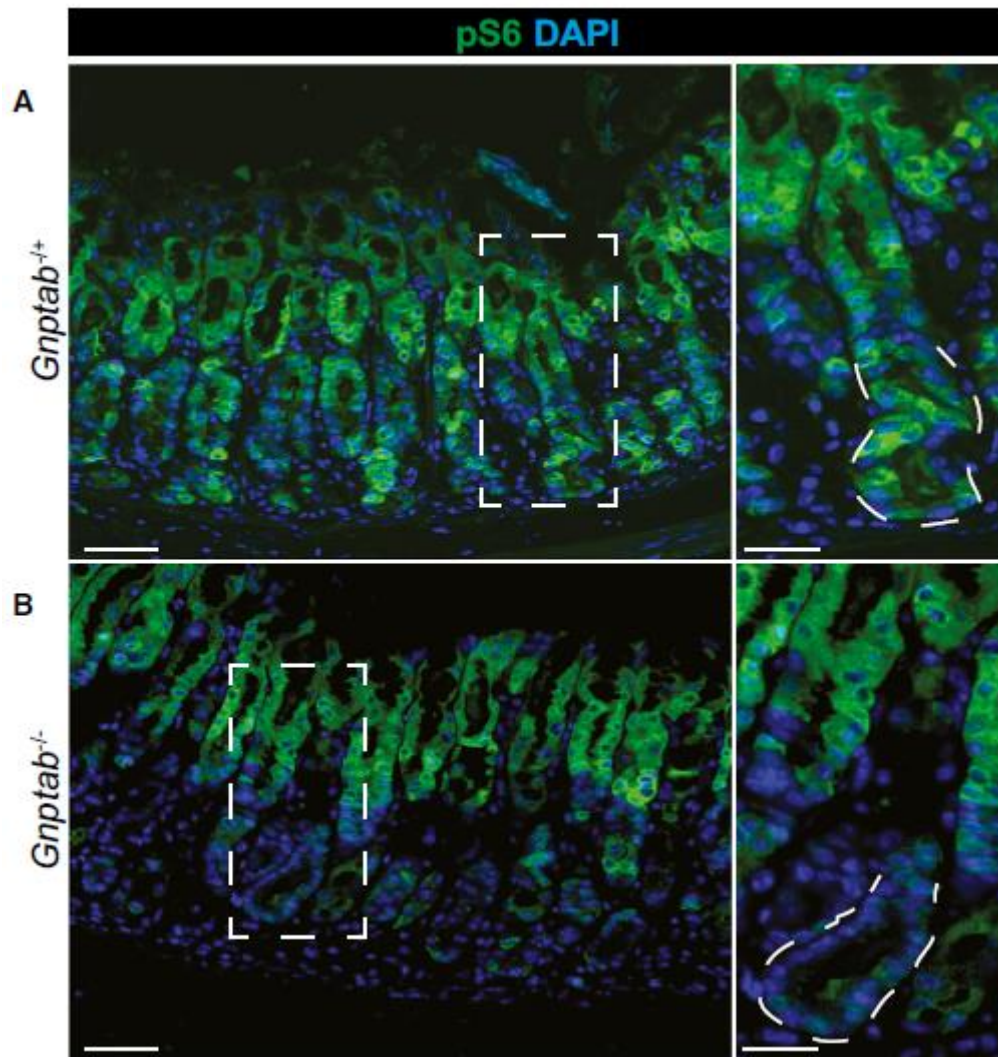


**Figure EV7.** Lysosomal activity is required to reactivate mTORC1 following HD tamoxifen injury.

A At peak metaplasia stages in *Gnptab*<sup>+/+</sup> tissue, pS6 is re-expressed throughout the stomach epithelium, including intense staining within the pit and metaplastic base. Scale bars: 50  $\mu\text{m}$ ; pullout, 25  $\mu\text{m}$ .

B In  $Gnptab^{-/-}$  issue, pS6 is not reactivated in the base, indicating lysosomal activity is required for mTORC1 re-activation at later stages following injury. Boxed regions are shown at higher magnification at right with a representative base (in which pS6 remains inactive without lysosomal activity) outlined by dotted line. Lysosomal activity appears dispensable for pit cells (at top of gastric unit) mTORC1 activity. Scale bars: 50  $\mu\text{m}$ ; pullout, 25  $\mu\text{m}$ .

## Chapter 2.6 REFERENCES

- Adami JG (1900) On growth and overgrowth. In “Festschrift” in honor of Abraham Jacobi, MD, LLD: to commemorate the seventieth anniversary of his birth, May sixth, 1900, Huber F, Sondern FE (eds), pp 422 – 432. New Rochelle, NY: Knickerbocker Press
- Adler G, Hahn C, Kern HF, Rao KN (1985) Cerulein-induced pancreatitis in rats: increased lysosomal enzyme activity and autophagocytosis. *Digestion* 32:10 – 18
- Becker FF, Lane BP (1965) Regeneration of the mammalian liver. I. Autophagocytosis during dedifferentiation of the liver cell in preparation for cell division. *Am J Pathol* 47: 783 – 801
- Blanc V, Sessa KJ, Kennedy S, Luo J, Davidson NO (2010) Apobec-1 complementation factor modulates liver regeneration by posttranscriptional regulation of interleukin-6 mRNA stability. *J Biol Chem* 285: 19184 – 19192
- Boerboom A, Reusch C, Pieltain A, Chariot A, Franzen R (2017) KIAA1199: a novel regulator of MEK/ERK-induced Schwann cell dedifferentiation. *Glia* 65: 1682 – 1696
- Boonen M, van Meel E, Oorschot V, Klumperman J, Kornfeld S (2011) Vacuolization of mucopolidosis type II mouse exocrine gland cells represents accumulation of autolysosomes. *Mol Biol Cell* 22: 1135 – 1147
- Buczacki SJ, Zecchini HI, Nicholson AM, Russell R, Vermeulen L, Kemp R, Winton DJ (2013) Intestinal label-retaining cells are secretory precursors expressing Lgr5. *Nature* 495: 65 – 69
- Buitrago-Molina LE, Pothiraju D, Lamle J, Marhenke S, Kossatz U, Breuhahn K, Manns MP, Malek N, Vogel A (2009) Rapamycin delays tumor development in murine livers by inhibiting proliferation of hepatocytes with DNA damage. *Hepatology* 50: 500 – 509

Burclaff J, Osaki LH, Liu D, Goldenring JR, Mills JC (2017) Targeted apoptosis of parietal cells is insufficient to induce metaplasia in stomach. *Gastroenterology* 152: 762 – 766 e7

Burkitt MD, Williams JM, Townsend T, Hough R, Pritchard DM (2017) Mice lacking NF-kappaB1 exhibit marked DNA damage responses and more severe gastric pathology in response to intraperitoneal tamoxifen administration. *Cell Death Dis* 8: e2939

Capoccia BJ, Jin RU, Kong YY, Peek RM Jr, Fassan M, Rugge M, Mills JC (2013) The ubiquitin ligase Mindbomb 1 coordinates gastrointestinal secretory cell maturation. *J Clin Invest* 123: 1475 – 1491

Carlisle RE, Brimble E, Werner KE, Cruz GL, Ask K, Ingram AJ, Dickhout JG

(2014) 4-Phenylbutyrate inhibits tunicamycin-induced acute kidney injury via CHOP/GADD153 repression. *PLoS One* 9: e84663

Chang-Panesso M, Humphreys BD (2017) Cellular plasticity in kidney injury and repair. *Nat Rev Nephrol* 13: 39 – 46

Choi E, Hendley AM, Bailey JM, Leach SD, Goldenring JR (2016) Expression of activated ras in gastric chief cells of mice leads to the full spectrum of metaplastic lineage transitions. *Gastroenterology* 150: 918 – 930 e13

Correa P, Piazzuelo MB (2012) The gastric precancerous cascade. *J Dig Dis* 13:2 – 9

Dhawan J, Laxman S (2015) Decoding the stem cell quiescence cycle—lessons from yeast for regenerative biology. *J Cell Sci* 128: 4467 – 4474

Direnzo D, Hess DA, Damsz B, Hallett JE, Marshall B, Goswami C, Liu Y, Deering T, Macdonald RJ, Konieczny SF (2012) Induced Mist1 expression promotes remodeling of mouse pancreatic acinar cells. *Gastroenterology* 143: 469 – 480

van Es JH, Sato T, van de Wetering M, Lyubimova A, Yee Nee AN, Gregorieff A, Sasaki N, Zeinstra L, van den Born M, Korving J, Martens ACM, Barker N, van Oudenaarden A, Clevers H (2012) Dll1+ secretory progenitor cells revert to stem cells upon crypt damage. *Nat Cell Biol* 14: 1099 – 1104

Espeillac C, Mitchell C, Celton-Morizur S, Chauvin C, Koka V, Gillet C, Albrecht JH, Desdouets C, Pende M (2011) S6 kinase 1 is required for rapamycin sensitive liver proliferation after mouse hepatectomy. *J Clin Invest* 121:2821 – 2832

Gelfman CM, Vogel P, Issa TM, Turner CA, Lee WS, Kornfeld S, Rice DS (2007) Mice lacking alpha/beta subunits of GlcNAc-1-phosphotransferase exhibit growth retardation, retinal degeneration, and secretory cell lesions. *Invest Ophthalmol Vis Sci* 48: 5221 – 5228

Giroux V, Rustgi AK (2017) Metaplasia: tissue injury adaptation and a precursor to the dysplasia-cancer sequence. *Nat Rev Cancer* 17: 594 – 604

He J, Kang L, Wu T, Zhang J, Wang H, Gao H, Zhang Y, Huang B, Liu W, Kou Z, Zhang H, Gao S (2012) An elaborate regulation of Mammalian target of rapamycin activity is required for somatic cell reprogramming induced by defined transcription factors. *Stem Cells Dev* 21: 2630 – 2641

Heid I, Lubeseder-Martellato C, Sipos B, Mazur PK, Lesina M, Schmid RM, Siveke JT (2011) Early requirement of Rac1 in a mouse model of pancreatic cancer. *Gastroenterology* 141: 719 – 730, 730.e1–7

Hingorani SR, Wang L, Multani AS, Combs C, Deramaudt TB, Hruban RH, Rustgi AK, Chang S, Tuveson DA (2005) Trp53R172H and KrasG12D cooperate to promote chromosomal instability and widely metastatic pancreatic ductal adenocarcinoma in mice. *Cancer Cell* 7: 469 – 483

Hu YY, Zhou CH, Dou WH, Tang W, Hu CY, Hu DM, Feng H, Wang JZ, Qian MJ, Cheng GL, Wang SF (2015) Improved autophagic flux is correlated with mTOR activation in the later recovery stage of experimental acute pancreatitis. *Pancreatology* 15: 470 – 477

Huh WJ, Khurana SS, Geahlen JH, Kohli K, Waller RA, Mills JC (2012) Tamoxifen induces rapid, reversible atrophy, and metaplasia in mouse stomach. *Gastroenterology* 142: 21 – 24 e7

Jessen KR, Mirsky R (2016) The repair Schwann cell and its function in regenerating nerves. *J Physiol* 594: 3521 – 3531

Jiang YP, Ballou LM, Lin RZ (2001) Rapamycin-insensitive regulation of 4e-BP1 in regenerating rat liver. *J Biol Chem* 276: 10943 – 10951

Karra R, Knecht AK, Kikuchi K, Poss KD (2015) Myocardial NF-kappaB activation is essential for zebrafish heart regeneration. *Proc Natl Acad Sci USA* 112: 13255 – 13260

Kato H, Nakajima S, Saito Y, Takahashi S, Katoh R, Kitamura M (2012) mTORC1 serves ER stress-triggered apoptosis via selective activation of the IRE1-JNK pathway. *Cell Death Differ* 19: 310 – 320

Khalaileh A, Dreazen A, Khatib A, Apel R, Swisa A, Kidess-Bassir N, Maitra A, Meyuhas O, Dor Y, Zamir G (2013) Phosphorylation of ribosomal protein S6 attenuates DNA damage and tumor suppression during development of pancreatic cancer. *Cancer Res* 73: 1811 – 1820

Lee C, Lee H, Hwang SY, Moon CM (2017) Hong SN (2017) IL-10 plays a pivotal role in tamoxifen-induced spasmodic polypeptide-expressing metaplasia in gastric mucosa. *Gut Liv* 11: 789 – 797

Lennerz JK, Kim SH, Oates EL, Huh WJ, Doherty JM, Tian X, Bredemeyer AJ, Goldenring JR, Lauwers GY, Shin YK, Mills JC (2010) The transcription factor MIST1 is a novel human gastric chief cell marker whose expression is lost in metaplasia, dysplasia, and carcinoma. *Am J Pathol* 177: 1514 – 1533

Leushacke M, Tan SH, Wong A, Swathi Y, Hajamohideen A, Tan LT, Goh J, Wong E, Denil S, Murakami K, Barker N (2017) Lgr5-expressing chief cells drive epithelial regeneration and cancer in the oxyntic stomach. *Nat Cell Biol* 19: 774 – 786

Lo HG, Jin RU, Sibbel G, Liu D, Karki A, Joens MS, Madison BB, Zhang B, Blanc V, Fitzpatrick JA, Davidson NO, Konieczny SF, Mills JC (2017) A single transcription factor is sufficient to induce and maintain secretory cell architecture. *Genes Dev* 31: 154 – 171

Logan CY, Desai TJ (2015) Keeping it together: pulmonary alveoli are maintained by a hierarchy of cellular programs. *BioEssays* 37: 1028 – 1037

Mills JC, Taghert PH (2012) Scaling factors: transcription factors regulating subcellular domains. *BioEssays* 34: 10 – 16

Mills JC, Sansom OJ (2015) Reserve stem cells: differentiated cells reprogram to fuel repair, metaplasia, and neoplasia in the adult gastrointestinal tract. *Sci Signal* 8: re8

Mills JC, Goldenring JR (2017) Metaplasia in the stomach arises from gastric chief cells. *Cell Mol Gastroenterol Hepatol* 4: 85 – 88

Mindos T, Dun XP, North K, Doddrell RD, Schulz A, Edwards P, Russell J, Gray B, Roberts SL, Shivane A, Mortimer G, Pirie M, Zhang N, Pan D, Morrison H, Parkinson DB (2017) Merlin controls the repair capacity of Schwann cells after injury by regulating Hippo/YAP activity. *J Cell Biol* 216: 495 – 510

Mizushima N, Yamamoto A, Matsui M, Yoshimori T, Ohsumi Y (2004) In vivo analysis of autophagy in response to nutrient starvation using transgenic mice expressing a fluorescent autophagosome marker. *Mol Biol Cell* 15: 1101 – 1111

Moreno-Torres M, Jaquenoud M, De Virgilio C (2015) TORC1 controls G1-S cell cycle transition in yeast via Mpk1 and the greatwall kinase pathway. *Nat Commun* 6: 8256

Morran DC, Wu J, Jamieson NB, Mrowinska A, Kalna G, Karim SA, Au AY, Scarlett CJ, Chang DK, Pajak MZ, Australian Pancreatic Cancer Genome I, Oien KA, McKay CJ, Carter CR, Gillen G, Champion S, Pimlott SL, Anderson KI, Evans TR, Grimmond SM et al (2014) Targeting mTOR dependency in pancreatic cancer. *Gut* 63: 1481 – 1489

Murtaugh LC, Keefe MD (2015) Regeneration and repair of the exocrine pancreas. *Annu Rev Physiol* 77: 229 – 249

Muzumdar MD, Tasic B, Miyamichi K, Li L, Luo L (2007) A global doublefluorescent Cre reporter mouse. *Genesis* 45: 593 – 605

Nam KT, Lee HJ, Sousa JF, Weis VG, O'Neal RL, Finke PE, Romero-Gallo J, Shi G, Mills JC, Peek RM Jr, Konieczny SF, Goldenring JR (2010) Mature chief cells are cryptic progenitors for metaplasia in the stomach. *Gastroenterology* 139: 2028 – 2037 e9

Nelsen CJ, Rickheim DG, Tucker MM, Hansen LK, Albrecht JH (2003) Evidence that cyclin D1 mediates both growth and proliferation downstream of TOR in hepatocytes. *J Biol Chem* 278: 3656 – 3663

Newberry EP, Kennedy SM, Xie Y, Luo J, Stanley SE, Semenkovich CF, Crooke RM, Graham MJ, Davidson NO (2008) Altered hepatic triglyceride content after partial hepatectomy without impaired liver regeneration in multiple murine genetic models. *Hepatology* 48: 1097 – 1105

Niederau C, Ferrell LD, Grendell JH (1985) Caerulein-induced acute necrotizing pancreatitis in mice: protective effects of proglumide, benzotript, and secretin. *Gastroenterology* 88: 1192 – 1204

Nomura S, Yamaguchi H, Ogawa M, Wang TC, Lee JR, Goldenring JR (2005) Alterations in gastric mucosal lineages induced by acute oxyntic atrophy in wild-type and gastrin-deficient mice. *Am J Physiol Gastrointest Liver Physiol* 288: G362 – G375

Nozaki K, Ogawa M, Williams JA, Lafleur BJ, Ng V, Drapkin RI, Mills JC, Konieczny SF, Nomura S, Goldenring JR (2008) A molecular signature of gastric metaplasia arising in response to acute parietal cell loss. *Gastroenterology* 134: 511 – 522

Peterson WL (2002) Review article: *Helicobacter pylori* and gastric adenocarcinoma. *Aliment Pharmacol Ther* 16(Suppl 1): 40 – 46

Radyk MD, Burclaff J, Willet SG, Mills JC (2018) Metaplastic cells in the stomach arise, independently of stem cells, via dedifferentiation or transdifferentiation of chief cells.

Gastroenterology 154: 839 – 843.e2

Radyk MD, Mills JC (2017) A chief source of cancer and repair in stomachs. EMBO J 36: 2318 – 2320

Ramsey VG, Doherty JM, Chen CC, Stappenbeck TS, Konieczny SF, Mills JC (2007) The maturation of mucus-secreting gastric epithelial progenitors into digestive-enzyme secreting zymogenic cells requires Mist1. Development 134: 211 – 222

Reich M, Liefeld T, Gould J, Lerner J, Tamayo P, Mesirov JP (2006) GenePattern 2.0. Nat Genet 38: 500 – 501

Robitaille AM, Christen S, Shimobayashi M, Cornu M, Fava LL, Moes S, Prescianotto-Baschong C, Sauer U, Jenoe P, Hall MN (2013) Quantitative phosphoproteomics reveal mTORC1 activates de novo pyrimidine synthesis. Science 339: 1320 – 1323

Rosenfeldt MT, O'Prey J, Morton JP, Nixon C, MacKay G, Mrowinska A, Au A, Rai TS, Zheng L, Ridgway R, Adams PD, Anderson KI, Gottlieb E, Sansom OJ, Ryan KM (2013) p53 status determines the role of autophagy in pancreatic tumour development. Nature 504: 296 – 300

Roth S, Franken P, Sacchetti A, Kremer A, Anderson K, Sansom O, Fodde R (2012) Paneth cells in intestinal homeostasis and tissue injury. PLoS One 7: e38965

Roux PP, Shahbazian D, Vu H, Holz MK, Cohen MS, Taunton J, Sonenberg N, Blenis J (2007) RAS/ERK signaling promotes site-specific ribosomal protein S6 phosphorylation via RSK and stimulates cap-dependent translation. J Biol Chem 282: 14056 – 14064

Rugge M, Correa P, Di Mario F, El-Omar E, Fiocca R, Geboes K, Genta RM, Graham DY, Hattori T, Malfertheiner P, Nakajima S, Sipponen P, Sung J, Weinstein W, Vieth M (2008) OLGA staging for gastritis: a tutorial. *Dig Liver Dis* 40: 650 – 658

Saenz JB, Burclaff J, Mills JC (2016) Modeling murine gastric metaplasia through tamoxifen-induced acute parietal cell loss. *Methods Mol Biol* 1422: 329 – 339

Saenz JB, Mills JC (2018) Acid and the basis for cellular plasticity and reprogramming in gastric repair and cancer. *Nat Rev Gastroenterol Hepatol* <https://doi.org/10.1038/nrgastro.2018.5>

Saluja A, Saito I, Saluja M, Houlihan MJ, Powers RE, Meldolesi J, Steer M (1985) In vivo rat pancreatic acinar cell function during supramaximal stimulation with caerulein. *Am J Physiol* 249: G702 – G710

Schmidt PH, Lee JR, Joshi V, Playford RJ, Poulsom R, Wright NA, Goldenring JR (1999) Identification of a metaplastic cell lineage associated with human gastric adenocarcinoma. *Lab Invest* 79: 639 – 646

Silvera D, Ernlund A, Arju R, Connolly E, Volta V, Wang J, Schneider RJ (2017) mTORC1 and -2 coordinate transcriptional and translational reprogramming in resistance to DNA damage and replicative stress in breast cancer cells. *Mol Cell Biol* 37: e00577 – 16

Spechler SJ, Merchant JL, Wang TC, Chandrasoma P, Fox JG, Genta RM, Goldenring JR, Hayakawa Y, Kuipers EJ, Lund PK, McKeon F, Mills JC, Odze RD, Peek RM Jr, Pham T, Que J, Rustgi AK, Shaheen NJ, Shivdasani RA,

Souza RF et al (2017) A summary of the 2016 James W. Freston conference of the American gastroenterological association: intestinal metaplasia in the esophagus and stomach: origins, differences, similarities and significance. *Gastroenterology* 153: e6 – e13

Storz P (2017) Acinar cell plasticity and development of pancreatic ductal adenocarcinoma. *Nat Rev Gastroenterol Hepatol* 14: 296 – 304

Subramanian A, Tamayo P, Mootha VK, Mukherjee S, Ebert BL, Gillette MA, Paulovich A, Pomeroy SL, Golub TR, Lander ES, Mesirov JP (2005) Gene set enrichment analysis: a knowledge-based approach for interpreting genomewide expression profiles. *Proc Natl Acad Sci USA* 102: 15545 – 15550

Syder AJ, Karam SM, Mills JC, Ippolito JE, Ansari HR, Farook V, Gordon JI (2004) A transgenic mouse model of metastatic carcinoma involving transdifferentiation of a gastric epithelial lineage progenitor to a neuroendocrine phenotype. *Proc Natl Acad Sci USA* 101: 4471 – 4476

Takahashi K, Yamanaka S (2006) Induction of pluripotent stem cells from mouse embryonic and adult fibroblast cultures by defined factors. *Cell* 126: 663 – 676

Wang S, Xia P, Ye B, Huang G, Liu J, Fan Z (2013) Transient activation of autophagy via Sox2-mediated suppression of mTOR is an important early step in reprogramming to pluripotency. *Cell Stem Cell* 13: 617 – 625

Wang WE, Li L, Xia X, Fu W, Liao Q, Lan C, Yang D, Chen H, Yue R, Zeng C, Zhou L, Zhou B, Duan DD, Chen X, Houser SR, Zeng C (2017) Dedifferentiation, proliferation, and

redifferentiation of adult mammalian cardiomyocytes after ischemic injury. *Circulation* 136: 834 – 848

Wu CY, Carpenter ES, Takeuchi KK, Halbrook CJ, Peverley LV, Bien H, Hall JC, DelGiorno KE, Pal D, Song Y, Shi C, Lin RZ, Crawford HC (2014) PI3K regulation of RAC1 is required for KRAS-induced pancreatic tumorigenesis in mice. *Gastroenterology* 147: 1405 – 1416 e7

Wu Y, Li Y, Zhang H, Huang Y, Zhao P, Tang Y, Qiu X, Ying Y, Li W, Ni S, Zhang M, Liu L, Xu Y, Zhuang Q, Luo Z, Benda C, Song H, Liu B, Lai L, Liu X et al (2015) Autophagy and mTORC1 regulate the stochastic phase of somatic cell reprogramming. *Nat Cell Biol* 17: 715 – 725

Yoshizawa N, Takenaka Y, Yamaguchi H, Tetsuya T, Tanaka H, Tatematsu M, Nomura S, Goldenring JR, Kaminishi M (2007) Emergence of spasmolytic polypeptide-expressing metaplasia in Mongolian gerbils infected with *Helicobacter pylori*. *Lab Invest* 87: 1265 – 1276

Zhou X, Liu W, Hu X, Dorrance A, Garzon R, Houghton PJ, Shen C (2017) Regulation of CHK1 by mTOR contributes to the evasion of DNA damage barrier of cancer cells. *Sci Rep* 7: 1535

Zoncu R, Bar-Peled L, Efeyan A, Wang S, Sancak Y, Sabatini DM (2011) mTORC1 senses lysosomal amino acids through an inside-out mechanism that requires the vacuolar H(+)-ATPase. *Science* 334: 678 – 683

# **Chapter 3: Increased IFRD1 Expression in Human Colon Cancers Predicts Reduced Patient Survival.**

Lewis MA\*, Sharabash N\*, Miao ZF, Lyons LN, Piccirillo J, Kallogjeri D, Schootman M, Mutch M, Yan Y, Levin MS, Castells A, Cuatrecasas M, Mills JC1, Wang ZN, Rubin DC12,13.

\*Co-first Author

## **Chapter 3.1 INTRODUCTION**

Colorectal cancer (CRC) is the third most common cancer in the world, and the global burden is expected to increase due to the growth and aging of the population. Despite advances in diagnosis and therapy, CRC remains the third most common cancer related cause of death in the United States among men and women, and the overall 5-year survival rate is 65% [1], and [1]. Colon cancer is a biologically heterogeneous disease that develops via distinct pathways involving combinations of genetic and epigenetic changes. Defining tumor subtypes based upon pathway-driven alterations has the potential to improve prognostication and guide targeted therapy [2]. However, it has become increasingly clear that there is marked heterogeneity in the “driver gene” mutational profiles within and among colon cancers. Some of these mutations are also found in non-tumor tissue [3], and are not sufficient to explain differences in colon cancer behavior and tumor response among patients [4]. Changes in the tumor landscape which may involve global modulation of gene expression have been suggested to play a role in these processes [4].

Interferon-related development regulator 1 (IFRD1, aka mouse Tis7, PC4) is a transcriptional co-regulator with a putative role in regulating intestinal lipid metabolism and

epithelial cell proliferation [5]. Expression of IFRD1 is increased in injury states in multiple organ systems, such as after massive intestinal resection [6], nerve [7] and muscle [8, 9] injury. Analysis of the intracellular localization of IFRD1 in cultured cells demonstrates cytoplasm or nuclear localization depending on the cellular differentiation state [10]. This suggests that the immediate early gene *IFRD1* may function in the cytoplasm as a sensor of cellular stimuli, and in the nucleus as a transcriptional modifier. In the nucleus IFRD1 has been shown to interact with the SIN3 protein complex, scaffold histone deacetylases [11], and regulates the expression of large gene cassettes in epithelial cells, myoblasts, hematopoietic cells, and neurons [12]. Review of the expression patterns of IFRD1 in 79 human tissues revealed that it is ubiquitous but particularly abundant in colorectal adenocarcinoma as well as in whole blood, testis, olfactory bulb, pancreas and other highly secretory tissues [13]. IFRD1 expression is increased in multiple cancers, as shown in large scale genomic/proteomic colon cancer analyses (including TCGA/Protein Atlas) [14, 15]. We have shown that IFRD1 expression is increased up to eightfold in the repairing small intestine following gut resection, and it is associated with a marked increase in gut epithelial cell proliferation [16]. Conversely, loss of IFRD1 inhibited the crypt cell proliferative adaptive response after massive intestinal resection [6].

Herein we aimed to explore the role of IFRD1 in human colon cancer pathogenesis. Specifically, we address the hypothesis that, given IFRD1's role in driving stress-induced proliferative response, increased IFRD1 expression in colon cancers would be associated with reduced survival. IFRD1 expression patterns of 378 human colon cancers and normal adjacent colon epithelium were analyzed by immunohistochemical analysis. We used a large, international multicenter, ethnically and racially diverse patient cohort to investigate how IFRD1 expression correlates with tumor severity, patient clinical demographics and overall survival.

## **Chapter 3.2 METHODS**

### **Subjects**

Formalin-fixed paraffin-embedded tissue (FFPE) from colon cancer (or colorectal carcinomas) and normal colonic mucosa from patients of three institutions from the United States, Spain and China were used for this analysis. The American cohort of colon cancer patients (n=72) were randomly selected from a subset of the Oncology Data Service cancer registry treated between 01/01/1999 and 06/30/2003 at the Barnes-Jewish Hospital in St. Louis, Missouri, a tertiary care institution affiliated with the Washington University School of Medicine Siteman Cancer Center. Data in the cancer registry includes demographic, clinical, and survival data in accordance with the American College of Surgeons Commission on Cancer guidelines. Pathological and surgical data was extracted from the medical chart. The Spanish cohort consisted of 227 consecutive stage II-III colon carcinoma patients obtained from Hospital Clinic, University of Barcelona, Barcelona, Spain, treated between 1993 and 2006 and, subjected to curative-intent surgical resection from 1998 to 2005. All cases were anonymized and the study was approved by the Hospital's Institutional Review Board and Ethics Committee. Patients were. The Chinese cohort of colon cancer patients (n=?), treated at the China Medical University between 2005 and 2009, were also anonymized and the study was approved by the China Medical University First Hospital Institutional Review Board and Ethics Committee. TNM stage was determined for all patients.

### **Immunohistochemistry**

Tissue microarray (TMA) sections containing representative cores from FFPE tissue from tumor and normal mucosa of all patients were used for immunohistochemistry (IHC) staining.

Two tumor sections from each patient were selected based on tissue quality and were used to score tumor staining. Monoclonal antibody anti-Tis7/IFRD1 (Sigma-Aldrich, St. Louis, MO; 1:500) was incubated overnight on deparaffinized 2-4  $\mu\text{m}$  thick TMA sections after decloaking with Diva antigen retrieval buffer (Biocare, Concord, CA). Antigen-antibody complexes were detected using biotinylated secondary antibody and streptavidin-horse radish peroxidase.

We used the H-score for IHC staining analysis. Three trained independent observers and a pathologist (JCM) graded the intensity of immunostaining of the tumors and normal mucosa on a 4-category scale of 0-3. The histological scoring system and individual specimen scoring were supervised by a pathologist (JCM). A score of 0 was assigned for no anti-Tis7/IFRD1 staining, a score of 1+ for traces or scattered staining in otherwise negative tumors, a score of 2+ for uniform staining of the entire tumor with light brown intensity, and a score of 3+ for uniform staining of the entire tumor with intense brown staining. The final score was the mean of the scores from the individual observers.

### **Statistical Analysis**

The association between IFRD1 expression with other demographic/clinical characteristics was assessed using Chi-square Nonparametric test. The primary clinical outcome was overall survival (OS) which was defined as the time from diagnosis to death due to cancer, and survivors were censored at the date of last contact. Kaplan-Meier method and Log-rank analysis were used to assess the association between IFRD1 expression and OS, while adjusting potential confounding effects of other demographic/clinical characteristics. Cox regression analysis was used to determine the independent effect of each variable on patient survival. All analyses were two-sided and significance was set at a p-value of 0.05. Statistical analyses were performed using SPSS 19.0.

## **Chapter 3.3 RESULTS**

### **Patient Characteristics**

Colon cancer specimens from 378 patients from the United States (n=72), Spain (n=105) and China (n=201) were analyzed by IHC staining for IFRD1 expression. The average age for the entire patient cohort was 66 years (Supplemental Table 1). There were 194 males and 184 females. Of 378 colon cancers, 6% were TNM stage I, 45% TNM stage II, 45% TNM stage III and 4% TNM stage IV.

The final IFRD1 staining score was the mean of the staining intensity scores of three independent observers as defined in the Methods. IFRD1 immunoreactivity scores were based on the intensity of stain (Figure 1A-1D). Overall, 36.2% of the tumors had a score of 0-1 (low) and 63.7% had a score of 2-3 (high) (Table 1).

### **IFRD1 expression is increased in colon adenocarcinomas compared to normal colon epithelium.**

Normal colonic mucosa demonstrated no or minimal IFRD1 immunoreactivity (Figure 1E). When present in normal mucosa, staining was low in intensity, scattered and localized in the nuclei of crypt enterocytes with minimal cytoplasmic immunoreactivity (Figure 1E inset). In contrast, almost all (373/378, 98.7%) of the colorectal cancers showed evidence of readily detectable IFRD1 expression (Figure 1B-D). Immunoreactivity was localized predominantly in the tumor cytoplasm (Figure 1B, C), with nuclear staining detectable in tumors with high-intensity, 3-score (Figure 1D). Tumor groups at the infiltrating border tended to exhibit more intense immunoreactivity (Figure 1F).

Most patients were 60 years or older at the time of diagnosis (69.8%, 264/378, Table 1). There was a significant association between age and IFRD1 immunostaining intensity, comparing patients < 60 or  $\geq$  60 and tumors with low vs. high expression ( $p = 0.013$ ). There was no significant association with gender.

We also found a significant relationship between tumor location, i.e.: right vs. left colon, and levels of IFRD1 expression (Table 2,  $p=0.036$ ). Seventy percent of right sided tumors had high IFRD1 expression compared to 59% of left sided tumors. TNM stage and IFRD1 expression showed no association (Table 2).

### **Increased IFRD1 expression in colon cancers is associated with reduced five-year patient survival.**

High IFRD1 colon cancer expression (score 2-3) correlated with decreased 5-year overall survival (Figure 2,  $p=0.025$ ). Subgroup analysis showed that patients in the American cohort with high IFRD1 colon cancer expression had a poorer prognosis and reduced 5-year survival compared to patients in the Chinese or Spanish cohorts ( $p<0.001$ ; Fig. 3). There was a significant relationship among the three cohorts with high IFRD1 expressing tumors for age ( $p=0.011$ , Table 3) gender ( $p=0.007$ ; Table 3) and tumor location, but not TNM stage (Table 4). There were more right-sided tumors in the Chinese cohort, more left-sided tumors in the Spanish cohort and a relatively equal distribution of right and left sided tumors in the American cohort ( $p=0.001$ ; Table 4).

On the multiple regression analysis, the levels of IFRD1 expression were not related to survival (Table 5). As expected, TNM stage ( $p<0.001$ ; Table 5) independently predicted patient

survival. In addition, country of origin ( $p < 0.001$ ; Table 5) independently predicted patient survival.

### **Chapter 3.4 DISCUSSION**

In the present study, we show that expression of the transcriptional co-regulator IFRD1 is increased in colon carcinomas compared to normal colon mucosa, and on the univariate analysis patients with high IFRD1-expression colon cancers have a reduced 5-year survival compared to patients with low IFRD1-expression. IFRD1 expression also correlated significantly with tumor location, being higher in right-sided carcinomas. The prognosis of right sided colon cancer is significantly worse than those in the left [17], thus, reduced survival associated with high IFRD1 expression and the higher percentage of right compared to left colon tumors with high IFRD1 expression suggest a role for IFRD1 as a modulator of increased tumorigenicity.

IFRD1 is a transcriptional co-regulator that interacts with the SIN3-histone deacetylase (HDAC) complex which then binds to DNA promoter sites and regulates global gene transcription [11] [12]. Depending on the cell type and context, IFRD1 may act as a transcriptional co-repressor or co-activator [12] to regulate a variety of cellular processes include cell proliferation and differentiation [8]. IFRD1 exhibits a low basal level of expression in multiple organs and cell types in normal homeostasis; in contrast, its expression is highly regulated in a wide variety of tissue injury models, suggesting a conserved role for IFRD1 in the cellular response to injury and stress [6, 9, 18]. For example, in the intestine, we have shown that IFRD1 plays a role in in regulating the adaptive increase in gut epithelial cell proliferation that occurs in response to resection-induced injury [6]. *Ifrd1*<sup>-/-</sup> mice show a blunted response to bowel resection with decreased crypt cell proliferation early after resection.

IFRD1 expression is regulated by growth factors including NGF, FGF and EGF [16] and glucagon-like peptide 2 [16]. IFRD1 also has effects on immune cell function and on tumor immune surveillance and plays a complex role in NF- $\kappa$ B signaling [19]. IFRD1 has been shown to regulate viral immune evasion mechanisms in human papilloma virus-induced keratinocytes with similar effects in cervical cancer cell lines, via suppression of immune driven RelA-associated NF- $\kappa$ B cytokine expression mediated by the EGFR [20]; in this model, IFRD1 acts downstream of the EGFR to deacetylate NF $\kappa$ B/RelA. In patients with cystic fibrosis who are homozygous for the F4508 deletion mutation, IFRD1 was identified as a modifier of lung disease via effects on neutrophil effector function [21]; in this study, IFRD1 deficiency was associated with decreased NF- $\kappa$ B p65 transactivation, mediated by effects on NF- $\kappa$ B induced transcription via HDAC. In contrast, IFRD1 is a repressor of NF- $\kappa$ B transcriptional activity in myoblasts via recruitment of HDAC3 in a murine model of muscle regeneration following injury [19]. Finally, IFRD1 deficiency increased p65 acetylation via inhibition of histone deacetylase-dependent deacetylation in bone marrow macrophages, repressing NF- $\kappa$ B dependent transcription of NFATc1 [22]. Thus depending on the cellular context and lineage, IFRD1 may increase or decrease NF- $\kappa$ B dependent transcriptional activity [22]. In sum, the observed worse prognosis for patients with high IFRD1 expressing colon cancers may result from alterations in multiple pathways, including direct effects on tumor cell proliferation [16], facilitating tumor immune surveillance evasion [20] or by changes in immune cell function [21].

We observed a worse prognosis for American patients with high IFRD1 expression compared to Spanish or Chinese cohorts. Although we were unable to identify a specific causal factor, our cohort has a high percentage of African Americans (55%) who exhibit a marked disparity in outcomes in colon cancer [23, 24]. Black vs. white disparities in mortality are

increased in each stage of disease but appear driven in large part by differences in late stage disease [25]. Due to the limited number of African American patients in our entire study cohort, we cannot determine whether increased IFRD1 expression in colon cancers is also significantly associated with African American populations; this will be the subject of future investigation in a larger cohort of American patients.

In summary, we have identified novel IFRD1 gene expression patterns in colon cancer which suggest a role for IFRD1 in increasing tumorigenicity and contributing to a worse prognosis. The precise mechanisms by which IFRD1 exerts its effects are unknown; the adverse effect on survival associated with high IFRD1 expression suggests that understanding these mechanisms may provide novel targets for colon cancer therapy.

Chapter 3.5 FIGURES

FIGURE 3.1

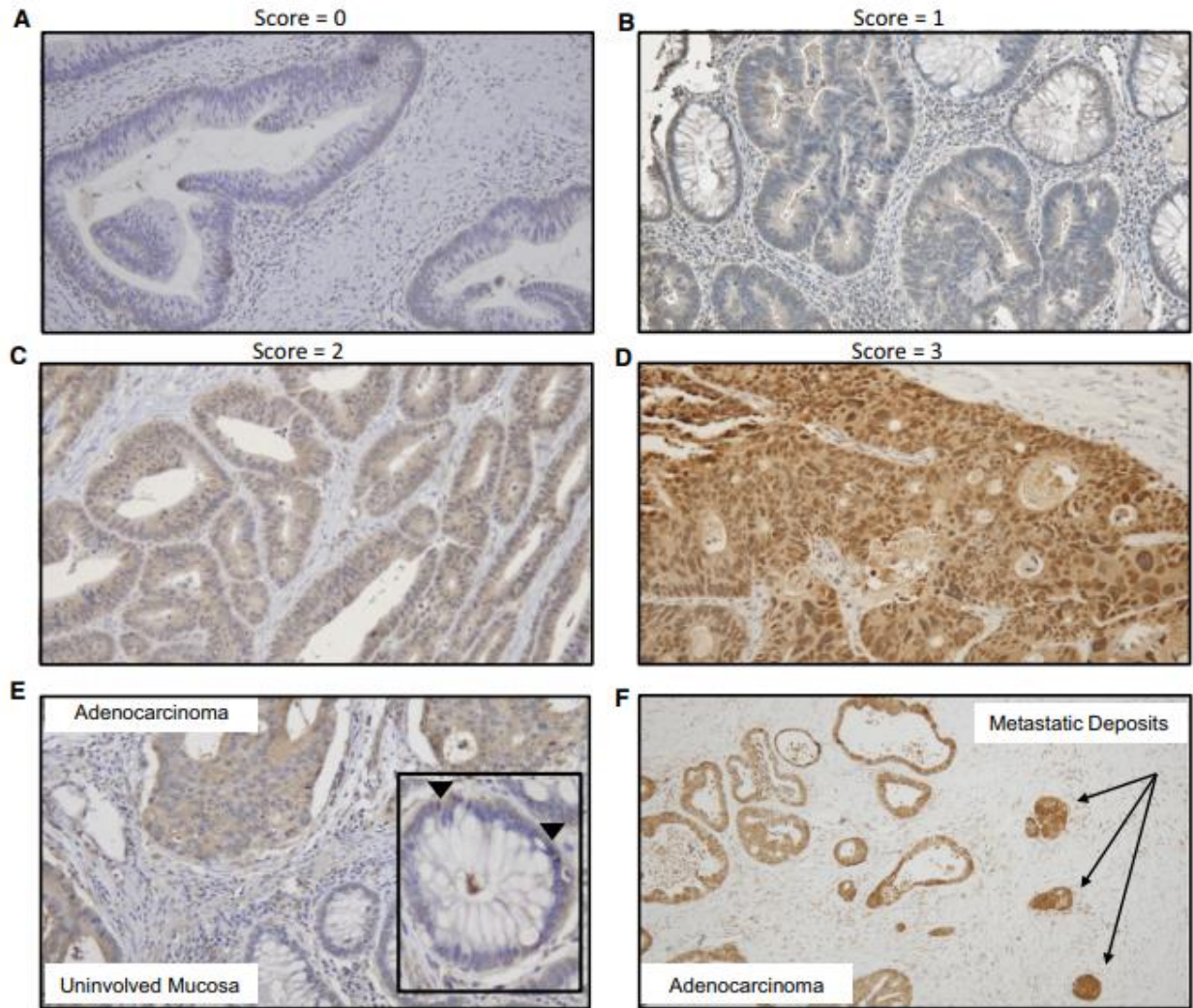


**Figure 1 IFRD1 immunohistochemical staining in colon carcinomas.**

Tumors were analyzed for IFRD1 expression using an anti-IFRD1 monoclonal antibody. IFRD1 immunostaining intensity was quantified by scoring on a scale of 0–3. a Tumors with a score of 0 had no to minimal IFRD1 immunoreactivity. Scattered light staining can be observed in the nuclei of well-differentiated tumors. b Immunohistochemical score of 1 showed light staining

throughout the tumor or more intense, but scattered staining. c Uniform staining of the entire tumor with medium intensity (score 2). d Uniform staining of the entire tumor with intense brown staining, often associated with increased nuclear staining (score 3). e Comparison of tumor and normal mucosal staining demonstrates that IFRD1 staining is readily detectable in colon cancer, but adjacent, uninvolved mucosa shows no or minimal IFRD1 immunoreactivity. When IFRD1 staining was detected in the uninvolved mucosa, it was low in intensity and localized in the nuclei of crypt cells with minimal cytoplasmic immunoreactivity (Fig. 1e inset). f Tumor clusters at the invasive margin show more intense staining.

TABLE 3.1

**Table 1** Patient demographics

---

<i>Patient demographics</i>	
Age range of patients	25–84
Mean age of patients	66
Gender	
Males	194
Females	184
Tumor location	
Right	146
Left	202
Other (transverse or flexures)	30
TNM stage	
Stage I	23
Stage II	169
Stage III	171
Stage IV	15

---

TABLE 3.2

**Table 2** Patient age and gender distribution in low compared to high IFRD1-expressing colon cancers

	Low IFRD1 ( <i>n</i> = 137)	High IFRD1 ( <i>n</i> = 137)	<i>p</i> value
<b>Age</b>			
< 60	52	62	0.013*
≥ 60	85	179	
<b>Gender</b>			
Male	79	115	0.063
Female	58	126	

IFRD1 immunostaining intensity was scored for each cancer on a scale of 0–3 (*n* = 378). Colon cancers were then classified as expressing low IFRD1 levels (score of 0–1, *n* = 137) or high IFRD1 levels (score of 2–3, *n* = 241)

TABLE 3.3

**Table 3** Clinical characteristics of low versus high IFRD1-expressing colon cancers

	Low IFRD1 ( <i>n</i> = 137)	High IFRD1 ( <i>n</i> = 137)	<i>p</i> value
<b>Tumor location</b>			
Right	44	102	0.036*
Left	83	119	
<b>TNM stage</b>			
Stage I	7	16	0.660
Stage II	65	104	
Stage III & IV	65	121	

IFRD1 immunostaining intensity was scored for each cancer on a scale of 0–3 (*n* = 378). Colon cancers were then classified as expressing low IFRD1 levels (score of 0–1, *n* = 137) or high IFRD1 levels (score of 2–3, *n* = 241)

FIGURE 3.2

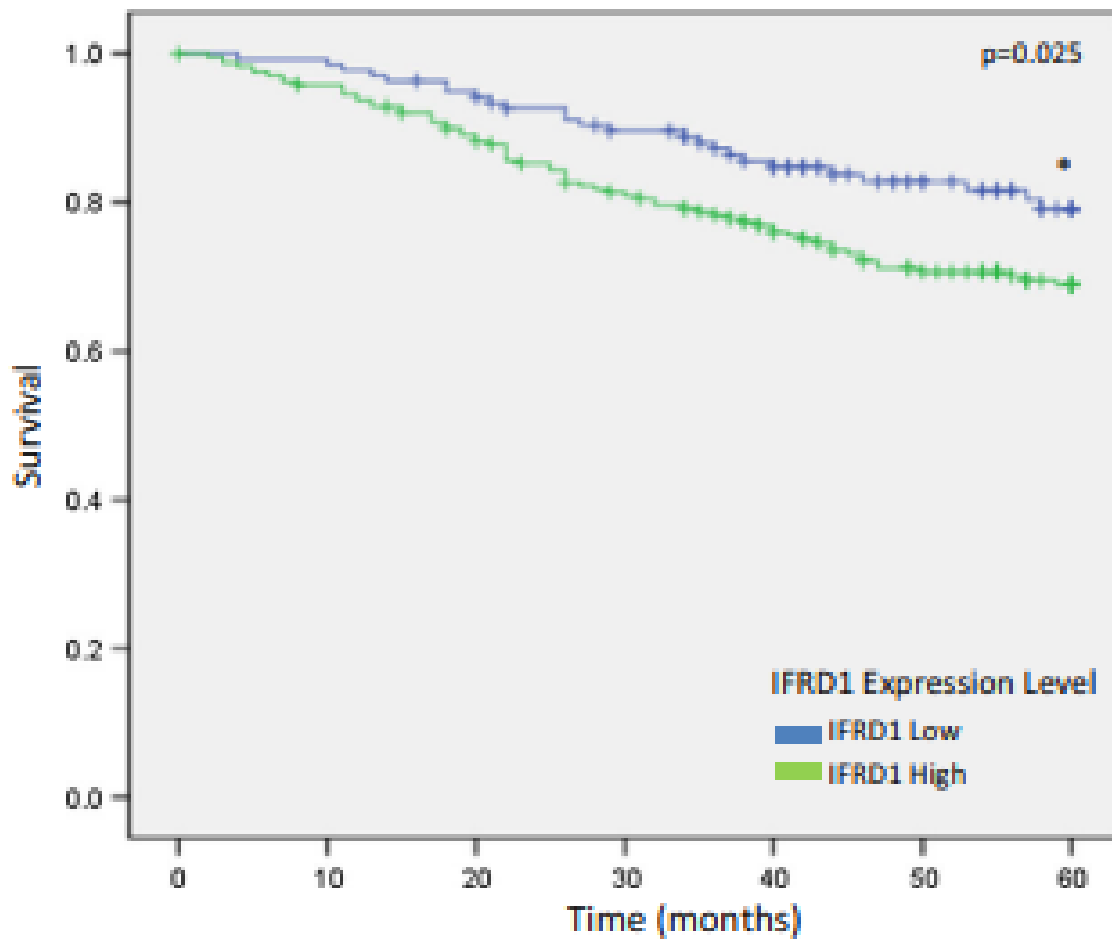


**Figure 2 Reduced 5-year survival in patients with high IFRD1-expression colon cancers.**

Censored patients with high IFRD1 expression in tumors significantly poorer survival at 5 years post diagnosis compared to patients with tumors with low IFRD1 expression (\* p = 0.025).

FIGURE 3.3

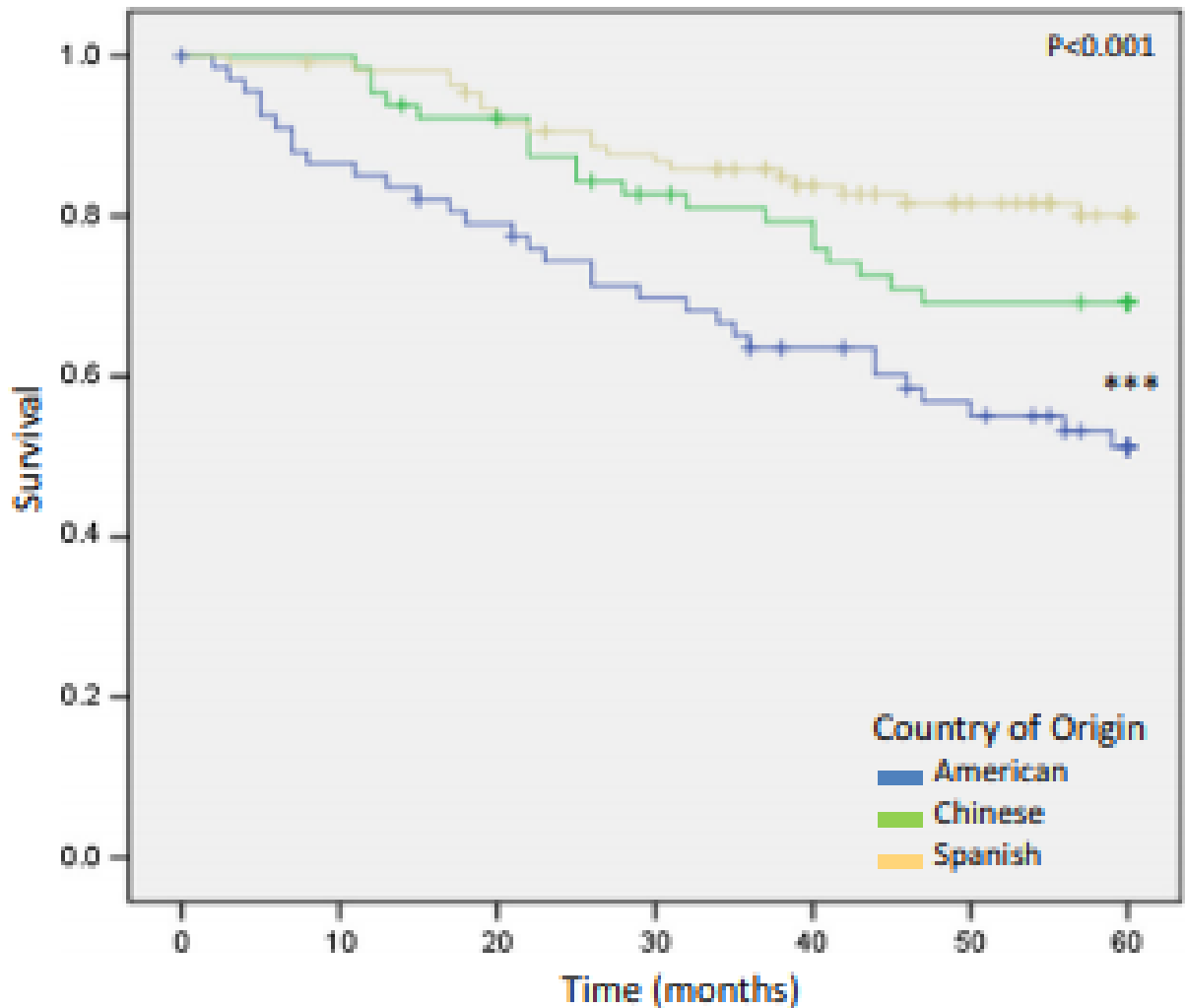


**Figure 3 American patients with high IFRD1-expressing tumors have reduced 5-year survival compared to Chinese and Spanish patients.** Five-year survival analysis was performed for all patients with high IFRD1-expressing tumors from American, Chinese, and Spanish cohorts. American patients with high IFRD1-expressing tumors had reduced 5-year survival compared to Chinese and Spanish patients with high IFRD1-expressing tumors \*\*\* p(0.001).

TABLE 3.4

**Table 4** Demographics of high IFRD1-expressing cancers by country of origin

	IFRD1 high American ( <i>n</i> = 68)	IFRD1 high Chinese ( <i>n</i> = 65)	IFRD1 high Spanish ( <i>n</i> = 108)	<i>p</i> value
<b>Age</b>				
< 60	17	32	35	0.011*
≥ 60	51	33	73	
<b>Gender</b>				
Male	22	33	61	0.007*
Female	46	32	47	

Tumor samples with a score of 2 or 3 were analyzed for relationship to age and gender based on country of origin

TABLE 3.5

**Table 5** Clinical analysis of colon cancer patient cohort samples by country of origin

	IFRD1 high American ( <i>n</i> = 68)	IFRD1 high Chinese ( <i>n</i> = 65)	IFRD1 high Spanish ( <i>n</i> = 108)	<i>p</i> value
<b>Tumor location</b>				
Right	32	45	32	0.001*
Left	36	20	76	
<b>TNM stage</b>				
Stage I	16	14	22	0.856
Stage II	20	25	35	
Stage III & IV	31	26	51	

Tumor samples with high IFRD1 expression (scored 2 or 3) were analyzed for tumor location and TNM stage based on country of origin

TABLE 3.6

**Table 6** Multiple regression analysis of patient variables

Cox proportional hazards regression model				
	<i>P</i> value	RR	95% CI for RR	
			Lower	Upper
Age	0.808	1.046	0.728	1.502
Gender	0.825	1.041	0.732	1.479
Location	0.768	0.968	0.783	1.198
TNM stage	0.000	2.138	1.67	2.737
Country of origin	0.000	0.491	0.391	0.615
IFRD1 expression	0.819	0.954	0.637	1.428

Patient variables were analyzed for their independent impact on colon cancer prognosis using Cox proportional regression model

## Chapter 3.6 REFERENCES

1. Siegel RL, Miller KD, Jemal A: **Cancer Statistics, 2017**. *CA Cancer J Clin* 2017, **67**(1):7-30.
2. Sinicrope FA, Shi Q, Smyrk TC, Thibodeau SN, Dienstmann R, Guinney J, Bot BM, Tejpar S, Delorenzi M, Goldberg RM *et al*: **Molecular markers identify subtypes of stage III colon cancer associated with patient outcomes**. *Gastroenterology* 2015, **148**(1):88-99.
3. Weaver JM, Ross-Innes CS, Shannon N, Lynch AG, Forshew T, Barbera M, Murtaza M, Ong CA, Lao-Sirieix P, Dunning MJ *et al*: **Ordering of mutations in preinvasive disease stages of esophageal carcinogenesis**. *Nat Genet* 2014, **46**(8):837-843.
4. Punt CJ, Koopman M, Vermeulen L: **From tumour heterogeneity to advances in precision treatment of colorectal cancer**. *Nat Rev Clin Oncol* 2017, **14**(4):235-246.
5. Garcia aM, Wakeman D, Lu J, Rowley C, Geisman T, Butler C, Bala S, Swietlicki Ea, Warner BW, Levin MS *et al*: **Tis7 deletion reduces survival and induces intestinal anastomotic inflammation and obstruction in high-fat diet-fed mice with short bowel syndrome**. *AJP: Gastrointestinal and Liver Physiology* 2014, **307**:G642-G654.
6. Yu C, Jiang S, Lu J, Coughlin CC, Wang Y, Swietlicki EA, Wang L, Vietor I, Huber LA, Cikes D *et al*: Deletion of Tis7 protects mice from high-fat diet-induced weight gain and blunts the intestinal adaptive response postresection. *J Nutr* 2010, **140**(11):1907-1914.
7. Dieplinger B, Schiefermeier N, Juchum-Pasquazzo M, Gstir R, Huber LA, Klimaschewski L, Vietor I: **The transcriptional corepressor TPA-inducible sequence 7 regulates adult axon growth through cellular retinoic acid binding protein II expression**. *Eur J Neurosci* 2007, **26**(12):3358-3367.
8. Micheli L, Leonardi L, Conti F, Maresca G, Colazingari S, Mattei E, Lira Sa, Farioli-Vecchioli S, Caruso M, Tirone F: **PC4/Tis7/IFRD1 stimulates skeletal muscle regeneration and is involved in myoblast differentiation as a regulator of MyoD and NF-??B**. *Journal of Biological Chemistry* 2011, **286**:5691-5707.
9. Vadivelu SK, Kurzbauer R, Dieplinger B, Zweyer M, Schafer R, Wernig A, Vietor I, Huber LA: **Muscle Regeneration and Myogenic Differentiation Defects in Mice Lacking TIS7**. *Molecular and Cellular Biology* 2004, **24**(8):3514-3525.
10. Guardavaccaro D, Montagnoli A, Ciotti MT, Gatti A, Lotti L, Lazzaro CD, Torrisi MR, Tirone F: **Nerve Growth Factor Regulates the Subcellular Localization of the Nerve Growth Factor-Inducible Protein PC4 in PC12 Cells**. *Journal of Neuroscience Research* 1994, **37**:660-674.

11. Vietor I, Vadivelu SK, Wick N, Hoffman R, Cotten M, Seiser C, Fialka I, Wunderlich W, Haase A, Korinkova G *et al*: **TIS7 interacts with the mammalian SIN3 histone deacetylase complex in epithelial cells.** *EMBO Journal* 2002, **21**(17):4621-4631.
12. Vietor I, Huber LA: **Role of TIS7 family of transcriptional regulators in differentiation and regeneration.** *Differentiation* 2007, **75**(9):891-897.
13. Uhlén M, Björling E, Agaton C, Szigyarto CA-K, Amini B, Andersen E, Andersson A-C, Angelidou P, Asplund A, Asplund C *et al*: **A Human Protein Atlas for Normal and Cancer Tissues Based on Antibody Proteomics.** *Molecular & Cellular Proteomics* 2005, **4**:1920-1932.
14. Sabates-Bellver J, Van der Flier LG, de Palo M, Cattaneo E, Maake C, Rehrauer H, Laczko E, Kurowski MA, Bujnicki JM, Menigatti M *et al*: **Transcriptome profile of human colorectal adenomas.** *Mol Cancer Res* 2007, **5**(12):1263-1275.
15. Zhang B, Wang J, Wang X, Zhu J, Liu Q, Shi Z, Chambers MC, Zimmerman LJ, Shaddox KF, Kim S *et al*: **Proteogenomic characterization of human colon and rectal cancer.** *Nature* 2014, **513**(7518):382-387.
16. Swietlicki E, Fritsch; HIC, Yi; L, Levin MS, Rubin aDC: **Growth Factor Regulation of PC4/TIS7, An Immediate Early Gene Expressed During Gut Adaptation After Resection.** *JOURNAL OF PARENTERAL AND ENTERAL NUTRITION* 2003, **27**(2):123-131.
17. Petrelli F, Tomasello G, Borgonovo K, Ghidini M, Turati L, Dallera P, Passalacqua R, Sgroi G, Barni S: **Prognostic Survival Associated With Left-Sided vs Right-Sided Colon Cancer: A Systematic Review and Meta-analysis.** *JAMA Oncol* 2016.
18. Benjamin Dieplinger, \*, □ Natalia Schiefermeier,1, □ Michaela Juchum-Pasquazzo,1 Ronald Gstir,1 Lukas A. Huber,1, Vietor1 LKaI: **The transcriptional corepressor TPA-inducible sequence 7 regulates adult axon growth through cellular retinoic acid binding protein II expression.** 2007.
19. Micheli L, Leonardi L, Conti F, Maresca G, Colazingari S, Mattei E, Lira SA, Farioli-Vecchioli S, Caruso M, Tirone F: **PC4/Tis7/IFRD1 stimulates skeletal muscle regeneration and is involved in myoblast differentiation as a regulator of MyoD and NF-kappaB.** *J Biol Chem* 2011, **286**(7):5691-5707.
20. Tummers B, Goedemans R, Pelascini LP, Jordanova ES, van Esch EM, Meyers C, Melief CJ, Boer JM, van der Burg SH: **The interferon-related developmental regulator 1 is used by human papillomavirus to suppress NFkappaB activation.** *Nat Commun* 2015, **6**:6537.
21. Gu Y, Harley IT, Henderson LB, Aronow BJ, Vietor I, Huber LA, Harley JB, Kilpatrick JR, Langefeld CD, Williams AH *et al*: **Identification of IFRD1 as a modifier gene for cystic fibrosis lung disease.** *Nature* 2009, **458**(7241):1039-1042.

22. Iezaki T, Fukasawa K, Park G, Horie T, Kanayama T, Ozaki K, Onishi Y, Takahata Y, Nakamura Y, Takarada T *et al*: **Transcriptional Modulator Irf1 Regulates Osteoclast Differentiation through Enhancing the NF-kappaB/NFATc1 Pathway**. *Mol Cell Biol* 2016, **36**(19):2451-2463.
23. Robbins AS, Siegel RL, Jemal A: **Racial disparities in stage-specific colorectal cancer mortality rates from 1985 to 2008**. *J Clin Oncol* 2012, **30**(4):401-405.
24. Simpson DR, Martinez ME, Gupta S, Hattangadi-Gluth J, Mell LK, Heestand G, Fanta P, Ramamoorthy S, Le QT, Murphy JD: **Racial disparity in consultation, treatment, and the impact on survival in metastatic colorectal cancer**. *J Natl Cancer Inst* 2013, **105**(23):1814-1820.
25. Howlader N, Noone AM, Krapcho M, Garshell J, Miller D, Altekruse SF, Kosary CL, Yu M, Ruhl J, Tatalovich Z, Mariotto A, Lewis DR, Chen HS, Feuer EJ, Cronin KA (eds). **SEER Cancer Statistics Review, 1975-2012, National Cancer Institute**. Bethesda, MD, [http://seer.cancer.gov/csr/1975\\_2012/](http://seer.cancer.gov/csr/1975_2012/), based on November 2014 SEER data submission, posted to the SEER web site, April 2015.

# **Chapter 4: IFRD1 promotes survival and proliferation in the conserved cellular regeneration program (paligenosis) by suppressing p53**

Mark A. Lewis, Zhi-Feng Miao, Dongkook Park, Jeffrey W. Brown, Charles Cho, Susan Kennedy, Jianyan Lu, Marcus Mahar, Ilja Vietor, Lukas A. Huber, Nicholas O. Davidson, Valeria Cavalli, Deborah C. Rubin, Jason C. Mills

## **Chapter 4.1 SUMMARY**

The capacity for mature cells to reprogram into a proliferative, regenerative state is a general feature of multicellular organisms and appears to proceed by a dedicated, evolutionarily conserved program (*paligenosis*). The fundamental cellular energy sensor and regulator of protein translation, mTORC1, is the central regulator of paligenosis. Here, we reasoned that, akin to apoptosis and other cellular programs, genes likely evolved to regulate paligenosis. We identified IFRD1 as a gene conserved throughout eukaryotes, upregulated by paligenosis-inducing injury, but not required for homeostatic regulation of proliferation and differentiation. IFRD1 was critical for the injury-induced recruitment of cells into the cell cycle in *Drosophila* intestine and multiple mouse tissues. *Ifrd1*<sup>-/-</sup> mice showed decreased mTORC1-mediated proliferation and increased apoptosis in gastric and pancreatic paligenotic cells. mTORC1 inhibition and *Ifrd1*<sup>-/-</sup>;*Trp53*<sup>-/-</sup> experiments showed that IFRD1 works largely by alleviating p53 repression of mTORC1 reactivation during stage 3 of paligenosis. Our results identify the first gene regulating the conserved cellular program that recruits mature cells for regeneration. A p53-mTORC1 balance dictates whether paligenosis is successful, and mature cells reenter

mitosis or whether it fails and cells die. Pro-paligenotic genes like IFRD1 might be harnessed to increase cellular reprogramming to promote regeneration; alternatively, because recruiting old cells with potential stores of somatic mutations increases risk for cancer, blocking paligenosis might prevent or treat cancer.

## **Chapter 4.2 INTRODUCTION**

Following large-scale injury, mature cells in pancreas and stomach use a common program (termed *paligenosis*) to reenter the cell cycle and fuel tissue regeneration<sup>1</sup>. Here, we hypothesize that paligenosis, akin to other cellular programs like apoptosis, will be governed by a conserved set of genes. We expect such genes to be: a) ubiquitously induced upon paligenosis-causing injury, b) conserved across species, and c) dispensable for normal development or stem cell homeostasis. Nearly all tissues, across numerous species, demonstrate examples of cellular plasticity in response to injury. We recently proposed a shared cellular program by which differentiated cells can change their fate to facilitate injury repair<sup>1</sup>. In our investigation of gastrointestinal organs (stomach, pancreas, liver, and intestine), we believe that each has the capacity to repair tissue damage through the recruitment of fully differentiated cells into a less differentiated, proliferative state to replenish lost or damaged cells. We also proposed that this process could be expanded to include other cells (kidney, neurons, etc.) because of the dynamic mTORC1 activity and proliferative or regenerative capacity that these tissues exhibit following injury. This cellular “reprogramming” to a proliferative, regenerative state can occur in various contexts, such as when tissue undergoes metaplasia following injury. In the acute setting, the metaplastic response appears to be a tissue repair mechanism and can be temporary, with full restoration of normal tissue architecture. Accordingly, we have shown that differentiated cells in the stomach and pancreas have the capacity to revert to the embryonic state, becoming mitotic

again to aid in tissue repair. In tissues with constitutively active stem cells, like stomach and intestines, the tissues would have the option of regenerating with either constitutive stem cells or recruited stem cells, depending potentially on type, extent, and location of injury.

Identification of genes that regulate this repair is crucial to understanding human diseases that are dependent on this process and has the potential to lead to breakthroughs in personalized medical treatment. We would hypothesize that a gene whose primary function is to regulate reserve stem cell function would be dispensable for normal cellular activity, but be called to action during an acute injury response.

Through an *in silico* screen, we have identified IFRD1 as such a gene. It is an immediate early gene that was originally found to respond to mitogens such as TPA, EGF, c-Jun and FGF. IFRD1 associates with the Sin3 complex and is, thus, reported to play a role as a transcriptional co-regulator with a putative function in regulating intestinal lipid metabolism and epithelial cell proliferation<sup>2,3</sup>. We and others have shown IFRD1 is a highly conserved, transcriptional co-regulator that: responds transiently and rapidly to cellular stimuli; is critical for induction of proliferation in intestinal repair but is dispensable for normal stem cell activity; has polymorphisms associated with gastric cancer; and elevated expression is associated with poorer survival in colon cancer patients<sup>3-6</sup>. IFRD1 levels positively correlate with the processes of cell and tissue injury response and regeneration in humans, mice and in lower species, such as, *S. pombe* and *D. melanogaster*. The activity of energy sensing protein mTORC1 governs proliferation in the stomach and pancreas. Analysis of tissues that depend on mTORC1 activity following injury revealed that there are 8 genes that are acutely upregulated following injury. Expanding the screen to lung and glial tissues reveals that *Ifrd1* and *Atf3* are two genes that may be critical for this injury response across multiple tissues. We are currently investigating the role

of *Atf3* in our models of paligenosis and, herein, we will describe the requirement of IFRD1 for the proliferative response of reserve stem cells across multiple tissues and species.

Following large-scale injury, mature cells in pancreas and stomach use a common program (termed *paligenosis*) to reenter the cell cycle and fuel tissue regeneration<sup>1</sup>. Here, we hypothesize that paligenosis, akin to other cellular programs like apoptosis, will be governed by a conserved set of genes. We expect such genes to be: a) ubiquitously induced upon paligenosis-causing injury, b) conserved across species, and c) dispensable for normal development or stem cell homeostasis.

## Chapter 4.3 RESULTS AND DISCUSSION

### **IFRD1 is highly conserved and is upregulated following regeneration-inducing injury in multiple tissues and species**

To identify tissue-independent paligenosis-regulating genes, we screened for mRNAs whose expression was induced following injury in all 4 organs we previously used to delineate the core paligenotic cellular response (stomach, pancreas, liver, kidney)<sup>1</sup>. We identified 8 genes and determined if they were also increased in two additional injury-induced gene expression profiles from tissues: lung and neural glia<sup>7 8</sup> that also are known to undergo dramatic, injury-induced reprogramming (Fig. 1 a, b). Only two genes were upregulated in all 6 tissues: *Ifrd1* and the transcription factor *Atf3* (Fig. 1b). *Atf3* is the subject of ongoing work in our group; we focus here on IFRD1.

We next tested if IFRD1 structure and function exhibited broad evolutionary conservation. Our multisequence alignment of IFRD1 orthologs demonstrated conservation of

nearly the entire protein from humans to the fission yeast *Schizosaccharomyces pombe* (Fig. 1c and Supplementary Fig. 1a). Our secondary structure prediction suggested extensive alpha-helical character with the mature protein likely obtaining an armadillo (or alpha-solenoid) fold, a structural motif used by other important scaffolding/signaling proteins like  $\beta$ -catenin (CTNNB1) and Adenomatous Polyposis Coli (APC). (Fig. 1c and Supplementary Fig. 1a). Further, a cryoEM structure of IFRD2 bound to the ribosome demonstrates that the homolog assumes an armadillo fold and secondary structure consistent with our unbiasedly prediction from the IFRD1 sequence (Supplemental Figure 1b). The yeast ortholog of IFRD1 (SPBC20F10.03) has not been specifically characterized, but mRNA and protein screens detailed at PomBase <sup>9</sup> showed that its expression increases following multiple stresses including H<sub>2</sub>O<sub>2</sub> and heat but does not change during normal cell cycle progression. Further, yeast null for the gene encoding IFRD1 do not seem to have a vegetative/cell cycle defect, suggesting that the protein is specific to stress response.

As in yeast, the *Drosophila melanogaster* ortholog of IFRD1, CG31694, has not been specifically characterized; however, again, examination of various published screens showed that *difrd1* is upregulated during stem-cell-recruiting injury in the gut in response to entomopathogenic *Pseudomonas* bacteria and implicated in the stem-cell recruiting Unpaired (orthologous to IL-6) pathway <sup>10</sup>. We confirmed that *difrd1* increased following intestinal stem-cell-recruiting stress using a strain expressing GFP under the *difrd1* promoter (Fig. 1d). Furthermore, whereas stem-cell-recruiting stress caused wildtype fly intestines to markedly increase proliferation as expected, two strains hypomorphic for *difrd1* failed to respond (Fig. 1e). As the hypomorphic strains showed no defects in normal development or stem cell homeostasis,

the regulation of proliferation by IFRD1 in *Drosophila* appears specific to situations where stem cells are recruited after stress.

Previous studies by us and others have shown that in the absence of IFRD1, mice, like yeast and flies, do not have substantial defects in development or adult organ stem cell homeostasis (<sup>3 11</sup>, unpublished observations, Supplementary Fig. 3 b-e). We investigated a cell-autonomous role for IFRD1 in two tissue types not represented in our initial screen. We generated organoids from the small intestine. The efficiency of organoid establishment is a function of how many stem cells can be recruited to grow in the ex vivo environment <sup>12 13 14</sup>. Enteroid forming efficiency and growth 7 days after passage were both significantly reduced in the absence of IFRD1 (Supplementary Fig. 2 a-d). In parallel, we used a well-characterized system that induces nuclear reprogramming of neurons along with expression of IFRD1: axotomy of ex vivo grown dorsal root ganglion neurons <sup>15,16</sup>. When IFRD1 was knocked down, the reprogramming-dependent regeneration of axons was significantly compromised (Supplementary Fig. 2c).

Therefore, IFRD1 is required for paligenosis and is: a) expressed in ubiquitous cell types undergoing paligenosis; b) broadly conserved across eukaryotes; and c) dispensable for normal homeostatic growth or development.

### **IFRD1 is required for stage 3 of paligenosis**

We next wanted to explore where IFRD1 acted during paligenosis. We turned to the injury models that we and others have shown induce canonical, three-stage paligenosis: high-dose tamoxifen (HD-TAM) for the stomach and injection of the cholecystokinin analog cerulein for the pancreas (<sup>1</sup> Figure 1 A, B). We analyzed effects of loss of IFRD1 during the sequential

stages of paligenosis: 1) autodegradation (when lysosomes and autolysosomes recycle existing cell architecture); 2) induction of embryonic/progenitor gene expression; and 3) cell cycle re-entry (Supplementary Figure 3a; <sup>1</sup>).

Injury to both organs caused the expected metaplastic responses in wildtype control mice. Gastric chief cells in the stomach became cuboidal-columnar cells characteristic of the differentiation pattern known as Spasmodic Polypeptide Expressing Metaplasia (SPEM; Fig. 2 a, b; Supplementary Fig. 3 b, c), and pancreatic acinar cells also showed the decreased cell volume with increased lumens in the pattern known as Acinar to Ductal Metaplasia (ADM; Fig. 2 e, f; Supplementary Fig. 3 d, e). Previously shown that IFRD1 is also induced precancerous and cancerous epithelial lesions in the human luminal gastrointestinal tract <sup>6</sup>; we show here that it also is strongly expressed in regions of acinar-ductal metaplasia in a patient with pancreatic ductal adenocarcinoma (Fig. 2g).

Mice lacking IFRD1 had aberrant paligenosis. In stomach, the base of the gastric unit, where paligenosis occurs, showed marked cell loss (Fig. 2 a, b), and pancreas also showed regions of epithelial loss with increased stroma and tissue edema (Fig. 2e). Proliferation was significantly decreased in paligenotic *Ifrd1*<sup>-/-</sup> cells (Fig. 2). In stomach, decreased proliferation was confined to the base where paligenosis occurs, whereas cells higher in the gastric unit in the constitutively proliferative stem cell zone (the isthmus) were largely unaffected either before or after HD-TAM (Fig. 2 c, d). In pancreas, proliferating paligenotic acinar cells were greatly reduced, while proliferating cells in the stroma were largely unaffected (Fig. 2 h, i). To further test the role of IFRD1 in paligenotic proliferation, we performed partial hepatectomies, which we and others have shown involve paligenotic recruitment of hepatocytes back to a proliferative

state<sup>1</sup>. Mitotic activity in *Ifrd1*<sup>-/-</sup> livers following partial hepatectomy was also compromised (Supplementary Fig. 2 g, h)

Re-entry into the cell cycle is the third stage of paligenosis, so the decreased proliferation in the absence of IFRD1 could be due to upstream failure of cells to progress through stages 1 or 2. In both the pancreas and stomach, the massive upregulation of LAMP1+ vesicles characteristic of the autodegradation phase occurred in *Ifrd1*<sup>-/-</sup> mice (Supplementary Fig. 3 b, d), so there was no obvious defect in the autodegradative stage 1. Likewise, the characteristic re-expression of the mucous neck cell pattern in paligenotic chief cells of the stomach (Supplementary Fig. 3c) and paligenotic expression of nuclear YAP1 (Supplementary Fig. 3e) and SOX9 (unpublished observations) in paligenotic acinar cells were observed as expected in *Ifrd1*<sup>-/-</sup> mice. Thus, paligenosis stage 2 was not markedly affected by loss of IFRD1.

### **Loss of IFRD1 causes increased activation of p53 and decreased expression of mTORC1-associated and cell-cycle-related transcripts**

We next explored the mechanism IFRD1 uses to regulate paligenosis. Our analysis of IFRD1 structure revealed a protein without catalytic domains that is remarkably conserved in both the recurring  $\alpha$ -helices in armadillo folds with scant variation in overall length across all eukaryotes. Overall, the structure and conservation suggest it acts as a scaffold that interacts with multiple other proteins throughout its entire length. Accordingly, previous reports have arrived at neither consistent function nor even cellular localization of IFRD1 with some studies showing interactions with nuclear histone deacetylases to govern chromatin modification<sup>17-19</sup>, others suggesting that it likely is cytosolic and interacts with ribosomes<sup>20</sup>, and still others indicating

interaction with multiple signaling pathways including IL6/JAK/STAT/NF- $\kappa$ B, MAP Kinases, Hippo, Wnt, and mTOR<sup>2 21 22 23 24</sup>.

Thus, IFRD1 is likely to function as a central hub with numerous potential binding partners in cytosol and nucleus. To begin to identify the most salient mechanisms, we performed global gene expression profiling of whole pancreas of *Ifrd1*<sup>-/-</sup> and control mice  $\pm$  cerulein at the time point when the greatest number of cells are in stage 3 of paligenosis, when the IFRD1 phenotype manifests. Gene Set Enrichment Analysis (GSEA) using publicly available cell cycle data sets (Molecular Signatures Database, Broad Institute<sup>25</sup>) confirmed dramatic, statistically significant de-enrichment for cell cycle transcripts in *Ifrd1*<sup>-/-</sup> mice (Fig. 3a), consistent with the histological data. Furthermore, when we analyzed the Broad Institute Hallmark collection of GSEA datasets (a compendium of gene sets designed for unbiased screens) for any gene sets that significantly distinguished cerulein-injured *Ifrd1*<sup>-/-</sup> pancreases from control, we noted marked de-enrichment again of additional cell cycle-related gene sets (G2M Checkpoint, Mitotic Spindle, myc Targets). In addition, in the absence of IFRD1, there was also de-enrichment for gene sets associated with p53, DNA repair, and mTORC1 (Fig. 3b).

The Hallmark p53 gene set comprises p53- upregulated and downregulated genes, as well as genes associated with or modifying p53. To determine which genes were principally responsible for the differential p53 gene expression between *Ifrd1*<sup>-/-</sup> mice and controls, we examined the most increased genes in wildtype (i.e. the ones primarily responsible for p53-associated gene enrichment in wildtype mice). The top 10 most-enriched transcripts in control vs. *Ifrd1*<sup>-/-</sup> mice were all either promoters of cell cycle progression (CCND1, CCND2, CCNG1, GTSE1, CDK1), anti-apoptotic (SESN2, SESN3, MDM2) or miscellaneous (SERPINB5, THBS1). Furthermore, Western blots for p53 in untreated and paligenotic stomachs and

pancreases showed that p53 expression was dramatically increased in *Ifrd1*<sup>-/-</sup> mice (Fig. 3c). The p53 activation in *Ifrd1*<sup>-/-</sup> mice likely explains why cell-cycle and anti-apoptotic genes – whose expression is inhibited by p53 – were upregulated in control mice vs. *Ifrd1*<sup>-/-</sup> mice, accounting for both the GSEA pattern and suggesting a p53-dependent mechanism to reduce proliferation in the absence of IFRD1.

Decreased mTORC1-associated transcripts in *Ifrd1*<sup>-/-</sup> pancreas during paligenosis suggested an additional possible mechanism for cell cycle blockade. Our previous studies demonstrated that mature acinar and chief cells maintain high levels of digestive enzyme translation and secretion via activated mTORC1 at homeostasis. However, mTORC1 is quenched during stages 1 and 2 of paligenosis then reactivated in stage 3 where it is required to drive cells from G1 to S-phase of the cell cycle<sup>1</sup>. Hence, given the defective proliferation in *Ifrd1*<sup>-/-</sup> mice, we would expect that the re-induction of mTORC1 function might be compromised.

### **IFRD1 is required for normal mTORC1 reactivation and cell survival in stage 3 of paligenosis**

To assay mTORC1 activity in individual paligenotic cells we used phosphorylated S6 (pS6) ribosomal protein, whose kinase is a target of mTORC1. We previously showed by multiple methods that pS6 is a faithful proxy for mTORC1 activity in individual cells<sup>1</sup>. At homeostasis, in mature chief and acinar cells, pS6 was not affected by loss of IFRD1 (Fig. 4 a, d). However, at the time points when control mice show maximal census of stage 3 paligenotic cells, pS6 expression was markedly aberrant. In stomach, all control paligenotic cells expressed abundant pS6 as expected, but in *Ifrd1*<sup>-/-</sup> mice, even in regions where the paligenotic portions of

glands had not been lost, pS6+ cells were both rarer and often showed less intense expression (Fig. 4a). In pancreas, scattered cells showed high pS6 expression (Figure 4d), but many others showed low to undetectable expression. To confirm aberrant mTORC1 activity following loss of IFRD1, we used HALO Image Analysis Software to quantify pS6 distribution. In control mice only 10% of acinar cells were negative for pS6, while nearly half of *Ifrd1*<sup>-/-</sup> acinar cells were negative at d5 of cerulein. (Fig. 4e and Supplementary Fig. 4).

Thus, the loss of proliferation in stage 3 of *Ifrd1*<sup>-/-</sup> mice correlated with decreased reactivation of mTORC1 and increased p53 activation. As mTORC1 and p53 are both associated with cell survival as well as proliferation, we next investigated the effects of loss of IFRD1 on cell death. Previously, we have shown that there is minimal apoptosis in paligenosis induced by HD-TAM or cerulein, as measured either by loss of tissue in regions of paligenosis or activation of cleaved caspase 3<sup>1</sup>. We also showed that aberrant paligenosis (e.g. by inhibiting stage 1 progression) can lead to increased apoptosis following injury. We confirmed low-level cleaved caspase 3 in control paligenotic stomach and pancreas; in contrast, *Ifrd1*<sup>-/-</sup> mice showed marked, significantly increased apoptosis (Fig. 4 b, c, f, g). Note that by d3 after HD-TAM, many of the paligenotic gland bases in stomach had entirely atrophied in *Ifrd1*<sup>-/-</sup> mice as described above, so the increased cleaved caspase 3 positive cells are in regions that have not yet been lost as depicted in Fig. 4b.

### ***Ifrd1*<sup>-/-</sup> cells fail to re-enter the cell cycle due to inappropriate activation of p53**

Failure of *Ifrd1*<sup>-/-</sup> cells to reactivate mTORC1 could be responsible for the block in proliferation. However, our previous work did not indicate that loss of mTORC1 caused marked increase in cell death, so the fact that loss of IFRD1 caused increased death as well as decreased

proliferation would not necessarily be explained by simple failure to reactivate mTORC1. Furthermore, even without IFRD1, there was a substantial fraction of strongly pS6+ cells, especially in pancreas, indicating that some paligenotic cells could activate pS6 as robustly as wildtype cells. Another possibility is that the overall decreased fraction of pS6+ cells was because mTORC1 activation in the absence of IFRD1 leads to apoptosis rather than mitosis, thus removing many pS6+ cells from the tissue.

Aberrant p53 activation can lead to cell cycle arrest or delay both by blocking mTORC1 activation and by blocking ribosome biogenesis using transcriptional and translational mechanisms<sup>26 27 28</sup>. Thus loss of IFRD1 could activate p53 to block mTORC1 and therefore entry into S-phase. We generated *Ifrd1*<sup>-/-</sup>; *Trp53*<sup>-/-</sup> mice and tested effects on paligenosis in stomach and in pancreas. In both stomach and pancreas, loss of p53 substantially and significantly rescued the proliferation block in *Ifrd1*<sup>-/-</sup> mice (Fig. 5 a - d, f - h). Thus, in the absence of p53, IFRD1 no longer was required for cells to progress through the cell cycle. As mTORC1 is required for S-phase, the results indicated that IFRD1 was not required for mTORC1 activation, and, accordingly, Supplementary Fig. 5 shows that S6 activation was similar to wildtype when both p53 and IFRD1 were deleted. In stomach, loss of both p53 and IFRD1 also significantly decreased the number of dying cells seen in paligenosis when only *Ifrd1* was deleted (Fig. 5e). However, in pancreas, loss of p53 did not change the *Ifrd1*<sup>-/-</sup> cell death phenotype, indicating p53 is required for *Ifrd1*<sup>-/-</sup> gastric paligenotic death but the pancreas may have additional, p53-independent factors that can still cause apoptosis (Fig. 5i).

## **mTORC1 suppresses p53 and is required for cell cycle entry and for cell death in the absence of IFRD1**

Overall, the results indicate that IFRD1 suppresses p53 in Stage 3 of paligenosis such that loss of IFRD1 activates p53 to block the cell cycle and, in the stomach, to cause death. IFRD1 appears to interact with mTORC1 only via p53, as pS6 was delayed but not blocked in *Ifrd1*<sup>-/-</sup> mice and, once p53 was also deleted (i.e. in *Ifrd1*<sup>-/-</sup>; *Trp53*<sup>-/-</sup> mice), mTORC1 activation and proliferation were similar to wildtype (Supplementary Fig. 5). We next sought to further determine the relationship of mTORC1 to p53 and IFRD1. We treated control and *Ifrd1*<sup>-/-</sup> mice with the mTORC1 inhibitor rapamycin during paligenotic injury, using the protocol previously detailed<sup>1</sup>. mTORC1 blockade did not rescue the proliferation block in stomachs of *Ifrd1*<sup>-/-</sup> mice, which was expected because entry into S-phase requires mTORC1 (Fig. 6 b, c). However, rapamycin did inhibit cell death, which was quantified in the stomach at maximal paligenosis (Fig. 6 a, b, d). mTORC1 suppresses p53 activation, and western blot showed that p53 was activated in the absence of mTORC1 (Supplementary Fig. 6). Thus, p53 activation alone does not cause death; death also requires mTORC1 activation.

In the pancreas, we can do more chronic injury to determine how loss of IFRD1 ±mTORC1 affects overall tissue regeneration, whereas HD-TAM causes mouse death if it is not discontinued after maximal paligenosis. Two-week cerulein in *Ifrd1*<sup>-/-</sup> mice caused near total destruction of acinar cells; thus, IFRD1 regulation of paligenosis is absolutely required for tissue repair/survival in this organ (Figure 6E). Rapamycin largely rescued the *Ifrd1*<sup>-/-</sup> cell death, though paligenotic proliferation was still impaired relative to wildtype (Figure 6F).

## Chapter 4.4 CONCLUSIONS

Here, we identify IFRD1 as the first evolutionarily conserved gene whose principal function seems to be to govern paligenosis. IFRD1 is remarkably conserved in structure and length from yeast to humans. Its expression is critical for injury response but mostly dispensable for homeostasis. It is critical for cell cycle re-entry and survival in stage 3 of paligenosis. Epistasis experiments indicate it principally works to suppress the p53-mediated suppression of mTORC1 (Fig. 7). The suppression of p53 is critical specifically in an injury-induced, mTORC1-dependent cell cycle re-entry context because a) *Ifrd1*<sup>-/-</sup> mice have constitutive p53 activation but have no proliferative or developmental phenotype in pancreas or stomach or liver in the absence of injury and b) when mTORC1 is inactive *Ifrd1*<sup>-/-</sup> mice and wildtype mice show similar phenotypes.

To our knowledge, this is the first report to show IFRD1-mediated repression of p53. The central location of IFRD1 as a regulator of p53 in the specific paligenotic context of increased mTORC1 during cell cycle reentry of mature cells makes teleological sense. Multicellular organisms have the advantage of being able to dedicate the vast majority of cells to specific functions; however, paligenosis also allows those cells to act as a large reservoir of potential stem cells to repair damage of organs throughout life. In the pancreas, as shown here, the inability to undergo paligenosis, in the absence of tissue stem cells, can be catastrophic (Fig. 6e). There are risks, however, in allowing long-lived cells to cycle between replicative and differentiated states, because mutations could potentially accumulate over time increasing cancer risk with each paligenotic event<sup>29,30</sup>. A robust licensing mechanism that is dedicated to regulating paligenotic cell cycle entry – and would not affect constitutive cycling of homeostatic tissue stem cells -- would make sense. That is, in fact, why it has been speculated p53 evolved in

multicellular organisms and not yeast <sup>31</sup>: Multicellular organisms can afford to waste cells via apoptosis to avoid cancer risk. Our previous results showing increased IFRD1 predicts poor outcome in colon cancer is consistent with the potential for tumor cells to exploit IFRD1 suppression of p53 to subvert cell cycle delay and apoptosis <sup>6</sup>.

Here, we outline a central hub that performs the key, conserved licensing steps allowing mature cells to re-enter the cell cycle, describing critical roles for mTORC1, p53, and a gene whose function seems to have evolved largely to dictate paligenosis. There is likely a dedicated cohort of other genes that govern this cellular program that acts on injured mature cells that reach the decision crux between apoptosis and mitosis. Because paligenosis is at the heart of both regeneration and tumorigenesis, delineating the underlying genes can lead to better understanding that might spur new therapeutic approaches.

Chapter 4.5 FIGURES

FIGURE 4.1

Lewis et al. Figure 1

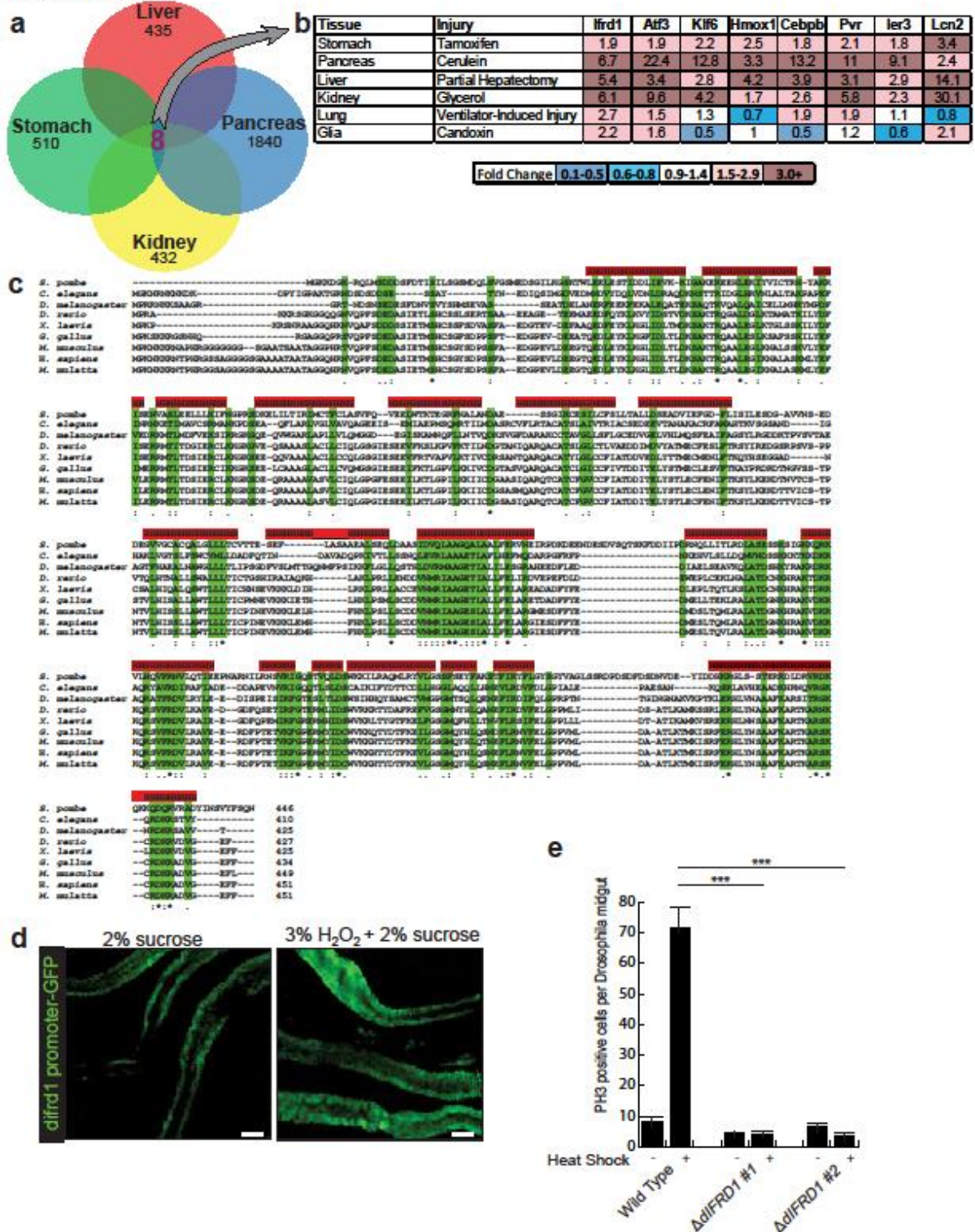


**Fig. 1 IFRD1 is highly conserved and is upregulated following regeneration-inducing injury in multiple tissues and species**

- a. Venn diagram depicting coinciding genes up-regulated in each model. Green = high-dose tamoxifen-induced gastric metaplasia (Spasmolytic Polypeptide Expressing Metaplasia), blue = cerulein injury-induced pancreatic metaplasia (Acinar-Ductal Metaplasia), red = partial liver resection, yellow = glycerol-induced acute kidney injury.
- b. Analysis showing the relative gene expression of coinciding genes in injury models.
- c. Multiple sequence alignment of *Ifrd1* across evolutionary spectrum. Secondary structural prediction from *H. sapiens* sequence.
- d. Image of the localization of GFP driven by *Ifrd1* promoter in *Drosophila melanogaster* intestine at baseline and under H<sub>2</sub>O<sub>2</sub> stress. Scale bar, 100μM
- e. Quantitative analysis of pHH3<sup>+</sup> cells in *Drosophila* intestine sections. Δ*I*FRD1 #1 and #2 are hypomorphic for *difrd1*. Statistical information: N.S. = not statistically significant, \*\*P < 0.01; \*\*\*P < 0.001 by t-test with unequal variance; data represented as mean ± SD from at least 3 independent experiments.

FIGURE 4.2

Lewis et al. Figure 2

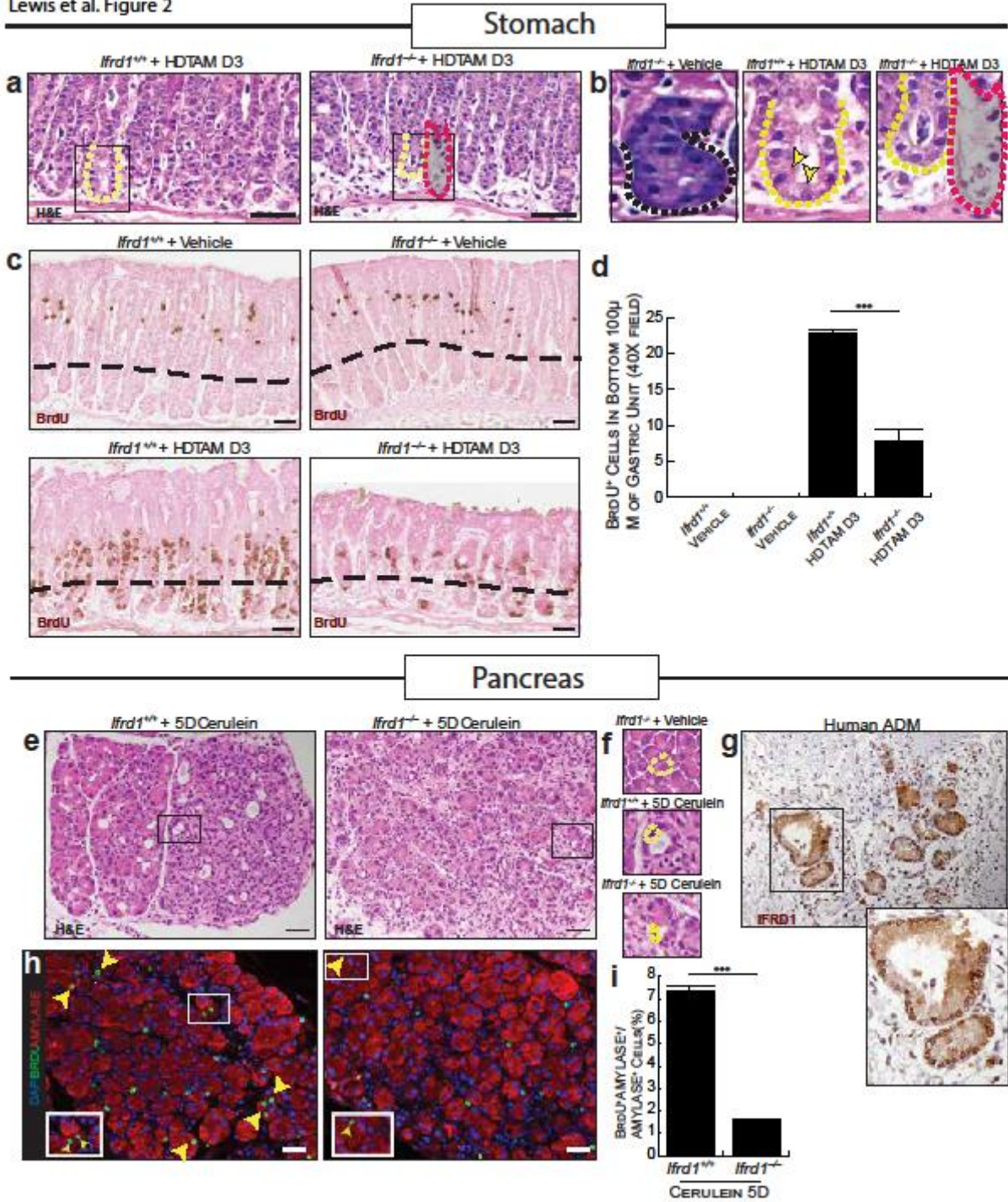


**Fig. 2 IFRD1 is required for stage 3 of paligenosis**

- a. Histological analysis of wildtype and *Ifrd1*<sup>-/-</sup> mice after day 3 high-dose tamoxifen (hdtam d3) treatment. Scale bar, 50μM.
- b. High magnification histological analysis of zymogenic chief cells from *Ifrd1*<sup>-/-</sup> vehicle, wildtype hdtam d3 and *Ifrd1*<sup>-/-</sup> hdtam d3. Black outline = normal chief cell histology, yellow outline = normal histological metaplasia (SPeM), yellow arrows = representative metaplastic changes in chief cells, red outline = area of zymogenic chief cell dropout.
- c. Immunohistological analysis of BrdU staining in gastric units from mice vehicle and hdtam d3 treated wildtype and *Ifrd1*<sup>-/-</sup> mice. Dotted line = representative chief cell zone (100μM perpendicular to muscularis mucosa). Scale bar, 50μM.
- d. Quantitative analysis of BrdU<sup>+</sup> cells the chief cell zone of vehicle and hdtam d3 treated wildtype and *Ifrd1*<sup>-/-</sup> mice. Statistical information: N.S. = not statistically significant, \*\*P < 0.01; \*\*\*P < 0.001 by t-test with unequal variance; data represented as mean ± SD from at least 3 independent experiments.
- e. Histological analysis of wildtype and *Ifrd1*<sup>-/-</sup> mice 5 days post cerulein treatment. Scale bar, 50μM.
- f. High magnification histological analysis pancreatic acinar cells of vehicle treated *Ifrd1*<sup>-/-</sup> mice, cerulein treated wildtype mice and cerulein treated *Ifrd1*<sup>-/-</sup> mice.
- g. Immunohistological staining of IFRD1 human pancreas tissue. Scale bar, 50μM.
- h. Immunofluorescent imaging of BrdU incorporation 5 days post-cerulein treatment in wildtype and *Ifrd1*<sup>-/-</sup> mice. Yellow arrow = AMYLASE/BRDU co-positive cells. Scale bar, 50μM.

- i.** Quantification of BrdU<sup>+</sup> cell number per 20X field at 5 days post cerulein. Statistical information: N.S. = not statistically significant, \*\*P < 0.01; \*\*\*P < 0.001 by t-test with unequal variance; data represented as mean ± SD from at least 3 independent experiments.

**FIGURE 4.3**

Lewis et al. Figure 3

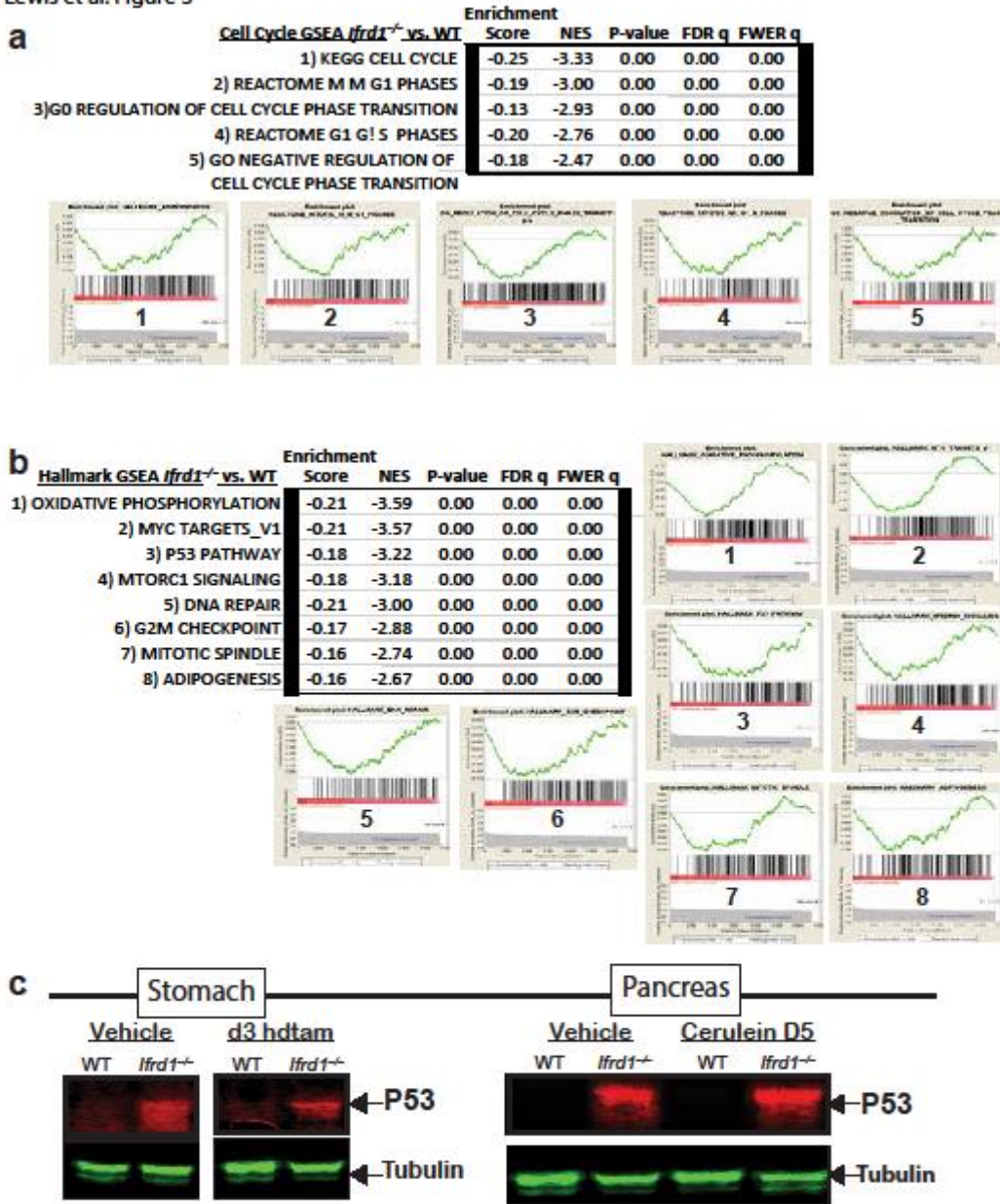


**Fig. 3 Loss of IFRD1 causes increased activation of p53 and decreased expression of mTORC1-associated and cell-cycle-related transcripts**

- a.** Global gene expression profiling of pancreas tissue *Ifrd1*<sup>-/-</sup> and control mice ±cerulein at 5 days post-cerulein using Gene Set Enrichment Analysis (GSEA) utilizing publicly available cell cycle data sets.
- b.** Unbiased screen of Broad Institute Hallmark data sets using GSEA to uncover gene sets that significantly distinguish cerulein-injured *Ifrd1*<sup>-/-</sup> pancreases from control.
- c.** Western blot for p53 untreated and paligenotic stomachs and pancreases.

FIGURE 4.4

Lewis et al. Figure 4

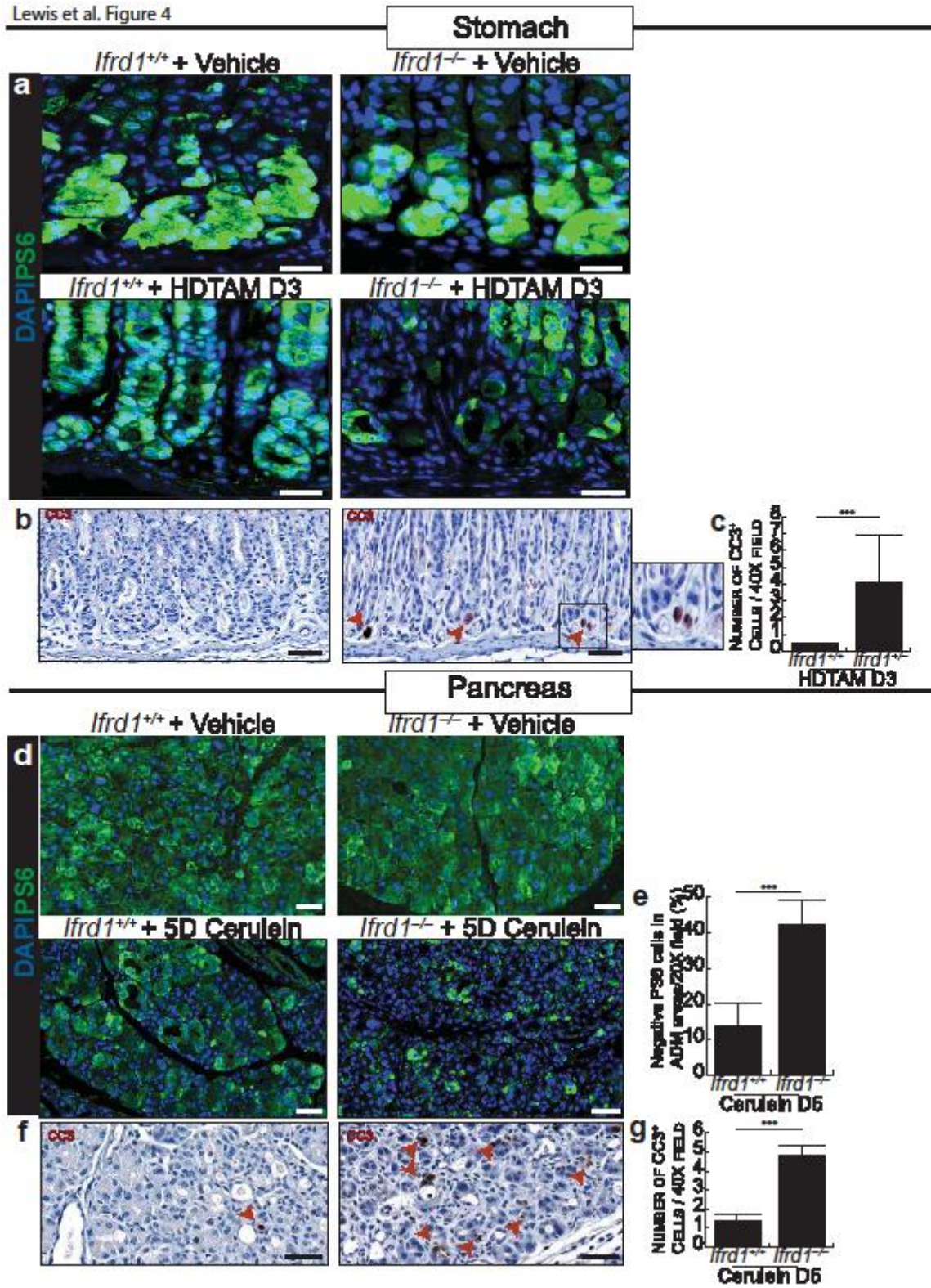


**Fig. 4 IFRD1 is required for normal mTORC1 reactivation and cell survival in stage 3 of paligenosis**

- a.** Immunofluorescent analysis of phosphorylated-S6 (pS6) staining in wildtype and *Ifrd1*<sup>-/-</sup> mice following vehicle or hdtam d3 treatment. Scale bar, 20 $\mu$ M.
- b.** Immunohistological analysis of Cleaved-Caspase 3 (CC3) staining in wildtype and *Ifrd1*<sup>-/-</sup> mice following hdtam d3 treatment. Scale bar, 50 $\mu$ M.
- c.** Quantification of CC3<sup>+</sup> cells per 20X field in wildtype and *Ifrd1*<sup>-/-</sup> mice following vehicle or hdtam d3 treatment. Statistical information: N.S. = not statistically significant, \*\*P < 0.01; \*\*\*P < 0.001 by t-test with unequal variance; data represented as mean  $\pm$  SD from at least 3 independent experiments.
- d.** Immunofluorescent analysis of pS6 staining in wildtype and *Ifrd1*<sup>-/-</sup> mice 5 days following vehicle or cerulein treatment. Scale bar, 50 $\mu$ M.
- e.** Quantitative analysis using the HALO imaging software of areas of the pancreas demonstrating ADM that are lacking pS6 expression per 20X field. N.S. = not statistically significant, \*\*P < 0.01; \*\*\*P < 0.001 by t-test with unequal variance; data represented as mean  $\pm$  SD from 5 images from 4 independent experiments.
- f.** Immunohistological analysis of CC3 staining in wildtype and *Ifrd1*<sup>-/-</sup> mice 5 days following cerulein treatment. Scale bar, 50 $\mu$ M.
- g.** Quantification of CC3<sup>+</sup> cells per 20X field in wildtype and *Ifrd1*<sup>-/-</sup> mice 5 days following cerulein treatment. Statistical information: N.S. = not statistically significant, \*\*P < 0.01; \*\*\*P < 0.001 by t-test with unequal variance; data represented as mean  $\pm$  SD from at least 3 independent experiments.

FIGURE 4.5

Lewis et al. Figure 5

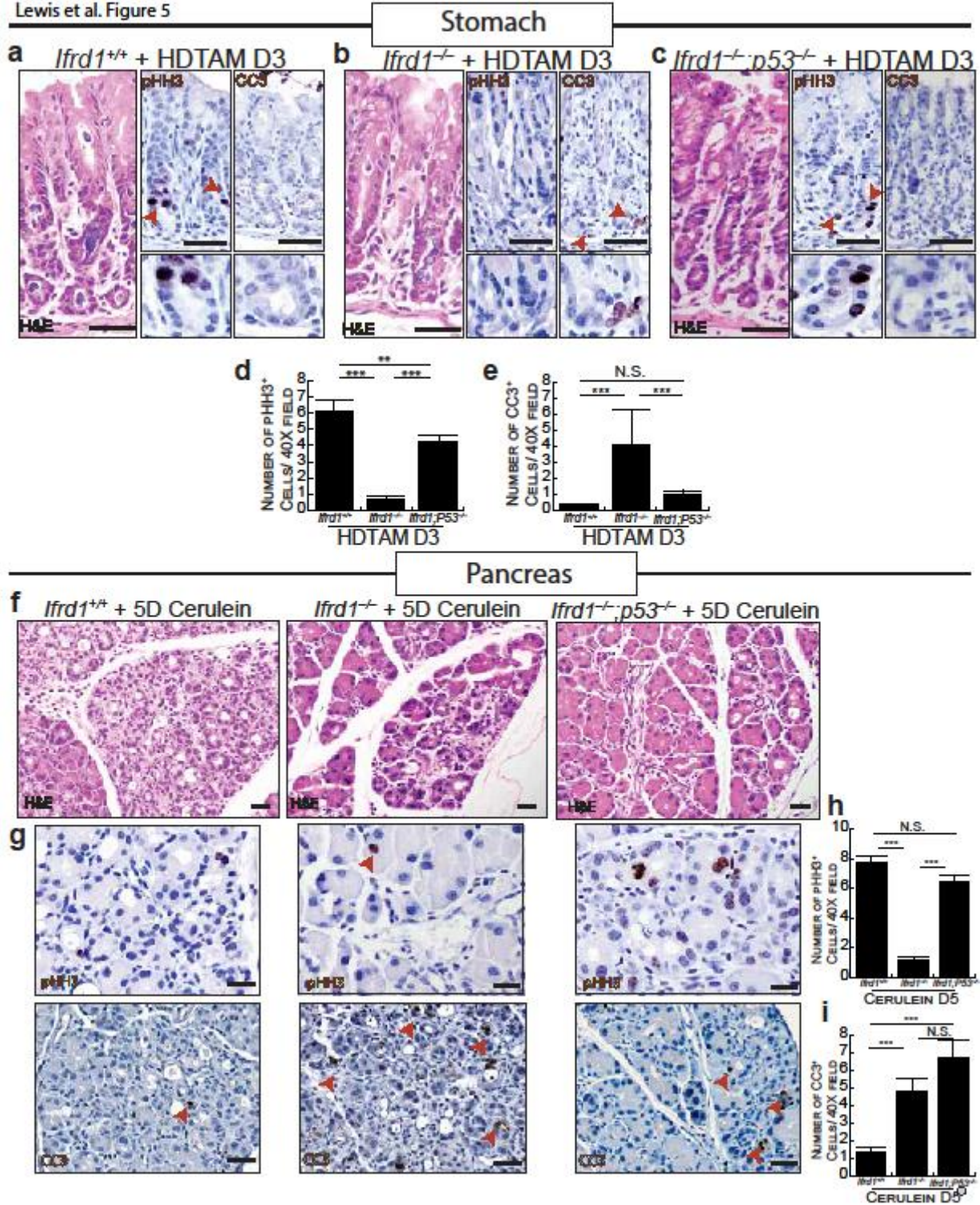


**Fig. 5 *Ifrd1*<sup>-/-</sup> cells fail to re-enter the cell cycle due to inappropriate activation of p53**

- a.** Histological analysis of wildtype mice treated with hdtam d3. Smaller panels show representative and high magnification immunohistological imaging of pHH3 and CC3 staining. Histology scale bar, 50μM. Immunohistological scale bar, 20μM.
- b.** Histological analysis of *Ifrd1*<sup>-/-</sup> mice treated with hdtam d3. Smaller panels show representative and high magnification immunohistological imaging of pHH3 and CC3 staining. Histology scale bar, 50μM. Immunohistological scale bar, 20μM.
- c.** Histological analysis of *Ifrd1*<sup>-/-</sup>; *p53*<sup>-/-</sup> mice treated with hdtam d3. Smaller panels show representative and high magnification immunohistological imaging of pHH3 and CC3 staining. Histology scale bar, 50μM. Immunohistological scale bar, 20μM.
- d.** Quantitative analysis of pHH3<sup>+</sup> cells in wild type, *Ifrd1*<sup>-/-</sup> and *Ifrd1*<sup>-/-</sup>; *p53*<sup>-/-</sup> mice treated with hdtam d3. Statistical information: N.S. = not statistically significant, \*\*P < 0.01; \*\*\*P < 0.001 by t-test with unequal variance; data represented as mean ± SD from at least 3 independent experiments.
- e.** Quantitative analysis of CC3<sup>+</sup> cells in wild type, *Ifrd1*<sup>-/-</sup> and *Ifrd1*<sup>-/-</sup>; *p53*<sup>-/-</sup> mice treated with hdtam d3. Statistical information: N.S. = not statistically significant, \*\*P < 0.01; \*\*\*P < 0.001 by t-test with unequal variance; data represented as mean ± SD from at least 3 independent experiments.
- f.** Histological analysis of wildtype, *Ifrd1*<sup>-/-</sup> and *Ifrd1*<sup>-/-</sup>; *p53*<sup>-/-</sup> mice 5 days following treatment with cerulein. Scale bar, 50μM.
- g.** Immunohistological analysis of pHH3<sup>+</sup> and CC3<sup>+</sup> wildtype, *Ifrd1*<sup>-/-</sup> and *Ifrd1*<sup>-/-</sup>; *p53*<sup>-/-</sup> mice 5 days following treatment with cerulein. Scale bar, 20μM.

- h.** Quantitative analysis of pHH3<sup>+</sup> cells in wild type, *Ifrd1*<sup>-/-</sup> and *Ifrd1*<sup>-/-</sup>;*p53*<sup>-/-</sup> mice 5 days following treatment with cerulein. Statistical information: N.S. = not statistically significant, \*\*P < 0.01; \*\*\*P < 0.001 by t-test with unequal variance; data represented as mean ± SD from at least 3 independent experiments.
- i.** Quantitative analysis of CC3<sup>+</sup> cells in wild type, *Ifrd1*<sup>-/-</sup> and *Ifrd1*<sup>-/-</sup>;*p53*<sup>-/-</sup> mice 5 days following treatment with cerulein. Statistical information: N.S. = not statistically significant, \*\*P < 0.01; \*\*\*P < 0.001 by t-test with unequal variance; data represented as mean ± SD from at least 3 independent experiments.

**FIGURE 4.6**

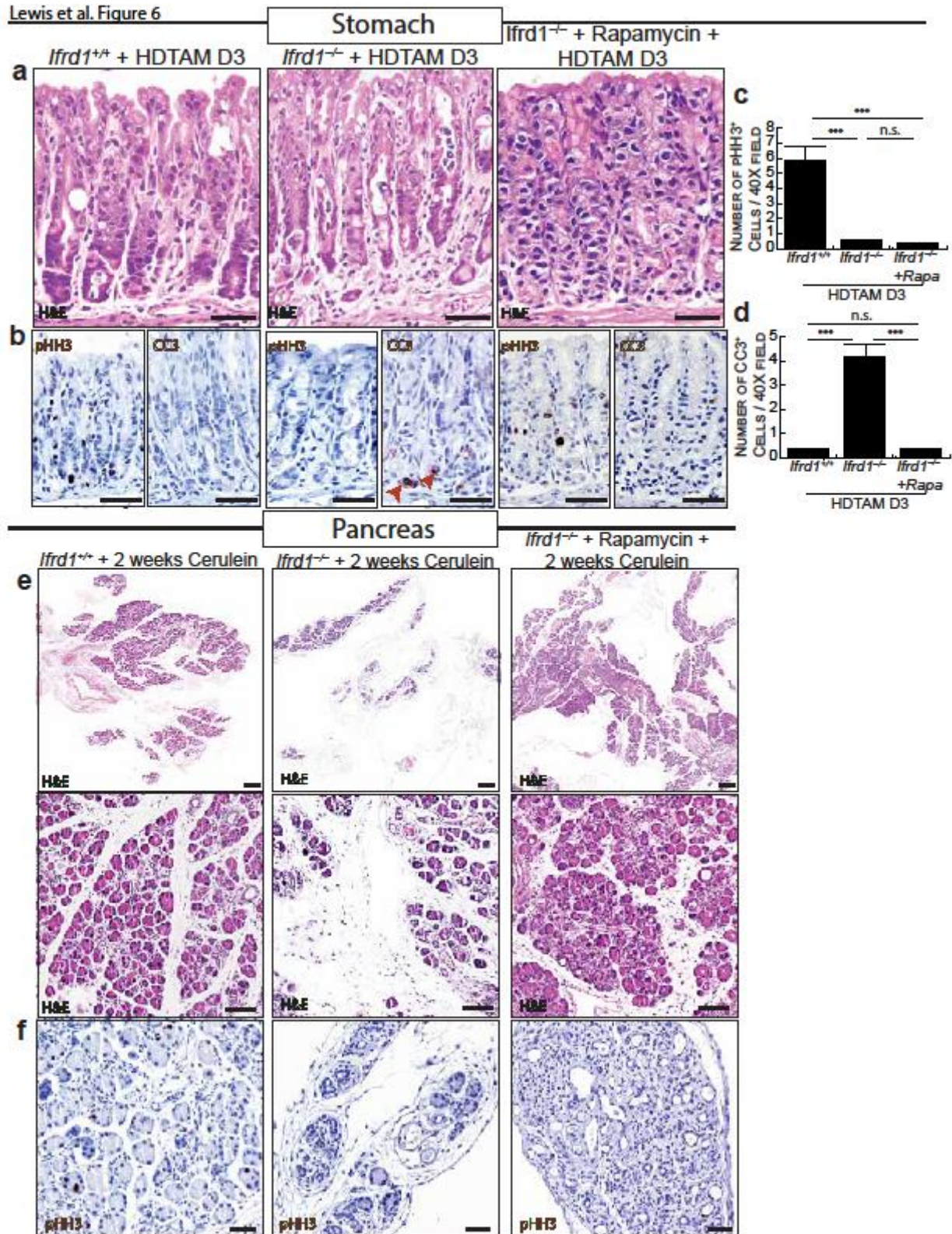
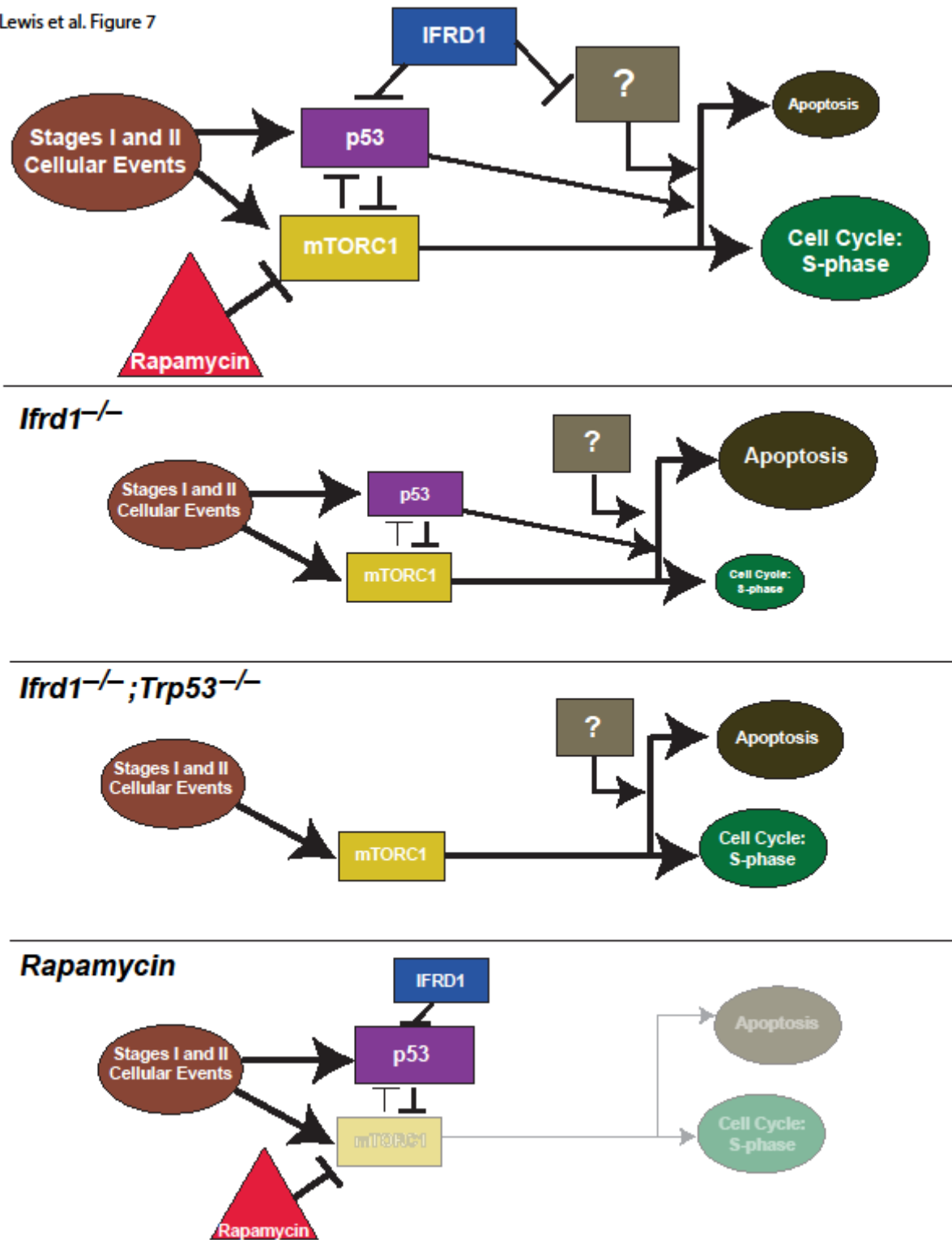


**Fig. 6 mTORC1 suppresses p53 and is required for cell cycle entry and for cell death in the absence of IFRD1**

- a.** Histological analysis of hdtam d3 treated wildtype, *Ifrd1*<sup>-/-</sup> and *Ifrd1*<sup>-/-</sup> + rapamycin mice. Scale bar, 50μM.
- b.** Immunohistological analysis pHH3<sup>+</sup> and CC3<sup>+</sup> cells of hdtam d3 treated wildtype, *Ifrd1*<sup>-/-</sup> and *Ifrd1*<sup>-/-</sup> + rapamycin mice. Scale bar, 20μM.
- c.** Quantitative analysis of pHH3<sup>+</sup> cells in wild type, *Ifrd1*<sup>-/-</sup> and *Ifrd1*<sup>-/-</sup> + rapamycin mice treated with hdtam d3. Statistical information: N.S. = not statistically significant, \*\*P < 0.01; \*\*\*P < 0.001 by t-test with unequal variance; data represented as mean ± SD from at least 3 independent experiments.
- d.** Quantitative analysis of CC3<sup>+</sup> cells in wild type, *Ifrd1*<sup>-/-</sup> and *Ifrd1*<sup>-/-</sup> + rapamycin mice treated with hdtam d3. Statistical information: N.S. = not statistically significant, \*\*P < 0.01; \*\*\*P < 0.001 by t-test with unequal variance; data represented as mean ± SD from at least 3 independent experiments.
- e.** Histological analysis of 2 weeks cerulein treated wildtype, *Ifrd1*<sup>-/-</sup> and *Ifrd1*<sup>-/-</sup> + rapamycin mice. Scale bars, 200μM (top), 50μM (bottom).
- f.** Immunohistological analysis pHH3<sup>+</sup> cells of 2 weeks cerulein treated wildtype, *Ifrd1*<sup>-/-</sup> and *Ifrd1*<sup>-/-</sup> + rapamycin mice. Scale bar, 20μM.

FIGURE 4.7

Lewis et al. Figure 7



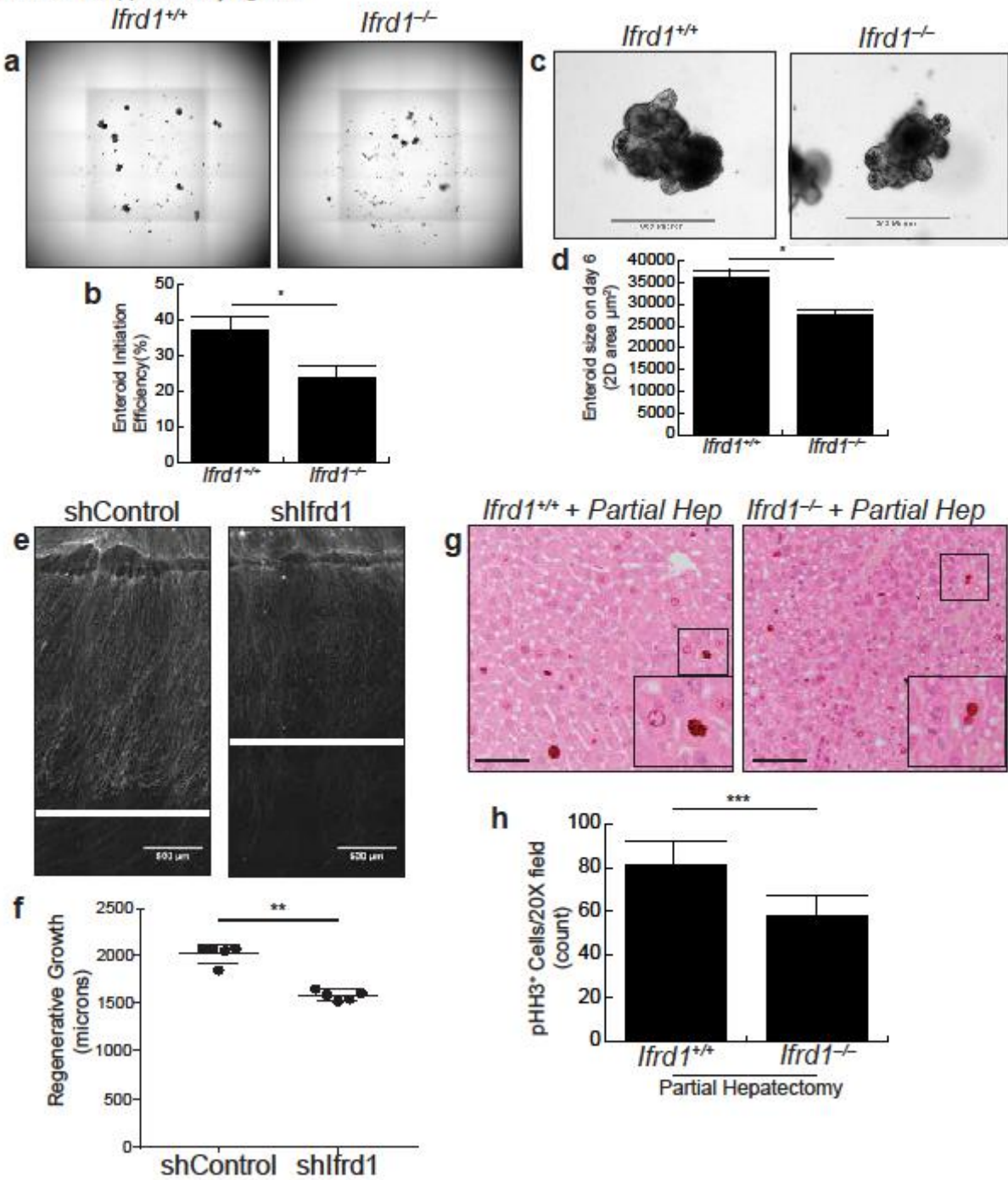


**Supplementary Fig. 1 IFRD1 structure exhibits broad evolutionary conservation**

- a. Phylogenetic tree generated from multisequence analysis of IFRD1 orthologs across numerous classes from three phyla using Clustal Omega webserver.
- b. Multisequence alignment of IFRD1 (*H. sapiens*) to IFRD2 (*O. cuniculus*). Secondary structure for IFRD1 was computed using JPred4 webserver and secondary structure for IFRD2 was computed from the atomic coordinates of the recently reported cryoEM structure of IFRD2 bound to the ribosome (PDB 6MTC).

SUPPLEMENTARY FIGURE S4.2

Lewis et al. Supplementary Figure 2

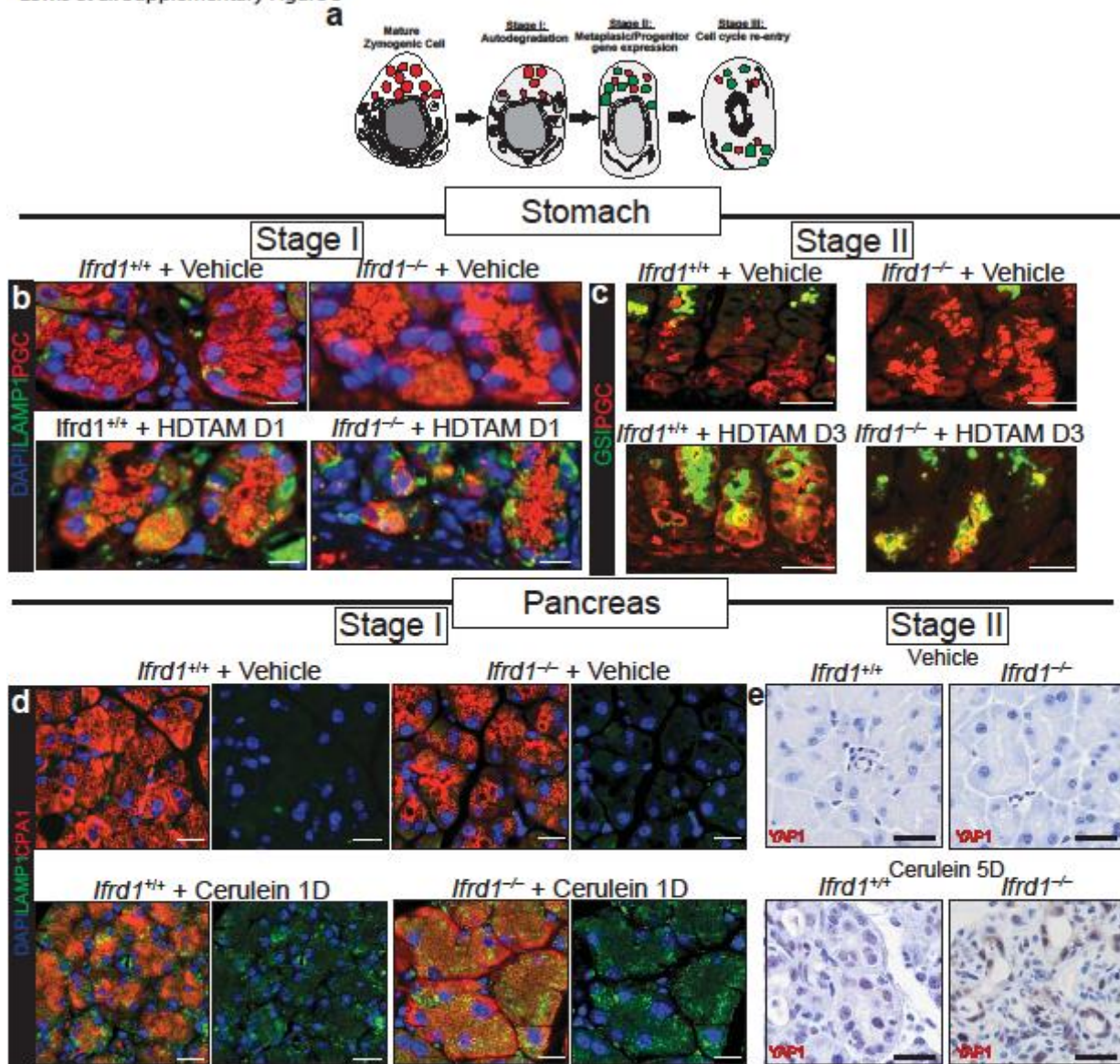


**Supplementary Fig. 2 IFRD1 function is cell-autonomous and is required  
proliferation/regeneration in multiple systems**

- a. Low (4X) magnification images of organoids derived from *wild type* and *Ifrd1*<sup>-/-</sup> mice.
- b. Quantification of enteroid initiation efficiency of *wild type* and *Ifrd1*<sup>-/-</sup> mice. Statistical information: N.S. = not statistically significant, \*\*P < 0.01; \*\*\*P < 0.001 by t-test with unequal variance; data represented as mean ± SD from at least 3 independent experiments.
- c. High power image of a single representative organoid from *wild type* and *Ifrd1*<sup>-/-</sup> mice. Scale bar, 300µM.
- d. Quantification of enteroid size on day 6 of *wild type* and *Ifrd1*<sup>-/-</sup> mice. Statistical information: N.S. = not statistically significant, \*\*P < 0.01; \*\*\*P < 0.001 by t-test with unequal variance; data represented as mean ± SD from at least 3 independent experiments.
- e. Representative images of axon regeneration following axotomy *ex vivo* of control and shRNA knockdown of *Ifrd1* (shIfrd1). Scale bar, 500µM.
- f. Quantification of axon regeneration following axotomy. Statistical information: N.S. = not statistically significant, \*\*P < 0.01; \*\*\*P < 0.001 by t-test with unequal variance; data represented as mean ± SD from 5 independent experiments.
- g. Histological analysis partially resected livers from *wild type* and *Ifrd1*<sup>-/-</sup> mice. Scale bar, 50µM.
- h. Quantification of pHH3+ cells per 20X field following partial hepatectomy in *wild type* and *Ifrd1*<sup>-/-</sup> mice.

SUPPLEMENTARY FIGURE S4.3

Lewis et al. Supplementary Figure 3

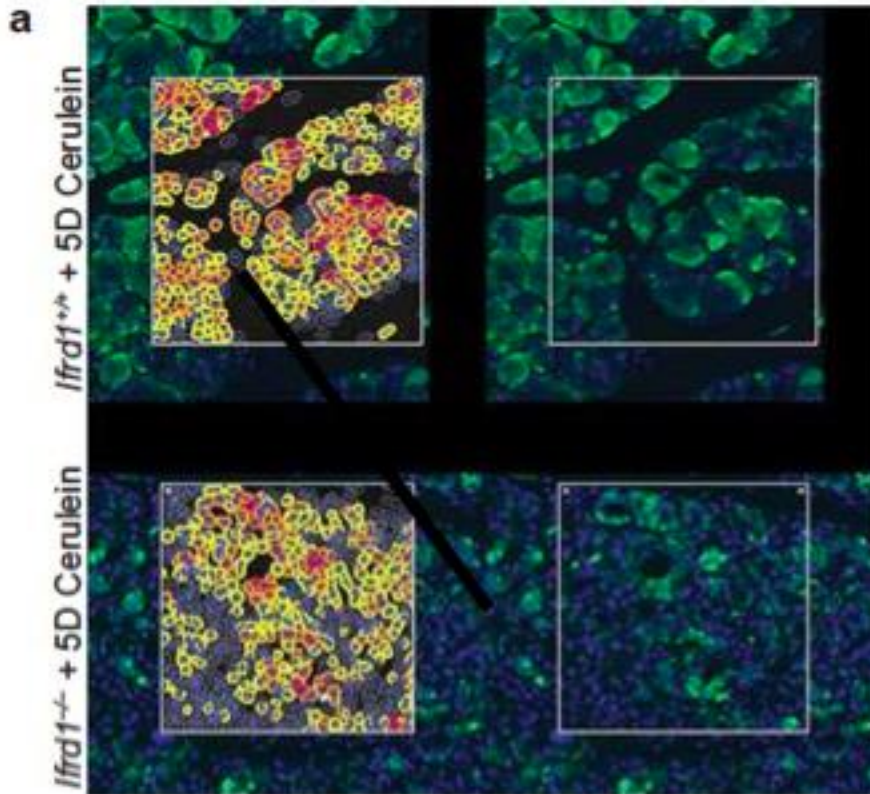


**Supplementary Fig. 3 In the absence of IFRD1, mice do not have substantial defects in development, homeostasis or early stages of paligenosis**

- a. Schematic image of the 3 stages of paligenosis.
- b. Immunofluorescent analysis of activation of lysosomal machinery (paligenosis Stage 1) in chief cells of wild type and *Ifrd1*<sup>-/-</sup> mice treated with d1 hdtam. DAPI: 4',6-diamidino-2-phenylindole (nucleus). LAMP1: lysosomal associated membrane protein (lysosomes). PGC: Pepsinogen C (protease secreted by gastric chief cell). Scale bar, 20μM.
- c. Immunofluorescent analysis of the metaplastic gene expression (paligenosis Stage 2) in chief cells of wild type and *Ifrd1*<sup>-/-</sup> mice treated with d3 hdtam. GSII: N-acetylglucosamine-binding lectins (neck cell). PGC: Pepsinogen C (protease secreted by gastric chief cell) Scale bar, 50μM.
- d. Immunofluorescent analysis of activation of lysosomal machinery (paligenosis Stage 1) in acinar cells of wild type and *Ifrd1*<sup>-/-</sup> mice 1 day following treatment with cerulein. DAPI: nucleus. LAMP1: lysosomes. CPA1: Carboxypeptidase A1 (digestive enzyme secreted by pancreatic acinar cells). Scale bar, 50μM.
- e. Immunofluorescent analysis of the metaplastic gene expression (paligenosis Stage 2) in acinar cells of wild type and *Ifrd1*<sup>-/-</sup> mice 5 days following treatment with cerulein. YAP1: Yes-associated protein 1 (baseline- duct cell; cerulein- acinar and duct cells). Scale bar, 50μM.

## SUPPLEMENTARY FIGURE S4.4

Lewis et al. Supplementary Figure 4

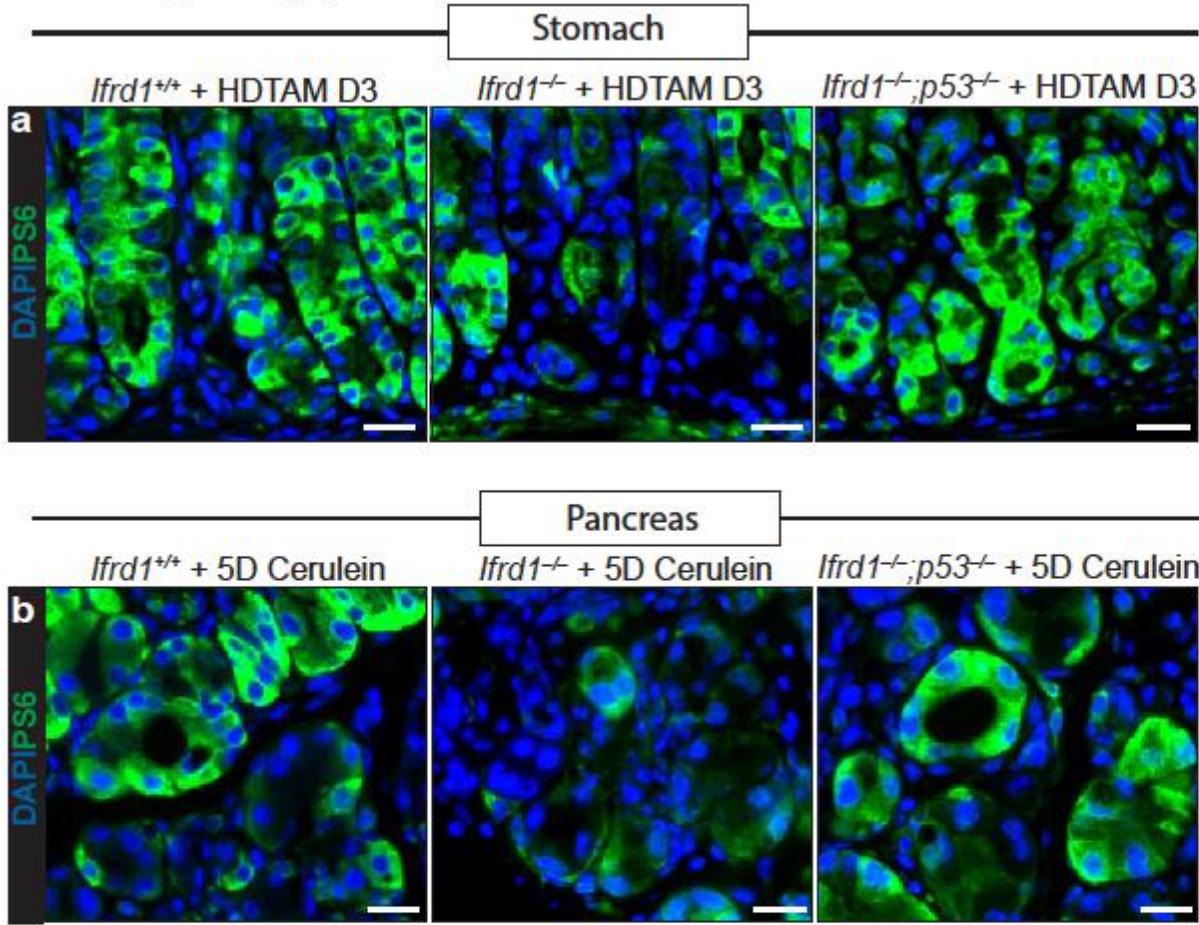


### Supplementary Fig. 4 Representative image of HALO imaging software

- a. Representative image of the identification of positive (yellow, orange, and red) and negative (no color) cells using the HALO imaging software in wild type and *Ifrd1*<sup>-/-</sup> mice 5 days following treatment with cerulein.

SUPPLEMENTARY FIGURE S4.5

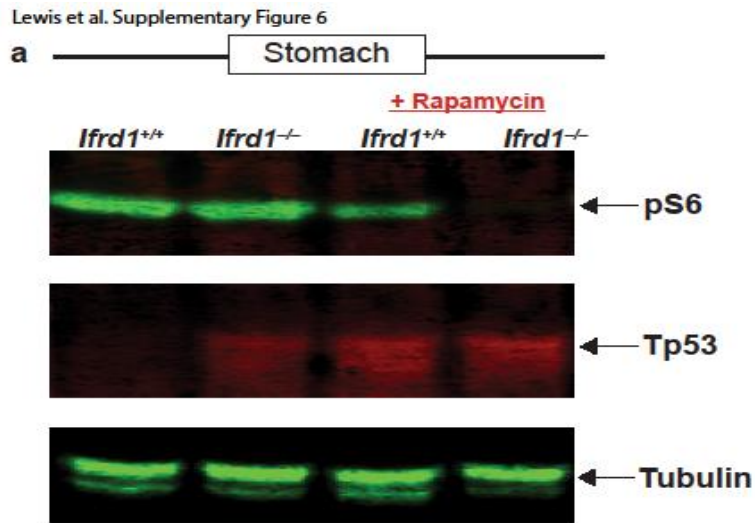
Lewis et al. Supplementary Figure 5



**Supplementary Fig. 5 Loss of p53 rescues the mTORC1 defect in *Ifrd1*<sup>-/-</sup> mice**

- a.** Immunofluorescent analysis of PS6 staining in wild type, *Ifrd1*<sup>-/-</sup> and *Ifrd1*<sup>-/-</sup>;*p53*<sup>-/-</sup> mice treated with hdm d3. Scale bar, 50μM.
- b.** Immunofluorescent analysis of PS6 staining in wild type, *Ifrd1*<sup>-/-</sup> and *Ifrd1*<sup>-/-</sup>;*p53*<sup>-/-</sup> mice 5 days following treatment with cerulein. Scale bar, 50μM.

## SUPPLEMENTARY FIGURE S4.6



### Supplementary Fig. 6 mTORC1 inhibition causes the stabilization of p53

**a.** Western blot for p53 and Ps6 in untreated and rapamycin treated stomachs.

## Chapter 4.6 METHODS

### Bioinformatics, microarray and *in silico* screening

GeneChips were analyzed with Partek Genomic Suite 6.6 (Partek, Inc.) analysis software using default settings (Lo et al. 2017). Gene sets include Tamoxifen (12 hour; generated by Jason Mills lab), Pancreas (6 hour; GDS1731), Partial Hepatectomy (2 hour, GDS2577), Acute Kidney Injury (24h, GDS4864), Ventilator-Induced Lung Injury (6 hour, GDS81240), and Candoxin Glia Injury (24 hour, GDS1414). Thresholds were set at 1.5-fold gene enrichment for all gene sets.

GSEA (Subramanian et al., 2005), was done using default 3.0 settings. GMX files were made using microarray data generated *de novo* from WT and *Ifrd1*<sup>-/-</sup> pancreas tissue treated with cerulein (GSE121925, available May 1, 2019). RNA was isolated using the RNEasy Micro Kit (Qiagen) following the manufacturers' instructions. Mouse Gene 2.0 ST Array (Affymetrix) was used to analyze gene expression. Multisequence alignments and phylogenetic analysis are presented as uncurated results from Clustal Omega Webserver (Sievers Mol System Biol, <http://msb.embopress.org/content/7/1/539>). Secondary structure prediction was computed with the JPred4 webserver (Drozdetskiy NAR, 2015) using the sequence of human IFRD1.

### Animal studies and reagents

All experiments using animals followed protocols were approved by the Washington University School of Medicine Animal Studies Committee. WT C57BL/6 mice were purchased from Jackson Laboratories (Bar Harbor, ME). *Ifrd1*<sup>-/-</sup> mice, previously described (Vadivelu et al. 2004), were a kind gift from Dr. Lukas Huber and Dr. Deborah Rubin. Tamoxifen (5 mg/20 g body weight; Toronto Research Chemicals) was injected intraperitoneally (IP) daily for 2–3 days

to induce maximal gastric injury (Huh *et al*, 2012; Saenz *et al*, 2016). Tamoxifen was prepared by first dispersing in 100% ethanol by sonication and then emulsifying in sunflower oil (Sigma-Aldrich) 9:1 (oil:ethanol). Pancreatitis was induced by 6 hourly IP injections of 50 µg/kg (in 0.9% saline) cerulein (Sigma-Aldrich) given every other day for up to 2 weeks. Mice were sacrificed 24h after the final cerulein injection. Rapamycin (60 µg/20 g body weight; LC Laboratories) was injected IP in 0.25% Tween-20, 0.25% polyethylene glycol in PBS for 3–7 days prior to starting and throughout injury time course. Mice were given an IP injection containing 5-bromo-2'-deoxyuridine (BrdU; 120 mg/kg) and 5-fluoro-2'-deoxyuridine (12 mg/kg) in sterile water 90 min before sacrifice for all BrdU labeling experiments.

### **Drosophila studies**

Mammalian *ifrd1* homolog is CG31694 (*difrd1* here). Fly stocks were obtained from the Bloomington Drosophila stock center. *yw*; P(EPgy2)EY11632 (BL#20811; designated as *difrd1* #1), *yw*; P(PTT-GA)CA07748 (BL#52520; designated as *difrd1* #2 or *ifrd1*-GFP). *w1118* or *Canton-S* are used as wild types. All flies were cultured on yeast-molasses based on food at the room temperature.

Flies were anesthetized by CO<sub>2</sub> gas and were stored on ice until dissection. Midguts were dissected in fly saline (182mM KCl, 46mM NaCl, 10mM Tris Base, 3mM CaCl<sub>2</sub>, pH adjusted to 7.2 with 1N HCl) and transferred to fixation solution (4% formaldehyde, 7% picric acid in 1X PBS) for 1h at room temperature while shaking. All samples were washed by Washing buffer (1X PBT: 1x PBS and 0.3% Triton X-100) several times for 1h and blocked in the pre-incubation buffer (1X PBT containing 1% BSA and 1% normal goat serum, 0.01% Sodium Azide). Primary antibodies were diluted in the same buffer. Midguts were incubated in antisera overnight at 4°C

with shaking. After intensive washing, midguts were incubated with secondary antibodies (Alexa-488/ -594/ -647 conjugated IgG antibodies, 1:1000) for 1h at room temperature. After washing twice for 15 minutes, midguts were stained with 1  $\mu$ g/mL DAPI in 1x PBT for 15min, followed twice more washing and mounted in Vectashield medium (Vector Laboratories).

For heat shock stress, female flies were incubated at 37°C for 90 minutes and recovered for more than 2 days at room temperature. For oxidative stress, female flies were raised in vials containing 1 mL of 2% sucrose solution with or without 3% hydrogen peroxide for overnight. Fly guts were dissected in saline and fixed (7% picric acid/4% paraformaldehyde, 1X PBS) for 60 min. The immunostaining was performed as previously described (Park et al., 2008). Primary antibodies used for immunocytochemistry included rabbit anti-PH3 (Cell Signaling, 1:1000) and mouse anti-GFP (DHSB, 1:200). Conjugated secondary antibodies were Alexa488 or Alexa594 (Molecular Probes).

### **Organoid culture**

Enteroid cultures were established from crypts isolated from WT or *Ifrdl*<sup>-/-</sup> proximal jejunum. Crypts were plated in Matrigel and grown into enteroids in media containing EGF, R-spondin, Wnt3a, noggin and Y27632 (Sata et al. 2009, Fuller et al. 2012). Enteroids were then re-passaged twice at 7 day intervals to measure replating efficiency, and harvested for RNA on day 21. Enteroid numbers and area were quantified from images of each well obtained on days 6, 13 and 20 using Cytation 3 Cell Imaging. The efficiency of enteroid establishment from crypts was calculated as the number of enteroids on day 6 normalized to the number of crypts plated. Enteroid area was measured at each time point using NIH ImageJ.

## **Axon Regeneration**

Embryonic DRG neurons were cultured as previously described (Cho and Cavalli, 2012). Briefly, e13.5 DRG neurons were dissected from CD-1 mice, trypsinized (.05%) for 25 minutes, and triturated 60x to dissociate the cells. Neurons were resuspended in neuronal media consisting of Neurobasal, 1x B27, 1x Glutamax, FDU, and pen/strep, and were plated in spots of 10,000 neurons on plates coated with poly-d-lysine and laminin. Lentivirus containing FCIV-Bclx1 was added at DIV 2 and shIFRD1 at DIV4. At DIV 9, spots were axotomized with an 8mm long microtome blade and fixed 48 hours after injury. Spots were immunostained for SCG10 and regenerative growth was measured from the blade mark to the axon tips. The experiments were completed in technical triplicate with 8 biological replicates.

## **Imaging and tissue analysis**

Mouse tissues were immediately excised and flushed with phosphate-buffered saline and fixed overnight in 4% paraformaldehyde in PBS. Tissues were washed, embedded in 3% agar, and then underwent routine paraffin processing. Sections prepared for immunofluorescence or immunohistochemistry underwent standard deparaffinization and rehydration protocols, were blocked in 5% normal serum, and left overnight with primary antibodies. Sections were washed in phosphate-buffered saline and incubated for 1 h with secondary antibodies and then washed prior to mounting. For antibodies used in this study, see (Supplementary Table \_).

Immunofluorescence images were taken on a Zeiss Apotome or LSM710 confocal (Zeiss).

Bright field images were taken on a Nanozoomer (Hamamatsu) whole slide scanner or DP70 microscope (Olympus). To account for frequent gland loss in the base of *Ifrd1*<sup>-/-</sup> mice, 10 random, 20X fields were chosen in three *Ifrd1*<sup>-/-</sup> and three control animals. The 10 fields were

further subdivided into two rectangular regions: a basal one 100  $\mu\text{m}$  perpendicular and 450  $\mu\text{m}$  parallel to the muscularis mucosa and a region of the same size immediately adjacent and encompassing the neck of the gastric unit. All BrdU<sup>+</sup> or pHH3 cells were scored and the proportion in each zone calculated. Quantification of proliferation in the pancreas was done by counting 10 randomly sampled whole 20X fields per condition. HALO image analysis platform (Indica Labs) to quantify intensity of fluorescent staining. We selected 5 pancreas images per four *Ifrd1*<sup>-/-</sup> and four control animals that exhibited pathological ADM. Exposure times were kept constant across all samples and images were analyzed based on the intensity of fluorescence per cell. The staining threshold was set based on control tissue for positive staining. Statistical analysis with both antibodies was done using ANOVA with a *post hoc* Dunnett's test.

## Chapter 4.7 REFERENCES

- 1 Willet, S. G. *et al.* Regenerative proliferation of differentiated cells by mTORC1-dependent paligenosis. *EMBO J* **37**, doi:10.15252/embj.201798311 (2018).
- 2 Garcia, A. M. *et al.* Tis7 deletion reduces survival and induces intestinal anastomotic inflammation and obstruction in high-fat diet-fed mice with short bowel syndrome. *Am J Physiol Gastrointest Liver Physiol* **307**, G642-654, doi:10.1152/ajpgi.00374.2013 (2014).
- 3 Yu, C. *et al.* Deletion of Tis7 protects mice from high-fat diet-induced weight gain and blunts the intestinal adaptive response postresection. *J Nutr* **140**, 1907-1914, doi:10.3945/jn.110.127084 (2010).
- 4 Swietlicki, E. *et al.* Growth factor regulation of PC4/TIS7, an immediate early gene expressed during gut adaptation after resection. *Journal of Parenteral and Enteral Nutrition* **27**, 123-131, doi:10.1177/0148607103027002123 (2003).
- 5 Xu, R., Peng, C., Xiao, S. & Zhuang, W. IFRD1 polymorphisms and gastric cancer risk in a Chinese population. *Medical Oncology* **31**, 135, doi:10.1007/s12032-014-0135-0 (2014).
- 6 Lewis, M. A. *et al.* Increased IFRD1 Expression in Human Colon Cancers Predicts Reduced Patient Survival. *Dig Dis Sci* **62**, 3460-3467, doi:10.1007/s10620-017-4819-0 (2017).
- 7 Ma, S. F. *et al.* Bioinformatic identification of novel early stress response genes in rodent models of lung injury. *Am J Physiol Lung Cell Mol Physiol* **289**, L468-477, doi:10.1152/ajplung.00109.2005 (2005).
- 8 Pachiappan, A., Thwin, M. M., Manikandan, J. & Gopalakrishnakone, P. Glial inflammation and neurodegeneration induced by candoxin, a novel neurotoxin from

- Bungarus candidus venom: global gene expression analysis using microarray. *Toxicon* **46**, 883-899, doi:10.1016/j.toxicon.2005.08.017 (2005).
- 9 Lock, A. *et al.* PomBase 2018: user-driven reimplementa-tion of the fission yeast database provides rapid and intuitive access to diverse, interconnected information. *Nucleic Acids Res*, doi:10.1093/nar/gky961 (2018).
- 10 Muller, P., Kutenkeuler, D., Gesellchen, V., Zeidler, M. P. & Boutros, M. Identification of JAK/STAT signalling components by genome-wide RNA interference. *Nature* **436**, 871-875, doi:10.1038/nature03869 (2005).
- 11 Vadivelu, S. K. *et al.* Muscle regeneration and myogenic differentiation defects in mice lacking TIS7. *Molecular and cellular biology* **24**, 3514-3525, doi:10.1128/MCB.24.8.3514-3525.2004 (2004).
- 12 Tetteh, P. W. *et al.* Replacement of Lost Lgr5-Positive Stem Cells through Plasticity of Their Enterocyte-Lineage Daughters. *Cell Stem Cell* **18**, 203-213, doi:10.1016/j.stem.2016.01.001 (2016).
- 13 Yu, S. *et al.* Paneth Cell Multipotency Induced by Notch Activation following Injury. *Cell Stem Cell* **23**, 46-59 e45, doi:10.1016/j.stem.2018.05.002 (2018).
- 14 Demitrack, E. S. *et al.* Notch signaling regulates gastric antral LGR5 stem cell function. *The EMBO journal* **34**, 2522-2536, doi:10.15252/embj.201490583 (2015).
- 15 Cho, Y. & Cavalli, V. HDAC5 is a novel injury-regulated tubulin deacetylase controlling axon regeneration. *EMBO J* **31**, 3063-3078, doi:10.1038/emboj.2012.160 (2012).
- 16 Dieplinger, B. *et al.* The transcriptional corepressor TPA-inducible sequence 7 regulates adult axon growth through cellular retinoic acid binding protein II expression. *Eur J Neurosci* **26**, 3358-3367, doi:10.1111/j.1460-9568.2007.05951.x (2007).

- 17 Vietor, I. *et al.* TIS7 interacts with the mammalian SIN3 histone deacetylase complex in epithelial cells. *The EMBO Journal* **21**, 4621-4631, doi:10.1093/emboj/cdf461 (2002).
- 18 Lammirato, A. *et al.* TIS7 induces transcriptional cascade of methylosome components required for muscle differentiation. *BMC biology* **14**, 95-95, doi:10.1186/s12915-016-0318-6 (2016).
- 19 Brown, A., Baird, M. R., Yip, M. C., Murray, J. & Shao, S. Structures of translationally inactive mammalian ribosomes. *Elife* **7**, doi:10.7554/eLife.40486 (2018).
- 20 Vietor, I., Kurzbauer, R., Brosch, G. & Huber, L. A. TIS7 regulation of the beta-catenin/Tcf-4 target gene osteopontin (OPN) is histone deacetylase-dependent. *J Biol Chem* **280**, 39795-39801, doi:10.1074/jbc.M509836200 (2005).
- 21 Micheli, L. *et al.* PC4/Tis7/IFRD1 stimulates skeletal muscle regeneration and is involved in myoblast differentiation as a regulator of MyoD and NF-kappaB. *J Biol Chem* **286**, 5691-5707, doi:10.1074/jbc.M110.162842 (2011).
- 22 Tummers, B. *et al.* The interferon-related developmental regulator 1 is used by human papillomavirus to suppress NFkappaB activation. *Nat Commun* **6**, 6537, doi:10.1038/ncomms7537 (2015).
- 23 Benhaddou, A. *et al.* Transcription factor TEAD4 regulates expression of myogenin and the unfolded protein response genes during C2C12 cell differentiation. *Cell Death Differ* **19**, 220-231, doi:10.1038/cdd.2011.87 (2012).
- 24 Subramanian, A. *et al.* Gene set enrichment analysis: A knowledge-based approach for interpreting genome-wide expression profiles. *Proceedings of the National Academy of Sciences* **102**, 15545, doi:10.1073/pnas.0506580102 (2005).

- 25 Feng, Z., Zhang, H., Levine, A. J. & Jin, S. The coordinate regulation of the p53 and mTOR pathways in cells. *Proc Natl Acad Sci U S A* **102**, 8204-8209, doi:10.1073/pnas.0502857102 (2005).
- 26 Fontoura, B. M., Atienza, C. A., Sorokina, E. A., Morimoto, T. & Carroll, R. B. Cytoplasmic p53 polypeptide is associated with ribosomes. *Molecular and Cellular Biology* **17**, 3146-3154, doi:10.1128/mcb.17.6.3146 (1997).
- 27 Horton, L. E. *et al.* p53 activation results in rapid dephosphorylation of the eIF4E-binding protein 4E-BP1, inhibition of ribosomal protein S6 kinase and inhibition of translation initiation. *Oncogene* **21**, 5325, doi:10.1038/sj.onc.1205662 (2002).
- 28 Burclaff, J. & Mills, J. C. Plasticity of differentiated cells in wound repair and tumorigenesis, part I: stomach and pancreas. *Disease Models & Mechanisms* **11**, dmm033373, doi:10.1242/dmm.033373 (2018).
- 29 Burclaff, J. & Mills, J. C. Plasticity of differentiated cells in wound repair and tumorigenesis, part II: skin and intestine. *Disease Models & Mechanisms* **11**, dmm035071, doi:10.1242/dmm.035071 (2018).
- 30 Wahl, G. M. & Carr, A. M. The evolution of diverse biological responses to DNA damage: insights from yeast and p53. *Nature Cell Biology* **3**, E277, doi:10.1038/ncb1201-e277 (2001).

# Chapter 5: Conclusions and Future Directions

## Chapter 5.1: Summary

In summary, the work described in this dissertation details significant advancements in the molecular basis of disease and injury in gastrointestinal tissues. We have described the process, paligenosis, by which mature cells can alter their differentiation state and become proliferative, in response to injury. We detailed the specific steps that occur during this process, and we have begun to highlight some of the major pathways involved. We began by investigating cellular dynamics that play an important role in whole tissue function in gastric chief cells and pancreatic acinar cells. We uncover the importance of mTORC1 as a central regulator of this process in both the stomach and pancreas. We investigated this process in numerous tissues and proposed that paligenosis is a conserved a shared mechanism. My work in the Mills lab has also specifically helped build upon the idea of paligenosis in two important ways: 1) establishment of the cerulein-based pancreatitis model that has enabled us to thoroughly characterize paligenosis as a shared process and 2) the identification of *Ifrd1* as a gene that is commonly upregulated in cells that undergo paligenosis. We characterized IFRD1 in numerous tissues, across several species and we now know that it is critical for the proliferation of cells undergoing paligenosis in diverse contexts. We discovered that IFRD1 is highly evolutionarily conserved, and this work has led to a burgeoning project in the lab focusing on paligenosis in *Drosophila*. My initial bioinformatic screen helped support projects in the lab characterizing paligenosis genes like *Ddit4* and *Atf3*. My work on paligenosis and *Ifrd1* uncovered new and

intersected with known hubs of cellular biology that are conserved to yeast including mTOR, P53, nucleolar stress and MAPK signaling<sup>1-4</sup>. Ultimately, our research aims to influence the understanding of human disease and paligenosis sheds light on the way that secretory cells can fuel GI adenocarcinomas. To that end, we analyzed IFRD1 in human colorectal cancers and observe a significant correlation between IFRD1 expression and patient survival.

## **Chapter 5.2: Future Directions**

Crafting a dissertation project around IFRD1 has been a mixed blessing. The scant literature on IFRD1 in relation to our model systems has made it so that we, along with Dr. Deborah Rubin, have been able to help set a foundational understanding of this gene. However, my dissertation research concludes with many unanswered questions that I will describe throughout the rest of this chapter.

### **IFRD1 in *ex vivo* culture**

We have previously experienced mixed results when attempting to generate gastroids from *Ifrd1*<sup>-/-</sup> mice. The most interesting result was achieved several times, whereby gastroids failed to form from mice that lacked *Ifrd1* (Figure 5.1). While this was a promising result, it was also surprising given our presumption that IFRD1 appears to function primarily on mature cells undergoing paligenosis; thus, we would not expect the constitutively active stem cell to be affected by *Ifrd1* mutation.

Further work is needed to answer several question about IFRD1 and the formation of organoids from gastric cells. The first experiment would be to find a consensus result from the generation of gastric organoids from gastric units isolated from *Ifrd1* null mice. Building on that

study would be to isolate chief cells from gastric units of mice with and without *Ifrd1* and determine the efficiency of organoid generation in that context.

Gastroids provide a cell autonomous system in which to test molecular mechanisms of paligenesis. Another system, for which I generated preliminary data, is the isolation and culture of pancreatic acinar cell ex vivo. This system has the advantage of requiring only crude isolation in order to enrich the cell population of interest (acinar cells), but a major disadvantage is that it is difficult to propagate these cells for more than a few days. Isolated acinar cells will naturally dedifferentiate and become more duct like in vitro (modeling acinar-ductal metaplasia in vivo), but many cells die due to the abundance of digestive enzymes that are released during isolation<sup>5</sup>. Developing this protocol further will enable large scale testing of paligenesis in a relatively homogenous cell population, which is important for understanding the molecular changes that occur during paligenesis.

There are numerous studies of interest in both gastric organoid and ex vivo acinar cell culture models. Since rapamycin has such a strong effect in vivo, it would be important to test the effects of rapamycin treatment on gastroid formation and dedifferentiation of isolated pancreatic acinar cells. Along the same lines, both of these systems enable the investigation of lysosome and autophagy dynamics. In relation to IFRD1, in vitro systems enable further analysis of the interaction between IFRD1 and P53. Co-immunoprecipitation could be done robustly in the cells of interest, as opposed to the mixed cell types in an in vivo tissue. Further, an epistatic relationship could be determined through the administration of Nutlin-3, which is an MDM2 antagonist (resulting in the stabilization of P53). Lastly, in vitro assays would enable the direct modulation of other major signaling pathways like JNK, HIPPO, MAPK and ribosomal stress

(e.g. treat with the transcriptional inhibitor actinomycin D), all of which would increase mechanistic evidence relating to IFRD1.

### **Single cell RNAseq in secretory cells undergoing paligenesis in the absence of *Ifrd1***

Rapid progress in the development of next-generation sequencing technologies in recent years has provided insights into biological systems. Sequencing based technologies for genomics, transcriptomics and epigenomics are now being focused on characterizing individual cells. Traditional expression profiling that assesses bulk populations can create noise when analyzing a process like paligenesis. Single cell RNAseq would be particularly useful in the pancreas, a tissue which is primarily composed of acinar cells, but those cells are not synchronized throughout injury. Characterizing the expression of pancreatic acinar cells (and gastric chief cells) undergoing paligenesis at various timepoints would help dissect specific expression profiles during the progression of paligenesis and potentially reveal regulatory relationships between genes. This technology has routinely been used in mouse and human pancreas, but not in the context of injury *en route* to metaplasia<sup>6-8</sup>.

### **IFRD1 Yeast 2 Hybrid**

In November of 2017, we performed a Yeast 2 Hybrid screen to uncover which proteins IFRD1 can interact with *in vivo*. This screen is a complementation assay that involves splitting a transcription factor into two fragments (bound to two proteins of interest) and observing the activation of a downstream reporter gene that is only transcribed when the two domains of the transcription factor interact. Initial review of the data produced a few interactions of note,

including: RPL19, RPL3, SMC6, ZNF574 and a screen of a short, but high identify match to LAMTOR4 (Figure 5.2). Ribosomal proteins RPL19 and RPL3 are highly conserved and involved in proliferation, ribosomogenesis, translation efficiency and management of nucleolar stress in relation to p53<sup>9-11</sup>. SMC6 is also highly conserved and manages DNA repair and replication stress<sup>12</sup>. In yeast, in addition to DNA repair and homologous recombination, SMC6 is essential for proliferation<sup>13</sup>. ZNF574 is one of seven genes that demonstrates highly differential expression in early onset colorectal cancer compared to late onset colorectal cancer<sup>14</sup>. ZNF574 is associated, like IFRD1, with the SIN3 complex, which, as described in Chapter 1, plays a role in scaffolding histone deacetylases, histone and DNA methylation and the regulation of P53. ZNF574 also interacts with NAT10, a nucleolar acetyltransferase that responds to stress by promoting a transition from rRNA synthesis to autophagy. Lastly, LAMTOR4 (late endosomal/lysosomal adapter and mitogen activated protein kinase and mechanistic target of rapamycin activator 4) is one of five proteins that make up the Ragulator complex. This complex is also conserved to yeast and its function is to anchor mTORC1 to the lysosomal membrane<sup>15</sup>. In the absence of the Ragulator complex mTORC1 becomes constitutively inactivated in the cytoplasm<sup>16</sup>.

None of the above described interactions can independently explain IFRD1 function, but together they provide insight into how IFRD1 may function in the injury response and they are each worthy of further exploration.

### **IFRD1 and Nucleolar Stress**

I performed an analysis of cerulein treated *Ifrd1* null vs WT mice in Partek that revealed that several DEAD-box helicases were down-regulated in mice lacking *Ifrd1* following 5 days of

cerulein treatment. This analysis led us to begin investigating ways to interpret and analyze the nucleolus in cells undergoing paligenosis. Immunofluorescent analysis of DDX21 revealed much less expression in *Ifrd1*<sup>-/-</sup> mice treated with cerulein compared to wild type mice treated with cerulein (Figure 5.3). Further, a relationship between IFRD1 and DDX21 was revealed through Cord analysis which displays genes that have been shown to be co-regulated in experimental contexts. I could not find a similar phenotype in the stomach so I have not continued to pursue DDX21, but the nucleolus has remained an area of active investigation in the lab.

Nucleolar/ribosomal stress is one of the few pathways that we know are shared among cells undergoing paligenosis and is conserved all the way to yeast. In the fly interactome (Drosophila Interactions Database), we see that the Drosophila version of *Ifrd1* interacts with Nucleostemin 1 and 2. Nucleostemin is required for DDX21 localizing to the nucleolus and is required for proliferating cells to pass through G1-phase<sup>17</sup>. A scenario where *Ifrd1* is required to scaffold Nucleostemin-DDX21 during stress, in order to maintain the suppression of p53 and enable cell cycle progression, is worth investigation.

The nucleolus is also important because it functions to maintain a balance between ribosomal RNAs (which are transcribed in the nucleolus) and ribosomal proteins is required to prevent p53 stability and progress through the cell cycle<sup>18</sup>; Figure 1.5). We believe that the apoptosis that we observe in stage 3 paligenotic cells of *Ifrd1*<sup>-/-</sup> mice is due to this stabilization of p53. The nucleolus integrates a ton of information because it requires: transcription (Pol-I, Pol-II and Pol-III), translation (of mTOR-dependent ribosomal proteins), nuclear import of ribosomal proteins and assembly of the entire ribosome complex. Any imbalance leading to the accumulation of ribosomal proteins that aren't attached to ribosomal RNAs leads to MDM2 binding. The binding of MDM2 by ribosomal proteins liberates and, therefore, stabilizes p53<sup>19</sup>.

Studies are underway in the lab to investigate morphological differences in the nucleoli of wild type and *Ifrd1*<sup>-/-</sup> gastric and pancreatic cells undergoing paligenosis. Early indications are that there is a difference in the number and size of nucleoli, however, more work is required to identify specific nucleolar markers that can be analyzed in each context and link those nucleolar markers to paligenosis-specific phenotypes.

### **IFRD1 and P53 transcription**

We analyzed gene sets from microarrays performed following 5 days of cerulein treatment in wild type and *Ifrd1*<sup>-/-</sup> mice. Given the stabilization of p53, we were interested in identifying a molecular expression signature that would differentiate *Ifrd1*<sup>-/-</sup> from wild type mice at the proliferation stage. Although we would expect all p53 target genes to be upregulated in *Ifrd1*<sup>-/-</sup> mice (due to the stabilization of p53 protein), instead we observed that a subset of p53 target genes were actually downregulated in *Ifrd1*<sup>-/-</sup> mice at this time point. In Knights et al., they describe how p53 is regulated by stress-induced posttranslational modifications<sup>20</sup>. Specific acetylated and phosphorylated residues of p53 influence gene expression patterns and, ultimately, cell fate. They describe that there is a cassette of p53 genes that are related to growth-arrest and another set which causes apoptosis. These gene sets can be delineated by their expression in relation to p53 acetylation status. P300 acetylates lysines 370, 372, 373 and 382 in the C-terminal portion of p53<sup>21</sup>. PCAF (p300-associated factor) has been linked to acetylation of lysine 320, which is located within a flexible linker domain which also contains a nuclear localization signal<sup>22,23</sup>. IFRD1 has been reported to form a complex with histone deacetylases, thus, we would propose that IFRD1 could plug into the Sin3 complex to influence p53 acetylation status<sup>24</sup>. In the Genechip data, we observe a decrease in growth-arrest p53 targets, like *cdkn1* and *sen2*. This suggests that there is a relative loss of K320 P53 in the absence of

IFRD1. If the loss of IFRD1 shifts the acetylation status of P53 from K320 to the K373 cassette, it may explain why there is more apoptosis following injury. Further investigation would include analyzing the difference between P53 gene cassettes and their relation to IFRD1. This would help uncover the functional relationship between IFRD1 and P53 and the consequences on paligenosis.

### **IFRD1 and Type I Interferons**

A new angle on paligenosis is emerging in the lab, in relation to the role of Type I Interferons and their effect on the injury observed in pancreas and stomach *en route* to metaplasia. IFRD1 is highly conserved, and we speculated that it evolved as a way for cells to differentiate between self and invading species that may try to take over host-protein translation mechanisms. *IFRDI* has been shown to be upregulated in human tissue following *H. pylori* infection and *Drosophila* tissue following *Pseudomonas* infection. The literature has also shown that IFRD1 can regulate viral immune evasion mechanisms in human papilloma virus-induced keratinocytes<sup>25</sup>. Type I Interferon (type 1 IFN) genes are cytokines that play a role in the induction of anti-viral gene program that is important for host defense against viruses. The type 1 interferon response, specifically genes associated with IFN- $\alpha$  and IFN- $\beta$ , are upregulated in *Ifrd1*<sup>-/-</sup> vs WT mice treated with cerulein. Further, IFN- $\alpha$  and IFN- $\beta$  responsive genes are upregulated in cerulein treated *Ifrd1*<sup>-/-</sup> vs. Rapamycin + Cerulein treated mice (Figure 5.4). This Type I IFN response may account for the increased death that we observe in *Ifrd1*<sup>-/-</sup> mice treated with long term cerulein compared to wild type mice.

## IFRD1 and Oxidative Phosphorylation

Metabolic reprogramming is a hallmark of tumor cell survival, proliferation and resistance to therapy. Cancer cells exhibit a wide range of metabolic profiles but tend to favor glycolysis over oxidative phosphorylation, even though glycolysis is much less efficient<sup>26</sup>. The Warburg effect describes this preference and one of the reasons that glycolysis may be preferred in cancer cells is due to impaired mitochondria, which function in apoptosis<sup>27</sup>. Mitochondrial function is generally intact in most cancers, but in some cases mitochondrial deficiencies can arise due to damage from the low-oxygen tumor environment or suppression by cancer genes<sup>27</sup>. In tumors, p53 is often inactivated or deleted, yet paradoxically recent studies have shown that activation of p53 impacts glucose metabolism and prevents more aggressive cancer phenotypes<sup>28</sup>. p53 has been shown to revert the Warburg effect and negatively influence the oncogenic metabolic adaptation of cancer cells<sup>29</sup>. A consistent molecular signature from the analysis of cerulein gene chips from *Ifrd1*<sup>-/-</sup> vs. wild type mice reveals that genes associated with the oxidative phosphorylation pathway are differentially expressed in *Ifrd1*<sup>-/-</sup> mice. As described earlier, p53 is stabilized in *Ifrd1*<sup>-/-</sup> mice, and aberrant p53, even in non-tumor cells, may result in a shift away from activation of genes associated with oxidative phosphorylation.

Previous work by the lab of Dr. Deborah Rubin has shown that overexpression of *Ifrd1* causes metabolic changes in enterocytes<sup>30</sup>. They observed an increase in fatty acid absorption and a decrease in the uptake of select amino acids in transgenic mice. Mice lacking *Ifrd1* also demonstrate metabolic deficiencies. For example, mice do not gain weight when chronically fed a high-fat diet and *tis7* deletion results in delayed lipid absorption and altered intestinal and hepatic lipid trafficking<sup>31</sup>. This investigation establishes a link between IFRD1-induced lipid metabolism, the inflammatory response to a high-fat diet, and survival after surgical resection<sup>32</sup>.

## **IFRD1 and human cancer screening**

As described earlier in Chapter 2, we find high IFRD1 expression is associated with poorer patient survival in colorectal cancer. We proposed that IFRD1 regulates metabolic processes in cancer cells, which may influence sensitivity to adjuvant chemotherapy. The precise mechanism by which IFRD1 may work is unknown, but the IFRD1 exhibits promise in cancer therapeutics as an indicator of high metabolic activity. We have shown, at the cellular level, that IFRD1 marks cells that have recently sensed injury. In the absence of IFRD1, these cells still sense damage, but they demonstrate a defect in the ability to resolve that injury. Our data show that IFRD1 may function as a signal to the cell that entry into the cell cycle is safe. Aberrant or hyperactivity of IFRD1 in tumors may suggest that these cells have the capacity to proliferate while ignoring normal cellular checkpoints. I view the impact of IFRD1 in future therapies as two-fold: 1) IFRD1 could serve as a marker on a genetic panel or screen that would highlight tumors with high metabolic plasticity and 2) as a drug target, inhibiting IFRD1 function, following the synchronization of tumor cells using chemotherapy. Since, IFRD1 seems dispensable for normal homeostatic activity, its inhibition would specifically drive tumor cells toward apoptosis.

## **Chapter 5.3 Conclusion**

Paligenosis establishes a new field that begins to explain a phenomenon observed during the injury response in numerous species and tissues. The characterization of IFRD1 in the context of paligenosis will influence the investigation of numerous tissues and disease research. The work described in this thesis details the launch of a new field of study and the first described regulator of it.

Figure 5.1

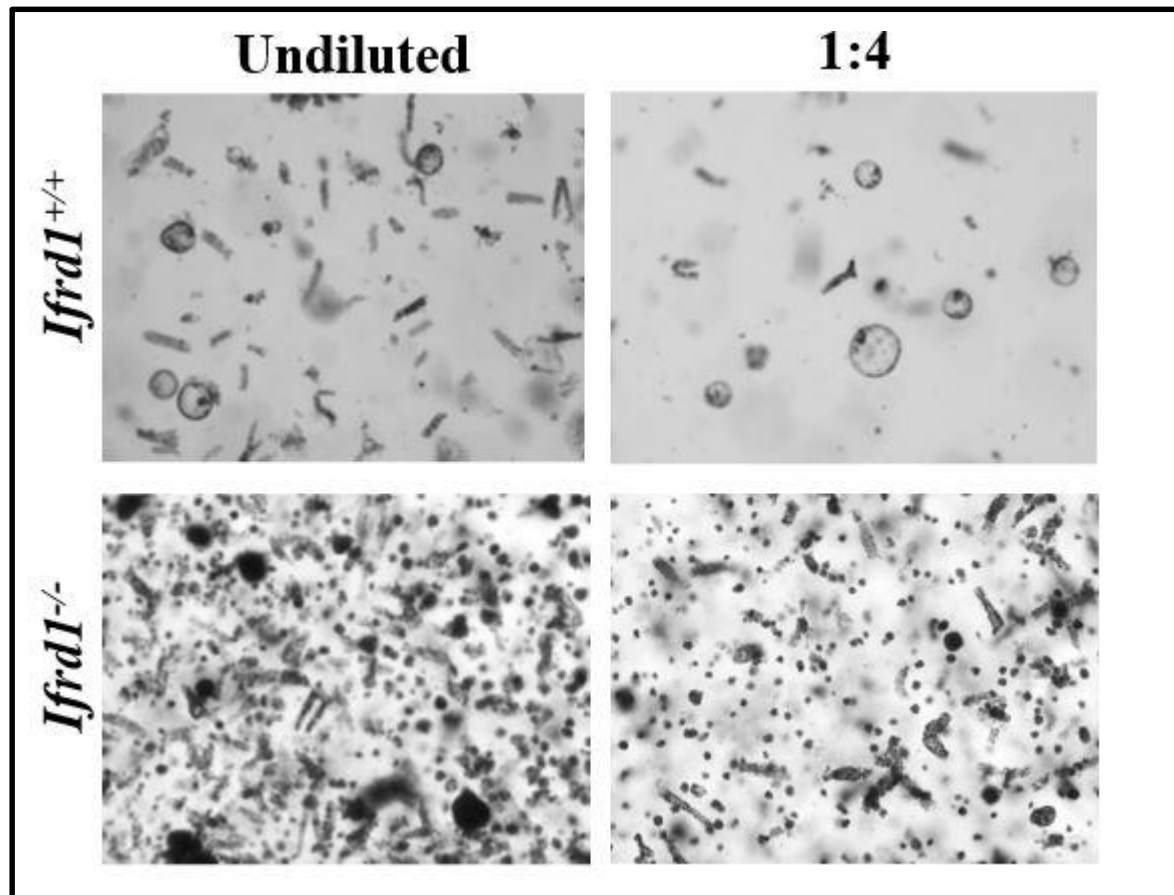


**Figure 5.1** Preliminary gastric organoid data generated from wild type and *Ifrd1* null mice. Initial results showed increased death and poor organoid establishment in null mice, but further experiments showed inconsistent results.

**Figure 5.2**

Clone Name	Type Seq	Gene Name (Best Match)	Start..Stop (nt)	Frame	Sense	%Id 5p	%Id 3p	PBS
pB66_B-2	5p/3p	<a href="#">Homo sapiens - KRT80</a>	1114..1409	×	OOF1	99.7	99.7	N/A
pB66_B-3	5p/3p	<a href="#">Homo sapiens - KRT80</a>	1114..1409	×	OOF1	99.7	99.7	N/A
pB66_B-8	5p/3p	<a href="#">Homo sapiens - KRT80</a>	1126..1642	×	OOF1	98.7	99.6	N/A
pB66_B-23	5p/3p	<a href="#">Homo sapiens - MISP</a>	1284..2095	×	IF	99.3	99.3	C
pB66_B-52	5p/3p	<a href="#">Homo sapiens - MISP</a>	1323..2095	×	IF	99.1	99.1	C
pB66_B-16	5p/3p	<a href="#">Homo sapiens - MORC3</a>	2025..1788		?? N	100.0	100.0	N/A
pB66_B-15	5p/3p	<a href="#">Homo sapiens - NUCB2</a>	1005..1348	×	IF	88.1	88.1	D
pB66_B-27	5p/3p	<a href="#">Homo sapiens - NUCB2</a>	1005..1348	×	IF	88.1	88.1	D
pB66_B-7	5p/3p	<a href="#">Homo sapiens - NUCB2</a>	1005..1348	×	IF	88.1	88.1	D
pB66_B-43	5p/3p	<a href="#">Homo sapiens - NUCB2</a>	1005..1348	×	IF	88.1	88.1	D
pB66_B-29	5p/3p	<a href="#">Homo sapiens - NUCB2</a>	1005..1348	×	IF	88.1	88.1	D
pB66_B-10	5p/3p	<a href="#">Homo sapiens - OGFOD2</a>	21..490		IF	100.0	100.0	D
pB66_B-32	5p/3p	<a href="#">Homo sapiens - OGFOD2</a>	21..490		IF	98.7	99.4	D
pB66_B-31	3p	<a href="#">Homo sapiens - RPL19</a>	..623		??		98.0	N/A
pB66_B-44	5p/3p	<a href="#">Homo sapiens - RPL3</a>	198..701		IF	100.0	100.0	D
pB66_B-50	5p/3p	<a href="#">Homo sapiens - SERBP1</a>	941..445		?? N	90.7	90.7	N/A
pB66_B-35	5p/3p	<a href="#">Homo sapiens - SETD2</a>	4269..3902		?? N	100.0	100.0	N/A
pB66_B-53	5p/3p	<a href="#">Homo sapiens - SMC6</a>	1008..1671		IF	98.5	98.5	C
pB66_B-21	5p/3p	<a href="#">Homo sapiens - SMC6</a>	1041..1624		IF	100.0	100.0	C
pB66_B-28	5p/3p	<a href="#">Homo sapiens - SORT1</a>	555..1354		IF	99.9	99.6	D
pB66_B-41	5p/3p	<a href="#">Homo sapiens - TAF1</a>	3245..4701		OOF2	96.2	99.0	N/A
pB66_B-42	5p/3p	<a href="#">Homo sapiens - TAF1</a>	3245..4701		OOF2	99.7	99.3	N/A
pB66_B-14	5p/3p	<a href="#">Homo sapiens - TRPM2</a>	3852..4531	×	IF	99.0	99.3	D
pB66_B-13	5p	<a href="#">Homo sapiens - XPOT</a>	748..518		?? N	99.6		N/A
pB66_B-49	5p/3p	<a href="#">Homo sapiens - ZNF574</a>	909..1512		IF	99.8	99.7	D
pB66_B-45	3p	<a href="#">Homo sapiens - GenMatch</a>	-1..130	×	IF		100.0	D
pB66_B-25	5p/3p	<a href="#">Homo sapiens - GenMatch</a>	-1..548	×	IF	97.5	88.6	D
pB66_B-9	5p/3p	<a href="#">Homo sapiens - GenMatch</a>	-1..412		IF	100.0	100.0	D
pB66_B-6	5p/3p	<a href="#">Homo sapiens - GenMatch</a>	-1..412		IF	99.8	100.0	D

**Figure 5.2** Results from Yeast 2 Hybrid assay listing the potential proteins that can interact in vitro.

**Figure 5.3**

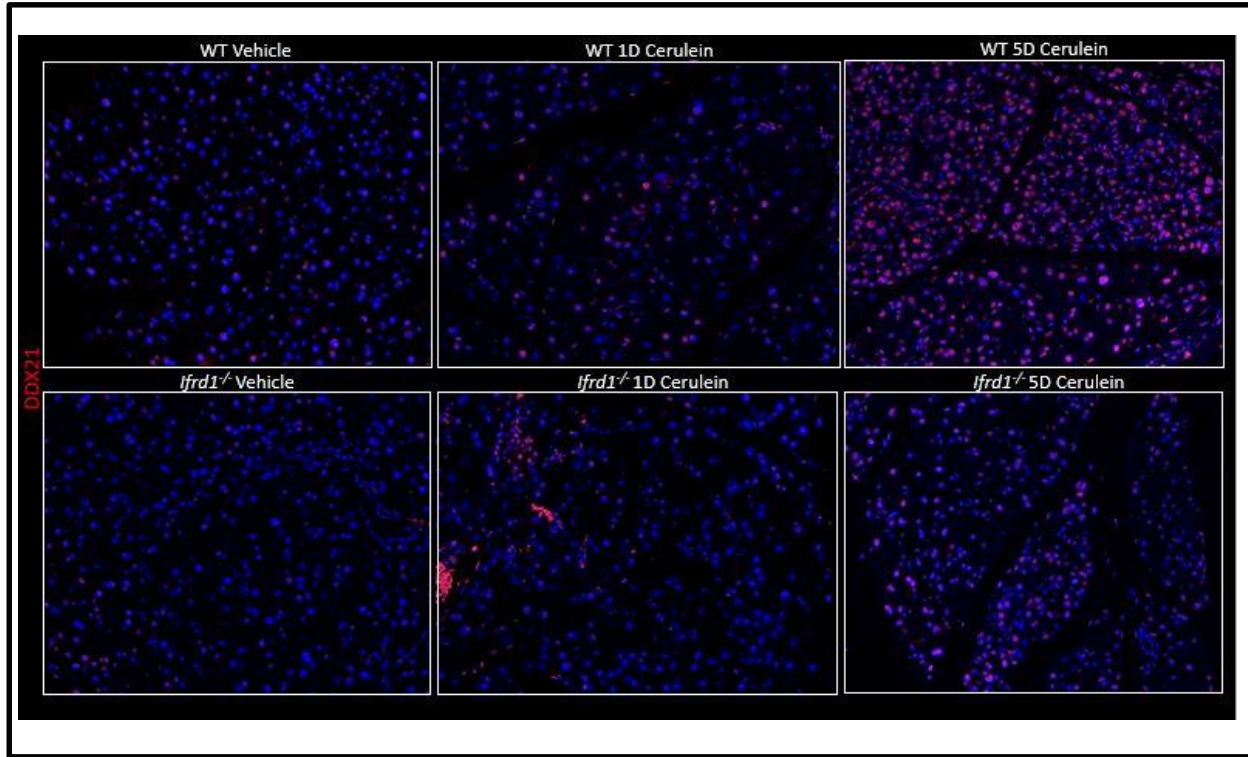


**Figure 5.3** Preliminary results showing decreased DDX21 expression in *Ifrd1* null mice treated with cerulein compared to wild type mice.

**Figure 5.4**

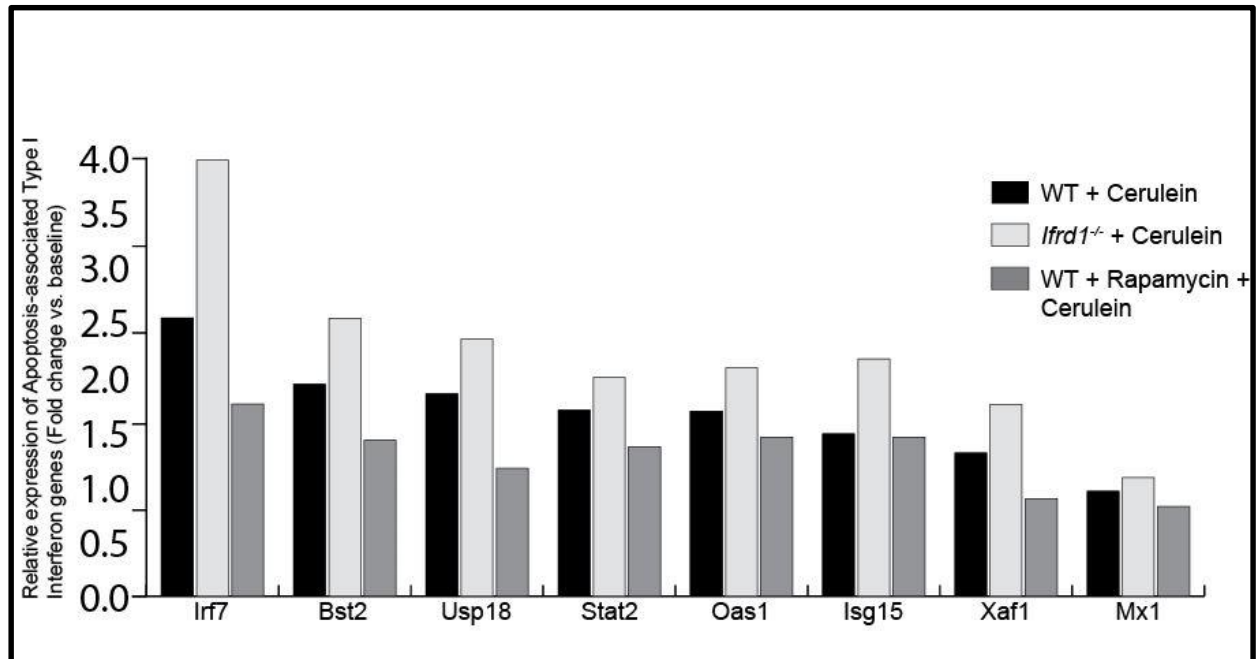


**Figure 5.4** Comparison of interferon related gene expression after cerulein treatment in wt, Ifrd1 null and wt mice + rapamycin. The results show that all of the Interferon type 1-related genes are upregulated in Ifrd1 nulls compared to wild type or rapamycin treated mice, which might account for the increases apoptosis in Ifrd1 null mice treated with cerulein.

## Chapter 5.5 REFERENCES

- 1 González, A. & Hall, M. N. Nutrient sensing and TOR signaling in yeast and mammals. *The EMBO journal* **36**, 397-408, doi:10.15252/embj.201696010 (2017).
- 2 Casso, D., Beach, D., Casso, D. & Beach, D. A mutation in a thioredoxin reductase homolog suppresses p53-induced growth inhibition in the fission yeast *Schizosaccharomyces pombe*. *Molecular and General Genetics MGG* **252**, 518-529, doi:10.1007/BF02172398 (1996).
- 3 Yu, Z.-Y. *et al.* Fission yeast nucleolar protein Dnt1 regulates G2/M transition and cytokinesis by downregulating Wee1 kinase. *Journal of cell science* **126**, 4995-5004, doi:10.1242/jcs.132845 (2013).
- 4 Toone, W. M. & Jones, N. Stress-activated signalling pathways in yeast. *Genes to Cells* **3**, 485-498, doi:10.1046/j.1365-2443.1998.00211.x (1998).
- 5 Gout, J. *et al.* Isolation and culture of mouse primary pancreatic acinar cells. *Journal of visualized experiments : JoVE*, 50514, doi:10.3791/50514 (2013).
- 6 Hwang, B., Lee, J. H. & Bang, D. Single-cell RNA sequencing technologies and bioinformatics pipelines. *Experimental & molecular medicine* **50**, 96-96, doi:10.1038/s12276-018-0071-8 (2018).
- 7 Enge, M. *et al.* Single-Cell Analysis of Human Pancreas Reveals Transcriptional Signatures of Aging and Somatic Mutation Patterns. *Cell* **171**, 321-330.e314, doi:10.1016/j.cell.2017.09.004 (2017).
- 8 Stanescu, D. E., Yu, R., Won, K.-J. & Stoffers, D. A. Single cell transcriptomic profiling of mouse pancreatic progenitors. *Physiological genomics* **49**, 105-114, doi:10.1152/physiolgenomics.00114.2016 (2017).
- 9 Tsubota, S. I. & Phillips, A. C. Drosophila Enhancer of Rudimentary Homolog, ERH, Is a Binding Partner of RPS3, RPL19, and DDIT4, Suggesting a Mechanism for the Nuclear Localization of ERH. *Molecular biology international* **2016**, 8371819-8371819, doi:10.1155/2016/8371819 (2016).
- 10 Russo, A. *et al.* Human rpL3 induces G<sub>1</sub>/S arrest or apoptosis by modulating p21 (waf1/cip1) levels in a p53-independent manner. *Cell cycle (Georgetown, Tex.)* **12**, 76-87, doi:10.4161/cc.22963 (2013).
- 11 Russo, A. *et al.* rpL3 promotes the apoptosis of p53 mutated lung cancer cells by down-regulating CBS and NFκB upon 5-FU treatment. *Scientific Reports* **6**, 38369, doi:10.1038/srep38369 <https://www.nature.com/articles/srep38369#supplementary-information> (2016).

- 12 Roy, M.-A. & D'Amours, D. DNA-binding properties of Smc6, a core component of the Smc5–6 DNA repair complex. *Biochemical and Biophysical Research Communications* **416**, 80-85, doi:<https://doi.org/10.1016/j.bbrc.2011.10.149> (2011).
- 13 Ju, L. *et al.* SMC6 is an essential gene in mice, but a hypomorphic mutant in the ATPase domain has a mild phenotype with a range of subtle abnormalities. *DNA Repair* **12**, 356-366, doi:<https://doi.org/10.1016/j.dnarep.2013.02.006> (2013).
- 14 Berg, M. *et al.* Distinct high resolution genome profiles of early onset and late onset colorectal cancer integrated with gene expression data identify candidate susceptibility loci. *Molecular cancer* **9**, 100-100, doi:10.1186/1476-4598-9-100 (2010).
- 15 Mu, Z., Wang, L., Deng, W., Wang, J. & Wu, G. Structural insight into the Ragulator complex which anchors mTORC1 to the lysosomal membrane. *Cell discovery* **3**, 17049-17049, doi:10.1038/celldisc.2017.49 (2017).
- 16 Su, M.-Y. *et al.* Hybrid Structure of the RagA/C-Ragulator mTORC1 Activation Complex. *Molecular cell* **68**, 835-846.e833, doi:10.1016/j.molcel.2017.10.016 (2017).
- 17 Romanova, L. *et al.* Critical role of nucleostemin in pre-rRNA processing. *The Journal of biological chemistry* **284**, 4968-4977, doi:10.1074/jbc.M804594200 (2009).
- 18 Nicolas, E. *et al.* Involvement of human ribosomal proteins in nucleolar structure and p53-dependent nucleolar stress. *Nature communications* **7**, 11390-11390, doi:10.1038/ncomms11390 (2016).
- 19 Volarević, S. *et al.* Proliferation, But Not Growth, Blocked by Conditional Deletion of 40<em>S</em> Ribosomal Protein S6. *Science* **288**, 2045, doi:10.1126/science.288.5473.2045 (2000).
- 20 Knights, C. D. *et al.* Distinct p53 acetylation cassettes differentially influence gene-expression patterns and cell fate. *The Journal of cell biology* **173**, 533-544, doi:10.1083/jcb.200512059 (2006).
- 21 Gu, W. & Roeder, R. G. Activation of p53 Sequence-Specific DNA Binding by Acetylation of the p53 C-Terminal Domain. *Cell* **90**, 595-606, doi:[https://doi.org/10.1016/S0092-8674\(00\)80521-8](https://doi.org/10.1016/S0092-8674(00)80521-8) (1997).
- 22 Sakaguchi, K. *et al.* DNA damage activates p53 through a phosphorylation-acetylation cascade. *Genes & development* **12**, 2831-2841 (1998).
- 23 Liu, L. *et al.* p53 sites acetylated in vitro by PCAF and p300 are acetylated in vivo in response to DNA damage. *Molecular and cellular biology* **19**, 1202-1209 (1999).
- 24 Vietor, I. *et al.* TIS7 interacts with the mammalian SIN3 histone deacetylase complex in epithelial cells. *The EMBO Journal* **21**, 4621, doi:10.1093/emboj/cdf461 (2002).
- 25 Tummers, B. *et al.* The interferon-related developmental regulator 1 is used by human papillomavirus to suppress NFκB activation. *Nature communications* **6**, 6537-6537, doi:10.1038/ncomms7537 (2015).

- 26 DeBerardinis, R. J., Lum, J. J., Hatzivassiliou, G. & Thompson, C. B. The Biology of Cancer: Metabolic Reprogramming Fuels Cell Growth and Proliferation. *Cell Metabolism* **7**, 11-20, doi:<https://doi.org/10.1016/j.cmet.2007.10.002> (2008).
- 27 Hsu, P. P. & Sabatini, D. M. Cancer Cell Metabolism: Warburg and Beyond. *Cell* **134**, 703-707, doi:<https://doi.org/10.1016/j.cell.2008.08.021> (2008).
- 28 Phan, L. M., Yeung, S.-C. J. & Lee, M.-H. Cancer metabolic reprogramming: importance, main features, and potentials for precise targeted anti-cancer therapies. *Cancer biology & medicine* **11**, 1-19, doi:10.7497/j.issn.2095-3941.2014.01.001 (2014).
- 29 Gomes, A. S., Ramos, H., Soares, J. & Saraiva, L. p53 and glucose metabolism: an orchestra to be directed in cancer therapy. *Pharmacological Research* **131**, 75-86, doi:<https://doi.org/10.1016/j.phrs.2018.03.015> (2018).
- 30 Lu, J. *et al.* Proline Absorption and SGK1 Expression are Inhibited in Intestinal *Tis7* Transgenic Mice. *Cellular Physiology and Biochemistry* **38**, 1532-1543, doi:10.1159/000443094 (2016).
- 31 Yu, C. *et al.* Deletion of *Tis7* protects mice from high-fat diet-induced weight gain and blunts the intestinal adaptive response postresection. *The Journal of nutrition* **140**, 1907-1914, doi:10.3945/jn.110.127084 (2010).
- 32 Garcia, A. M. *et al.* *Tis7* deletion reduces survival and induces intestinal anastomotic inflammation and obstruction in high-fat diet-fed mice with short bowel syndrome. *American journal of physiology. Gastrointestinal and liver physiology* **307**, G642-G654, doi:10.1152/ajpgi.00374.2013 (2014).

## Mark Anthony Lewis

860-655-6993(cell) - mark.a.lewis07@gmail.com - St. Louis, Missouri

### SUMMARY

- Academic training on the molecular mechanisms of reserve stem cell recruitment and development of pre-cancerous lesions in the gastrointestinal tract
- Excellent communication and presentation skills
- Demonstrated excellence in research project management and development
- Accomplished graduate level research scientist
- Intrinsically motivated and consistently looking for opportunities to develop personally and professionally

### EDUCATION

**Ph.D.** (expected January 2019), Molecular Cell Biology, Washington University

**M.A.**, Biology, Washington University, May 2012

**B.S.**, Biochemistry, Eastern Connecticut State University, May 2008

### PUBLICATIONS

1. **Lewis, M.A.**, Sharabash, N., Miao, ZF. et al. Increased IFRD1 Expression in Human Colon Cancers Predicts Reduced Patient Survival. *Dig Dis Sci* (2017) 62: 3460.  
<https://doi.org/10.1007/s10620-017-4819-0>
2. Willet, S.G, **Lewis, M.A.\***, Miao, ZF. et al. Regenerative proliferation of differentiated cells by mTORC1-dependent Paligenosis. *The EMBO J* (2018) 37:4 DOI: 10.15252/embj.201798311  
\*Co-first author
3. **Lewis, M.A.** et al. IFRD1 promotes survival and proliferation in the conserved cellular regeneration program (paligenosis) by suppressing p53 *Manuscript in submission*

### SELECTED ACADEMIC RESEARCH EXPERIENCE

**Graduate Research Associate**, September 2013-present, Mentor: Dr. Jason Mills, Gastroenterology Washington University School of Medicine

- Bioinformatic screen of pancreas, stomach, liver and kidney injury models to identify genes involved in the acute injury response.
- Development of a pancreas injury model that has allowed the lab to increase the scope and generalizability of our molecular basis of gastrointestinal disease in manuscripts and grants.
- Facilitated a collaboration between research and clinical leaders in pancreatic disease via the identification of macrophage type (resident or bone-marrow derive) and their function in pancreatic cancer progression.
- Dissertation research will culminate in the identification of a gene that is extremely well-conserved, dispensable for normal growth and development, but essential for the recruitment of reserve stem cells following injury in multiple organs.

### SELECTED AWARDS & RECOGNITION (last 5 years):

2017 – **Oral Presenter**, FASEB Gastrointestinal Tract XVII, Steamboat Springs, Colorado (1 of 4 invited graduate trainee speakers)

2016 - **Oral Presenter**, Keystone Symposia on Cell Biology, Keystone, Colorado  
(Global Cell Biology Conference with more than 500 attendees)  
(1 of 2 invited graduate trainee speakers)

2016 - **Young Investigator Travel Award**, Keystone Symposia on Cell Biology, Keystone, Colorado (1 of 8 travel award recipients)

### INDUSTRY EXPERIENCE

**Research Associate**, June 2007- September 2013

*Monsanto Company*, St. Louis Missouri- Monsanto (acquired by Bayer Corp.) was a global agriculture company specializing in products and tools that help farmers grow crops, while using energy, water and land in a more efficient manner.

- Optimization of high throughput, next generation sequencing machinery, bioinformatic sequence analysis and molecular quality control
- Project management and the development of a Laboratory Information Management System (LIMS) to centralize sample and project information in a high throughput environment
- Developed several programs written in PERL to analyze, align, and assemble plant and bacterial genome sequences in support of the Monsanto pipeline.
- Nucleic acid extractions and molecular analysis utilizing Taqman real-time, end point and inverse PCR methods.

### PROFESSIONAL DEVELOPMENT

2018 – Trained Consultant, The Biotechnology and Life Sciences Advising (BALSA)

2018 – Market Research Consultant, Canopy Biosciences

2015 – Mentor, AMGEN scholar program, Washington University

2014-2016 – Executive Board Member, Connections (student-led initiative to increase bias literacy)

2013-2015 – Mentor, Young Scientist Program, Washington University

2013 – Six Sigma Green Belt in Process Optimization, Monsanto Company

### RESEARCH SUPPORT

**Predoctoral Pediatric Digestive Disease Research T32-DK077653**

**03/01/2018-02/28/2019**

The criteria for appointment are likelihood of advancing to a career in biomedical research as assessed by classwork and research successes prior to and in the first 2 years of the graduate program, and interest in an area of inquiry relevant to juvenile diseases. T32 support offers membership in a community of scholars one training level senior to the predoctoral candidate.

**Diversity supplement to Mills-R01-DK-094989-03 Mills (PI)**

**01/01/2015-03/31/17**

This application proposes several experiments to learn how stem cells in the body (corpus) of the lining of the stomach respond to loss of acid-secreting parietal cells.